**PhD thesis**

Roald Kommedal

# Degradation of polymeric and particulate organic carbon in biofilms

NTNU Trondheim
Norwegian University of Science and Technology

PhD thesis [2003:101]
Telemark University College
Faculty of technology

# Degradation of polymeric and particulate organic carbon in biofilms

**Roald Kommedal**

Telemark University College
Faculty of Technology
Porsgrunn, Norway

Thesis submitted to the
Norwegian University of Science and Technology
for the PhD degree

*True churchmen's primary goal never is to serve the community ahead of everything else. Their primary goal is to serve, through reason, the goal of truth.*

Phædrus on "the Church of Reason"
Robert M. Pirsig

# Acknowledgements

Fulfilment of this research project was made possible by an unconditional grant from the Norwegian Ministry of Education and Research. The European Commissions program on Training and Mobility of Researchers enabled my research stay at the Technical University of Denmark under the BioToBio project (contract no. ERBFMRXCT970114).

Even though I am not supposed to credit my supervisor (Eco, 1997)[1], I would still take this opportunity to thank Rune Bakke for his support on and of the stage throughout the last ten years. His influence on my academic development, and commitment of providing me with the best of possibilities are highly appreciated. Rune and Kari Magrethe always kept their doors and minds open for positive reflections, and a good night sleep.

I would also thank my colleagues at Telemark University College for their interest and support in this project. Twofold credit to professor Poul Harremoës and Environment & Resources at DTU for including me in their PhD training, and giving me the opportunity of joining them on the BioToBio project. As part of the same project, Professor Eberhard Morgenroth, now at University of Illinois, provided profound help and support. Thanks to Professor Paul Stoodley and the Center for Biofilm Engineering at Montana State University for an interesting and stimulating period of research and learning. Dr. Kjetil Rasmussen and the people at Institutt for Bioteknologi at NTNU are thanked for having me up for training and discussions, and professor Torleiv Bilstad at Stavanger University College enabled means for the completion of this thesis.

Gratitude goes out to all the students and colleagues that helped and played important parts in this work, especially to Kim Milferstedt for his supreme work on HPLC and enzyme activity analysis, and his committed and talented contributions inside and out of the lab.

No structure is standing on a fragile fundament. Thanks to family and friends for support and tolerance of this provoking individual. Love and respect to Monika. It is all yours…

[1] Eco, Umberto *Kunsten at skrive speciale*, Akademisk Forlag, 1997, ISBN 8750034774

# Abstract

Polymeric and particulate organic carbon (POM) are fundamental compounds in the global cycling of carbon, and constitute significant amounts of BOD in municipal wastewater. The main objective of this work is to study molecular size effects on degradation dynamics in biofilm systems. Specifically, the effect of substrate molecular weight on degradation kinetics and transport dynamics, location of depolymerisation enzyme activity and depolymerisation intermediate formation dynamics are assessed. A mathematical model for biofilm degradation dynamics is presented, and used for data interpretation and simulations.

Dextran, an α-1,6 Glucan, was used as model substrate during batch degradation in a Rototorque biofilm reactor, in addition to batch tests on biofilm sub samples retrieved from the Rototorque, and during pure endo- and exo-Dextranase studies. Oxygen utilisation rate (OUR) estimates and bulk phase TOC mass balances were used to evaluate the effect of variable initial molecular weight on the observed half order removal coefficient (Harremoës, 1978; Rittmann and McCarty, 1980). Size exclusion-HPLC analysis for determination of bulk phase depolymerisation intermediates, and specific enzyme assays were used to evaluate transport dynamics of polymers and location of enzyme activity in the enhanced mixed population biofilm system.

Dextran removal rate decrease with increasing Dextran molecular weight. The observed areal half order removal rate coefficient, $k_{1/2,A}$, demonstrate an approximate 10-fold decrease in the 1-500 kDa range, showing negative logarithmic correlation to the initial $M_W$ of Dextran. A less distinct correlation is observed above this transition limit (1-10 MDa). Evaluation of the Thiele moduli, from one step depolymerisation modelling, suggests that the logarithmic reduction in observed removal rate is caused by combined reaction rate and transport limitations. Transport limitations dominates as the polymeric substrate size increase and hinders biofilm matrix diffusion, and the removal rate becomes a surface limited process. Removal of Dextran is biomass dependent in what appears to be a non-linear dependency on biofilm thickness. Expressed as biomass areal density ($g/m^2$), no depolymerisation is observed for thin biofilms (0.7 $g/m^2$), slow for medium (3.7 $g/m^2$) and high for thicker biofilms (5.2 $g/m^2$).

Depolymerisation intermediates accumulated in the bulk phase over the entire Dextran size range during pure Dexranase studies, with even size distributions. Final products were oligo-isomaltoses (DP 2-6). Dextran was not depolymerised by α-Glucosidase nor Oligo-α-1,6 Glucosidase. During biofilm reactor and slide sub-sample tests, low $M_W$ Dextran intermediates (1-10 kDa) accumulated in the bulk during depolymerisation of 160 kDa Dextran at 250 and 200 mg/l initial concentrations, but were not detected during experiments with 100 mg/l initial concentrations. Intermediate range Dextran (10-100 kDa) did not accumulate in either case. At the same conditions, some assimilable range Dextran (0.2-0.9 kDa) accumulated in the bulk liquid during initial 250 and 200 mg/l batches, but was not detected during 100 mg/l initial Dextran concentrations. The extent of bulk phase accumulation seems to depend on the biofilm growth rate, where more bulk phase accumulation is observed during experiments with starved compared to more actively growing biofilms. More intermediates accumulate during low $M_W$ initial standards, compared to higher. These observations indicate that the extent of bulk phase intermediate accumulation is balanced by the rate of depolymerisation, and the substrate uptake rate (growth). Accumulation of intermediate hydrolysis products in biofilm systems is therefore dependent on the slowly biodegradable organic (SBCOD) loading rate.

Dextranase was detected in the cellular fraction of the biofilms. The enzyme activity was not detected in any other biofilm sub compartments, implying that the exogenous enzyme remains attached to the cells while working on polymers. These findings support the conceptual model of Confer and Logan (1998), implying that bulk phase intermediate accumulation observed in this study and by others, is not a result of enzymatic activity in the bulk phase, but transport of intermediates from the biofilm matrix.

# Table of Contents

# List of Figures

# List of Tables

# Abbreviations

| | |
|---|---|
| SBOM: | Slowly biodegradable organic matter |
| RBOM | Readily biodegradable organic matter |
| TOC: | Total organic carbon |
| COD: | Chemical oxygen demand |
| BOD: | Biological oxygen demand |
| Da: | Daltons |
| RBCOD: | Readily biodegradable COD |
| SBCOD: | Slowly biodegradable COD |
| OUR: | Oxygen utilisation rate |
| POM: | Particulate organic matter |
| EC: | Enzyme Commission |
| DOM: | Dissolved organic matter |
| SBR: | Sequencing batch reactor |
| EPS: | Extracellular polymeric substances |
| SEC: | Size exclusion chromatography |
| HPLC: | High performance liquid chromatography |
| RID: | Refractive index detector |
| PBS: | Phosphate buffered saline |
| RIU: | Refractive index units |
| ASM | Activated sludge model |
| DP: | Degree of polymerisation (number of monomers) |
| CSTR: | Completely stirred tank reactor |

(For symbols, see Table 3-1.)

# 1 Introduction

Natural occurring organic matter is found in most environments of the biosphere. From the deep parts of sedimentary rocks such as oil, via soil and sediments to the water bodies of the oceans and fresh water sources, reduced organic molecules persist as slowly biodegradable or almost inert polymeric compounds. The continuous reduction of carbon species by photosynthesis is counterbalanced by the abiotic and biotic oxidations in oxic and anoxic environments resulting in a dynamic steady state of readily and slowly degradable organic matter. Thermodynamically, organic carbon is susceptible to chemical oxidation converting the reduced carbon to inorganic oxidised species. The absence of readily biodegradable organic substances in natural environments, such as soil, the ocean and freshwater bodies, indicate that the recycling of inorganic carbon is limited by the degradation of polymeric organics. Even though degradation is thermodynamically favourable, the chemical structure and size of the polymers provide a high degree of chemical stability causing the kinetics of the degradation to strongly limit the recycling. Thus, biological catalysis through the action of enzymes is the main route of degradation of organic matter, of which most catalysts are of microbial origin. By ecologists called the microbial loop, microbial degradation is the major route of re-mineralisation of organic carbon from photosynthesis. However, polymeric structure and high molecular weight prevent polymeric carbon molecules from entering microbial cells, necessitating preconditioning of the chemical structure before mineralisation. Depolymerisation, i.e. splitting a long polymer into its fragmented building blocks of mono- and oligomers, is the most important pre-processing as the cytoplasmic cell membrane prevents molecules larger than two to three atoms of passively diffuse into the cell, and more importantly, facilitated transport is by most organisms restricted to molecules less than about 600-1000 g/mole. Thus, enzymatic depolymerisation outside the cell membrane, either anchored to the membrane, in the periplasmic space, attached to the cell wall or even excreted into the surrounding media, produce readily biodegradable organic products that may enter the cell for intracellular terminal mineralisation.

Microbial degradation of slowly biodegradable organic matter (SBOM) is also of major importance in biotechnological applications, especially in wastewater and solid waste treatment. While degradation of readily biodegradable organic matter (RBOM) has

received most attention during the last century, focus on the kinetics and stoichiometry of SBOM degradation has become more important lately, both for operational and design purposes. Most of this work has been aimed at understanding the role of RBOM synthesis in suspended biological nutrient removal systems (Activated sludge nutrient removal systems), and in sludge stabilisation processes. Less attention has been offered the other major microbial community structure found in nature, the attached microorganisms forming biofilms. In this work focus is aimed at investigating the process of depolymerisation of polymeric carbon in biofilms. The main objectives are evaluation of the effects of molecular weight on depolymerisation kinetics, the combined kinetic and transport effects of intermediate dynamics in diffusive gradient bioaggregates (here: biofilms) and location of depolymerisation in these systems.

Knowledge provided will give a better understanding of degradation processes in structured microbial systems, such as biofilms and activated sludge flocs, and provide designers and operators of biotechnological processes quantitative information on the mechanisms of depolymerisation.

# 2 Background

This section contains information on definitions and concepts used. It is not intended to provide a general background, but rather introduce the necessary ideas and nomenclature used during the rest of the thesis.

## 2.1 Degradation of polymeric and particulate organic matter

Classification of organic matter is a relativistic exercise dominated by system related definitions. The lack of generalised terms is a source of confusion preventing exchange of quantitative information between, and within, disciplines.

### 2.1.1 Classification of organic substrates

Heterogeneity and diversity of organic compounds in natural and wastewater systems has resulted in the use of lumped terms representing the sum of carbon (TOC) or its oxygen demand upon oxic degradation (COD/BOD). Related to physical size, carbon exists as part of molecules over six orders of magnitude (0.001-1000 µm, Levine et al., 1985), and organic matter in wastewater has been organized into several sub-categories (Balmat, 1957; Heukelekian and Balmat, 1959; McKinney and Ooten, 1969; Dold et al., 1980). Organic substrates may be classified based on: 1) physical size, and 2) degradability.

Traditionally, two size fractions have been identified by filtration through a filter of nominal pore size of 0.2-2 µm (Clesceri et al., 1998), dissolved organic matter (DOM) defined to be the total organic carbon (TOC), or chemical oxygen demand (COD), in the filtrate, while the retentate represented the particulate organic matter fraction (POM). Sometimes the filtrate is further separated into the colloidal fraction, defined as the 1-1000 nm size range by ultrafiltration or precipitation (Tchobanoglous and Burton, 1991), and the dissolved fraction remaining. The particulate fraction within the range 1-100 µm has sometimes been called the supra-colloidal, defining particles above this limit as settleable (Levine et al., 1985). Figure 2-1 show typical organic content of wastewater in the traditional size fractions. Even though composition is site specific and large variations are inevitable, these data indicate that significant fractions of inlet organic matter (~70%) is colloidal and particulate. More over, the

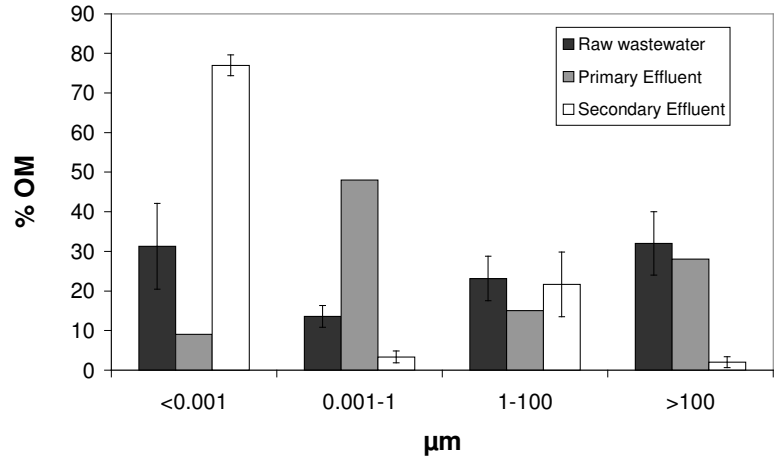


Figure 2-1. Typical organic content of traditional size ranges of wastewater particles (Levine et al., 1991)

colloidal fraction increases relatively much during primary sedimentation (~50%) emphasising the importance of this particular fraction. Characterisation based on size does not distinguish chemical properties of the particles. Characterisation may also be based on system factors. Larsen (1992) fractionated particles as diffusible and non-diffusible in a biofilm matrix based on their molecular size (diffusible cut-off limit set at $10^5$ g/mole (Daltons, Da), and the readily biodegradable fraction below 1000 Da.

Traditionally, three particulate substrate groups have been specified based on chemical composition; polysaccharides (sugars), lipids (fats) and proteins. As substance groups these also include their shorter chain oligo- and monomers (carbohydrates, peptides, amino acids, fatty acids). Heukelekian and Balmat (1959) reported detailed on the composition of domestic wastewater. While only 36 % (w/w) of the total solids occurred as particulate material (i.e. colloidal, supracolloidal and settleable), 69 % of the volatile organics were particulate. Of these, total grease (fats) accounted for 32 %, nitrogenous (proteins) 36 %, 20 % carbohydrates (polysaccharides) and 12 % was unspecified. This indicates that the major fraction of volatile organics (69 %) in wastewater is non-dissolved, and that most of this fraction consists of polysaccharides, proteins and particle bound fats (88 %). Other lumped organic molecules, such as nucleic acids (RNA and DNA), vitamins and humic acids, may also be singled out representing different characteristics as the three standard components. Figure 2-2 show how organic substrate (and inorganic nutrients) groups relate to molecular size in terms of their molecular weight and hydrodynamic radius (assuming flexible chain tertiary structure). Also indicated are traditional separation and analytical techniques applicable for each size fraction, and particular fraction distributions. Polymers are almost exclusively related to the colloidal

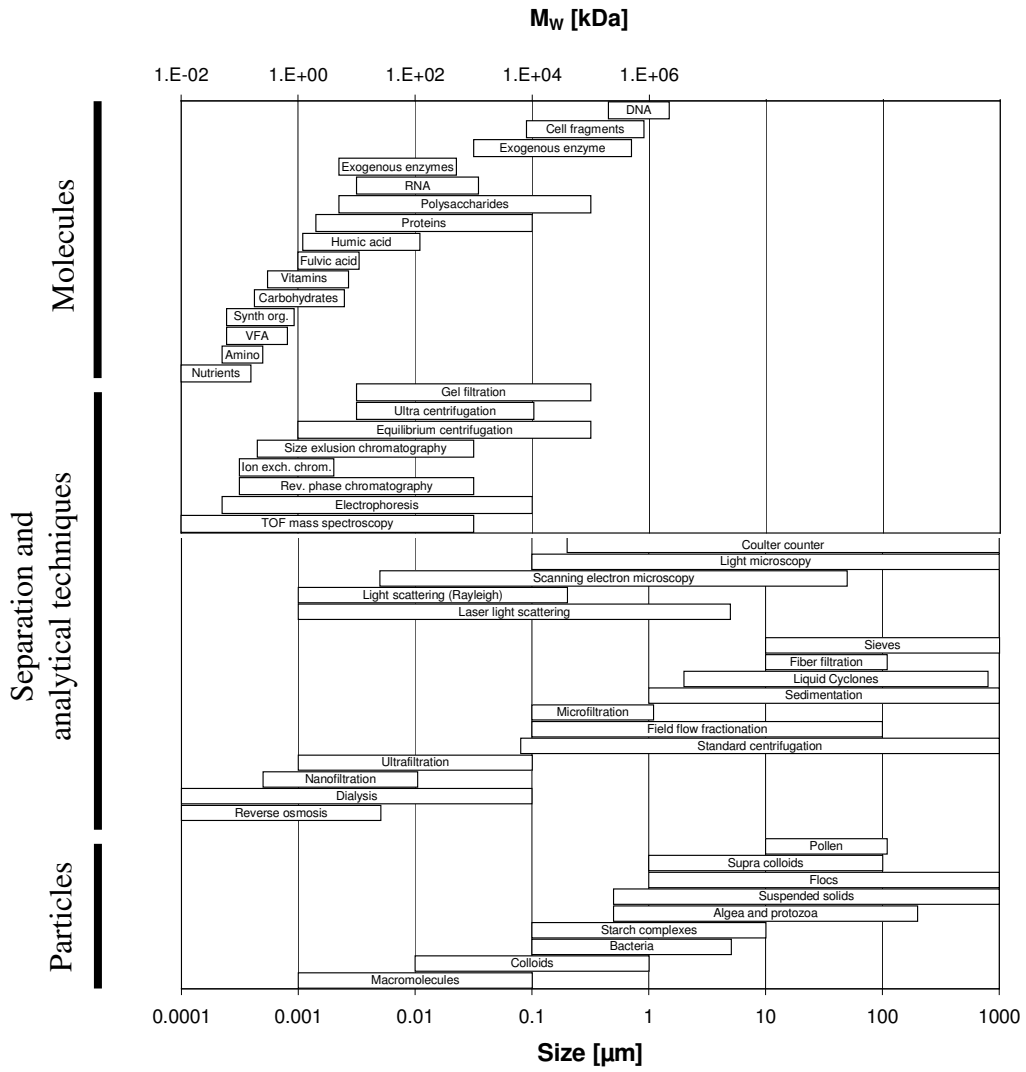


Figure 2-2. Biomolecules, particles and separation and analytical techniques used for classification and characterisation based on molecular weight and/or flexible chain size (Compiled on data from Levine et al., 1985; Tchobanoglous and Burton, 1991; Cheryan, 1998)

and macromolecular fraction of organic particles. Only very large polymers (like DNA, cellulose and starch) are big enough to be regarded as colloidal. Therefore, major fractions of organic particles found in wastewater are colloidal and particulate aggregates of polymers making up cellular fragments, and coagulated conglomerates. Thus, degradation of wastewater particles involves degradation of several unspecific polymers, parts of undefined structure and variable size fractions.

Fractionation based on traditional filtering into suspended and dissolved solids (at about 1 µm), in the wastewater literature often used to separate the readily from the slowly biodegradables, largely overestimate the true readily biodegradable fraction defined as substrates that may be taken up directly by microorganisms without any preconditioning. Ekama and Marais (1977) developed a respirometric method for determination of the

readily (RBCOD) and slowly biodegradable (SBCOD) organics in wastewater, further developed by Ekama et al. (1986) and Sollfrank and Gujer (1991). This method is based on estimating the oxygen utilization rate (OUR) during batch operated activated sludge on influent wastewater. Contrary to the filter based separation, SBCOD and RBCOD are estimated by the true biodegradability of the fractions, and not by molecular size. Unfortunately, this method involves significantly more equipment (in terms of technicalities and costs) and data interpretation.

The IWA task group on mathematical modeling for design and operation of biological wastewater treatment (popularly called the ASM group) have based the characterization of biodegradable wastewater organics on the OUR procedure of Ekama and Marais (1977) and Ekama et al. (1986), separating into RBCOD ($S_S$), SBCOD ($X_S$), particulate inert organic matter ($X_I$) and soluble inert organic matter ($S_I$) (Henze et al., 1987), implementing the notation proposed by Grau et al. (1982). By combining the OUR test with filtrates from wastewater, these fractions may be estimated based on degradability, providing a more representative characterization of the organic fractions compared to strict filtration. However, intrinsic filtration steps are required introducing some uncertainties regarding, especially, the estimation of the heterotrophic yield, $Y_H$. Henze et al. (2000) suggested fractionation of the true RBCOD by ultrafiltration using a 1 kDa cut of membrane, and assuming the inert fraction of the filtrate to be less than 10 %. In a recent calibration study, Koch et al. (2000) used the approach described above and found the $S_S$ fraction of the total primary effluent COD to be 10 %, $X_S$ was 50-60 %, $X_I$ varied from 15 to 25 %, $S_I$ was found constant at 6 % and the inlet heterotrophic biomass amounted to about 9 %. In the same study, the filtrate passing a 0.45 µm membrane filter was found to be 40 % of the total COD, of which 23 % was slowly biodegradable and 15 % was readily. This indicates that slowly biodegradable particulate COD and inert particular COD amounts to 60 % of the total primary effluent COD and only 15 % may be regarded as readily biodegradable. The colloidal/polymeric fraction (passing the 0.45 µm filter) is as high as 23 % of the total. Thus, significant fractions (approx. 50 %) of the dissolved substrates (<0.45 µm) are not to be regarded as readily biodegradable, but slowly biodegradable dissolved substrates. This fraction contains dissolved particles, colloids and polymers. These data are similar to the results reported by Sollfrank and Gujer (1991) and those of Henze et al. (2000) and Henze et al. (2002), who found the slowly biodegradable dissolved fraction to be 50 %,. Ohron and Çokgör (1997) report on primary influent compositions that typically show higher particulate fractions (67 %), a ratio that is reduced

| | $C_T$ [mg/l] | $X_S$ [%] | $X_H$ [%] | $X_I$ [%] | $S_S$ [%] | $S_H$ [%] | $S_I$ [%] | References |
|---|---|---|---|---|---|---|---|---|
| *Primary influent* | | | | | | | | |
| South Afrika | 530 | 62 | | 13 | 20 | | 5 | Ekama et al. (1986) |
| Denmark | | 40 | 20 | 18 | 20 | | 2 | Henze (1992) |
| Turkey | 315 | 39 | | 13 | 13 | 29 | 6 | Ohron and Cokgör (1997) |
| Turkey | 670 | 64 | | 8 | 9 | 16 | 3 | Ohron and Cokgör (1997) |
| Turkey | 585 | 64 | | 10 | 13 | 10 | 3 | Ohron and Cokgör (1997) |
| Switzerland | 250 | 53 | 7 | 9 | 11 | | 20 | Kappeler and Gujer (1992) |
| Switzerland | 430 | 60 | 15 | 8 | 7 | | 10 | Kappeler and Gujer (1992) |
| Switzerland | 325 | 55 | 15 | 10 | 8 | | 12 | Kappeler and Gujer (1992) |
| *Primary effluent* | | | | | | | | |
| South Africa | 370 | 60 | | 4 | 28 | | 8 | Ekama et al. (1986) |
| Switzerland | 220 | 45 | | 11 | 32 | | 11 | Henze et al. (1987) |
| Switzerland | 190 | 56 | | 26 | 10 | | 8 | Siegrist et al. (1994) |
| Switzerland | 250 | 58 | | 24 | 10 | | 8 | Siegrist et al. (1994) |
| Switzerland | 320 | 31 | 22 | 8 | 14 | 16 | 9 | Sollfrank and Gujer (1991) |
| Switzerland | 390 | | | | 4 | 33 | 7 | Koch et al. (2000) |
| Switzerland | 400 | | | | 9 | 33 | 6 | Koch et al. (2000) |
| Switzerland | 390 | | | | 10 | 27 | 6 | Koch et al. (2000) |
| Switzerland | 565 | | | | 10 | 18 | 6 | Koch et al. (2000) |
| Switzerland | 330 | | | | 9 | 27 | 6 | Koch et al. (2000) |
| Switzerland | 435 | | | | 16 | 26 | 6 | Koch et al. (2000) |
| Switzerland | 345 | | | | 9 | 25 | 6 | Koch et al. (2000) |
| Switzerland | 545 | | | | 14 | 16 | 6 | Koch et al. (2000) |
| Switzerland | 480 | | | | 33 | 13 | 6 | Koch et al. (2000) |
| Switzerland | 315 | | | | 27 | 25 | 6 | Koch et al. (2000) |
| Switzerland | 140 | | | | 25 | 14 | 7 | Koch et al. (2000) |
| Switzerland | 520 | | | | 7 | 27 | 6 | Koch et al. (2000) |
| Switzerland | 280 | | | | 25 | | 5 | Koch et al. (2000) |
| Switzerland | 350 | | | | 17 | 11 | 6 | Koch et al. (2000) |
| Hungary | 350 | 43 | | 20 | 29 | | 9 | Henze et al. (1987) |
| Spain | 340 | 33 | 15 | 25 | 18 | | 9 | de la Sota et al. (1994) |
| Denmark | 515 | 49 | | 19 | 24 | | 8 | Henze et al. (1987) |
| Denmark | | 43 | 14 | 11 | 29 | | 3 | Henze (1992) |
| France | 450 | 44 | | 13 | 33 | | 10 | Lesouf et al. (1992) |
| France | 345 | 41 | | 8 | 25 | | 6 | Lesouf et al. (1992) |
| *Pre-precipitated primary effluent* | | | | | | | | |
| Denmark | | 26 | 8 | 5 | 56 | | 5 | Henze (1992) |

Table 2-1. Literature values on the relative [%] composition of organic fractions as determined by filtration and respirometric estimations.

during primary treatment (typically 50-70 % reduction, Henze et al., 2002). However, the readily biodegradable fraction is again about one third of the total dissolved COD (37 %), and the slowly biodegradable is 52 %. A summary of literature studies on characterisation is given in Table 2-1.

### 2.1.2 Polymers

As the particles enter the sub-micron range it is more appropriate to use the term polymers (*poly* = many, and meros = parts) or macromolecules, indicating that the particles are now small enough to exhibit molecular properties (Mortimer, 2000). Contrary to particles, the size of polymers is normally given as the molecular weight of the macromolecule. Relating that to the more common particle diameter depends on both molecular composition and conformations within the molecule (Smidsrød and Moe, 1995). Polymer size is often represented by the radii of gyration, $R_G$ (also called the radii of inertia). The size of macromolecules, in terms of physical extent, is correlated to their molecular weight as shown in Figure 2-3. Stiff polymers, like DNA, Cellulose and Xanthan, show close to direct correlation ($R_G$~M) up to about 200-300 nm, while molecules resembling ideal spheres are related by the cubic root ($R_G$~$M^{0.33}$) (Smidsrød and Moe, 1995). Most macromolecules, like proteins and water soluble polysaccharides, and stiff molecules of high molecular weight, behave as flexible chains with varying degree of flexibility around each polymer bond. Intermediate correlation values are typical for these (~$M^{0.4\text{-}0.8}$) with a typical root relation as an average. Hydrodynamic radii, representing radii of the hydrated macromolecule, is given as 80 % (flexible chain polymers) of the $R_G$ (Smidsrød and Moe, 1995), and this value may be used for comparing molecular size with nominal pore sizes in

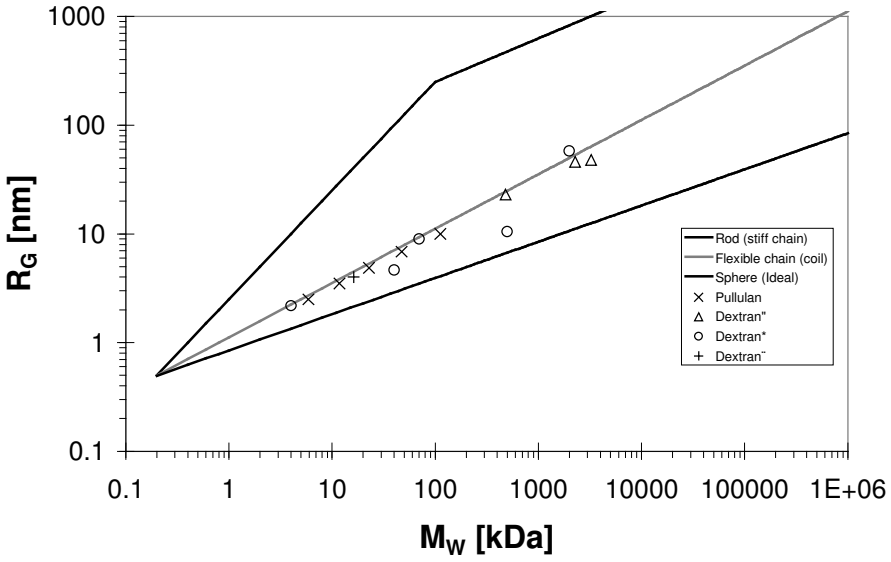


Figure 2-3. Correlation between macromolecular radii of gyration, $R_G$, and molecular weight. Upper boundary indicates the maximum correlation between stiff rods like molecules, while lower represents ideal spheres. The grey line in the middle shows the intermediate correlation for flexible chains. Experimental studies on Dextran (o, +, Δ) and Pullulan (x) are indicated. Data from Rogers et al., (2000), Wu, (1993) and Lawrence et al., 1994) and Smidsrød and Moe, (1995).

filters and gel structures. Wastewater polymers and typical hydrodynamic size ranges are indicated in Figure 2-2. As indicated, large polymers are well within the colloidal size range, while macromolecules of about 10 nm (or $M_W$ ~ 100 kDa) are defined as dissolved.

### 2.1.3 Depolymerisation

Depolymerisation may be defined as cleavage of covalent bonds, connecting monomers in a polymer, into products of sub-polymers of molecular weights less than the mother polymer. This process represents the opposite of the various polymerisation mechanisms used during polymer synthesis, and may come about through several mechanisms. Of these, hydrolysis and lysis of polymer bonds are most common.

Hydrolysis represents a broad range of chemical reactions of which water is consumed during the breakdown of covalent bonds. The process is energetically favourable at standard conditions ($\Delta S$ is always positive, $\Delta H$ is normally very low, and often negative), however, at rates too low for industrial applications (Goldberg and Tewari, 1994). The use of chemical and/or physical treatment combined with catalysts is therefore common in industrial processes. Chemical hydrolysis under acidic conditions, by thermal action and by combinations of these, has been used to enhance the rate of depolymerisation by hydrolysis. Chemical hydrolysis in natural habitats occurs slowly, however, *in situ* catalysts, such as soil, may enhance the process. In biological systems depolymerisation reactions are dominated by the action of hydrolytic enzymes.

Figure 2-4 lists identified hydrolytic (group 3) and lytic (group 4) enzymes and sub-classifications of these in accordance with the *Recommendations of the Nomenclature Committee of the International Union of Biochemistry and Molecular Biology* (IUBMB) *on the Nomenclature and Classification of Enzyme-Catalysed Reactions* (Webb, 1992). The sub groups are related to the type of substrate or bonds that are subject of depolymerisation. Several databases are available on the internet listing various information on specific enzymes (IUBMB: http://www.chem.qmw.ac.uk/iubmb/enzyme/, BRENDA: http://www.brenda.uni-koeln.de/, Expasy: http://www.expasy.org/, NCBI: http://www.ncbi.nlm.nih.gov/, WIT base: http://wit.mcs.anl.gov/, EMP project: http://wit.mcs.anl.gov/EMP/, Protein data bank (PDB):

| Group | Sub group | | | | | | | | | | | | | |
|---|---|---|---|---|---|---|---|---|---|---|---|---|---|---|
| | 1 | 2 | 3 | 4 | 5 | 6 | 7 | 8 | 9 | 10 | 11 | 12 | 13 | 99 |
| 3 (Hydrolases) | Acting on ester bonds (Esterases) | Acting on Glucosidic bonds (Glucosylases) | Acting on ether bonds (Etherases) | Acting on peptide bonds (Peptidases) | Acting on carbon-nitrogen bonds, other than peptide bonds (Amidases) | Acting on acid anhydrides (Anhydrases) | Acting on carbon-carbon bonds (Ketonases) | Acting on halide bonds | Acting on phosphorus-nitrogen bonds | Acting on sulfur-nitrogen bonds | Acting on carbon-phosphorus bonds | Acting on sulfur-sulfur bonds | Acting on Carbon-Sulfur Bonds | |
| 4 (Lyases) | Carbon-Carbon Lyases | Carbon-Oxygen Lyases | Carbon-Nitrogen Lyases | Carbon-Sulfur Lyases | Carbon-Halide Lyases | Phosphorus-Oxygen Lyases | | | | | | | | Other Lyases |

Figure 2-4. Groups and main sub groups of depolymerising enzymes as organised by the *Nomenclature Committee of the International Union of Biochemistry and Molecular Biology* (NC-IUBMB).

Systers: http://www.rcsb.org/pdb, http://systers.molgen.mpg.de, Protein Mutant Database: http://spock.genes.nig.ac.jp). IUBMB lists a total of 3196 identified and systematically categorised enzymes of which 1009 are hydrolytic and 314 are lyases (Webb, 1992). Relevant enzyme groups for polymer and POM degradation is the lipases, polyphosphatases and nucleases of EC 3.1, the glucosylases of 3.2, proteinase of EC 3.4, and the lytic enzyme groups of EC 4.2 acting on C-O bonds, especially sub-sub group EC 4.2.2 listing the polysaccharide lyases. Appendix 1 and 2 presents the full list of identified depolymerising enzymes.

## 2.2 Microbiology of polymer and POM degradation

Degradation of substrates involves numerous transport and reaction mechanisms attributed to cellular, but also community actions (Atlas and Bartha, 1998). While the terminal mineralisation refer to the reactions of the main intracellular metabolic pathways, exogenous mechanisms are often necessary to facilitate uptake of substrates. Fundamentally, the cellular membrane defines the outside of living cells, however, important reactions occur in the periplasm, on the surface of microbial cell walls and in the media surrounding the cell and/or the cellular community.

Microorganisms have developed fundamentally two different strategies to utilise organic substrates of polymeric and particulate origin. Eukaryotic organisms lacking a rigid cell wall may engulf particles and water containing dissolved polymers by wrapping the cytoplasmic membrane around the substrate, forming intracellular vacuoles for enzymatic breakdown (Priest, 1984). Pinocytosis (uptake of dissolved substrates) and phagocytosis (POM uptake) have also been observed by certain prokaryotes (Hashimoto et al., 1999), however, the rigidity and low permeability of the prokaryotic cell wall makes these mechanisms impossible for most bacteria.

Microbial cell membranes inhibit transport of macromolecules and particles into (and out of) the cytosol (Maxham and Majer, 1978). Only small non-charged molecules (like gases, small hydrophobic and water molecules) may passively diffuse trough the phospholipid bi-layer, limiting transport of other molecules to be transported by enzymes (Mathews and van Holde, 1990). Carbohydrates (Glucose, Mannose, Mannitol, etc.) are transported by the phosphotranspherase system (PTS), while separate systems exists for oligomers (maltose-maltohexose and melibiose transport system) and other non-PTS system substrates (lactose, glycerol, intermediates of the citric acid cycle). Transport and uptake of maltose and maltodextrins in $G^-$ bacteria has been reviewed by Boos and Schuman (1998), and serve as an excellent illustration of the mechanisms involved.

The maltose transport system consists of a membrane intrinsic enzyme complex ($MalFGK_2$) that transports maltose and maltose-oligomers up to six glucose units (maltohexaose) into the cytosol under ATP consumption. Intracellular degradation of maltodextrins are conducted by cytosolic amylomaltase (*malQ*), Maltodextrin glucosidase (*malZ*) and maltodextrin phosphorylase (*malP*), to produce maltose, glucose and glucose-1-phosphate. These end products are readily mineralised by glycolysis or polymerised for storage as glycogen. In the outer membrane of the $G^-$ bacteria, a dedicated porin for maltose and maltodextrin (and other carbohydrates) specific diffusion is encoded by the *lamB* gene, known as the λ-receptor. This porin has a pore diameter of approx. 1 nm, allowing facilitated diffusion of maltodextrins of small enough (approx. 1 kDa) to enter the periplasmic space. Inside the periplasmic space a high affinity maltose binding protein (MBP or MalE) transport protein binds maltodextrin, and release it upon binding to the $MalFGK_2$ translocation complex of the cytosolic membrane.

The activity of the maltoporin, and especially the extreme high affinity of the MBP protein, enables the cell to scavenge carbohydrates and small polysaccharides at very low exogenous concentrations ($K_M$ of MBP is as low as 1 μM). The maltose system is typical for many $G^-$ bacteria, like *E.Coli* and *Pseudomonads*, but is generally absent in $G^+$ prokaryotes. Maltose and small maltodextrins are thought to be transported through the peptidoglygan layer by passive diffusion, while proton motive force transport systems and PTS systems take up maltose. A similar system of depolymerisation and uptake mechanisms has been found for chitin (Baty III et al., 2001), and it may represent a general model for degradation and transport of large molecules in bacterial cells.

Several authors have listed general cut off limits to the uptake of oligomers from the surrounding media (White, 2000; Confer and Logan, 1997b; Larsen, 1992). The above

description of the maltose transport system of $G^-$ and $G^+$ bacteria indicate that this limit is in the range of 400 to 1000 Da for sugar oligomers. White (2000) lists a general average value of 600 Da for $G^-$ prokaryotes.

Substrates of molecular weight higher than the cut off limit of the various transport systems have to be depolymerised by enzymes outside the cell membrane before entrance and terminal mineralisation can complete degradation. Enzymes transported across the membrane but remaining in the periplasm or anchored to the cell wall, are called ectoenzymes, while those excreted into the surrounding media are called extracellular enzymes (Priest, 1984; Chróst, 1990). Extracellular enzymes may be excreted intentionally by living cells, enter the media by lysis or cell damage, or result from grazing activity by zooplankton and protozoan (Chróst, 1991). In this work the term exogenous enzymes is used to represent both kinds of enzymes located outside the inner cell membrane.

Depolymerisation of polymers and POM are exothermic reactions mainly catalysed by hydrolytic extracellular and ectoenzymes, attacking intra-polymeric bonds (bonds inside the second monomer) or by cleavage of the last bond connecting the terminal monomer to the polymer chain, called endo- and exoenzymes respectively (Priest, 1984). Extracellular depolymerisation enzymes are most common for Gram positive bacteria, however, some may attach to the outer surface as surface bound ectoenzymes. The more complex structure of the $G^-$ cell wall enable excreted enzymes to occupy the periplasmic space, the outside of the inner cell membrane, fixed to the inner or outer surface of the outer cell membrane, and anchored to the cell wall surface (Priest, 1984). It is suggested that the multi-layered cell wall of $G^-$ bacteria generally result in high levels of ectoenzymes, whereas the $G^+$, due to the relative open cell wall structure, release exogenous enzymes to the surrounding media (Cembella et al., 1984).

The peptidoglycan layer in bacteria is thought to resemble a gel like network of the aminosugar N-acetylglucosamine and N-acetylmuramic acids, and additional peptides for crosslinkages and teichoic acids (White, 2000). In $G^+$ bacteria the average net size is thought to be 5-6 nm (White, 2000), while peptidoglucan of $G^-$ are thought to cut off at around 50 kDa (Rydman and Bamford, 2002), ref. Figure 2-3. Ton B proteins found in $G^-$ bacteria protrude the bacterial cell wall and are known to be required for proton motive force driven translocation of substrates that do not diffuse through porins into the periplasm (White, 2000). It is therefore likely that small polymers, larger than the cut off limits of the porins and cytosolic membranes, accumulates in the immediate vicinity of the

membrane (inside the peptidoglycan of $G^+$, and in the periplasm of $G^-$), and that ectoenzymes depolymerise these into monomers of translocational size.

Location of exogenous enzymes has profound biochemical and ecological effects. Enzymes released to the bulk phase solutions are known to have higher turnover rates compared to ectoenzymes or enzymes immobilised to gel structures (Wentzel, 1991). From the cellular point of view, releasing enzymes to the environment would appear energetically inefficient, and the investment would become even more uneconomical as the distance between the enzymatic activity and the cell increase. Cells would, however, still energetically benefit from their investment up to about 500 µm in suspended cultures (Wentzel, 1991). Ectoenzymes would grant it's producer most of the product of their activity. However, these enzymes are subjected to substrate transport limitations. Therefore, releasing enzymes could be beneficial to the cell after all, since increased substrate availability would compensate the loss of products. Intuitively, substrate sufficient conditions would probably make the extracellular depolymerisation strategy more favourable than during starvation regimes, as it seems more important to retain the products during substrate scarcity. For the important genera *Bacillus sp.*, specific growth rate and growth phase have shown to have profound implications on the location of alkaline phosphatase (Hulett, 1986). Increased substrate availability is especially important for depolymerisation enzymes that attack substrates exhibiting low diffusivity and complex conformations. Immobilisation of extracellular enzymes or at least restricted diffusivity by extracellular matrix structures could provide a mean of ecological optimisation towards polymer scavenging. This will be dealt with in chapter 2.4.

## 2.3 Extracellular and ectoenzymes

According to the Enzyme Handbook (Schomburg et al., 19972002) 237 extracellular and 130 ectoenzymes have been identified. True extracellular enzymes (those that has been extracted from the growth media) are dominated by hydrolases that attack polymer bonds, i.e. EC 3.1, EC 3.2, EC 3.4 and EC 3.5. Most lyases extracted belong to the 4.2.2 subgroup, the polysaccharide lyases. This is not surprising in view of the transport mechanisms involved as discussed in section 2.2. EC 2.4 contains enzymes that transfer glycosyl groups from oligosaccharides to another carbohydrate, and some are known to

catalyse reactions that may be regarded as hydrolysis (strictly they transfer glycosyl groups to water). Hexosyl transferases (EC 2.4.1) are the major found extracellularly, in accordance with the abundance of hexoses in natural environments. Also, phosphotransferases (EC 2.7) has been extracted from the surrounding media, maybe as parts of phosphorous scavenging mechanisms. Extracellular oxido-reductases (EC 1) of the subclass dehydrogenase, especially the oxidases (EC.1.1.3) that oxidise glucose, galactose and alcohols (EC 1.1.3.4, 7, 9, 10, 18, 25 and 30) and dismutase (EC 1.15.1.1) are common detoxification enzymes (Harth and Horwitz, 1999). Group 1.10 enzymes (laccase oxidising benzenediol, ascorbate oxidase and rifamycin oxidase) and peroxidases (EC 1.11.1.7, 10, 13, 14) involved in -detoxification, have also been found extracellular. It is not surprising to find enzymes of these types in the surrounding media, as their function is related to scavenging of organic and phosphorous containing substrates unable to cross into the cells (hydrolases, lyases and phosphotransferases), and defence mechanisms acting upon antimicrobial agents and toxic compounds (Frere, 1995; Kharazmi, 1991).

Exogenous enzymes cross the cell membrane as part of the translation process (co-translational secretion) through ribosome-transport protein complexes (Priest, 1992). Most of the depolymerisation enzymes do not rely on cofactors or prosthetic groups. The enzyme substrate specific activity is thought to follow traditional Michaelis-Menten kinetics. However, early studies reports 1. order kinetics (Tauber, 1948) but that might be due to relative low substrate affinity and high $V_{max}$. They generally show wide temperature and pH ranges, and many have low specificity which makes them versatile for cells scavenging various substrates, providing microorganisms with an adaptive tool during static conditions. This is demonstrated as many exogenous enzymes are synthesized (or synthetically up-regulated) during late exponential and stationary growth conditions. Most extracellular enzymes reported in enzyme databases (like BRENDA, http://www.brenda.uni-koeln.de/) have been studied in vitro, and it is questionable how representative kinetic and stoichiometric coefficients are for in vivo situations.

Priest (1984) reviewed the regulation of exogenous enzymes. He suggested that control is exerted primarily at transcriptional level, and that inducible enzymes are governed by repressor or activator proteins. Further, inducible enzymes are thought to be activated by enzyme products due to the inability of primary substrates (polymers) to cross the cell membrane. Exogenous enzyme synthesis is found to be under strong catabolite repression by easily metabolised carbon substrates (e.g. acetate, glucose, intermediates of the citric acid cycle). For example, scavenging of maltodextrins is prepared by endogenous

induction after exponential growth on glucose or other carbohydrate carbon sources (Boos and Shuman, 1998). Similarly, synthesis of proteases is repressed by easily assimilable nitrogen sources, such as ammonium and amino acids (Priest, 1984). Many exogenous enzymes are up-regulated during late exponential and early stationary phase. That indicates substrate scavenging functions, and may also be indicative that some enzymes are involved in cell differentiation (White, 2000).

### 2.3.1 Exogenous enzymes in natural systems

Enzymatic activity in natural environments outside the cell has been observed for a long time. Overbeck (1991) gives a comprehensive historical review of papers published on the theme. He refers to Fermi (1906) as the first time proteolytic enzyme activity was observed in stagnant water pools, and Harvey (1925) reporting on extracellular oxidase and catalase activity in seawater. Kreps (1934) detected nitrate and ammonia oxidation in filtrate of seawater, while Elster and Einsele (1937) suggested extracellular phosphatase activity. ZoBell and Rittenburg (1937) reviewed degradation of high molecular weight chitins in natural habitats and concluded that these are found widely distributed in marine sediments, on the surface of plants, in the gut of marine mammals and associated with marine POM. More recently, Amon and Benner (1994) and Benner et al. (1992) reviewed the importance of exogenous enzymes in the recycling of DOM in the marine environment, emphasizing the importance of the microbial loop in primary production (Atlas and Bartha, 1998). Marine sediments harbour high levels of exogenous enzyme activity (Arnosti, 1995; Arnosti et al., 1994; Novitsky, 1986; Meyer-Reil, 1991) similar to activity found in brackish and estuarine waters (Hoppe, 1983; Smucker and Kim, 1991) and fresh water sediments (Cotner and Wentzel, 1991; Jones, 1979). Even deep-sea sediments and near bottom water have been studied and found to contain exoenzymatic activity associated to benthic macrofauna (Köster et al., 1991) and organic particles (Tholosan et al., 1999). Exoenzyme activity has also been studied in freshwater streams and rivers of epilithic and biofilm bacteria (Romani and Sabater, 1999; Chappell and Goulder, 1994; Jones and Lock, 1991).

Extracellular enzymes in the soil environment have been known for over 100 years (Skujins, 1976). Exoenzyme activities in soil are thought to be due to extracellular enzymes associated with, or as part of biofilm communities covering, the soil matrix (Hattori and Hattori, 1976), or originating from plants and macro invertebrates (Ladd,

1972; Hartenstein, 1982). Extracellular enzymes are also important for degradation of dead material in forest habitats, like fungal and bacterial degradation of cellulose (Bayer et al., 1998; Beguin and Aubert, 1994; Gilbert and Hazlewood, 1993; Coughlan, 1992; Coughlan, 1985). Exoenzymes are also part of bacterial virulence strategy during infections. *Erwinia cartotovora* and *Pseudomonas aeruginosa* are examples of opportunistic pathogens that secrete exogenous enzymes (Pectinases, Cellulases, Elastase, Lipases and Proteases) contributing to pathogenesis of plant and mammal infections, respectively (Jones et al. 1993; Kharamzi, 1991; Wicker-Böckelmann et al, 1987). Extracellular Dextranase has been isolated from *Streptococci salivarius* biofilms on tooth surfaces retarding plaque deposition (Ohnishi et al., 1995).

All these examples point to the widespread occurrence of exogenous enzymes. In fact, this is not at all surprising considering that easily biodegradable substrates are rare in natural habitats while POM and organic polymers are abundant from decaying biomass. A priori, bacterial infections would also imply exogenous enzyme activity during early stages of virulent infections, as well as host responses involve counter acting by exogenous protease activity. Also, it is understandable that detoxification enzymes would have to be exogenous by nature, since the effect of antibacterial and aggressive chemicals are known to attack intracellular processes.

### 2.3.2 Exogenous enzymes in wastewater systems

Numerous studies of enzymatic activity of enzymes in activated sludge have been used to characterize the activity of the sludge (Vaicum et al., 1965, Klapwijk et al., 1974; Teuber and Brodisch, 1976). Most studies focused on the activity of exogenous hydrolases (Thiel and Hattingh, 1967; Sridhar and Pallai, 1973; Nybroe et al., 1992; Boczar et al., 1992; Frølund et al. 1995). Richards et al., 1984) screened a number of activated sludge plants for the activity of eight enzymes, among these α-Glucosidase and Protease (both exogenous hydrolytic enzymes). They found indications of positive correlation between hydrolytic activity and COD loading rate. Nybroe et al., 1992) correlated activated sludge enzymatic activity with biomass concentration and microbial activity. However, α-Glucosidase did not seem to be affected by activity, indicating constitutive synthetic regulation. San Pedro et al., 1994) did not find any significant effect of biomass concentration on starch hydrolysis rate. In contrast, they did see an effect of

acclimatisation time, which may indicate an inducible long term effect. Hydrolysis of starch correlated well with first order hydrolysis kinetics, and interestingly, the activity of hydrolysis did not seem to be affected by changing electron acceptor conditions. Dold et al. (1995), however, reported higher α-Amylase activity under anaerobic conditions compared to aerobic, and located the Glycosylase activity to the cell fraction. Goel et al., 1997) also established a strong dependency between incubation electron acceptor conditions and hydrolytic activity in batch operated *Bacillus amyloliquefaciens* and *Pseudomonas saccharophilia* pure cultures. Contrary to Dold et al. (1995), they detected higher enzyme activity at aerobic conditions. However, their findings suggested that it was not the specific activity of hydrolytic enzymes that were affected, but rather the hydrolytic enzyme synthesis rate. The same authors demonstrated no electron acceptor effect on the specific activity of α-Glucosidase, Protease and Alkaline- and Acidic phosphatase in SBR activated sludge (Goel et al., 1999). However, in this study the stability and location of hydrolytic enzymes could explain the independence of electron acceptor conditions. Adsorption of extracellular enzymes to single sludge flocs subjected to varying conditions with characteristic times far below the degradation rate of hydrolytic enzymes could explain this effect. Interestingly, Protease activity increased during anaerobic phase. Batch tests under anaerobic and aerobic incubation all showed increased exogenous hydrolase activity (Phosphatase, Protease and α-Glucosidase) after exhaustion of TOC (undefined media). This may indicate an inducible enzyme synthetic stationary response by catabolite repression.

Location of exogenous hydrolytic activity was also studied by Goel et al., 1997), Goel et al., 1998a), Goel et al., 1999). Their major conclusion was that bulk phase extracellular hydrolysis was significant in two pure cultures studied, while the activity in SBR sludge was associated with the sludge flocs. Boczar et al. (1992) also showed that activated sludge contained most hydrolytic activity, with negligible bulk water activity. Frølund et al. (1995) later found that Esterase and Leucine aminopeptidase activity was 18 – 32 times higher in the activated sludge flocs compared to bacterial culture. This strongly suggests that the extracellular matrix may immobilize large amounts of extracellular enzymes. Vetter et al. (1998) concluded that released extracellular enzymes provide individual bacteria with a powerful feeding mechanism, especially in typical wastewater conditions (high surface area, high particulate organic concentrations). By comparing net energy gain, they showed that to a limited distance, cell free enzymes provide an important carbon

source even without taking mutualistic effects into account. This is significant when comparing biofilm and activated sludge systems, as cell free enzymes are thought to be more effected by hydraulic washout in activated sludge systems. Confer and Logan (1998) found that Leucine aminopeptidase and α-Glucosidase activity was cell mass associated, both for biofilm and suspended growth batch systems. Similar results were found when analysing trickling filter effluents. Hydrolytic
intermediates, however, were found to accumulate to some degree in the bulk phase. They explained this by suggesting a model were hydrolytic fragments may diffuse into the bulk phase (Confer and Logan, 1997a; Confer and Logan, 1997b). This is in accordance with Kepkay, 1994) who saw that bacteria attached to an organic particle hydrolyse significantly more organic substrate than they can use for their own metabolism. However, this is contrary to the model suggested by Larsen and Harremoës, 1994) were enzymes are thought to diffuse into the liquid bulk phase, and hydrolytic products diffuse back to be metabolised in the bio aggregates. The location of the enzymatic depolymerisation is especially important for the understanding of hydrolysis of particulate matter in biofilm systems. Larsen, 1992) and later Rohold and Harremoës, 1993) demonstrated an effect of bulk phase washout rates in biofilm reactors. However, these reports are not conclusive to whether washout influenced intermediates, enzymes or both.

Most of the works listed above have been aimed at estimating the enzymatic activity in the samples analysed, often by enzyme assays involving labelled substrates that are different from the natural substrates. For depolymerisation enzymes this difference is very important since substrate properties, especially monomeric composition and molecular size, differ a lot from typical model substrates used during assaying (e.g. nitrophenyl, fluorescein labels, and methylumbelliferyl or methylcoumarinylamid). In addition to the reaction kinetic differences, transport mechanisms of the bio-aggregate involved very much depends on the molecular size of the model substrate. Using a significantly smaller (most model substrates are small compared to polymer substrates of depolymerising enzymes) substrate overestimate removal rates during transport limitations, conditions that are very significant in activated sludge flocs and biofilms. Therefore, generalisation of enzyme activity from data obtained by extraction and assayed using model substrates involve systematic uncertainties and errors that must be taken into consideration, especially during quantitative analysis. Some of these problems may be eliminated by the use of polymeric model substrates labelled with small side groups or small ligands (like Dextran Blue), or

by quantification of the reaction products like the endoglucanase assay based on reducing sugars quantification (Ashwell, 1957; Schellhorn and Forsberg, 1984).

## 2.4 Biofilms

Biofilms, as first introduced by Zobell and Allen (1935) and Zobell and Anderson (1937), may be defined as cells immobilised on a substratum and frequently embedded in an organic matrix of microbial origin (Characklis and Marshall, 1990). Both open culture (mixed population) and pure culture biofilms form heterogeneous dynamic structures (Costerton et al., 1995; Costerton et al., 1997; Costerton et al., 1999; Stoodley et al., 2002) of principally three components; cells, extracellular polymeric substances (EPS) and liquid void spaces (Christensen and Characklis, 1990). Numerous papers have been published on the biology of bacterial biofilms (see Watnick and Kolter (2001) for an interesting review), and the gradient environment biofilm cells are subjected to (e.g. Characklis et al. 1990; Harremoës, 1978). Recent methodological developments have established fundamental biological properties of sessile bacteria (Sauer and Camper, 2001; Sauer et al., 2002), and confirmed the typical substrate gradient environment resulting from transport limitations (de Beer et al., 1994b; Lewandowski et al., 1995; de Beer et al., 1997). These two aspects, the phenotype of bacterial biofilms and the transport limitations, together with the mechanical and structural properties of EPS, are the main features distinguishing sessile bacterial systems from suspended cultures. For further details into the field of general biofilm science, the assembled works of Characklis and Marshall (1990), Bryers (2000) and Wuertz et al. (2003) may be good starting points.

### 2.4.1 Polymer and particle dynamics in biofilms

Successful removal of organic particles and polymers in biofilm systems rely on four separate processes linked in series: Transport of particle/polymer to the biofilm surface, attachment to the biofilm matrix, depolymerisation and subsequent mineralisation (Sprouse and Rittmann, 1990). O'Melia (1987) described how particles are transported and attached to surfaces. Transport and attachment to the surface of biofilms was theoretically

investigated by Bouwer (1987) which proposed first order particle transport to be controlled by diffusion, interception or sedimentation mechanisms, depending on system configurations and molecular size of particle/polymer. Upon close approach to the biofilm surface, short range surface interactions such as hydrodynamic retardation, van der Waals attraction, electrostatic repulsion and overlapping double layers would all affect the attachment of the particles. In addition, net attachment would depend on the detachment forces exerted by hydraulic shear forces. Attachment and transport was lumped into a single process by reducing the process rate of transfer (transport to and attachment onto) to the biofilm by a sticking factor similar to the description of cell attachment proposed by Characklis (1990) and Escher and Characklis (1990). As both the surface charge of the cell walls, and the EPS of biofilms are negatively charged around neutral pH, electrostatic forces are important for the attachment and transport of especially charges particles and polymers (Horan and Eccles, 1986; Morgan et al., 1990). The effect of ionic strength on the forces stabilising activated sludge flocs are of the same type as the ones between particles and biofilm surfaces, except for the geometries involved. Zita and Hermansson (1994) suggested increase of the electric double layer thickness to explain the deflocculation of activated sludge during reduced ionic strength according to the DLVO theory. Keiding and Halkjær Nielsen (1997) emphasized the importance of divalent cations, especially $Ca^{2+}$, for the sorption of organic macromolecules to the activated sludge EPS. Zita and Hermansson (1997) also suggested cell and polymer hydrophobicity as important during adhesion to sludge flocs. Carlson and Silverstein (1998) discussed how molecular size and surface charge of polymers affected the sorption to biofilms, concluding that increased molecular weight reduced surface adhesion to biofilms, as well as negative surface charge. Bouwer (1987), however, found the net transport to surfaces to be inversely correlated to particle size, especially due to increased sedimentation. Even though transport to the biofilm surface seems to be well understood, and that attachment can be modelled using DLVO theory, adsorption of macromolecules and organic particles to biofilms are influenced by biofilm specific properties and multi dependency towards surface and liquid composition, making generalisations difficult. O'Melia (1987) summarised by stating that during favourable attachment situations, existing theories are sufficient for practical modelling, while during unfavourable situations adsorption is underestimated. In addition, surface heterogeneity and matrix transport, factors related to the biology and history of the biofilms (Lewandowski et al., 1995; de Beer et al., 1994a; de

Beer et al., 1994b) further complicates the understanding of mass transfer, making qualitative evaluations just as appropriate as quantitative.

For activated sludge systems, adsorption and/or enmeshment are thought to be fast, and that for modelling purposes the process may be described by equilibrium expressions (Henze, 1979; Dold et al., 1980; Gujer, 1981). Adsorption of organic films prior to biofilm formation is regarded as very fast (Characklis, 1990), and may be represented by a logistic saturation function (Characklis et al., 1990). For biofilms Bouwer (1987) suggests an empirical first order adsorption kinetics in bulk phase particle concentration compensated by the sticking efficiency, $\alpha$. Characklis et al. (1990) regards $\alpha$ to be dependant on surface roughness, EPS composition and liquid ionic strength, and suggests it to be low ($<<0.01$). Sprouse and Rittmann (1990) reported $\alpha \approx 0.04$ for adsorption of milk colloids in a methanogenic fluidised bed biofilm reactor.

As mentioned earlier, introduction of techniques from molecular biology has enabled the biofilm research community to identify phenotypic changes of the biofilm bacteria (Stoodley et al., 2002; Sauer and Camper, 2001). Interestingly, Holligbaugh and Azam (1983) have observed higher proteolytic activity of attached marine bacteria compared to their suspended counterparts. This might result from genetic regulation mechanisms, or simply by loss reduction due to transport restriction s in the biofilm matrix. Either way, sessile systems might have systematic or biological opportunities of enhancing scavenging of particulate and polymeric substances.

Another biological response to polymer and POM substrates is the restructuring of the biofilm architecture to optimise the transport mechanisms to and from the biofilm matrix (de Beer and Stoodley, 1995; Tanyolac and Beyenal, 1997). As polymer transport and degradation rates are thought to be limiting for the degradation and terminal mineralisation (Ubukata, 1992;1997; 1999), quasi steady state depolymerisation products (RBCOD) are thought to be rather low, causing the biofilm to experience substrate limiting conditions. It has been suggested that substrate limiting conditions promote formation of porous biofilms enhancing advective transport and reducing diffusive path lengths into the biofilm matrix (Picioreanu et al., 1998). A mixed population biofilm from a biofilm airlift suspension reactor showed this morphological adaptation when transferred from growing on glucose to soluble starch (Mosquera-Corral et al., 2003).

Degradation of polymers and POM in biofilm systems are governed by the chemical and physical properties of the polymers and enzymes involved in the depolymerisation. Biofilm communities have several levels of adaptation to the nature of limiting substrates,

including regulations at gene levels related to the synthesis of exogenous enzymes, their location and their activity. In addition, biofilm communities have shown adaptation on the morphological and structural level by changing the biofilm matrix to promote optimised transport mechanisms of the limiting substrate. Lag phases are thought to be involved in all these processes, especially on the structural level adaptation. This has consequences for experimental designs as well as for engineering applications.

## 2.5 Mathematical Modelling

Mathematical modelling has become the most important framework of interpreting experimental data and theories in the wastewater scientific society during the last 20 years. Even though microbiologists have not adopted the same strategy to the same extent, quantitative understanding and the use of mathematical formulations have been adopted to describe the fundamental processes such as growth, maintenance, decay, product formation and attachment/detachment. Especially the emergence of technological applications within the terms of biotechnology, has promoted the use of quantitative formulations and communication. In the wastewater engineering community the successful use of mathematical models to describe the activated sludge process, has spurred development of other models for systems like river water quality, anaerobic sludge digesters and biofilm reactors.

### 2.5.1 The activated sludge an mixed population biofilm models

Among the first attempts to propose a comprehensive model for the activated sludge process was the group at university of Cape Town (Dold et al., 1980, Ekama and Maris, 1979). Building one their work, the *IAWPRC task group on mathematical modelling for design and operation of biological wastewater treatment process* was founded, and reported the Activated Sludge Model no. 1 (ASM1) in 1987 (Henze et al., 1987). The model described heterotrophic growth on carbonaceous substrates, nitrification and denitrification. It was extended in 1995 to include chemical and biological phosphorous removal (ASM 2), with further extensions in 1998 (denitrifying phosphorous accumulating organisms, ASM 2d). A restructured model based on storage as the central substrate uptake mechanism was presented in 1998 (ASM 3). These models contain stoichiometric and

kinetic expression for the conversion of substrates and growth of functional biomass without taking transport mechanisms into account.

Harremoës (1978) proposed a steady state model successfully describing substrate gradients in biofilms. A similar model was put forward by Rittmann and McCarty (1980), while Gujer and Wanner (1990) made the necessary theory for a one-dimensional dynamic model for a mixed population biofilm. This model was implemented in a purpose made software (AQUASIM) by Reichert (1994), and extended to include advanced spatial heterogeneity and functions, and transport (interfacial) mechanisms (Wanner and Reichert, 1996; Reichert and Wanner, 1997). Lately, the 1-dimensional models have been solved for three dimensions, opening up new possibilities for modelling structural properties and functions (Piceraneau et al., 1998; Hermanowicz, 1998). The biofilm models do not contain mass balance equations for kinetics and stoichiometry, but reflect the transport mechanisms involved in spatial heterogeneous growth. The practise has been to implement the stoichiometries and kinetics of the activated sludge models into the transformation equations of the mixed population biofilm models, for simulation and data interpretation.

### 2.5.2 Modelling depolymerisation

Degradation of POM and polymeric substances in the wastewater engineering literature has been equivalent to the process called "hydrolysis" without paying attention to whether the depolymerisation mechanisms are hydrolytic or not. That might be due to the fact that most depolymerisation enzymes are hydrolytic, and that the common macromolecules (fats, proteins, polysaccharides and nuclei acids) are depolymerised naturally by hydrolases. Thus, hydrolysis should not, in the wastewater treatment literature, been taken literarily, but rather representing the sum of mechanisms depolymerising POM and organic substrates into readily biodegradable matter.

Morgenroth et al. (2002) recently reviewed processes and modelling of hydrolysis in aerobic wastewater treatment, and the following paragraph is based on their work.

Early models of particulate substrate degradation were based on direct growth (Stenstrøm, 1975) or adsorption followed by direct growth (Ekama and Maris, 1979; Dold et al., 1980). Hydrolysis of slowly biodegradable into easily biodegradable substrates was adopted by the IAWQ group as a one step hydrolysis process (Henze et al., 1987) based on the kinetic

expression proposed by Dold et al. (1980). Frigon et al. (2001) defined two distinct active biomasses, one growing on RBCOD whereas a second degraded SBCOD, for a structured model taking intracellular constituents into account. Several authors have expanded on the lumped substrate model of the IAWQ group to describe the kinetics of slowly, intermediate and rapidly hydrolysable substrates in order to reflect the chemical heterogeneity and molecular weights of particulate substrates. Sollfrank and Gujer (1991); Orhon et al., (1998); Janning, (1998) and Vollertsen and Hvidtved-Jacobsen (1999) defined parallel hydrolysis into easily biodegradable substrates, while Novak et al. (1995), Bjerre (1996), Confer and Logan (1997a; 1997b) and Spérandino and Paul, (2000) applied sequential hydrolysis. Separation into substrate classes based on degradability reflects the complexity of particle and polymer degradation. Table 2-2 shows a summary of empirical model stoichiometries from the wastewater literature. Kinetic expressions are shown in Table 2-3.
Dold et al., 1980) developed a kinetic expression for hydrolysis based on Stenstrom, 1975), that assumed that slowly biodegradable organic matter adsorbs to the surface of the organisms and is degraded by direct growth. This results in surface limited hydrolysis kinetics as described by model no. V and VI in Table 2-3. Based on experimental results with variations in sludge age and sludge concentration, Dold et al., 1980), suggested that hydrolysis kinetics cannot be sufficiently described with simple Monod kinetics (Table 2-3, model IV).

A subject of ongoing debate is whether hydrolysis rates are influenced by redox conditions as can be seen by changes in the activated sludge models. In ASM1 and ASM2 (Table 2-3, model VI) a reduction factor $\eta$ that reduced hydrolysis rates if no oxygen was present. In ASM1 $\eta$ was 0.4 and in ASM2 $\eta$ was 0.1 or 0.6 for anaerobic and anoxic conditions respectively (values for 20°C). In ASM3, no reduction factor was considered any more. This modification was supported by Goel et al., 1998b) who showed that enzyme activity was not significantly affected by redox conditions. Probable reasons for the observed reduction of hydrolysis rates during anoxic and anaerobic conditions by some authors (Henze and Mladenovski, 1991; San Pedro et al. 1994), might be reduction in grazing activity by higher organisms (amoebae and protozoan), and reduced synthesis rate of exogenous enzymes in anaerobic conditions. Simplified models for hydrolysis kinetics have been proposed as zero order, first order, or saturation type kinetics (Table 2-3, model 0-IV). Most of these models have been developed for specific situations (very high or very low substrate to microorganism ratios) and it can be shown that under these cases the surface limited hydrolysis rate expression in model V can be simplified: For $X_{S,i} << X_H$ the

| Processes | $X_{S,1}$ | $X_{S,2}$ | $X_{S,3}$ | $X_{Sads}$ | $S_S$ | $S_{O2}$ | $X_H$ | $X_{H,2}$ |
|---|---|---|---|---|---|---|---|---|
| *Model Nr. 1:* | | | | | | | | |
| *Direct growth on both soluble and particulate organic matter* | | | | | | | | |
| Growth on $X_{S,1}$ | $-1/Y_H$ | | | | | $-(1-Y_H)/Y_H$ | 1 | |
| Growth on $S_S$ | | | | | $-1/Y_H$ | $-(1-Y_H)/Y_H$ | 1 | |
| *Model Nr. 2: Adsorption model* | | | | | | | | |
| Adsorption of hydrolysable COD ($X_{S,1}$) | -1 | | | 1 | | | | |
| Direct growth on adsorbed COD | | | | $-1/Y_H$ | | $-(1-Y_H)/Y_H$ | 1 | |
| Growth on soluble COD | | | | | $-1/Y_H$ | $-(1-Y_H)/Y_H$ | | 1 |
| *Model Nr. 3: One step hydrolysis* | | | | | | | | |
| Hydrolysis of hydrolysable COD ($X_{S,1}$) | -1 | | | | 1 | | | |
| Growth | | | | | $-1/Y_H$ | $-(1-Y_H)/Y_H$ | 1 | |
| *Model Nr. 4: Parallel hydrolysis* | | | | | | | | |
| Hydrolysis of slowly hydrolysable COD ($X_{S,1}$) | -1 | | | | 1 | | | |
| Hydrolysis of intermediate hydrolysable COD ($X_{S,2}$) | | -1 | | | 1 | | | |
| Hydrolysis of rapidly hydrolysable COD ($X_{S,3}$) | | | -1 | | 1 | | | |
| Growth | | | | | $-1/Y_H$ | $-(1-Y_H)/Y_H$ | 1 | |
| *Model Nr. 5: Sequential hydrolysis* | | | | | | | | |
| Hydrolysis of slowly hydrolysable COD ($X_{S,1}$) | -1 | 1 | | | | | | |
| Hydrolysis of intermediate hydrolysable COD ($X_{S,2}$) | | -1 | 1 | | | | | |
| Hydrolysis of rapidly hydrolysable COD ($X_{S,3}$) | | | -1 | | 1 | | | |
| Growth | | | | | $-1/Y_H$ | $-(1-Y_H)/Y_H$ | 1 | |
| *Model Nr. 6: Two biomass model* | | | | | | | | |
| Hydrolysis of particulate COD ($X_{S,1}$) | -1 | | | | 1 | | | |
| Direct growth on hydrolysed COD | | | | | $-1/Y_H$ | $-(1-Y_H)/Y_H$ | 1 | |
| Growth on soluble COD | | | | | $-1/Y_H$ | $-(1-Y_H)/Y_H$ | | 1 |

where:
*Model No. 1*: Direct growth on both soluble and particulate organic matter. Hydrolysis is not considered as a separate process (e.g., Stenstrom, 1975).
*Model No. 2*: Adsorption system (Ekama and Marais, 1979; Dold et al., 1980).
*Model No. 3*: One step hydrolysis (e.g., Henze et al., 1987 (=ASM1); Henze et al., 1995 (=ASM2), Henze et al., 1999 (=ASM2d), Orhon et al., 1999, Gujer et al., 1999 (=ASM3), Sollfrank, 1988; Larsen, 1992; Spanjers and Vanrolleghem, 1995).
*Model No. 4*: Parallel hydrolysis (e.g., Sollfrank and Gujer, 1991; Janning, 1998; Orhon et al., 1998, Vollertsen and Hvitved-Jacobsen, 1999, Vollertsen, 1998).
*Model No. 5*: Sequential hydrolysis (e.g., Bjerre, 1996; Confer and Logan, 1997a; Spérandio and Paul, 2000)
*Model No. 6*: Two biomass system (Frigon et al., 2001)
$X_{S,1}$, $X_{S,2}$, $X_{S,3}$ = slowly biodegradable organic matter (in models with multiple $X_S$ fraction $X_{S,1}$ is slowly and $X_{S,3}$ is rapidly hydrolysable. $X_{S,ads}$ = adsorbed $X_S$, $S_S$, readily biodegradable organic matter, $S_{O2}$ = oxygen, $X_{H,1}$, $X_{H,2}$ = separate heterotrophic bacterial populations.

Table 2-2. Stoichiometries applied in literature models for various hydrolysis regimes (from Morgenroth et al. 2001)

| Nr. | Kinetic expression | References |
|---|---|---|
| 0 | $k_{H,0}$ | Larsen, 1992, Cliff, 1980, Andrews and Tien, 1977, Dennis and Irvine, 1981, Tsuno, 1978 |
| I | $k_{H,I} \cdot X_S$ | Gujer, 1980, Henze and Mladenovski, 1991, Sollfrank and Gujer, 1991, Janning, 1998, Kappeler and Gujer, 1992, San Pedro et al., 1994, Spérandio and Paul, 2000, Spanjers and Vanrolleghem, 1995, Goronszy and Eckenfelder, 1991 |
| II | $k_{H,II} \cdot X_H$ | Goel et al., 1997 |
| III | $k_{H,III} \cdot X_S \cdot X_H$ | Eliosov and Argaman, 1995, Argaman, 1995, Mino et al., 1995 |
| IV | $k_{H,IV} \cdot \frac{X_S}{K_{X,IV} + X_S} X_H$ | Larsen, 1992, Mino et al., 1995, Goel et al., 1998a |
| V | $k_{H,V} \cdot \frac{X_S / X_H}{K_{X,V} + X_S / X_H} X_H$ | Stenstrom, 1975, Mino et al., 1995, Janning, 1998, Gujer et al., 1999 (=ASM3) |
| VI | $k_{H,VI} \cdot \left( \frac{X_S / X_H}{K_{X,VI} + X_S / X_H} \cdot \frac{S_{O2}}{K_{O2} + S_{O2}} X_H + \eta_H \cdot \frac{X_S / X_H}{K_{X,VI} + X_S / X_H} \cdot \frac{K_{O2}}{K_{O2} + S_{O2}} X_H \right)$ | Dold et al., 1980, Henze et al., 1987 (=ASM1), Henze et al., 1995 (=ASM2), Henze et al., 1999 (=ASM2d) |

Table 2-3. Kinetic expressions for the hydrolysis models listed in Table 2-2 (from Morgenroth et al. 2001).

original Model V can be approximated with first order substrate kinetics (model I, with $k_{H,I} = k_{H,IV} / K_X$). For $X_{S,i} >> X_H$ model V can be approximated also with a first order model, in terms of the biomass concentration (model II, with $k_{H,II} = k_{H,IV}$ ). Likewise model IV simplifies to model III and II for $X_{S,i} << X_H$ and $X_{S,i} >> X_H$, respectively.

All models described above are empirical models not taking substrate composition, enzyme concentration, enzyme location nor substrate molecular size or intermediate formation into account. That is not a surprise with respect to the complexity of natural populations and the justified assumption can drastically reduce model complexity. Use of Monte-Carlo simulations is a well applied stochastic approach used for modelling starch liquefaction, lignin hydrolysis and α-amylase activity (McDermott et al., 1990; Nakatani 1996; Carbonell et al., 1998). Most kinetic expression used, both for deterministic and

stochastic models, is based on Michalis-Menten kinetics, or deduced variants taking into account model structure details, such as intermediate competitive substrate inhibition, endo- and exo-enymatic synergism, reversible dynamics and non-reversible binding (inhibition). Wojciechowski et al. (2001) give an updated review of recent models. For polysaccharide depolymerisation modeling, Fujii et al. (1981) used a lumped polymer model to show synergistic effects between simultaneous exo- and endo amylase activity. Suga et al. (1975) very early recognised the importance of intermediate modelling, and suggested a Michaelis-Menten based set of equations for each polymer intermediate. Dean and Rollings (1992) further extended the model of Suga et al. (1975) by including restrictions to bonding by a Dextranase- Dextran system at branching points.
In this work a model for the endo- and exo-depolymerisation of a model substrate (Dextran) will be presented, and simulations compared to time series data of model enzymes and open culture biofilms.

# 3 Hypothesis

This section outlines the fundamental ideas and viewpoints that form the foundation of which hypothesis, experimental and mathematical methods and data interpretation is developed from. A conceptual model of the biofilm system and the dynamics and reactions involved in polymer and particle degradation is suggested. The main hypotheses deduced from the conceptual model are also presented as separate sub-chapters.

## 3.1 Conceptual model

Naturally, conceptual biofilm models have been developed from the current understanding of the structure and functions of biofilms. Several factors such as substrate loading, shear stress, substrate type(s), hydraulic and particulate retention times are known to have an effect on the macroscopic structure and properties of biofilms (van Loosdrecht et al., 1995; van Loosdrecht et al., 2002). The effect is mutual, since substrate and particulate transport are also affected by the same structure and properties. Early models considered the biofilm to be a homogenous slab of equal thickness and distribution (Harremoës, 1978), but recent methodological developments in microscopy and microelectrode technology has revealed the true heterogeneous structures and transport regimes governing most natural (and

established) biofilms (Bakke, 1986; Revsbech and Jørgensen, 1986; Neu and Lawrence, 1997; de Beer et al., 1997; Schramm et al., 1997). Structure is influenced by the physical shear acting on the biofilm surface distributed into the cellular and EPS network and finally on the fimbriae and surface proteins and polysaccharides connecting the surface layer to the substratum (Characklis, and Marshall, 1990). The central role of EPS as the connective tissue and gel forming transport barrier has been known for quite some time (Geesey, 1982; Boyd and Chakrabarty, 1995; Flemming and Wingender, 2001), however, only recently has this profound property been considered in modelling and structure/function analysis (Kommedal et al., 2001); Horn et al., 2001; Kreft and Wimpenny, 2001; Boyd and Chakrabarty, 1995). EPS is likely to have an important effect on biofilm detachment (Boyd and Chakrabarty, 1994; Kommedal et al. 2000a). Chemical properties like composition, charge density, hydrophobicity, ion complexation, molecular weight, degradability etc. are all important factors when considering the dynamics of EPS (Christensen and Characklis, 1990). Environmental factors like pH, ionic strength and divalent cation activity strongly affects the EPS gel properties (Christensen and Characklis, 1990a; Keiding and Nielsen, 1997; Keiding et al., 2001), as well as biological controlled factors like polymer synthesis and degradation rates (Boyd and Chakrabarty , 1994; Boyd and Chakrabarty, 1995). The ability of biofilms to adsorb substrates in oligotrophic environments is another aspect of EPS function (Flemming, 1995), an ability that also provide means of controlling the extracellular activity of active enzymes, optimising a local microniche (Costerton et al., 1995). These, and recent insight into the effects of cell-cell signalling and biofilm genotype behaviour (Davies et al., 1998; Sauer et al., 2002; Stoodley et al., 2002), seems to have profound effects on the structure and function of biofilms, but little is known regarding the quantitative aspects and how these studies can be generalised into open mixed population cultures. The complexity of EPS (composition, synthesis, degradation) has therefore been regarded, together with the companioning process of detachment, as the "untouchables" of biofilm science, especially among the modellers. This is a surprising paradox considering their essential role in biofilm dynamics, but has nevertheless resulted in a very limited quantitative understanding of the dynamics. The conceptual model being outlined here will therefore take these factors into account on a qualitative level. Structurally and conceptually, the model suggested here is strongly influenced by the models put forward by Wanner and Reichert (1996) and Nielsen et al. (1997), which again built on Bryers and Mason (1987), Hseih et al. (1994) and Characklis(1990).

| Model constituents | Symbol | Unit |
|---|---|---|
| *Components* | | |
| Heterotrophic cellular biomass | $X_H$ | $g/m^3$ |
| Dissolved readily biodegradable substrate | $S_S$ | $g/m^3$ |
| Dissolved oxygen | $S_O$ | $g/m^3$ |
| Particulate slowly biodegradable substrate | $X_S$ | $g/m^3$ |
| Dissolved slowly biodegradable polymers | $S_P$ | $g/m^3$ |
| Dissolved Exogenous enzymes | $S_E$ | $g/m^3$ |
| Structural EPS | $X_{EPS}$ | $g/m^3$ |
| Inert particulate organic matter | $X_I$ | $g/m^3$ |
| Biofilm void (liquid) fraction | $\varepsilon_l$ | 1 |
| *Conversion Processes* | | |
| Cellular growth rate | $\mu_c$ | $g/m^3 \cdot h$ |
| Cellular endogenous decay rate | $r_d$ | $g/m^3 \cdot h$ |
| Cellular lysis rate | $r_d$ | $g/m^3 \cdot h$ |
| Substrate maintenance conversion rate | $r_{se}$ | $g/m^3 \cdot h$ |
| Substrate conversion rate | $r_s$ | $g/m^3 \cdot h$ |
| EPS synthesis rate | $\mu_{EPS}$ | $g/m^3 \cdot h$ |
| Oxygen uptake rate, OUR | $r_o$ | $g/m^3 \cdot h$ |
| Depolymerisation rate | $r_h$ | $g/m^3 \cdot h$ |
| Dissolution rate | $r_{diss}$ | $g/m^3 \cdot h$ |
| *Transport Processes* | | |
| Attachment rate | $r_{att}$ | $g/m^2 \cdot h$ |
| Detachment rate | $r_{det}$ | $g/m^2 \cdot h$ |
| Adsorption rate | $r_{ads}$ | $g/m^2 \cdot h$ |
| Desorption rate | $r_{des}$ | $g/m^2 \cdot h$ |
| Diffusion rates | $J$ | $g/m^2 \cdot h$ |
| Advection rates | Q | g/h |
| *Locations (sub compartment subscripts)* | | |
| Bulk phase | B | - |
| Biofilm matrix | $F_M$ | - |
| Biofilm void | $F_V$ | - |
| Biofilm surface | $F_S$ | - |

Table 3-1. Components, transport and conversion processes, and sub compartment (location) subscripts.

The objective of the model is to conceptually describe the location, transport mechanisms and conversion of POM and polymeric substrates, the synthesis, location and activity of depolymerising enzymes, the growth, decay and transport/transfer mechanisms of active cells and illustrate the heterogeneity of the biofilm structure and substrate gradients. Table 3-1 shows model symbols of components, processes, transport mechanisms and location indicators of the conceptual biofilm model. Figure 3-1 is a graphical representation of the model showing the biofilm structure and morphology, components (full text naming), transport and conversion mechanisms. Cellular conversion processes (growth, substrate uptake, endogenous and lytic decay) are thought to be no different than kinetics and stoichiometry for suspended bacteria (Bakke et al., 1984). This might be in contradiction to recent discoveries of the biofilm phenotype (Sauer and Camper, 2001; Sauer et al., 2002), however, limited (if any) knowledge has been published on the kinetic and stoichiometric consequences of changes in gene expression as bacteria form biofilms. Thus, anticipating the same conversion regime as adopted by the ASM group seems to be the only and best alternative (Henze et al., 2000). Molecular diffusion may be described by Fick's laws, and advection by classical mechanics. Adsorption and desorption may be modelled using the expressions suggested by Ekama and Marais (1978), while attachment of bacteria and POM might follow the mechanisms formulated in the model of Escher and Charaklis (1990) and Characklis et al. (1990). Biofilm detachment caused by surface shear force distribution cause erosion from the biofilm surface, while disintegration of internal matrix structures may lead to sloughing (Bakke, 1986), defined as detachment of larger chunks of biofilm. Sloughing, and probably also erosion, also provides EPS of a transport mechanism into the bulk phase. Often EPS and cells are lumped into the expression "biomass". All these mechanisms and processes have been described in detail elsewhere (see Bryers, 2000, for a recent comprehensive description). Thus, details regarding the conceptual model (Figure 3-1) will focus on polymer and POM transport and conversion. The key components of the degradation of polymers and POM are microbial cells, exogenous enzymes and dissolved and particulate polymers/particles. Exogenous depolymerising enzymes synthesised by the active cells in the biofilm are exported to the periplasm, surface or excreted into the liquid phase (void) of the biofilm matrix. Extracellular enzymes may be transported away from the mother cell and diffuse into the bulk liquid. Based on the matrix properties, they may also adhere to the biofilm matrix. Dissolved polymers follow the same transport mechanisms, and may adsorb to the

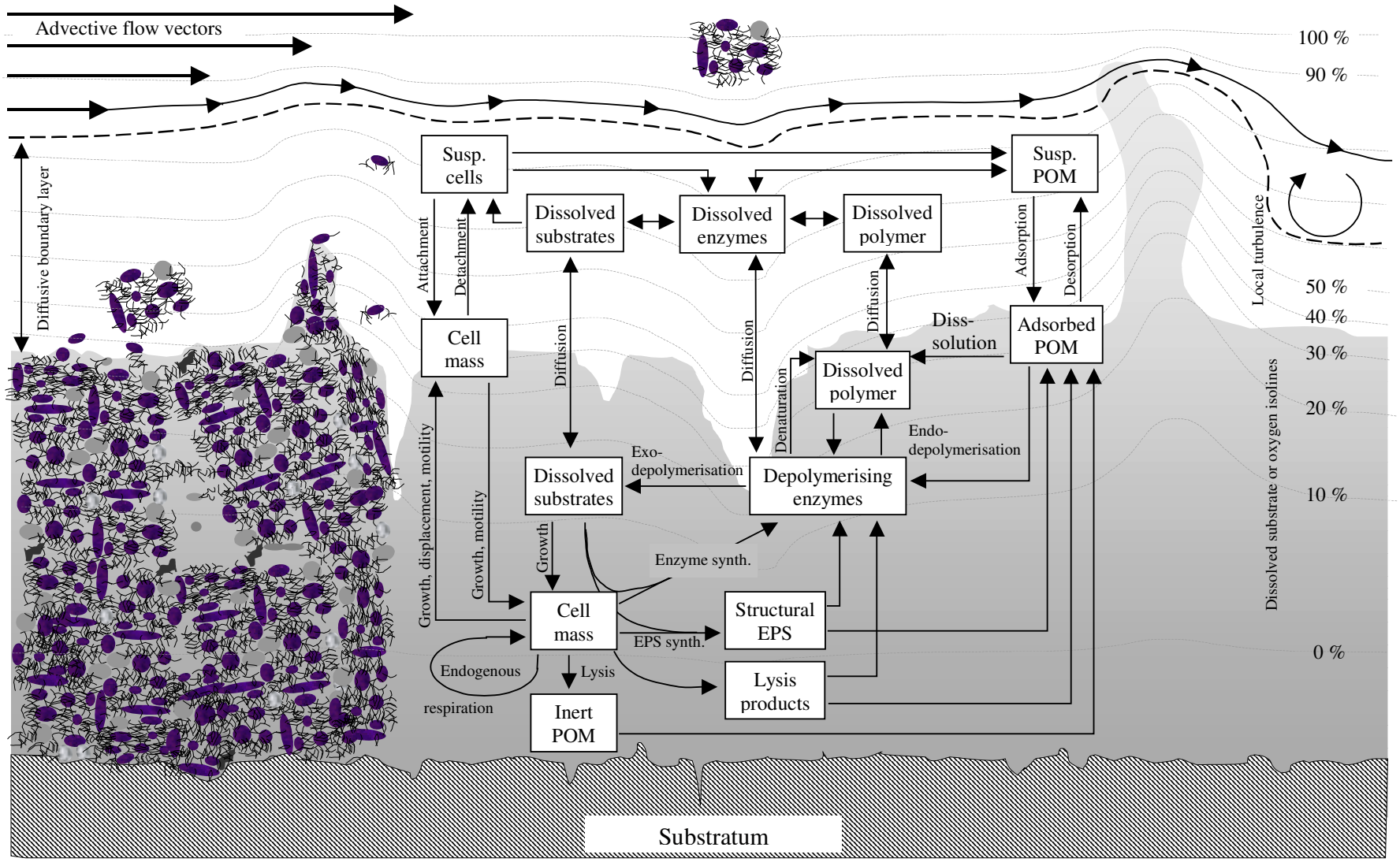


Figure 3-1. Conceptual model of biofilm compartment.

biofilm matrix at the surface or inside the biofilm. The important factors for the mobility of dissolved polymers and extracellular enzymes are the chemical properties of the matrix (cells and EPS), and the network mesh size of the EPS causing an inner filter effect. In addition, channels and pores may facilitate advective transport into the matrix of polymers (de Beer et al., 1994a), and even micro range particles (Drury et al., 1993). Advective transport into the biofilm matrix in channels and pores does not really change the regime fundamentally. Particles and dissolved substrate will still have to adsorb and diffuse into the matrix of the biofilm, however, the surface available for diffusion greatly increase. In addition, diffusion distances inside the matrix are significantly reduced. The 3-D "Swiss cheese" morphology resembles transport and diffusion in porous media, where the media may be regarded as the biofilm. Stoodley et al. (1997) suggests the biofilm matrix to be microporous, with pore diameters between 50 - 200 Å, however, Bryers and Drummond (1998) points out that the biofilm matrix is heterogeneous in terms of porosity, and that macropores and channels are common for heterogeneous biofilms suggesting the matrix pore diameter to vary from micro- to macropores (200-1000 Å) within a considerable range of pore diameters. Diffusive transport limitation due to the structural EPS matrix stresses the importance of the substrate molecular weight. Not only does this property greatly affect the diffusivity of the molecule, but the enmeshment into the polymer network effectively provides the EPS matrix a diffusive cut-off limit (Tanaka et al., 1984; Jimenez et al., 1988). POM may adsorb to the biofilm matrix surface, but rely on depolymerisation in order to enter the matrix. As the size of these substrates are thought to be 100 fold larger than typical spherical depolymerisation enzymes (typical exogenous enzyme size is 20-200 kDa, BRENDA database[2]), extracellular enzymes, or surface enzymes of bacteria colonising the particles, degrade POM by adsorbing to the particulate substrate and depolymerise particle polymers. This surface limited degradation is fundamentally different from the depolymerisation of dissolved polymers (small). These are of similar sizes as the enzymes, and both may diffuse in the matrix or adsorb at specific sites. The reaction mechanism may therefore be viewed as similar to traditional enzyme-substrate degradation regimes, and modelled similar to the established Michaelis-Menten kinetics and stoichiometry. A transition range is most likely to exist as the dissolved molecules become large enough to bind to several depolymerising enzymes. It is therefore probable that depolymerisation kinetically should be described by different expressions as the reaction mechanisms change according to molecular weight. As diffusive transport mechanism also

[2] BRENDA: http://www.brenda.uni-koeln.de/

depend on solute molecular weight, observed degradation in biofilm systems are most probably significantly affected by the molecular weight of macromolecular substrates, both kinetically and physically.

As cells and exogenous enzymes diffuse and detach into the bulk liquid, they are still active and show the same activity as for the sessile organisms. Bulk phase versus biofilm depolymerisation of SBCOD has been a matter of controversy the last decade (Larsen, 1992; Roholt and Harremoës, 1993; Confer and Logan 1998), and this concept allows for both.

## 3.2 Location of depolymerisation

Location of depolymerising enzymes has profound implications on interpretation of observed degradation kinetics and process design. From an ecological point of view, exogenous enzymes of biofilm system origin would provide the individuals and their community best substrate outcome if the enzymes were retained in the biofilm matrix. However, in case of transport limitations, enzymatic activity in the bulk phase could be just as possible, and conditionally advantageous, with products diffusing back to the biofilm matrix. The key factors here would be the exogenous enzyme synthesis and transport rate into the bulk, and the bulk phase washout rate.

Numerous workers have reported on the location of exogenous activity (see section 2.2, 2.3 and 2.4). Conceptually, two mechanisms have been proposed for biofilm reactor systems. Larsen (1992), Larsen and Harremoës (1994) and Roholdt and Harremoës (1993) all advocated enzymes to diffuse from their cellular origin within the biofilm matrix, into the bulk phase whereupon polymers and POM are depolymerised into readily biodegradable products that enter the biofilm by diffusion. Their motivation was based on the observed correlation between bulk phase washout rate, and the observed removal rate of slowly biodegradable substrates (Roholdt and Harremoës, 1993). Contrary to this model, Confer and Logan (1998) argued that the enzyme activity is retained in the biofilm matrix, and that depolymerisation products (intermediates) may diffuse back into the bulk phase. Even though some results indicated limited exogenous activity in the bulk phase, Goel et al. (1999) and Mosquera-Corral et al. (2003) supported the model outlined by Confer and Logan (1998). Fundamentally, both models predict loss of observed activity as the washout rate increase; enzyme and intermediate losses, respectively. Thus, direct analysis of enzymatic activity and chemical analysis of bulk phase intermediates are necessary in order to determine the location

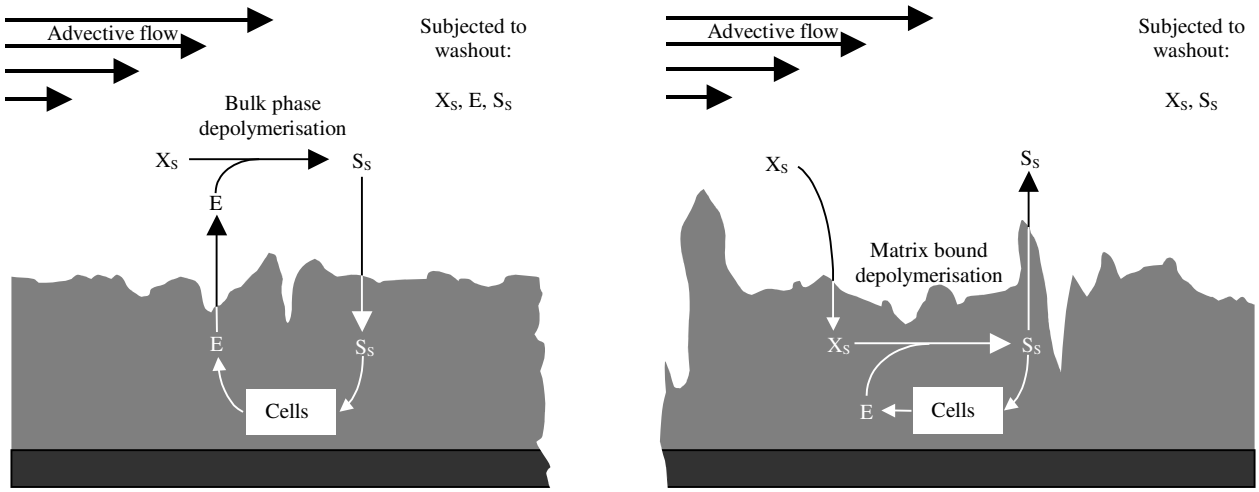


Figure 3-2. Illustration of the two conceptual location models as suggested by Larsen and Harremoës (1994) and Roholdt and Harremoës (1993) (left), and the model of Confer and Logan (1998) assuming cell/matrix bound exogenous enzyme activity (right).

of depolymerisation. Figure 3-2 show how these models differ when it comes to location of depolymerisation, and the implications for the transport mechanisms involved.

In this study the model presented by Confer and Logan (1998) is assumed representative of the fundamental mechanisms involved during polymer and POM degradation. The hypothesis evaluated is that the location of enzymatic activity is found in the biofilm matrix. Significant bulk phase activity would support the alternative hypothesis represented by the model by Harremoës and Larsen (1994).

## 3.3 Effect of polymer size on depolymerisation kinetics

As discussed in section 2.3.2, the size (or rather the molecular weight, $M_W$) of substrates subject to depolymerisation has not been taken into account in kinetic nor stoichiometric expressions. Even though some authors have implemented di- or multi- slowly biodegradable substrate classes (see section 2.5.2 and Table 2-2) as part of their modelling efforts, the true effect of polymer $M_W$ and POM size (typical diameter or filter characteristics) have not been studied into detail, neither in the wastewater engineering nor the biochemical and biotechnological literature.

In addition to the kinetic effects, molecular size will have consequences on the transport dynamics in biofilm systems (section 2.3.2 and 2.4.1). From a modelling point of view, molecular size will therefore have an effect on the true kinetic coefficients related to the

reaction mechanism, and the observed removal coefficient which is a combination of reaction mechanism and transport rates. Due to the intrinsic transport dependency of observed kinetic coefficients in biofilms (Harremoës, 1978), distinguishing transport from true kinetic correlations is difficult, however, the Thiele modulus may be used (Henze et al., 2002). The hypothesis tested here is whether or not the molecular size shows a systematic effect on observed removal rate coefficients.

## 3.4 Intermediate formation and transport

Both endo- and exo-enzymatic activity will result in the formation of products of molecular weight lower than the initial polymer or particle. Intermediate formation during degradation of initial size polymers and POM will affect the transport dynamics and the degradation kinetics. Molecular diffusion relates to the inverse of molecular weight according to the Stoke Einstein relation (Cussler, 1984). In biofilms, intermediates of higher diffusive mobility will reach further into the depths of the matrix, or the other way, into the bulk phase. On the cellular level, intermediates formed may enter cellular compartments not accessible for their larger predecessors and combine with new enzymes. The relative contribution to the overall depolymerisation will also depend on the molecular weight distribution of the intermediates. Exo-enzymatic activity depends on the concentration of molecular ends, while endo-enzyme substrate-enzyme complex formation is often dependent on a minimal size of the substrate (see BRENDA[3] for numerous examples among the exogenous enzymes; Appendix). Therefore, intermediate formation and time dependant substrate molecular weight distribution is of great importance when interpreting enzymatic activity, modelling degradation of SBCOD and interpretation of observed removal rates. Haldane and Logan (1994) and Confer and Logan (1997a; 1997b) all reported accumulation of bulk phase low molecular weight polymer intermediates in pure and mixed culture biofilms. Loss of substrate by hydraulic washout of the bulk phase may be an alternative explanation to the observed loss of removal rate reported by Larsen and Harremoës (1994) and Roholdt and Harremoës (1993). Related to the location hypothesis outlined above, this work will try to identify accumulation of bulk phase intermediates, their molecular weight and concentrations. In addition, intermediate formation will be used to evaluate model formulations (see next section). Under the regime suggested by Confer and Logan (1998) and in accordance with the observations of the same

[3] http://www.brenda.uni-koeln.de/

authors (Confer and Logan, 1997a; 1997b) and Haldane and Logan (1994), bulk phase accumulation of intermediates are formed and are susceptible to washout. The alternative hypothesis is that intermediates do not accumulate in the bulk.

## 3.5 General mathematical model for polymer depolymerisation

Mathematical models for degradation of SBCOD in wastewater systems are based lumped variables, often limited to two or three substrate classes (section 2.5). However, systematically, depolymerisation bears similarities to other processes, especially fragmentation theory (Ziff and McGrady, 1986). Also chemists, and to a certain extent biochemists, have proposed different kinetic models to the dynamics of depolymerisation. Some of them are based on statistical structures (Montroll and Simha, 1940), while others are combination of classical enzyme kinetics (Michaelis-Menten) and statistical interpretations (Wojciechowski et al., 2001). Based on a mechanistic regime as described earlier (section 2.5), a model for the kinetic and stoichiometric effects of molecular weight on depolymerisation rate is suggested. The model will be compared to the observed intermediate formations, and compared to the models found in the literature.

## 3.6 Degradation rate of wastewater particles

Degradation of wastewater particles extracted from municipal wastewater is also studied. As the studies outlined above are conducted using defined model substrates (see Materials and Methods section), comparison of the observed degradation rates using realistic particle composition and sizes is valuable for the projection of results. Quantitative evaluation of the degradation rates by comparing observed kinetics is used to evaluate whether degradation of wastewater particles may be described by the same model as for the observed kinetics of model substrates (comparing results to the results of the experiments used to test the hypothesis presented in section 3.3).

# 4 Materials and methods

This section describes in detail the experimental set up used to test the hypothesis presented in chapter 2, the composition and extraction of culture media, substrates and inocula, the operation and control of the experimental set up, sampling and analytical techniques. Also included is a section on data handling and analysis, and finally a section on error analysis.
Two experimental set ups were used. An annular Rototorque reactor system similar to the one described by Charaklis (1990b) was used during model substrate studies, while a tubular biofilm reactor (Bakke, 1986; Characklis, 1990b) was used during degradation studies of extracted POM from wastewater. In addition, culture tube batch tests were performed on biofilm samples from the annular reactor.

## 4.1 Rototorque biofilm reactor

The laboratory rotating annular biofilm reactor consists of a rotating inner cylinder concentrically housed inside an outer cylinder. Removable slides inside the outer, or on the outer surface of the inner cylinder, provide easy sampling of the biofilm without disrupting the biofilm structure. The reactor bulk phase is mixed by eccentrically drilled channels through the inner cylinder (close to the centre of the bottom towards the edges of the upper part of the rotor) to set up a circulating flow regime perpendicular to the direction of rotation (Characklis, 1990a). Constant fluid shear stress at the cylinder surfaces is directly related to the controlled speed of rotation of the rotor. By keeping the reactor hydraulic retention times low (10-20 min) sessile biomass are selected to the surfaces of the system representing true biofilm reactor conditions.

### 4.1.1 Experimental set up

The annular Rototorque reactor system is presented in Figure 4-1. Two parallel systems based on a model LJ 1120 Rototorque biofilm reactor from Biosurface Technologies (Bozeman MT, USA) were equipped with external recirculation loops (Watson-Marlow 313 U pump at approx. 500 ml/min) providing enhanced mixing (Trulear, 1983; Turakhia 1986), online pH and oxygen control, and a counter current bubble column for re-oxygenation of the reactor

| Experiment | Period | Reactors | Objectives |
|---|---|---|---|
| 1 | 01.03-10.03 | 1,2 | Assessing the influence of logging rate (# $O_2$ loggings mer $O_2$ readings) and OUR estimation rate (# of $O_2$ readings per OUR estimation) on the accuracy and sensitivity of the system. |
| 2 | 01.04-04.04 | 1,2 | Reactor characteristics using conductivity measurements and salt (NaCl) water as tracer. Conducted on empth (clean) reactor. |
| 3 | 20.04-23.04 | 1,2 | $K_L$a estimations on clean systems for OUR compensation during experiments, and for modelling. |
| 4 | 01.05-30.05 | 1,2 | Test injections. |
| 5 | 06.06-30.06 | 1,2 | Initial experiments for evaluation of size effects ($M_W$)of Dextran on OUR and the effects of variable initial concentrations (F/M). |
| 6 | 10.07-16.07 | 1 | Culture tube batch test experiments for the determination of intermediate formations |
| 7 | 24.07-28.07 | 1,2 | Evaluation of size effects and varoius initial concentrations on OUR and bulk phase TOC. Culture tube tests performed on selected $M_W$ standards |
| 8 | 07.08-08.08 | 1,2 | Washout experiment for the preparation of biofilm for location determination by coupon and bulk phase sampling followed by biofilm fractionation and enzyme assays |
| 9 | 02.09-05.09 | 1 | Evaluation of initial polymer concentration of 160 kDa dextran on OUR and bulk phase TOC |
| 10 | 06.09-09.09 | 1 | Evaluation of 100 mg/l dextran polymers of variable initial $M_W$ on OUR and TOC |
| 11 | 10.09-11.09 | 1 | Evaluation of eukaryotic versus prokaryotic activity on degradation of dextran using eukaryotic inhibitors and OUR analysis |

Table 4-1. Overview of experiments conducted using the Rototorque biofilm reactors and model substrate Dextran. The system was built during Oct. 00-Feb. 01 and periods refer to the spring and summer of 2001.

bulk water. The reactor consists of an inner slotted polycarbonate rotor connected to top mounted DC motor, and a glass outer cylinder. Twenty slides are flush mounted on the rotating inner cylinder. These slides are removed by stopping the rotation and pulling the slides out of their bevelled slots through an access port on the top of the reactor. An outer glass cylinder provides an outer jacketing for temperature control by circulating coolant/heated liquids. Total reactor system volume was 1160 ml, and the total wetted surface area was 2890 $cm^2$, giving a specific biofilm area of 250 $m^2/m^3$ (see Table 4-2 for details regarding the physical dimensions and operational settings). The bubble column was attached to a debubbler through a narrow tube connection to minimize diffusive backward re-oxygenation. Hydrodynamic bulk phase conditions were kept constant by fixed rotor speed. Liquid phase dissolved oxygen concentration (DO) was monitored using a WTW Oxi 340A meter attached to an Ox 325 polarographic (Clark Type) probe placed in a flow through mixing cell with magnetic stirring. An additional flow cell was used for online pH measurements using a by an Advantech PCL 818L (Advantech Co. Ltd, Taiwan) data acquisition card.

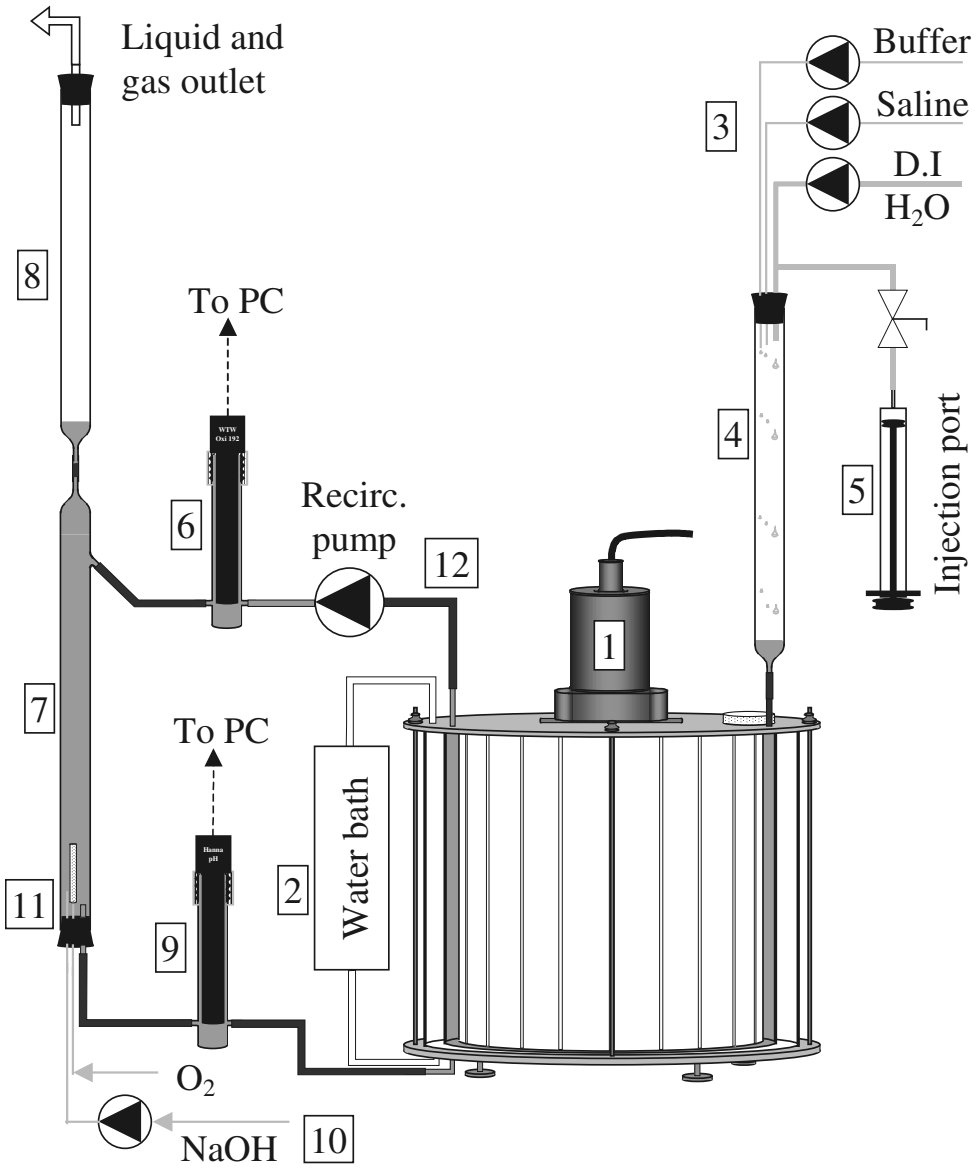


Figure 4-1. Experimental set up indicating flow directions and reactor connections to external units. 1) Rototorque reactor with outer jacketing and top drive motor, 2) External water bath with recirculation pump, 3) Inlet pumps, 4) Inlet back-growth preventer, 5) Standard injection syringe, 6) Oxygen probe in flow through cell, 7) Counter current oxygenation column, 8) Oxygenation column debubbler, 9) pH probe in flow through cell, 10) pH control pump, 11) Diffuser for pure oxygen addition.

Hanna HI 1910B probe attached to a Metrohm 692/691 meter. Both signals were logged using custom made software (LabVIEW 6.0e, National Instruments, Austin TX, US) on desktop PC Oxygen and pH control was provided by automatic operation of a solenoid valve (Kuhnke nw.1) of pure oxygen gas, and pump control (Ismatech Mini-S 860) connected to a 2 M NaOH reservoir. Computer controlled operation of saline/substrate and dilution water pumps (Ismatech Reglo Analog MS4/6-100 and Ole Dich Digital, respectively) provided controlled

| Parameter | Unit | $R_1$ | $R_2$ |
|---|---|---|---|
| Volume | ml | 1175 | 1160 |
| Total wetted surface area | $cm^2$ | 2890 | 2890 |
| Recirc. rate (40% max.) | ml/min | 570 | 570 |
| Dia. air column | mm | 22 | 22 |
| Length air column | mm | 265 | 265 |
| Water level debubbler (from lower edge debubbler) | mm | 50 | 50 |
| Volume Ox. sensor flow cell | ml | 10 | 10 |
| Volume pH sensor flow cell | ml | 7 | 7 |
| Wetted area Ox flow cell | $cm^2$ | 15 | 15 |
| Wetted area pH flow cell | $cm^2$ | 19 | 19 |
| Tube length column-debubbler (Tygon 3803 5/8 mm) | mm | 55 | 75 |
| Recirc. pump tubing (Marprene 7/10) | mm | 100 | 100 |
| Tubing (Tygon 3803 5/8 mm) | mm | 56 | 56 |

Table 4-2. Physical data for both Rototorque reactor systems. All numbers are based on physical measurements (volumes based on weight, flow on volumes, lengths by ruler).

loading through a drop chamber for back growth prevention. Temperature control was established using an external water bath (Hetofrig, Birkerøed DK) with local temperature control, recirculating distilled water (at approx. 500 ml/min) through the outer cylinder of the jacketed LJ 1100 reactor. The reactor system was kept at a slight overpressure to prevent air or temperature control water from leaking into the bulk phase. The rotor housed 18 removable plastic coupons for biofilm sampling for analysis (biomass and thickness) and sub-batch experiments. A 5 ml plastic syringe was used to introduce substrate to the reactor bulk phase through the debubbler.

System mixing and oxygenation properties were evaluated in order to test the assumptions underlying the experiment: Complete system bulk phase mixing, and insignificant oxygen loss by diffusion through system boundaries. Complete mixed conditions were tested on empty (cleaned) reactors by dilution (distilled water) of a strong salt solution (NaCl) and continuously measuring the bulk liquid conductivity (WTW Cond 340i meter with a Tetra on 325 conductivity cell) placed in the oxygen probe flow cell. The conductivity meter was logged using the $O_2$ meter analogue input. Oxygen uptake rate and loss rate were determined by oxygenating pre-disinfected (40 % Ethanol for 2 hours) reactors filled with distilled water, and measure bulk phase dissolve oxygen under and after oxygenation.

### 4.1.2 Model substrate: Dextran

Dextran is a water soluble α1-6 Glucan found in sugar cane production facilities, and as part of the EPS in oral cavity biofilms (Smidsrøed and Moe, 1995). It consists of linear glucose chains with 3-4 % α1-2, α1-3 and α1-4 branching points (Lehninger et al. 2000). Dextran serves as soluble storage compound for several yeast and bacterial species. Industrial applications include synthesis of gel beads for column chromatography, gel structure during immobilisation in biotechnology and plasma extenders in medicine. Dextran is commercially available as molecular weight standards, and serves as an excellent model substrate for degradation studies. In this study, Dextran from the lactic acid bacteria *Leuconostoc mesenteroides* strain B-512F was obtained from Sigma-Aldrich Chemicals (http://www.sigmaaldrich.com/). Dextran from this specie show variable structures according to the strain and growth conditions (Smidsrøed and Moe, 1995), but have a relatively linear secondary structure (>95% α1-6) with comb-like α1-3 short chain branches (1-2 monomers). Assuming 95% α1-6 glucosidic linkages, gives an average molecular formula of $(C_6H_{9.9}O_{4.95})_{n-1}C_6H_{12}O_6$ with an estimated molecular weight of:

$$M_W = 180.16 + 161.24 \cdot (n-1) \qquad (4\text{-}1)$$

where *n* is the number of monomers. Dextran of $M_W$ >10 kDa behaves as typically branched flexible polymers, while standards of 2-10 kDa exhibit the properties of a random

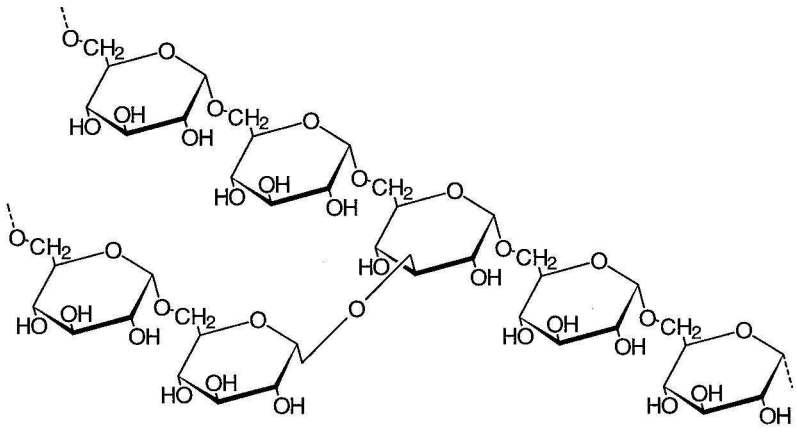

Figure 4-2. α1-6 linked glucose monomers making up the backbone of Dextran, also showing an α1-3 bifurcation (From Smidsrøed and Moe, 1995).

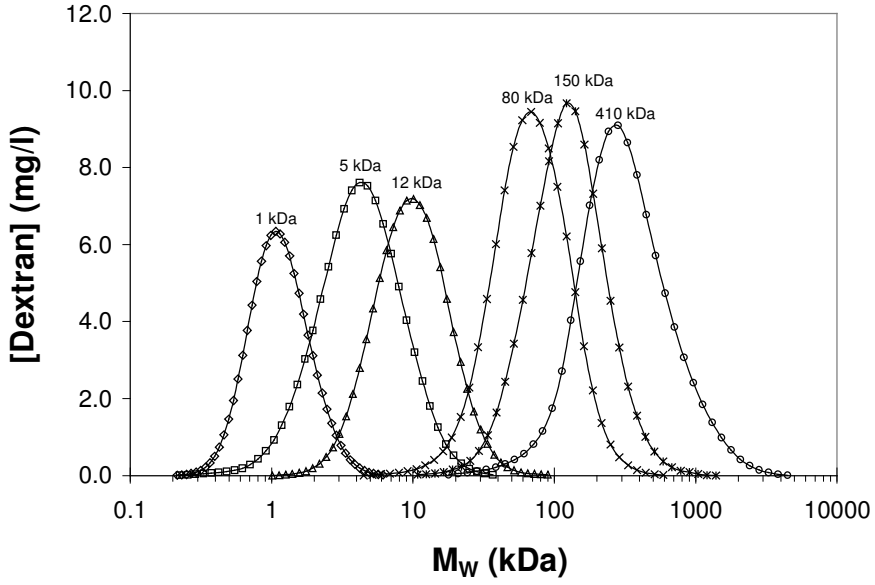


Figure 4-3. Log-Normal distributions of calibration standards used for HPLC calibration. The total standard concentration is 100 mg Dex/l, and is based on the analysis provided by the producer (Sigma Chemicals[4]).

chain/expandable coil, and below 2 kDa as stiff chain or rod like molecules (Product information Sigma-Aldrich). These properties are comparable to polymers found in wastewater (proteins and flexible polysaccharides), and Dextran should therefore be a good representative for the behaviour of such molecules in biofilm systems.

Commercial Dextran is synthesised from native Dextran of molecular weight of 9-500 MDa, and lower molecular weight standards are produced by limited acid hydrolysis and fractionation by size exclusion chromatography (SEC) and ethanol fractionation (Sigma product information[4]). Standards are analysed using HPLC-SEC and laser diffraction, and show a typically normal distribution to the logarithm of the average molecular weight (Kuhn distributed, Smidsrøed and Moe, 1995). Figure 4-3 show the distributions of HPLC analytical standards used for the calibration of the HPLC analysis reported later (section 4.1.5). These standards have a more narrow range than the degradation standards used during the batch degradation experiments, and therefore give a conservative indication of the polymer distributions. The broad distributions are important when analysing degradation data as even medium and high molecular weight standards have significant concentrations of low molecular weight intermediates.

[4] http://www.sigmaaldrich.com/cgi-bin/hsrun/Distributed/HahtShop/HAHTpage/HS_ProdDetail

### 4.1.3 Substrate, nutrients and buffer media

Separate minimal salt solution, buffer and dilution water flasks (10, 10, 5, 200 l respectively) were prepared according to Table 4-3. All reagents were analytical grade, and diluted in double distilled deionised water (DI water). All flasks were covered with alum foil in order to prevent algae growth, and Tedlar bags (SKC 232-15) containing $N_2$ gas provided gas relief as liquid was withdrawn from the flasks. Substrate standards (Table 4-3) were prepared by dissolving the appropriate carbon source in buffer, and stored at 2°C. During continuous operation (see section 4.1.4) reactor hydraulic retention times were controlled by simultaneously varying the flow rate of the dilution and saline/buffer pump maintaining the inlet ionic strength constant at 3.5-4 mM. Reactor inlet carbon concentration (diluted) was kept at 200 mg Dex/l (88.9 mg C/l), and sufficient minimal salt solution and phosphate buffer were added to secure carbon limited growth.

| Component | $M_W$ (g/mole) | Stock solution (mmole/l) | Continuous inlet (µmole/l) | Batch initial (µmole/l) |
|---|---|---|---|---|
| *Saline* | | | | |
| $(NH_4)_2SO_4$ | 114.10 | 1.75 | 54.8 | 54.8 |
| $NH_4Cl$ | 53.49 | 28.0 | 876 | 876 |
| NaCl | 58.44 | 17.1 | 535 | 535 |
| $MgCl_2 \cdot 6H_2O$ | 203.30 | 6.04 | 189 | 189 |
| $MnCl_2 \cdot 2H_2O$ | 161.87 | 0.121 | 3.77 | 3.77 |
| $CuSO_4 \cdot 5H_20$ | 249.68 | 0.067 | 2.09 | 2.09 |
| $CoCl_2 \cdot 6H_2O$ | 237.93 | 0.060 | 1.89 | 1.89 |
| $(NH_4)_6Mo_7O_{24} \cdot 4H_2O$ | 1235.86 | 0.0085 | 0.265 | 0.265 |
| $Na_2B_4O_7 \cdot 10H_2O$ | 381.37 | 0.015 | 0.471 | 0.471 |
| $ZnCl_2$ | 136.29 | 0.110 | 3.44 | 3.44 |
| $FeCl_3$ | 162.21 | 0.123 | 3.85 | 3.85 |
| $CaCl_2 \cdot 2H_2O$ | 147.02 | 1.36 | 42.5 | 42.5 |
| Allyl-thio Urea (ATU) | 116.19 | 5.87 | 183 | 183 |
| *Buffer* | | | | |
| $K_2HPO_4$ | 174.18 | 1.37 | 0.043 | 48.6 |
| $KH_2PO_4$ | 136.09 | 9.48 | 0.296 | 337 |
| *Substrates* | | | | |
| Dextran (as C) | - | 236.8 | 7400 | 3653 |
| Glucose (as C) | 180.15 | 213.3 | 6666 | 3288 |
| Yeast Extract (mg C/l) | - | 170 | 3.15 | 0 |

Table 4-3. Minimal salt solution, buffer and substrate stock solution concentrations, diluted inlet concentrations during continuous operation and during experiments (Batch operation).

| | CSTR inlet concentrations | Component/ C ratio | Batch initial concentrations | Component/ C ratio |
|---|---|---|---|---|
| | (mmole/l) | (%) | (mmole/l) | (%) |
| Total C | 7.4 | - | 7.3 | - |
| Total N | 0.99 | 13.3 | 0.99 | 13.5 |
| Total P | 0.34 | 4.6 | 0.43 | 5.9 |
| Total K | 0.38 | 5.2 | 0.38 | 5.2 |
| Total Ca | 0.043 | 0.57 | 0.043 | 0.58 |
| Total Mg | 0.19 | 2.5 | 0.19 | 2.6 |
| Total Na | 0.53 | 7.2 | 0.53 | 7.3 |
| Total Fe | 0.0039 | 0.052 | 0.0039 | 0.05 |
| Total S | 0.057 | 0.77 | 0.06 | 0.78 |

Table 4-4. Molar ratio's during continuous and batch operations of the Rototorque systems. The batch example represents injection of 10 ml 200 mg/l Dextran.

Batch experiments were conducted by injecting Dextran substrate standards with weight averaged molecular weights ($\overline{M_W}$) of: 0.18 (Glucose), 6.0, 10.5, 38.1, 41.3, 160, 473, 513 and 35000 kDa, of 30, 80, 200 and 500 mg/l each. Under continuous and batch operations, ionic strength and relative composition was carefully controlled such that growth limiting conditions were controlled by carbon availability. Table 4-4 shows the molar ratios during batch and continuous operation. When injecting 10 ml 500 mg/l Dextran (experiment 5 and 9, Table 4-1) additional saline was injected to secure carbon limited conditions. During batch experiments the initial ionic strength was estimated to be 3.6 - 3.9 mM.

### 4.1.4 Operation and control

Basic reactor characteristics were estimated ($V_{tot}$ and $K_La$) and mixing conditions tested using clean empty bed reactors (see Table 4-1). Biocarbone$^{TM}$ biofilm carrier material from the anoxic reactor of Hundested WWTP Sjælland, Denmark, was harvested and placed in a packed bed laboratory reactor as described by Janning (1998). A steady state biofilm was established using high $M_W$ Dextran (35 MDa) as substrate. After two months of continuous anoxic operation to allow a permanent polymer degrading biofilm to be established (Mosquera-Corral et al., 2003), 5 litres of effluent was collected, and filtered through GF/A filter paper (Whatman, Springfield Mill in Maidstone, Kent, UK) to remove eukaryotic organisms >1.6 µm. The retentate was dissolved in 10 ml buffer/saline, and used to inoculate

the Rototorque reactors by adding 4 ml of enhanced culture inocula to bulk phase concentrations of 500 mg/l Dextran (160 kDa) and 100 mg/l Difco yeast extract (YE). Following 30 h of aerobic batch operation, continuous loading of 200 mg/l Dextran 160 KDa and 7 mg/l YE was initiated, and retention time was stepwise reduced from 1 h to 20 min. An approximate steady state biofilm was observed after three weeks by microscopic apparent thickness estimation (Bakke and Olsson, 1986) on removable coupons from the rotor. During start up, bulk phase pH and DO were controlled at 6.2 and 10-20 mg/l, respectively.

Oxygen concentrations where logged automatically by the software every 100 mS. Electronic noise in the logging loop was dampened by averaging the measurements every 5 seconds, and this value (average of ~50 measurements) was stored and used for respiration rate estimation. Based on linear approximation of the last stored oxygen measurements, the oxygen utilisation rate (OUR) was estimated. The number of measurements used for each approximation was determined automatically based on the previous respiration rate estimation in order to minimize standard deviation, and at the same time keep the frequency of estimation high enough to detect short term changes. Thus, at background respiration rates (i.e. ~ 5 mg $O_2$/l·h) ~50 measurements were used, while at high rates (~ 25 mg $O_2$/l·h) 15 measurements were used for estimating OUR. Super saturated bulk phase oxygen concentration was imposed (by on-off aeration control) in the range [10, 24] mg $O_2$/l for experiment 5, [22-32] experiment 7 and [22, 30] mg $O_2$/l during experiment 11, in order to prevent oxygen depletion in the deeper parts of the biofilm.

After establishing a relatively constant biofilm thickness at approx. 300 µm, the reactor was flushed with PBS/DI water for 6 retention times, and background respiration was established during batch operation. At stable background respiration, 5 or 10 ml Dextran standard was injected, bringing the total bulk phase concentration to: 15, 30, 40, 80, 100, 200, 250 or 500 mg Dex/l. No yeast extracts or any other carbon source were added during batch experiments. Six separate experiments (or campaigns) were conducted (5-10 in Table 4-1). Respiration rates were estimated continuously, and bulk phase samples were collected for chemical analysis. Batch operation continued until stable background respiration rates were re-established. During batch experiments, dissolved oxygen and pH was controlled between 22 and 30 mg/l, and 5.75 and 6.0, respectively. Temperature was controlled (P-control) at 25°C. The procedure was repeated for the defined series of Dextran standards. Daily washout routines were established by increasing the rotor speed and recirculation rate to maximum (288 rpm and 1200 ml/min, respectively) under maximum hydraulic loading rates ($T_H$ at 8

min) without changing the ionic strength of the inlet. $O_2$ and pH sensors were cleaned (for biofilm and precipitations on the sensor membranes) and recalibrated before, and checked after, each experiment. Insignificant drift was observed for both reactors over a 7 days period. Following each experiment, evaluation of the operational procedure and settings were conducted, and minor adjustments introduced. These will be specified in the appropriate section of the results chapter. Following the last experiment (10), eukaryotic inhibition by 15 mg Nystatin and Cyclohexamid during degradation of 100 mg/l Dextran (160 kDa) was performed to evaluate eukaryotic contribution to the observed OUR.

### 4.1.5 Sampling and analytical techniques

Liquid bulk samples (approx. 3 ml) were withdrawn through the debubbler by a syringe. Samples were immediately filtered through a 0.45 µm nylon filter (Millipore) into acid washed glass vials (scintillation vials (10 ml) capped with alum foil seal caps). Each sample was conserved by adding 4 M $H_2SO_4$ (pH in sample <1.5) and stored at 2°C. An additional 1 ml was filtered directly into autoclaved Eppendorf tubes, and immediately heated in a water bath (80°C) for 2 min. to assure complete denaturation of depolymerising enzymes (Lee and Fox, 1985). According to Sigma Chemicals[4] Dextran standards are autoclavable, and precursor experiments showed that the size distribution of the polymers did not change by heat mediated hydrolysis (data not shown). Eppendorf samples were capped and stored for not more than 24 hours before HPLC analysis.

Samples for TOC analysis were transferred to acid washed and carbon free (heated to 250°C overnight) autosampler vials, and analysed on an IO Analytical Model 700 TOC analyser within three weeks. Samples for HPLC analysis were filtered through a sterile 0.22 µm PTFE membrane filter prior to analysis in order to remove gas bubbles. Dextran molecular weight distributions were analysed on an Agilent 1100 series HPLC system (Agilent Technologies, http://www.agilent.com/) equipped with an Agilent refractive index detector (RID). Separation according to molecular weight was achieved by a PL Aquagel-OH 30 column (Polymer Labs, MA, US) serial connected to a Zorbax GF-250 column from Agilent and a Zorbax pre-column. A custom made analytical software was designed and implemented in LabView 6.0e (National Instruments, Austin TX, US). Details regarding the analytical settings, mobile phases and buffers are listed in Table 4-5. In order to increase sensitivity, a

| | | |
|---|---|---|
| RID | Model | Agilent 1100 Series (G1362A) |
| | Sensor temp. | 32℃ |
| | Postrun purge time | 6 min. |
| | Prerun baseline compensation | 6 min. |
| Autosampler | Model | Agilent 1100 Series (G1313A) |
| | Injection loop | Agilent Multi Draw Kit (G1313A) |
| | Injection volume | 500 µl |
| | Sampler vials | Autosampler vials, 1 ml |
| Pump | Model | Agilent 1100 series binary pump (G1312A) |
| | flow rate | 1 ml/min |
| Pump $_{(Exp.10)}$ | Model | Agilent 1100 series quaternary pump (G1354A) |
| | flow rate | 1 ml/min |
| Datalogging | Software | Custom made LabView 6.0e |
| | Signal I/O | Adam 4012 |
| | Resolution | 0.01 mV (16 bit) |
| | Range | 0-150 mV |
| | Logging rate | 110 Hz |
| | Control I/O | Advantech 812 |
| Datalogging$_{(Exp.10)}$ | Agilent original system | Chemstation |
| SEC Column 1 | Model | PL Aquagel-OH 30 |
| | Manufacturer | Polymer Labs |
| | Dimensions | 7.5 x 300 mm |
| | Separation range | 0.1-30 kDa |
| | Particle size | 8 µm |
| | Stationary phase | Hydrophilic polyhydroxyl |
| SEC Column 2 | Model | Zorbax GF-250 |
| | Manufacturer | Mac-Mod Analytical Inc. |
| | Dimensions | 9.4 x 250 mm |
| | Separation range | 4-400 kDa |
| | Particle size | 4 µm |
| | Stationary phase | Hydrophilic diol bonds |
| Pre-column | Model | Diol Guard |
| | Dimensions | 4.6 (i.d.) x 12.5 |
| Column oven | Model | Supertherm |
| | Manufacturer | MikroLab, Aarhus (DK) |
| | Column Temp. | 32℃ |
| Mobile phase | Bulk | Milli-Q water |
| | Filtration | 0.45 µm Cellulose nitrate |
| | Degassing | Ultrasonication (45 min) |
| | pH | 6.4 |
| | Ionic strength | 0.17 mM |
| | Buffer composition | PBS (see table 2.3 last column) |

Table 4-5. HPLC system details and settings used during SEC analysis of Dextran samples.

500 µl sample injection volume loop was installed. Adjusting the buffer concentration of the mobile phase minimized buffer/stationary phase interactions. That resulted in a rather long elution time, giving a total HPLC run time of 63 min./sample. The HPLC system was calibrated by injection of six certified (DIN standards from Fluka GmBH, Sigma Aldrich Chemicals) Dextran calibration standards of $M_W$ (kDa): 0.342 (Isomaltose), 1, 12, 80, 150 and 410 (see Figure 4-3 for distributions). For each standard, four concentrations were injected in order to calibrate the peak height (RID signal/concentration response) in addition to the peak elution time.

### 4.1.6 Enzyme location assay

Two enzyme assays were used to test for exo- and endo- enzymatic activity in sub-compartments of the biofilm reactors. These are thoroughly described by Milferstedt (2001).

Endo-dextranase activity was assayed using the method developed by Mattiason (1980), with minor modifications (Milferstedt, 2001). In short, 200 µl Blue Dextran (30 g/l in 0.1 M PBS at pH 6), Reactive Blue 2 labelled 2 MDa Dextran, is added to an acid washed test tube containing 200 µl of sample. Following 30 min of incubation on a shaker (3 Hz), 0.9 ml PEG 4000 (polyethylene glycol, 430 g/l) and 2.5 ml $MgSO_4 \cdot 7\ H_2O$ (430 mg/l) are added, and vortexed. Two-phase separation for 7 min allows the labelled intermediates (Reactive Blue is strongly hydrophobic) to accumulate in the organic phase. An appropriate amount of organic phase (here: 500 µl) is then transferred to a microcuvette (plastic) for spectrophotometric determination at 620 nm (Perkin Elmer Lambda 2). The method is calibrated against a dextranase standard acquired from Sigma Chemicals (Dextranase *Paecilomyces lilacinus*, BioChemika Merck Index 13/2966) and reported as units of Dextranse activity $U_{dex}$). In the initial polymer, the hydrophobic labelled groups of Blue Dextran are balanced by the strongly hydrophilic Dextran backbone, giving an overall hydrophilic nature. As the endo-dextranase activity proceeds, the increasing relative amount of Reactive Blue in intermediates cause a change of hydrophobicity, enabling low Dextran containing intermediates diffusion and dissolution into the top organic phase.

Exo-dextranase activity was assayed using Amplex™ Red glucose assay kit from Molecular Probes (A-12210). This assay determines the concentration of glucose monomers as they are released by exo-dextranase enzymes (Zhou et al., 1998). The assay is based on colorimetric detection of $H_2O_2$, a Glucose oxidase product that reacts with the Amplex Red reactant catalysed by Horseradish peroxidase (Molecular Probes Inc[5]). In order to detect glucose, microbial uptake was avoided by sterile filtration (0.45 µm PTFE membrane syringe filters) and/or $NaN_3$ inhibition (5 mM). 90 µl samples were applied on a 96 well microplate together with 10 µl substrate assay solution[2], and 100 µl buffer (pH 7.4, kit solution) was added. The fluorescent chromophore Resorufin is liberated from the Amplex Red reactant, and measured by an automated microplate reader (BMG FLUOstar Galaxy[6] equipped with BMG 560-10 and BMG 590-EM filters). End point adsorption after 61 min of incubation (28°C) was used to

[5] Molecular Probes Inc. (2001) Instructions for use, Amplex Red Glucose Assay Kit (A12210), http://www.probes.com

[6] Kindly made available by NovoNordisk, Copenhagen.

determine the exo-enzymatic dextranase activity by the presence of glucose oxidised (cumulative). The assay was calibrated against glucose in the range (0.05 - 10.8 mg/l, or 10-2160 ng well plate mass). Samples for enzyme location determination was taken from the bulk phase just after experiment 8 (dilution experiment) at relatively high $T_H$ (75 min), from the biofilm surface by flushing biofilm coupons withdrawn from the inner rotor of the Rototorque with PBS (2 ml), and from the biofilm matrix by scraping of directly into a test tube. The biofilm matrix sample was disintegrated and homogenised by gentle sonication (Branson 2510, 40 kHz for 2 min). All samples were then centrifuged at 4°C for 10 min at 10.000 G. One sub-volume of the supernatant was filtered (0.45 µm PTFE) while the other half represented the unfiltered dissolved fraction. The biofilm matrix sample separated into: active native biofilm, native inactivated ($NaN_3$) biofilm, the cellular/matrix solid phase biofilm (represented by the re-suspended pellet) and the void volume represented by the supernatant (also sterile filtered by 0.45 µm PTFE syringe filter). All samples were kept on ice. For details on sampling procedure and sample preparations, see Milferstedt (2001)[7].

## 4.2 Culture tube batch tests

Small scale batch tests were developed in order to study intermediate formation and dynamics by coupon samples from the annular reactor. These batches are similar to the annular batch whole reactor experiments described above (section 4.1.4), but provided enough samples (coupons) to perform simultaneous intermediate experiments on biofilms at the same time, on samples of identical initial conditions (same biofilm thickness, growth history, etc.). In addition, biofilm mass and thickness were determined just after an experiment in order to relate the observed activity to the biomass present. Biofilm slides were sampled from $R_1$ and the effect of biofilm mass density and the extent of intermediate formation was evaluated using 250 mg/l initial Dextran 160 kDa standards. Inactivation by Azide ($NaN_3$) was performed on two slides to evaluate the pure exogenous enzymatic effects on the Dextran standards. Coupons were transferred to 60 ml Pyrex culture tubes immediately after sampling, pre-incubated at room temperature with 20 ml of PBS and Dextran standard, to give an area to bulk volume ratio of 70 $m^2/m^3$. Compared to the annular reactor this reduced S/V was necessary in order to provide enough bulk volume for sampling (10 x 1 ml samples). The Pyres batch was kept on a shaker, and samples were heated immediately after sampling for 2

[7] Appendix B, table 18.

min in an Eppendorf 2.5 ml tube, and centrifuged for 10 min at 10000 g and filter supernatant directly into the HPLC vial and stored at 2°C.

Pure enzyme studies were also performed in the culture tubes for evaluation of pure exogenous enzyme activity and effect on intermediate dynamics. 3.2.1.11 Dextranase, derived from the fungi *Paecilomyces lilacinus*, and 3.2.1.20 α-Glucosidase from *Bacillus stearothermophilus* and 3.2.1.10 oligo-1,6 Glucosidase from *Saccharomyces cerevisae* were used representing endo- and exo- exogenous activity, respectively. Lyophilised Dextranase were dissolved in 0.05 M acetate buffer, pH 5.2, while the lyophilised exo-enzymes were dissolved in 0.05 M phosphate buffer of pH 5.5 (pH selected based on information from the Brenda database[8]). Representative aliquots were then stored at -20°C until batch tests were conducted. The same procedure was followed during sampling as for the annular reactor intermediate experiments described above (section 4.1.5), except for the filtration step which was omitted (no suspended materials present). All details regarding sampling and handling may be found in Milferstedt (2001).

## 4.3 Tubular biofilm reactor

Tubular reactor biofilm systems may be operated as once through systems, representing the ideal plug flow reactor, or with recirculation that may provide close to ideal mixed conditions. The advantage of this system is the uniform and well controlled fluid dynamics of the reactor that provides a close to uniform biofilm thickness. Rectangular designs allow for direct microscopic inspection (Bakke, 1986) that may be used for direct apparent biofilm thickness measurements (Bakke and Olsson, 1986). Indirect determination of the true biofilm surface shear is possible by measuring the pressure drop over a specific tube distance (Bakke, 1986).

### 4.3.1 Experimental set up

The tubular reactor system is presented in Figure 4-4, and was kindly provided by Norsk Hydro Research department, Porsgrunn Norway[9]. A glass loop of approximately 2060 mm with an inner diameter of 13.5 mm, was connected via 5 mm (i.d.) Marprene pump tubing to a recirculation pump (Watson-Marlow 313 U) providing a recirculation rate of 675 ml/min (i.e.

[8] http://www.brenda.uni-koeln.de search on 3.2.1.11, 3.2.1.10 and 3.2.1.20
[9] contact person: Jon Hovland Norsk Hydro, Porsgrunn.

2.3 retention time per min.). The total loop (incl. tubing) volume was 299 ml, providing a specific wetted surface area of 333 $m^2/m^3$. An Ismatech Reglo Analog MS4/6-100 peristaltic pump loaded the system (143 ml/min) from four substrate flasks via a system of solenoid valves (Type Sirai, Z231A, 12 V three way tube valves) connected through Tygon 3603, 5 mm (i.d.) tubing. Dissolved oxygen was monitored by a CellOx 325 probe placed in a flow through mixing cell with magnetic stirring, connected to an Oxi 340 A dissolved oxygen meter (WTW GmBH, Germany). pH was kept constant at 7.7 using a phosphate buffer (see section 4.1.3) while temperature was kept at room temperature (25°C). Dissolved oxygen was logged using a custom made software (LabVIEW 5.0, National Instruments, Austin TX, USA) on desktop PC (Digital P90) by an Advantech PCL 818L (Advantech Co. Ltd, Taiwan) data acquisition card. The outlet from the top connection of the loop was equipped with an optical level switch (Hatteland AS) that controlled the filling cycle of the reactor (see operation below). All substrate flasks (10 l Nalgene flasks equipped with gas relief 20 l Tedlar Bags (SKC 232-15) filled with $N_2$) were kept anaerobic by stripping with $N_2$, except the Nutrient/Buffer flask which was supersaturated with oxygen by sparging with pure oxygen gas. Removable plastic coupons were attached to plastic brackets, sealed to the tubular reactor

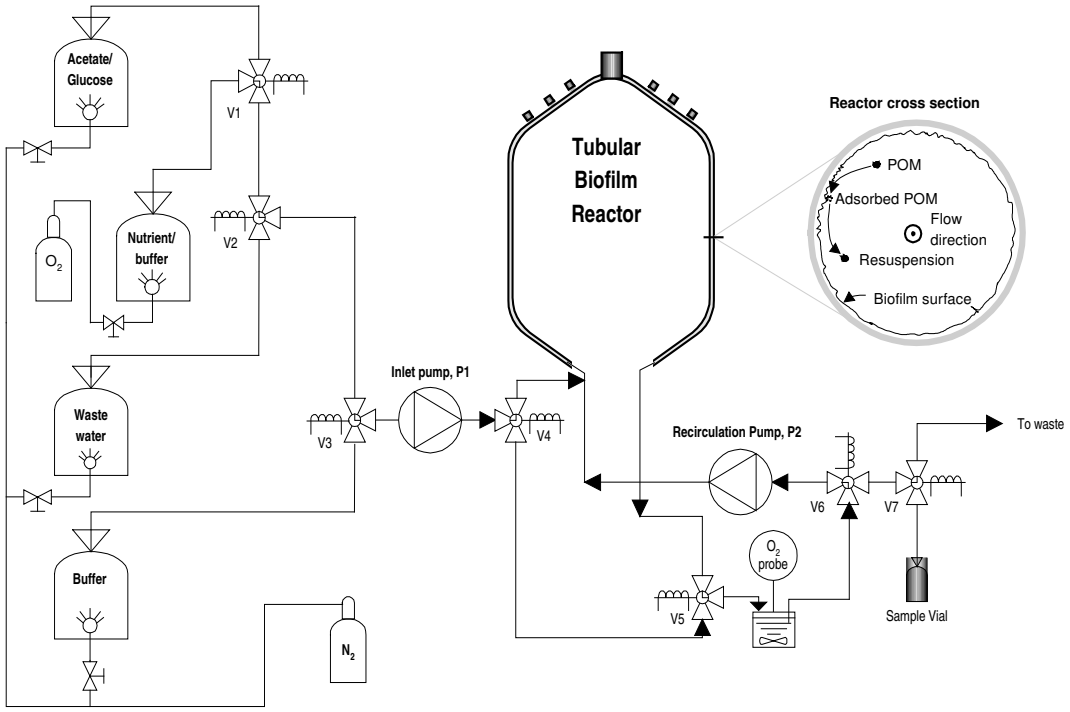


Figure 4-4. Tubular reactor system set up used for degradation studies on extracted POM from wastewater.

by rubber O-rings connected by custom made Schott caps. pH was controlled by a strong buffer (Janning, 1998). Three experiments were performed on the tubular reactor. The objective of all experiments was estimation of the depolymerisation/hydrolysis rate coefficient. All experiments followed the same procedure (section 4.3.4) and involved injection of 70 mg/l POM (as TOC) (experiment 1 and 2), and 275 mg/l POM (experiment 3). Experiment 3 also involved an evaluation of initial adsorption dynamics, and particle characterisation of pre- and post adsorbed bulk phase.

### 4.3.2 Substrate extraction

Primary influent from Knardalstrand WWTP (Porsgrunn, Norway) was collected (20 l) and immediately filtrated by test sieves (Prüfsieb, DIN 4188) of 20 and 125 µm. Filter retentate was washed and diluted in buffer (same ionic strength as the bulk liquid). Before injection to the tubular reactor system, samples were kept on ice, or stored at 2°C.

### 4.3.3 Nutrient media and buffer

Phosphate buffered saline was prepared as reported by Janning (1998). 40 mg/l $MgSO_4 \cdot 7 H_2O$, 2.7 mg/l $FeSO_4$, 20 mg/l $CaCl_2 \cdot 2 H_2O$, 4.5 mg/l $NH_4Cl$, 12 mg/l ATU (Allylthiourea), 2.5 µg/l HCl, 17.5 µg/l ZnCl, 25 µg/l $MnCl_2 \cdot 4 H_2O$, 1.5 µg/l $H_3BO_3$, 1.5 µg/l $CoCl_2 \cdot 6 H_2O$, 6 µg/l $NiCl_2 \cdot 6 H_2O$, 0.5 µg/l $CuCl_2 \cdot 2 H_2O$, 9 µg/l $Na_2MoO_4 \cdot 2 H_2O$, 1.39 g/l $NaH_2PO_4 \cdot 2 H_2O$ and 0.179 g/l $Na_2HPO_4 \cdot 2 H_2O$ were dissolved in 10 liter distilled water (MilliQ), autoclaved, and re-oxygenated by pure oxygen sparging for 20 min. Another flask was stripped using $N_2$ to produce anaerobic PBS following autoclavation. Easily biodegradable substrate was prepared by dissolving 20 mg/l acetate, 20 mg/l Glucose and 15 mg/l Yeast Extract (Difco) in 10 l PBS (giving a total organic carbon content of 25 mg/l), and autoclaved before super saturation by pure oxygen sparging. pH of all buffered solutions was maintained at pH 7.7 (Janning, 1998).

Three wastewater substrate standards were produced by dissolving extracted POM in PBS. One high TOC sample of 275 mg C/l was used during the adsorption and hydrolysis experiment, while two standards of 70 mg C/l was used for the hydrolysis experiments.

### 4.3.4 Operation and control

The reactor was inoculated by incubating primary inlet wastewater collected at Knardalstrand WWTP with PBS in the reactor for 24 hours. Following the mixed batch operation, the tubular reactor was loaded with easily biodegradable substrate/PBS by reducing the hydraulic retention time from 2 hours to 20 min. The reactor was continuously aerated during the incubation and growth phase. After about 3 days of continuous operation a thick biofilm was established, with a maximum OUR above 100 mg/l·h. Batch tests were performed following a modified procedure originally published by Janning (1998). PBS of supersaturated oxygen (30-33 mg/l) was fed the reactor after draining the reactor bulk liquid. Once filled, the reactor is mixed by the recirculation pump, and dissolved oxygen is measured at fixed intervals (here 6 sec.). Logged values are used to estimate OUR by least square fitting to 30 measurements. As soon as the dissolved oxygen concentration falls below the lower 0. order set point (here 15 mg/l), the bulk phase is drained and fresh oxygenated PBS is loaded (30 mg $O_2$/l). In order to condition the biofilm for the batch depolymerisation experiments, each experiment was performed by going through specific batch steps. Figure 5-23 (left) shows the main steps during preparation for the depolymerisation step. In order to remove residual organic substrates from the biofilm matrix (e.g. adsorbed SBCOD, storage compounds, degradable EPS) the biofilm as subjected to a relative long starvation phase of typically 4-6 hours. Background respiration was estimated by the end of the starvation phase. Reactivation using readily biodegradable substrates at high initial concentrations (120 mg $CH_3OH$/l) was then imposed for estimation of maximum OUR, and to avoid lag-phase behaviour caused by the prolonged starvation. Another short starvation period of about an hour then followed to metabolise adsorbed readily biodegradable substrates, and possible storage compounds (Janning, 1998). As soon as the OUR reached background respiration, anaerobic substrate standard for the depolymerisation stage was loaded and allowed to adsorb to the biofilm for about 0.5 h. Remaining bulk phase TOC was removed by a short washing (about three retention times) by anaerobic PBS. The hydrolysis phase (strictly depolymerisation phase) was then initiated by loading the reactor with supersaturated (oxygen) PBS. OUR was estimated until background respiration was re-established.

### 4.3.5 Sampling and analytical techniques

For all experiments, samples were taken from each draining of the reactor. During the adsorption phase (loading) of experiment 3, samples were also taken directly from the bulk phase by recirculating the bulk via a small external batch, and sample directly from that batch by pipettes. All samples were transferred to acid washed TOC vials (5 ml), and immediately analysed for TOC (Skalar Formacs TOC analyser, Skalar Breda NL). Initial and final particle distributions during the adsorption phase were investigated using laser diffraction scanning (Sympatec HELOS Laser diffraction pattern analyser).

## 4.4 Data acquisition and system control

Both experimental systems were equipped with full automatic control facilities, and automatic data logging and data evaluation. Custom made programs for data acquisition and control by PC interface were developed in LabView 5.0 (Tubular system) and 6.0e (Annular reactor). Suitable I/O interface cards and hardware for power supply and relay controls were designed and configured to the software. Detailed description of the tubular and annular biofilm system software may be found in Appendix 3.

## 4.5 Calibrations, estimations and error analysis

Even though some calibration and estimation details have been presented above, this section presents a comprehensive description of calibration, estimation and error analysis methods and strategies. The objective is to present the rationale behind determination of random and systematic error contribution.

### 4.5.1 Oxygen measurements and OUR estimation

The central parameter for activity estimation and experiment control was dissolved oxygen. In both systems, the Oxi 340 meter connected to the CellOx 325 polarographic (Clark type) probe provided oxygen readings to the system. The probe calibration was checked before each experiment, and recalibrated (in 100% humidity air, OxiCal-SL) if the cell constant was too low (<0.9). Accuracy of the probe and meter is listed at 0.5% of reading, which means about

0.1 mg/l (at 20 mg/l). Using the super saturated range of the meter (0-100%), 0.1 mg/l is equivalent to the resolution of the meter. The analogue output from the meter ranged 0-2 V from 0-100% saturation. The PCL 818L logging card had a 12 bit A/D converter covering the most appropriate ± 2.5 V range. The digital resolution thus becomes 1.22 mV, corresponding to 0.06 % oxygen resolution. At 20°C this is equivalent to about 0.025 mg/l. The accuracy of the A/D converter is 1 bit, or 1.22 mV. Thus, the system accuracy seems to be set by the meter/probe identical to the system resolution of 0.1 mg/l. Random errors were immediately observed, probably caused by 50 Hz net noise, and electrostatic interference from pumps and solenoid valves. This was especially observed during the annular reactor experiments. By increasing the $O_2$-logging rate drastically (from 0.25/s to 50/s) and calculate the average value over 4 s (assuming noise was normal distributed, or at least approximately normal distributed, N = 50-200), random noise effects were minimised without changing the original logging frequency (0.25 Hz). The standard deviations of the measurements per $O_2$ logging was estimated continuously by the Standard Deviation and Variance.vi of LabView, and was never found to exceed 0.05 mg/l. Thus, measurement error of dissolved oxygen was set to the meter/probe accuracy at ± 0.1 mg/l (95% confidence).

OUR was estimated using a fixed number (tubular system: 30) of oxygen measurements, or a variable number, depending on the last estimated OUR (annular system), between 15 and 50. LabView estimated OUR as the slope of the $O_2$ versus time curve, by the least squares method of the Linear Fit.vi (LabView 6.0i manual[10]). By calculating the standard error of the slope estimation according to Taylor (1982), an estimate of the uncertainty of the OUR estimation was available. This was found to be very constant and independent of OUR level (Covariance of OUR and St.error OUR was 0.1). Using six molecular weight standards and three concentration standards, the average constant standard error of the OUR estimations was found to be 0.38 ± 0.06 mg $O_2/l \cdot h$.

### 4.5.2 pH measurements

Even though the pH measurements were stable, pH logging followed the same regime as $O_2$ measurements. Both systems were calibrated using two point calibration standards (pH 4.01 and 7.00, Radiometer Copenhagen, DK) before each experiment. Tests showed that the Hanna electrodes were very stable over time. The cell constants hardly changed during the entire

[10] National Instruments Corporation (2000) LabVIEW Help, Part Number 370117A-01

experimental campaign (six months). The meters (Metrohm 691 and 692) had an accuracy of ± 0.01, and resolution of 0.01. The Amphel HI 1910 B electrode (Hanna Instruments) was preamplified by an internal battery, providing extended life time and stable signal to the meter. The electrode potential was shunted via a buffer to the meter output and logged by the ±1250 mV range of the PCL 818L board. That provided an A/D converter resolution of 0.6 mV, i.e. more than sufficient for the meter resolution (1 mV). The overall resolution of the pH logging system was therefore <0.01 and with an accuracy of ±0.01.

### 4.5.3 TOC analysis

Both TOC analysers used in this study were based on high temperature combustion and NIR detection of the combusted $CO_2$ gas. The Skalar analyser estimated standard deviations for each sample from three (or four) replicates, while the OI analytical analyser provided a fixed standard error (in %) from replicates of internal standards.

### 4.5.4 HPLC analysis

Size exclusion chromatography requires column and detector calibration. The column separate samples according to molecular weight by different column retention times (represented by the elution time). Thus, elution time is directly proportional to molecular weight. Refractive index sensors basically respond to almost all chemical compounds, unfortunately by variable degrees of response factors. Thus, each compound has to be calibrated by a set of concentration standards to calibrate the sensor response for that particular compound. Six different certified (DIN) Dextran $M_W$ standards were used for the calibration of the elution time (see section 4.1.5), four concentrations (5, 40, 100, 250 mg/l) were used for each size standard (i.e. 24 calibration samples), except for experiment 10 calibration which were based on nine calibration standards of: 0, 5, 20 and 100 mg/l. As the samples are typically Log-Normal distributed (see Figure 4-3), only a fraction of the standards are found under the weighted mean $M_W$. Thus, the peak height is equivalent to a much lower actual concentration than the standard. For example, all standards shown in Figure 4-3 are 100 mg/l, however, the actual concentrations of the peaks are approximately 10 times lower depending on the spread of the peaks. The total standard concentration may be found

summing the peak response by each polymer class (i.e. integrate the curve using a d($M_W$) of 162.15 g/mole). By using the certified analysis data provided by the manufacturer, a 2-dimensional theoretical response curve may be constructed and used as a theoretical calibration curve. The actual response curve of the HPLC system will be projected on the intrinsic spreading of the Dextran standards, and will be modified by column and detector properties. The actual calibration curve (the one recoded by analysing the standards on the HPLC system) was constructed by using the elution time and peak height as representative of the sample concentration (concentration of the polymer directly under the peak). By comparing this calibration response curve to the theoretical, the relative concentration and elution time errors of the system could be determined.

The Agilent 1100series HPLC system described above was equipped with custom made data acquisition soft- and hardware developed as part of this work. The RID detector provided mV direct output (1:1 buffered signal) that was logged using an ADAM 4012 A/D converter read by an ADAM 4520 I/O converter (RS 232). Control signals (start, stop signals) were read using a PCL 818L IO card. All hardware was purchased from Advantech Corp (KGS systems, Tromsø NOR). Logging and operation program was developed in LabView 6.0i and run from a Pentium II PC. The ADAM A/D converter provided 16 bit band width over a ±150 mV range, providing digital resolution of 5 µV. The analogue output from the RID detector provided resolution of 10 µV, equivalent to 60 nRIU (refractive index units). This is a relative low sensitivity (the short term S/N is 2.5 nRIU), but good enough compared to the long term drift stability (200 nRIU/h). Thus, the error of the RID sensor system was ± 60 nRIU, and the logging system 167 nRIU per 10 µV. That gives an overall system error of ± 167 nRIU.

### 4.5.5 Enzyme assays

Dextranase (from the fungus *Paecilomyces lilacinus*) was used to calibrate the Dextranase assay (Mattiasson, 1980). Six Dextranase standards (0, 6, 10, 20, 40, and 60 mU) were used for calibration against Blue Dextran (6 mg/3.8 ml) by measuring the water phase adsorption at 620 nm. Duplicates were used to establish standard deviations and errors. The assay detection limit was chosen to be three times the mean standard error of the calibrants (8%), found to be 1.5 mU. This gives an assay working range of 1.5 - 60 mU. During the experiments, duplicate samples were assayed and compared to the Dextranase activity standard curve.

Similarly, the α-Glucosidase an assay was calibrated by 10 substrate standards, standard errors estimated from triplicate standards and calibration range selected in accordance with the assay kit instructions to 0.05-10.8 mg/l.

## 4.6 Mathematical modelling

This chapter presents the development of a kinetic and stoichiometric model for exo- and endo-hydrolytic depolymerisation of Dextran. Expressions have been deduced as part of this work, but bears similarities to the models suggested by Suga et al. (1975) and Dean and Rollings (1992).

### 4.6.1 Endo-dextranase activity

Figure 4-5 show the reaction scheme for endo-hydrolysis of the mono-specie polymer. Let $P_j$ represent an intermediate polymer during the degradation of $P_{n,}$ and intermediates, to $P_k$. The proper substrate for enzymatic activity is the polymer bond between each monomer. Assuming the mechanism of hydrolysis of any bond inside the polymer chain to be equal, we assume the basal affinity for each bond to be equal (analogue to the equal probability of bond attach of stochastic models, and in a Michaelis-Menten expression, equivalent of assuming size independent $K_M$ values). Also, the rate of conversion of all enzyme-substrate complexes are assumed equal, regardless of the substrate size ($k_0$ for all reactions are equal). The

| | | | | | | | | | | |
|---|---|---|---|---|---|---|---|---|---|---|
| | + | $P_n$ | ↔ | $E{\cdot}P_n$ | → | E | + | $P_{n-k}$ | + | $P_k$ |
| | ⋮ | | | | | | | | | |
| | + | $P_{j+1}$ | ↔ | $E{\cdot}P_{j+1}$ | → | E | + | $P_{j+1-k}$ | + | $P_k$ |
| E | + | $P_j$ | ↔ | $E{\cdot}P_j$ | → | E | + | $P_{j-k}$ | + | $P_k$ |
| | + | $P_{j-1}$ | ↔ | $E{\cdot}P_{j-1}$ | → | E | + | $P_{j-1-k}$ | + | $P_k$ |
| | ⋮ | | | | | | | | | |
| | + | $P_{k+2}$ | ↔ | $E{\cdot}P_{k+2}$ | → | E | + | $P_2$ | + | $P_k$ |

Figure 4-5. Stoichiometries for endo-depolymerisation activity against a linear homopolymer (e.g. Dextran)

competition for free enzyme among all intermediates leads to an apparent competitive inhibition by all other reactions catalysed by the same enzyme. By projection of the bi-substrate competitive model presented by Cornish-Bowden (1995) into a multi-substrate expression, the formation rate of intermediate *k* may be represented by:

$$r_{P_k} = \sum_{j=k+2}^{n} \frac{k_0 \cdot e_0 \frac{P_j}{K_{M_j}}}{1 + \sum_{i=4}^{n} \frac{P_i}{K_{M_i}}} \qquad (4\text{-}2)$$

where: $k_0$ is the endo-specific activity [mole/mg·s], $e_0$ is the total endo-acting enzyme concentration, $K_{Mj}$ is the Michaelis-Menten coefficient for the binding to polymer *j* and $K_{Mi}$ is the same coefficient for polymer *i*. This rate expression was developed from Briggs-Haldane treatment (Cornish-Bowden, 1995) of a tri-substrate system, and projected onto *n* substrates. Mathematical proof may be achieved by induction (not shown here). Since each endo-hydrolytic reaction is stochastic in terms of which bond are attached, products may be assumed distributed with equal probabilities in a mixture of many enzymes and substrate molecules. This implies the following stoichiometric product coefficient for product $P_k$ from substrate $P_j$ :

$$\nu_{P_k/P_j} = \frac{2 \cdot k}{j^2 - 3 \cdot j} \quad , \quad k = 2,3, \ldots, j-2 \qquad (4\text{-}3)$$

where $\nu_{Pk/Pj}$ is the monomer based stoichiometric coefficient stating how many monomers of the original polymer *j* is converted to the product polymer *k*. This implies *j-2* stoichiometric coefficients which have to satisfy the mass balance:

$$\sum_{k=2}^{j-2} \left[ \frac{2 \cdot k}{j^2 - 3 \cdot j} \right]_j = 1 \qquad (4\text{-}4)$$

Proof:

$$\sum_{k=2}^{j-2} \frac{2 \cdot k}{j \cdot (j-3)} = \frac{2}{j \cdot (j-3)} \sum_{k=2}^{j-2} k$$

The depolymerisation products: $2,3,4,\ldots, j-2,$ has the row element no.: $1,2,3,\ldots, j-3.$ The sum over $k$ is an arithmetric sum defined by

$$\sum_{i=1}^{n} a_i = \frac{a_1 + a_n}{2} \cdot n, \quad \text{which gives:}$$

$$\sum_{k=2}^{j-2} k = \frac{2 + (j-2)}{2} (j-3) = \frac{j \cdot (j-3)}{2}$$

which, when inserted in the stoichiometric sum, gives

$$\sum_{k=2}^{j-2} \frac{2 \cdot k}{j \cdot (j-3)} = \frac{2}{j \cdot (j-3)} \cdot \frac{j \cdot (j-3)}{2} = 1 \quad \text{(QED)}$$

Depolymerisation rate of the formed intermediate is deduced the same way, with the rate expression:

$$r_{P_k} = \frac{k_0 \cdot e_0 \frac{P_k}{K_{M_k}}}{1 + \sum_{i=4}^{n} \frac{P_i}{K_{M_i}}} \qquad (4\text{-}5)$$

and the stoichiometric coefficient -1. These expressions relate to the substrate concentrations as mass per volume, and not molar concentrations (see below).

### 4.6.2 Exo-dextranase activity

Figure 4-6 presents the reaction mechanisms and stoichiometry of the exo-depolymerisation activity of a linear homo-polymer. Let $P_j$ represent the concentration of the j-monomer polymers. Exo-hydrolysis (hydrolysis of monomers from the non-reducing end of the polymer) of any polymer and oligomers will be subjected to the same kind of multi-substrate

| | | | | | | | | | | |
|---|---|---|---|---|---|---|---|---|---|---|
| | + | $P_n$ | ↔ | $E{\cdot}P_n$ | → | E | + | $P_{n-1}$ | + | S |
| | : | | | | | | | | | |
| | : | | | | | | | | | |
| | + | $P_{j+1}$ | ↔ | $E{\cdot}P_{j+1}$ | → | E | + | $P_j$ | + | S |
| E | + | $P_j$ | ↔ | $E{\cdot}P_j$ | → | E | + | $P_{j-1}$ | + | S |
| | + | $P_{j-1}$ | ↔ | $E{\cdot}P_{j-1}$ | → | E | + | $P_{j-2}$ | + | S |
| | : | | | | | | | | | |
| | : | | | | | | | | | |
| | + | $P_2$ | ↔ | $E{\cdot}P_2$ | → | E | + | S | + | S |

Figure 4-6. Reaction mechanisms and stoichiometry of exo-dextranase activity.

competitive inhibition as for endo-hydrolysis. Exo-hydrolysis activity will, however, be further reduced due to it's affinity for only one linkage (the closest polymer bond to the non-reducing end) of the polymer chain. Thus, the number of monomers of the polymer will reduce the affinity factor in the rate equation when weight per volume units is used. The competitive inhibition factors are also reduced by the same factor. Using the same arguments as outlined for the deduction of the endo-depolymerisation kinetics, formation by exo-depolymerisation may be described by:

$$r_S = \sum_{j=2}^{n} \left[ \frac{k_0 \cdot e_0 \dfrac{P_j}{K_{M_j} \cdot (j-1)}}{1 + \sum_{i=2}^{n} \dfrac{P_i}{K_{M_i} \cdot (i-1)}} \right] \qquad (4\text{-}6)$$

There are only two stoichiometric coefficients (mass per mass) for each reaction, one for the monomer liberated and one for the remaining polymer. Both are only dependant on the polymer size,

$$\nu_{S/P_j} = \frac{1}{j} \qquad (4\text{-}7)$$

for the monomer, and

$$\nu_{P_{j-1}/P_j} = \frac{j-1}{j} \tag{4-8}$$

for the remaining polymer, and so that they do obey the mass balance requirement:

$$\nu_{S/P_j} + \nu_{P_{j-1}/P_j} = \frac{j-1}{j} + \frac{1}{j} = 1 \tag{4-9}$$

Depolymerisation of intermediate *k* will be, analogue to the endo acting depolymerisation rate of *k*:

$$r_{P_k} = \frac{k_0 \cdot e_0 \dfrac{P_k}{K_{M_j} \cdot (k-1)}}{1 + \sum_{i=2}^{n} \dfrac{P_i}{K_{M_i} \cdot (i-1)}} \tag{4-10}$$

multiplied with the stoichiometric coefficient -1.

Now, the Michaelis coefficients in both the exo- and endo-enzyme rate equations are the true substrate affinity coefficients, both in the substrate affinity factor ($K_{Mj}$) and the substrate competitive inhibition factors ($K_{Mi}$). Using the assumption of equal affinities regardless of substrate size, the formation expressions for the endo- and exo depolymerisation mass balances reduces to:

$$\frac{dP_k}{dt} = \sum_{j=k+2}^{n} \left[ \frac{k_{0,endo} \cdot e_{0,endo} \cdot P_j}{K_{M,endo} + \sum_{i=4}^{n} P_i} \cdot \nu_{P_k/P_j} \right] \tag{4-11}$$

and

$$\frac{dS}{dt} = \sum_{j=2}^{n} \left[ \frac{k_{0,exo} \cdot e_{0,exo} \dfrac{P_j}{(j-1)}}{K_{M,exo} + \sum_{i=2}^{n} \dfrac{P_i}{(i-1)}} \cdot \nu_{S/P_j} \right] \tag{4-12}$$

respectively, and for the remaining polymer

$$\frac{dP_{j-1}}{dt} = \sum_{j=2}^{n} \left[ \frac{k_{0,exo} \cdot e_{0,exo} \dfrac{P_j}{(j-1)}}{K_{M,exo} + \sum_{i=2}^{n} \dfrac{P_i}{(i-1)}} \cdot \nu_{P_{j-1}/P_j} \right] \tag{4-13}$$

The same simplification will apply to the depolymerisation rate expression of the endo- and exo-activity substrates. The overall dynamic expression for the intermediate *k* thus becomes (rate multiplied by the appropriate stoichiometric coefficient):

$$\frac{dP_k}{dt} = \sum_{j=k+2}^{n} \left[ \frac{2 \cdot k \cdot k_{0,endo} \cdot e_{0,endo} \cdot P_j}{j(j-3)\left( K_{M,endo} + \sum_{i=4}^{n} P_i \right)} \right] - \frac{k_{0,endo} \cdot e_{0,endo} \cdot P_k}{K_{M,endo} + \sum_{i=4}^{n} P_i} + \frac{k_{0,exo} \cdot e_{0,exo} \cdot P_{k+1}}{(k+1)\left( K_{M,exo} + \sum_{i=2}^{n} \dfrac{P_i}{(i-1)} \right)} - \frac{k_{0,exo} \cdot e_{0,exo} \cdot P_k}{\left( K_{M,exo} + \sum_{i=2}^{n} \dfrac{P_i}{(i-1)} \right)} \tag{4-14}$$

In case of molar units, the equation of endo-depolymerisation formation changes to:

$$r_{P_k} = \sum_{j=k+2}^{n} \frac{k_{0,endo} \cdot e_{0,endo} \cdot P_j \cdot (j-3)}{K_{M,endo} + \sum_{i=4}^{n} P_i \cdot (i-3)} \tag{4-15}$$

due to endo-enzymes affinity for polymer bonds rather than the molecule itself, and the stoichiometric coefficient changes to:

$$\upsilon_{P_k/P_j} = \frac{2}{j-3} \tag{4-16}$$

For exo-depolymerisation, the affinity is again limited to the non-reducing end bond, which gives the following rate expression:

$$r_S = \sum_{j=2}^{n} \left[ \frac{k_{0,exo} \cdot e_{0,exo} \cdot P_j}{K_{M,exo} + \sum_{i=2}^{n} P_i} \right] \quad (4\text{-}17)$$

and

$$r_{P_{k-1}} = \frac{k_{0,exo} \cdot e_{0,exo} \cdot P_k}{K_{M,exo} + \sum_{i=2}^{n} P_i} \quad (4\text{-}18)$$

Stoichiometric coefficients for exo-hydrolysis are both one. The overall batch mass balance thus becomes:

$$\frac{dP_k}{dt} = \sum_{j=k+2}^{n} \left[ \frac{2 \cdot k_{0,endo} \cdot e_{0,endo} \cdot P_j}{K_{M,endo} + \sum_{i=4}^{n} P_i \cdot (i-3)} \right] - \frac{k_{0,endo} \cdot e_{0,endo} \cdot P_k \cdot (k-3)}{K_{M,endo} + \sum_{i=4}^{n} P_i \cdot (i-3)} + \frac{k_{0,exo} \cdot e_{0,exo} \cdot P_{k+1}}{K_{M,exo} + \sum_{i=2}^{n} P_i} - \frac{k_{0,exo} \cdot e_{0,exo} \cdot P_k}{K_{M,exo} + \sum_{i=2}^{n} P_i} \quad (4\text{-}19)$$

which is identical to the model proposed by Suga et al. (1974).

# 5 Results

This section presents system evaluation, calibration, experimental and modelling results.

## 5.1 System performance and calibrations

System mixing conditions were evaluated using a strong saline bulk solution, and continuously measure bulk phase conductivity (initially 2180 and 2650 µS/cm, $R_1$ and $R_2$ respectively) during inlet dilution ($Q_{in,1}$: 17.33 and $Q_{in,2}$: 16.66 ml/min). Figure 5-1 show the dilution curves for the reactors. Based on the estimated dilution rates, the reactor volume could be estimated. However, flow rate measurements showed that the flow rate changed during the progression of the experiment (after 320 min: 16.17 and 16.75 ml/min, respectively). By linear approximation of flow rate change, and using the least square approximation on the data, $V_{R1}$ and $V_{R2}$ were found to be 1156 and 1181 ml ($R_1$ and $R_2$). That is close to the measured volumes (using weight and distilled water) of 1175 and 1168 ml ($R_1$ and $R_2$, respectively). The exponential match indicates very close to perfect mixed conditions in the reactors at a recirculation flow rate of 40% (570 ml/min).

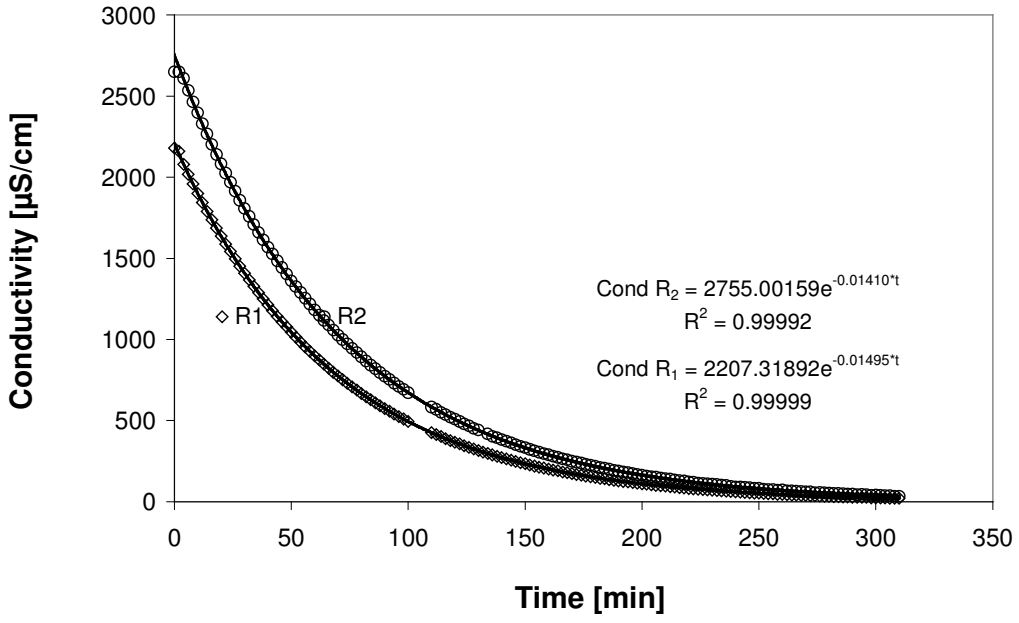


Figure 5-1. Dilution experiment of $R_1$ and $R_2$ using NaCl as tracer and conductivity measurements.

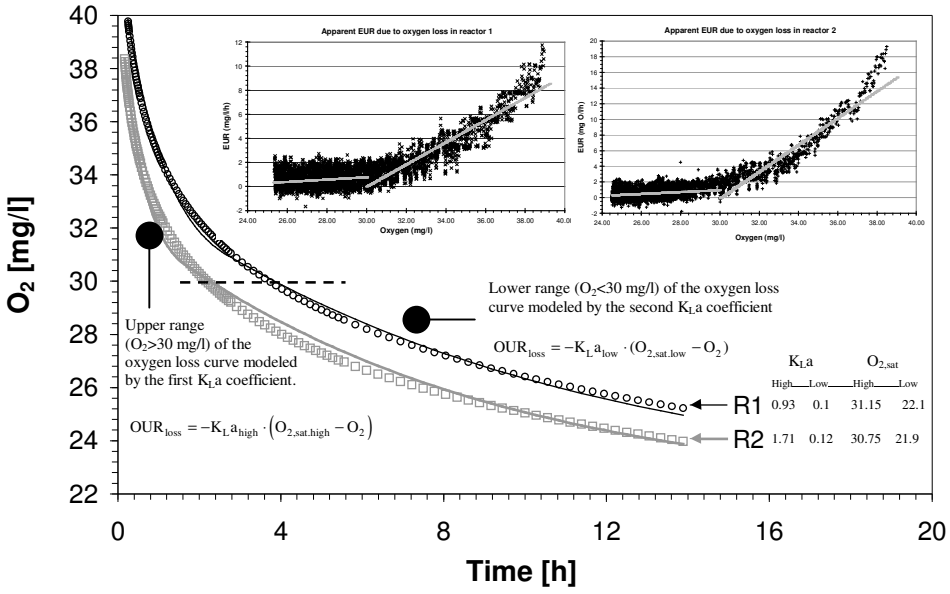


Figure 5-2. Oxygen loss from empty reactor (distilled water) following 40% Ethanol disinfection and oxygenation. Inserts show the estimated relation between $OUR_{loss}$ and bulk phase $O_2$ used to compensate for the apparent OUR recorded. Also indicated are the range split used for the compensation (high and low $OUR_{loss}$ ranges). O and □ represent data of $R_1$ and $R_2$ respectively, while lines show the two range $K_La$ models used.

Figure 5-2 shows the results of the system oxygen loss experiment. An ordinary $K_La$ model did not fit the $O_2$ data to the extent required, however, splitting the observed range (24-40 mg/l) into a high and low OUR loss range was sufficient to represent the observed $OUR_{loss}$ rate. This resulted in the calibration of a two range $K_La$ model that was implemented in the Rototorque reactors software to compensate for apparent OUR due to oxygen diffusion losses over the system boundaries (models and parameters are listed in Figure 5-2). Above 30 mg/l the loss effect is quite significant for both reactors, while a rather limited and constant effect were found below this limit. As most experiments were conducted in the 22-30 mg/l range, the effects were restricted to the endogenous phase OUR.

The SEC-HPLC and endo-enzyme assay developed (or modified) in this study were calibrated according to section 4.1.5. Complete description and discussion of the methodology and calibration procedures are given by Milfersted (2001). Details regarding the calibration methodology and calibration results are found in Appendix (9.3).

## 5.2 Effect of polymer size on depolymerisation kinetics

Effect of polymer size on depolymerisation kinetics is evaluated by observing degradation rates the batch operated annular biofilm reactor. Experiment 5, 7 and 10 (Table 4-1) all focused on this objective by analysing the observed bulk phase TOC and OUR results from injection of various sample standards.

### 5.2.1 Experiment 5, pilot testing

The objective of experiment 5 is to compare respiration rates from injections of sample standards at variable initial concentrations. Also, both reactors were fed the same substrates up to and during the experiment. By comparing the response from the reactors, conclusions could be drawn about the reproducibility and variability of the respirometric method.

Figure 9-5and Figure 9-6 (appendix 9.4) show the results of various Dextran standards and initial concentrations for both reactors on the observed OUR (experiment 5). No clear effect of the larger molecular weight standards can be seen, even though some curves show indications of gradually decreasing degradation rates as the initial molecular weight distribution increase. The obscurity of the data may be explained by oxygenation and base addition failure (software timing failure due to overloaded memory) during the 200 mg/l 160 kDa sample standard batch, which caused both reactors to become anaerobic, and suffering a pH drop. Injection of repeats of 200 mg/l 160 kDa was degraded in a distinct different fashion compared to the ones before the software failure (Figure 5-3, left panel). However, before the

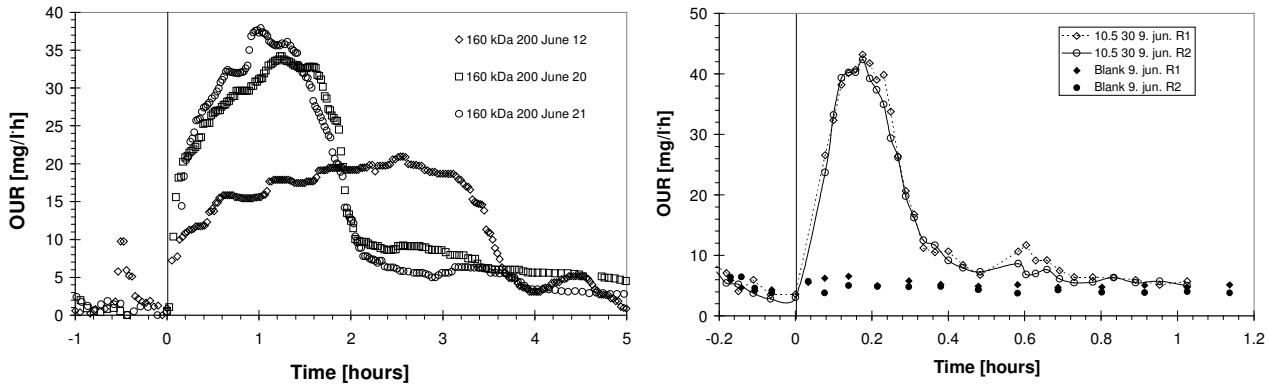


Figure 5-3. OUR results following injection of 160 kDa to $R_1$ just after the process disturbance (June 11) and a week later (left panel). All data were zeroed (i.e. reduced by the OUR prior to injection) in order to compare the relative OUR peaks. During the batch experiments before the anaerobic accident, peaks were almost identical between the reactors (right panel).

process disturbance, the system showed good correlation between samples and strikingly similar behaviour in the two reactors (Figure 5-3). Being a pilot experiment, experiment 5 showed that equal and constant operating conditions must be provided in order to compare the kinetic effects of various molecular weight standards. Further, unknown high oxygen concentration OUR losses were observed and compensated for in order to provide consistent data (ref. discussion in Appendix 9.4). This problem was solved by increasing the oxygen range applied during the batch tests, from [10-24] to [22-30]. Several batch runs also failed due to accumulation of oxygen/gas bubbles around the inner cylinder shaft of the reactors. Increasing the distance between the bottom stopper of the oxygenation column and the oxygen diffuser reduced flow trapping of oxygen bubbles in the bubble column. The results of variable initial sample concentrations suggested that the optimal sample standard was 80 to 200 mg/l. This is based on the necessary signal to noise ratio required, and the batch time per sample. Thus, initial sample concentrations of 100 and 200 mg/l were chosen for later experiments.

An important conclusion from the pilot experiment is that in order to compare degradation effects between samples of different molecular weight, injections had to be conducted as close as possible (time factor) with reactors of similar growth history. Two "close in time" late experiment 5 injections were performed in order to compare standards of different molecular weight (equal initial concentrations). Figure 5-4 show the results of 80 mg/l initial concentration of 38.1 and 513 kDa sample standards injected to both reactors June 27 (17:33) and 28 (10:30). Significant difference between the two molecular weight standards was observed, especially for $R_1$. An additional injection of 80 mg/l Glucose emphasize the size

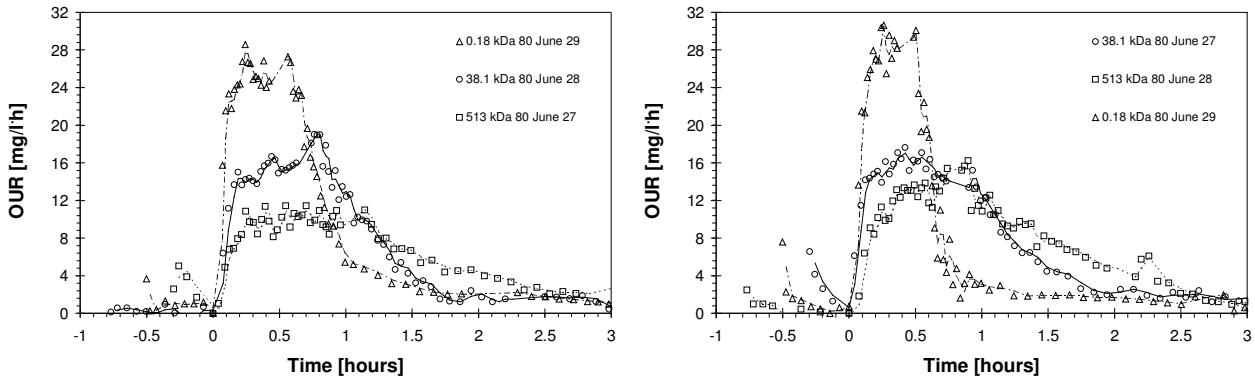


Figure 5-4. Respirograms of "close in time" injections to $R_1$ (left) and $R_2$ of 80 mg/l Dextran 38.1 and 513 kDa. Data are zeroed to the OUR at injection, providing ΔOUR data for relative comparison

effects providing both a stronger initial OUR response as well as shorter overall degradation times. This result also supports the assumption for the depolymerisation experiments; that depolymerisation is the rate limiting step during total degradation of Dextran polymers.

### 5.2.2 Experiment 7

Experiment 7 involved the same standards as applied during experiment 6, except that degradation batch tests were only performed on 200 mg/l initial concentrations, and that additional analysis on bulk phase TOC and SEC-HPLC analysis of intermediate dynamics were conducted. This section will only report OUR and bulk phase TOC data, whereas intermediate data will be presented later.

After the end of experiment 5 clogging of tubes and abnormal OUR under starvation conditions indicated that too much biomass accumulated in the reactors. This was concluded from draining and opening the reactors for direct inspection. By introducing regular "detachment" events under minimum hydraulic retention time ($\Theta_H$ = 8 min.), maximum recirculation rate ($Q_R$ = 1200 ml/min) and maximizing shear forces by increasing rotor speed to maximum (from 40%), settled and attached biomass from the bottom plate was re-suspended and washed out over 45-60 min. Both reactors were also checked for gas accumulation around the rotor shaft, and evacuated if occurring through the slide sample port. Detachment events and gas removal were performed before each injection to secure equal biomass and gas free conditions. Biofilm mass was also reduced by reducing the organic loading to the reactors during the 14 days of acclimatisation prior to the experiment (10 mg/l Dextran 160 kDa, $\Theta_H$ = 28 min, or about 2.2 g COD/$m^2$·d). Oxygen range was set to [22, 32] mg/l and $pH_{min}$ at 5.75.

Assuming hydrolysis of Dextran to be the rate limiting step during mineralisation (Ubukata, 1992; 1997; 1999), observed bulk phase carbon and OUR dynamics represent the rate of depolymerisation of the initial and intermediate polymers. For the biofilm batch system, the following mass balance describe the Dextran dynamics

$$V \cdot \frac{dX_s}{dt} = -r_A \cdot A_f \qquad (5\text{-}1)$$

where $V$ is the bulk phase reactor volume [$m^3$], $A_f$ is the total biofilm area, $X_S$ is the polymer bulk phase concentration [g TOC/$m^3$] and $r_A$ is the direct growth areal removal rate [g TOC/$m^2$·h]. Janning (1998) showed how kinetic batch experiments could be interpreted using the kinetics developed by Harremoës (1978). Depending on the bulk substrate concentration, the observed kinetics would change from 0.order via ½. order to 1. order, according to shift in the intrinsic biofilm degradation rate from 0 to 1.order kinetics. Assuming the biofilm is at any time partly penetrated, intrinsic Monod kinetics may be used to describe the observed bulk phase substrate concentration using a single equation (Rittmann and McCarty, 2001). This approach is advantageous when the shift between intrinsic kinetics is hard to define based on the data. The areal removal rate is given by:

$$r_A = k_{1/2,A}\sqrt{S_b - K_S \cdot ln\left[\frac{K_S + S_b}{K_S}\right]} \qquad (5\text{-}2)$$

where $k_{1/2,A}$ is the areal specific removal rate coefficient [$(g/m^3)^{0.5}$/d], $K_S$ is the Monod half saturation coefficient [$g/m^3$] and, according to Harremoës and Henze (2002), $k_{1/2,A}$ relates to the biofilm specific removal rate as:

$$k_{1/2,A} = \sqrt{2 \cdot k_{0,f} \cdot D_{X_S,f}} \qquad (5\text{-}3)$$

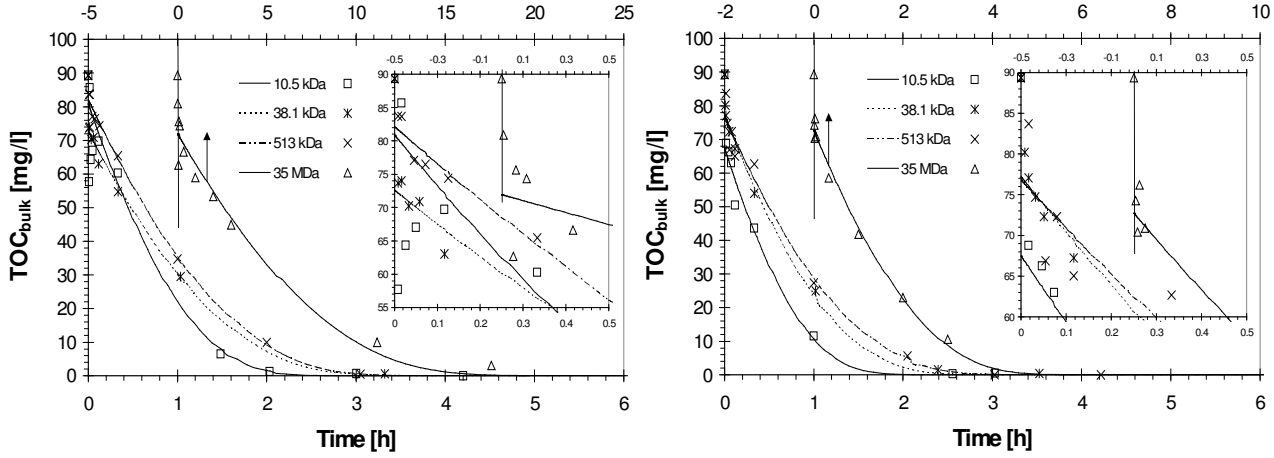


Figure 5-5. Bulk phase TOC concentrations after injection of 200 mg/l (reactor concentration) Dextran standards of varying molecular weight (average molecular weight) to $R_1$ and $R_2$ (right). Insert shows the bulk phase concentration immediately after the injection (expand of main figure).

where $D_{Xs,f}$ is the substrate diffusion coefficient in the biofilm [$m^2$/d]. $k_{0,f}$ is the zero order intrinsic reaction rate coefficient, and represents the maximum substrate removal rate, defined by:

$$k_{0,f} = \frac{\mu_{max} \cdot X_f}{Y_{X/S}} \quad (5\text{-}4)$$

where $\mu_{max}$ is the maximum specific growth rate of biofilm biomass [1/d], $X_f$ [g/$m^3$], and $Y_{X/S}$ is the maximum biomass yield coefficient [g/g].

Bulk phase TOC (mg C/l) during injection of 200 mg/l Dextran standards (equivalent to 89.4 mg TOC/l) is presented in Figure 5-5. Samples were taken after 0.5, 1, 2, 3, 7, 20, 60 min, and then at appropriate times depending on respiration rates. Table 5-1 lists the half order areal specific degradation coefficients for each initial size standard following linearised regression analysis, and the fitted correlation coefficient obtained. $K_S$ was kept constant at 1.5 g TOC/$m^3$ based on literature values for the hydrolysis product (Glucose; Henze et al., 2000), while $k_{0,f}$ was adjusted by least squares minimisation. As can be seen from the insert in Figure 5-5 the initial bulk phase TOC was for all sample injection significantly lower than the calculated concentration (89.3 mg TOC/l). This could be the result of fast initial adsorption of the polymers to the biofilm surface/matrix, or degradation of the polymers during storage (this is a possibility since rather old standards, about 6 weeks, were used in this experiment). As no mechanism of adsorption is included in the model used for interpretation, the latter was anticipated during rate estimations. Dextran diffusion coefficients were estimated using the Stoke-Einstein equation (5-5) compensated for biomass density, $D_{Xs,f} = 0.3 \cdot D_{Xs,b}$, (Stewart, 2003b),

| **Init. $M_W$** [kDa] | **Est. $D_f \cdot 10^{10}$** [$m^2$/s] | **Est. $k_{0,f}$** [kg COD/$m^3$·d] | | **Est. $k_{1/2,A}$** [kg COD/$m^3$·d] | | **δ $k_{1/2,A}$** [g/$m^3$·d] | | **Number of data points** | | **$k_{1/2,A}$ Correlation coeff. [$r^2$]** | |
|---|---|---|---|---|---|---|---|---|---|---|---|
| | | **$R_1$** | **$R_2$** | **$R_1$** | **$R_2$** | **$R_1$** | **$R_2$** | **$R_1$** | **$R_2$** | **$R_1$** | **$R_2$** |
| 10.5 | 0.88 | 132 | 216 | 0.86 | 1.11 | 0.07 | 0.04 | 10 | 9 | 0.949 | 0.990 |
| 38.1 | 0.50 | 346 | 226 | 0.66 | 0.86 | 0.02 | 0.02 | 9 | 10 | 0.996 | 0.998 |
| 513 | 0.139 | 502 | 608 | 0.67 | 0.74 | 0.01 | 0.04 | 10 | 9 | 0.995 | 0.975 |
| 35000 | 0.019 | 108 | 1380 | 0.12 | 0.41 | 0.01 | 0.02 | 10 | 9 | 0.935 | 0.960 |

Table 5-1. Effect of Dextran initial molecular weight on the estimated half order degradation rate coefficient $k_{1/2,A}$, estimated diffusion coefficients, $D_f$, and intrinsic degradation rate coefficient, $k_{0,f}$.

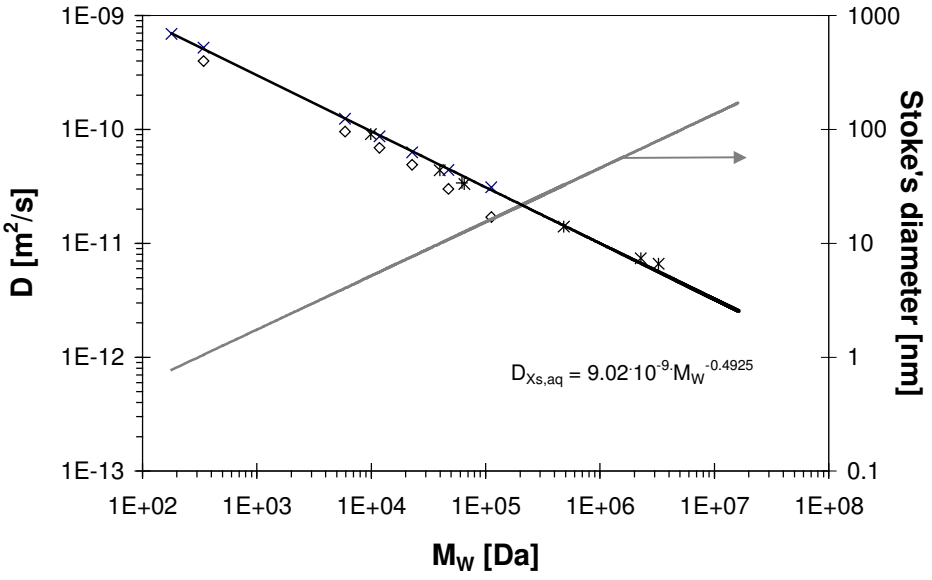


Figure 5-6. Pullulan (×) and Dextran (⤫) diffusion coefficients in water (Roger et al., 2000; Wu, 1993) including Stoke-Einstein estimation , and Pullulan effective diffusion coefficients as measured in agarose gels (◊). The best estimate through the liquid diffusion data is indicated. Stoke diameter (nested sphere) related to molecular weight is indicated on the second (right) ordinate.

$$D = \frac{k_B \cdot T}{6 \cdot \pi \cdot \mu \cdot R_e} \qquad (5\text{-}5)$$

where $k_B$ is the Boltzman constant, $T$ is the temperature, $\mu$ is the solvent viscosity and $R_e$ is the hydrodynamic (equivalent sphere) polymer radius [m]. Dextran is polymerised through three separate bonds, a property resulting in a range of rotational and vibrational states between each monomer unit. Thus, the polymer chain becomes extremely flexible, and takes on the structure of a nested sphere (Smidsrød and Moe, 1995). The hydrodynamic radius may be represented by the radii of inertia, $R_G$

$$R_e = \xi \cdot R_G \qquad (5\text{-}6)$$

where $\xi$ is a size independent constant at approximately 0.8 (Smidsrød and Moe, 1995). Due to the flexible and partial branching of the polymer chain, Dextran has a low $R_G$ and relates to the molecular weight as

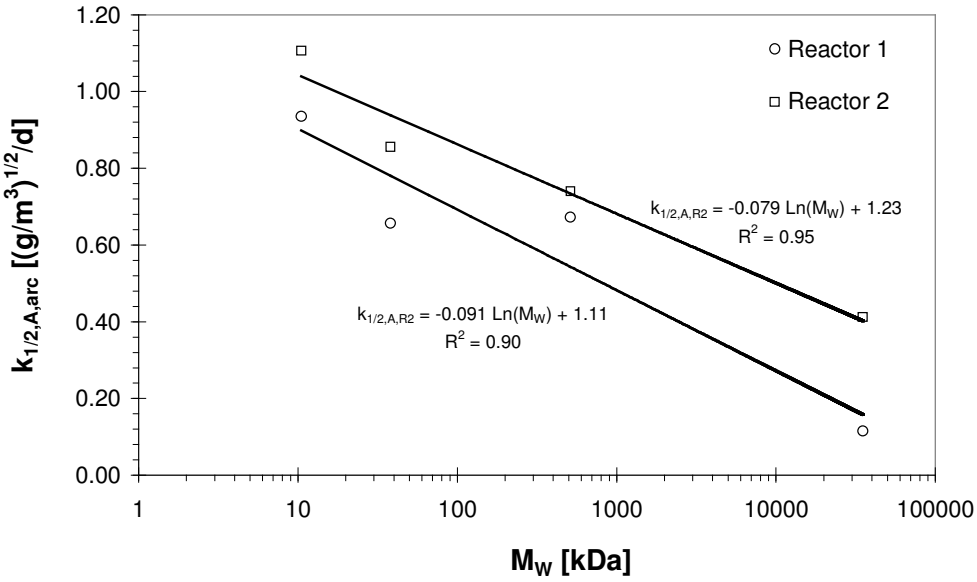


Figure 5-7. Estimated half order areal removal rate coefficients plotted against initial Dextran molecular weight (initial concentrations of 200 mg/l).

$$R_G \propto M^{0.5} \qquad (5\text{-}7)$$

for a polymer dissolved in a "good" solute. Thus, the diffusion coefficient of Dextran theoretically relates to the inverse root of their molecular weight. Figure 5-6 show reported relations between Dextran and Pullulan molecular weights (Roger et al., 2000; Wu, 1993) and the observed diffusion coefficient in water and hydrated gels. As indicated, the diffusion coefficient relates to the Dextran molecular weight very close to the theoretical anticipated value.

From Figure 5-5 it is possible to evaluate whether degradation rates decrease systematically as the initial average molecular weight of the Dextran substrate increase. The half order removal coefficient is plotted against the average molecular weight of the initial substrate standard in Figure 5-7. Even though the data are limited, there seems to be a systematic reduction in $k_{1/2,A}$ as the initial molecular weight of the polymers increase.

Respirograms of the same Dextran standards are presented in Figure 5-8. Background (endogenous) respiration is indicated by the OUR level before injection at t = 0 h. OUR could not be estimated during re-oxygenation, observed in the respirograms as gaps on the OUR curves. This effect was especially pronounced during high respiration rates when more frequent re-oxygenation was required. An immediate response can be seen for all standards

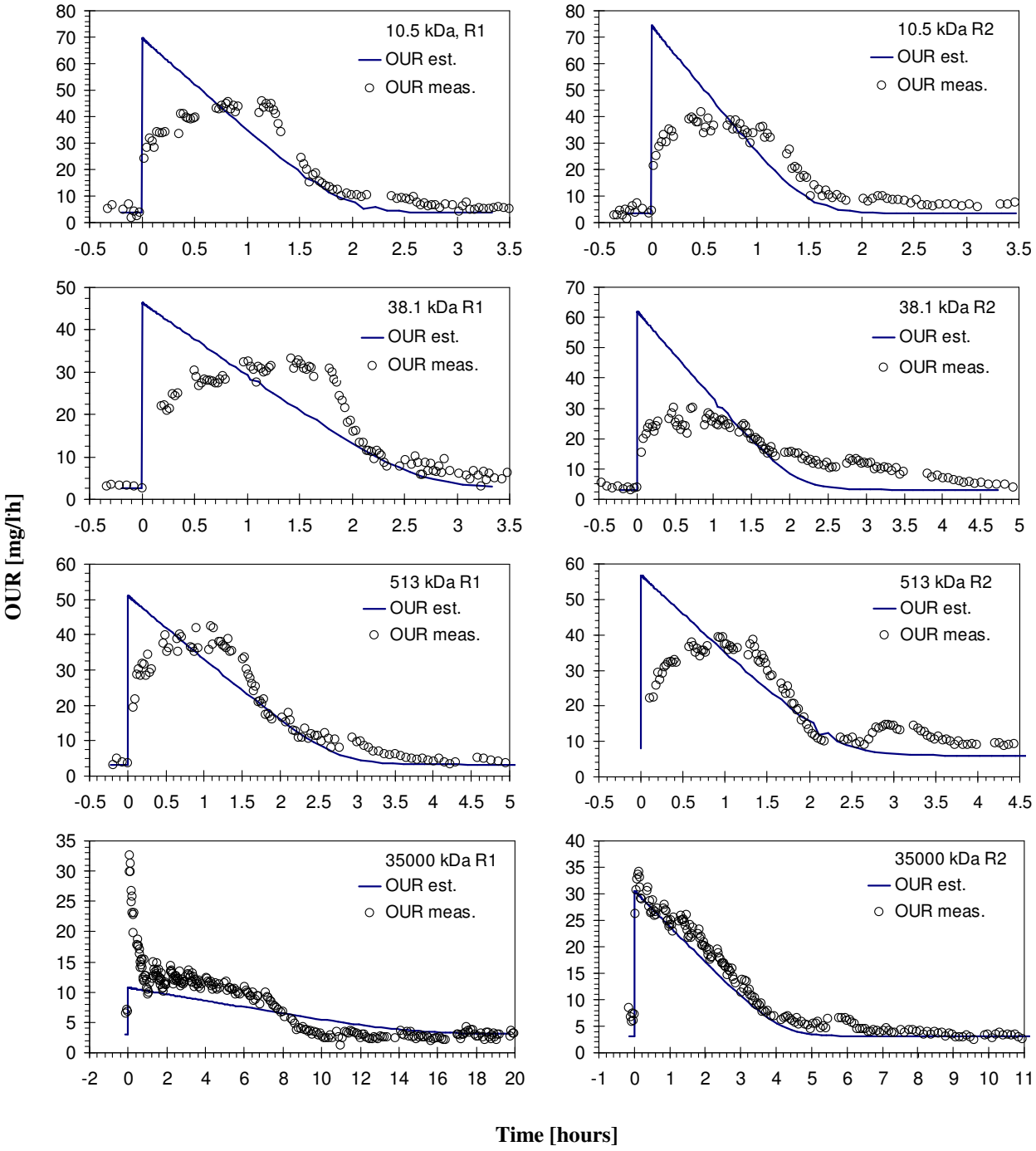


Figure 5-8. Respiration rates during depolymerisation and degradation of Dextran size standards in experiment 7. Lines represent the modelled OUR based on the half order kinetics in (5-2), using the estimated half order removal rate coefficient listed for each standard in Table 5-1.

upon injection except for the blank (pure PBS standard; not included in the figure). This indicates the presence of low molecular Dextran in all standards. Apart from the immediate response, all OUR curves resemble a log-normal response as would be expected from the log-normal $M_W$ distribution of the Dextran standards (ref. Figure 4-3). Also shown in Figure 5-8 is the estimated OUR based on the TOC removal rate estimated from the TOC data, found by

multiplying the TOC removal rate with the theoretical stoichiometric coefficient of 0.79 g $O_2$/ g TOC. By comparing the estimated OUR to the measured, some information regarding the adequacy of the modelling approach can be made. Both the shape and, especially, the initial OUR estimation indicate that the single direct substrate degradation model does not reflect the complexity and multi reaction set involved. Nevertheless, the half order rate estimation is an applicable tool to investigate the effects of initial polymer size as intrinsic reaction or transport rate effects are reflected in the coefficient. The peak like OUR estimation simply reflects the result of not taking diffusion time nor gradients into account, but treating the transport limiting effects as part of the reaction kinetics (deviation introduced by the model structure). In addition, assuming the polymers standards to be directly degradable without taking possible intermediate dynamics into account, produce the linear reduction response form which is very different from the almost bell shaped measured OUR curve (deviation introduced by the substrate structure). Nevertheless, the OUR estimation comparison is useful in order to evaluate the bulk phase TOC rate analysis. The areas under the OUR estimation and measured data curves are approximately equal, indicating that the stoichiometry of the model is correct. Also, the estimated OUR fairly good reflects the measured OUR during the latter phase of the batch were the system is not that influence by the initial injection. That is really not surprising as the reaction-diffusion intrinsic model has been developed and applied on steady state situations, rather than non-steady state batch systems. Interestingly, the model seems to be more accurate for the higher molecular weight standards (excluding the colloidal injection) during the initial phase. This may indicate that the lower size standards are transport limited, while the higher are limited by the depolymerisation rate.

### 5.2.3 Experiment 10

Experiment 7 showed that it is possible to evaluate the effects of initial polymer molecular weight on the observed degradation kinetics by applying a direct growth model with transport limitations intrinsic in the reaction rate expression. However, limited number of sample standards and uncertainties related to the initial concentrations suggested repeating the experiment using several freshly prepared standards. Thus, 100 mg/l standards of Glucose (0.18 kDa), 5, 10.5, 41.3, 160, 473, 513 and 35000 kDa were applied to $R_1$ (only) while

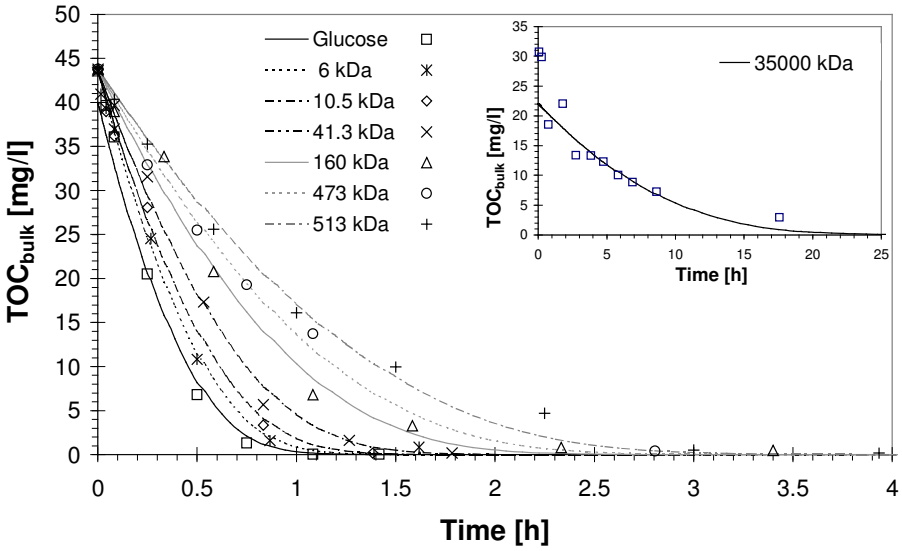


Figure 5-9. Bulk phase TOC concentrations after injection of 100 mg/l (reactor concentration) Dextran standards of varying molecular weight (average molecular weight). Insert show the 36 MDa standard degradation kinetics.

sampling for bulk phase TOC and intermediate dynamics. The experiment was performed just after experiment 9 where initial concentration effects were studied using 160 kDa standards. Therefore, the biofilm was active and adapted to Dextran substrate. Detachment events and gas evacuation were performed as described in section 5.2.2.

Figure 5-9 shows the bulk phase TOC development following injection of 100 mg/l Dextran/Glucose sample standards to reactor 1. Note that all initial concentrations (measured after 30 and 60 sec.) are close to the estimated initial TOC (44 mg/l for Dextran, 40 mg/l for Glucose) suggesting the observed deviation during the initial stages of batches in experiment

| **Init. $M_W$** [kDa] | **Est. $D_f \cdot 10^{10}$** [$m^2/s$] | **Est. $k_{0,f}$** [$g/m^3 \cdot d$] | **Est. $k_{1/2,A}$** [$g/m^3 \cdot d$] | **$\delta k_{1/2,A}$** [$g/m^3 \cdot d$] | **Number of data points** | **$k_{1/2,A}$ Correlation coeff. [$r^2$]** |
|---|---|---|---|---|---|---|
| 0.18 | 2.07 | 261918 | 1.88 | ±0.07 | 8 | 0.9998 |
| 6 | 1.14 | 289218 | 1.51 | ±0.03 | 8 | 0.998 |
| 10.5 | 0.88 | 294565 | 1.34 | ±0.04 | 7 | 0.996 |
| 41.2 | 0.46 | 373043 | 1.08 | ±0.04 | 8 | 0.997 |
| 160 | 0.24 | 383541 | 0.79 | ±0.06 | 8 | 0.990 |
| 473 | 0.144 | 463810 | 0.67 | ±0.05 | 6 | 0.996 |
| 513 | 0.139 | 342205 | 0.57 | ±0.03 | 9 | 0.997 |
| 35000 | 0.019 | 26356 | 0.057 | ±0.009 | 11 | 0.89 |

Table 5-2. Effect of Dextran initial molecular weight on the estimated half order degradation rate coefficient $k_{1/2,A}$, estimated diffusion coefficients, $D_f$, and intrinsic degradation rate coefficient, $k_{0,f}$.

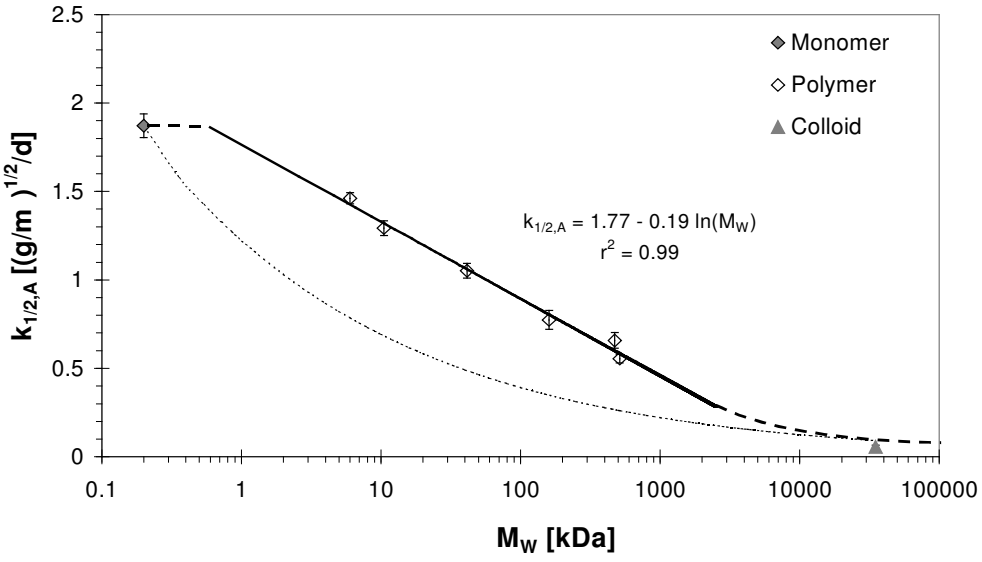


Figure 5-10. Half order hydrolysis rate dependency of initial Dextran molecular weight. Dashed lines (thick) indicate transitions zones between dissolved polymer and colloidal polymer kinetics (1-10 MDa), and the membrane transport system cut off limit (0.6-1 kDa). Regression is estimated for the dissolved polymers. Error bars indicate estimated standard deviations. Dotted line represents a theoretical half order limited rate as defined by equation (5-2) using diffusion coefficients from equation (5-5) and constant degradation kinetics, $k_{0,f}$.

7 to be the result of degradation of sample standards and negligible adsorption. Applying the same mathematical framework as described in section 5.2.2, Table 5-2 lists degradation rate coefficients, estimated uncertainties (from linearised regression analysis) and correlation coefficients for the modelled degradation rates in Figure 5-9. Using the diffusion coefficients estimated from Figure 5-6 (also listed in Table 5-2), half order degradation rate coefficients are estimated by least square approximation between modelled and observed bulk phase TOC concentrations. Figure 5-10 shows the result of the correlation between the half order degradation coefficient and initial molecular weight. Depending on the initial average molecular weight there seems to be three distinct dynamics involved in the Dextran degradation. The first region comprising the monomer (Glucose) up top about 0.8-1 kDa seems to have no effect on $k_{1/2,A}$, while a logarithmic reduction between 6 to 500 kDa fits the data quite well ($r^2 = 0.99$). The one standard from the substrate region above 1 MDa indicate that the degradation follow a different rate, with distinctively different dynamics as the substrate move into the colloidal size spectra (0.05-0.5µm). Also shown is the estimated degradation rate effect on $k_{½,A}$ due to the reduced diffusion coefficients inserted in equation (5-3) keeping the intrinsic degradation rate coefficient, $k_{0,f}$, and $K_S$ constant. As can be seen, the effect of transport rate reductions would suggest a stronger reduction in the observed degradation

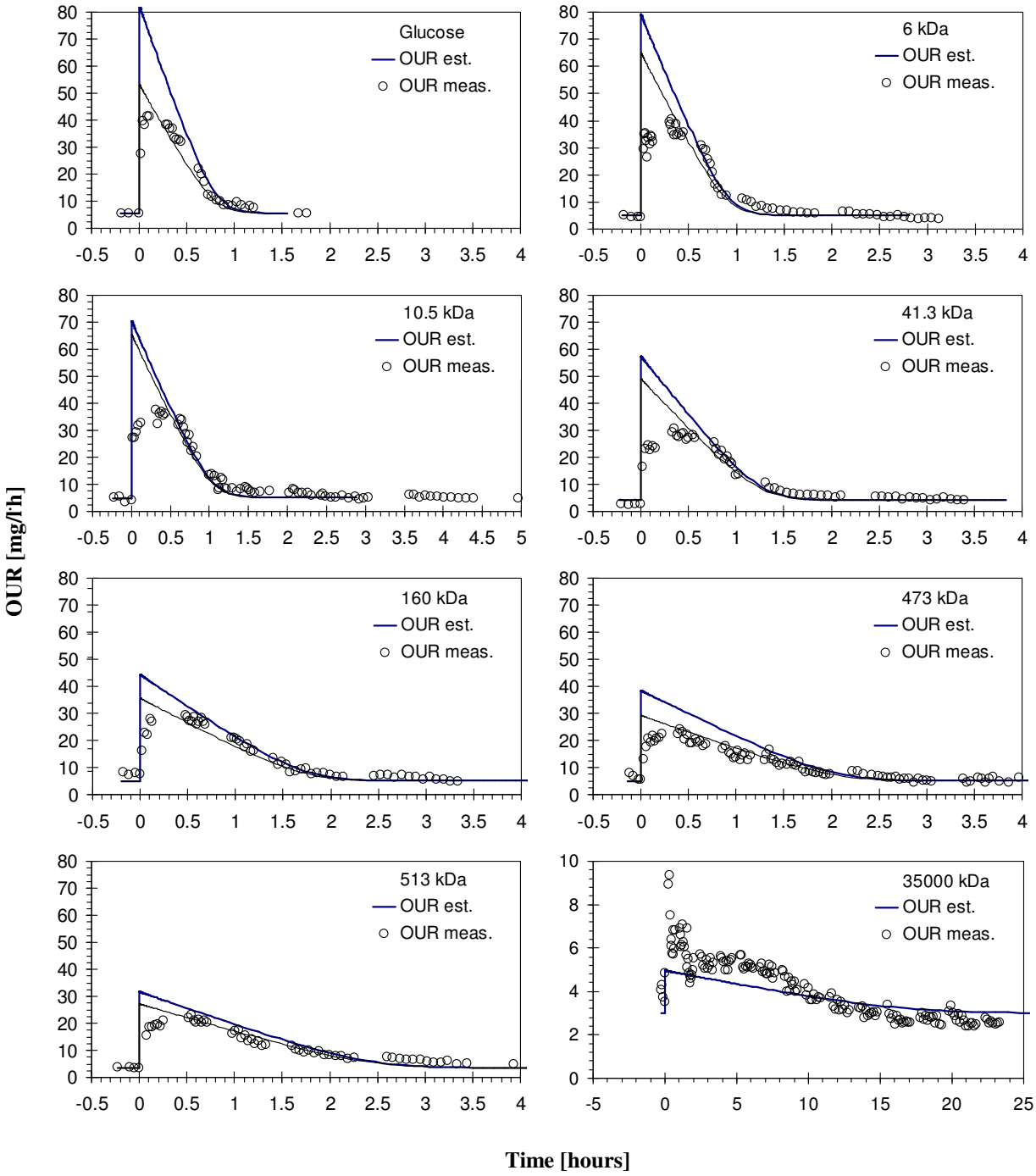


Figure 5-11. Respiration rates during depolymerisation and degradation of Dextran size standards. All plots are shown in similar scales in order to compare OUR for the various size standards, except the colloidal standard due to low degradation rates. Lines represent the modelled OUR based on the half order kinetics (5-2), using the estimated half order removal rate coefficient listed for each standard. The thick (upper) lines represent OUR estimates based on the theoretical stoichiometry, while the thin line show the OUR using the measured stoichiometric coefficient.

rates, indicating that elevated transport dynamics due to intermediate formation and dynamics must be involved.

Respirograms of the same Dextran standards are presented in Figure 5-11. An immediate response can be seen for all standards upon injection except for the blank (pure PBS standard; not included in the figure), again indicating the presence of low molecular weight Dextran in all standards. Apart from the immediate response, all OUR curves resemble a log-normal response similar to experiment 7. The highest OUR response resulted from Glucose injection. Also, final degradation, defined as the time of which background respiration is re-established, was accomplished first for the glucose standard, increasing gradually as the initial Dextran standard size increased. The maximum OUR response followed a systematic trend as substrate initial average molecular weight increased. Peak OUR responses for the injected Dextran standards and Glucose are presented in Figure 5-12. The reduction in net peak response correlates well with the logarithm of the average initial size of the Dextran standard.
As both the total degradation time is shorter, and peak response for the monomer is always higher than the polymer standards, and both factors are changing systematically according to average initial molecular weight, depolymerisation of Dextran is most likely the limiting step during Dextran degradation, validating the methodological assumption underlying the experiments. Figure 5-12 also shows another interesting correlation. The slope of OUR relaxation was defined as the slope of the OUR data as the batch OUR declines back to background respiration levels. This part of the OUR curve represent the most undisturbed part of the batch degradation test, and shows the respirometric response during low concentration of bulk TOC (ref. Figure 5-9). Similar logarithmic correlation between this indicator

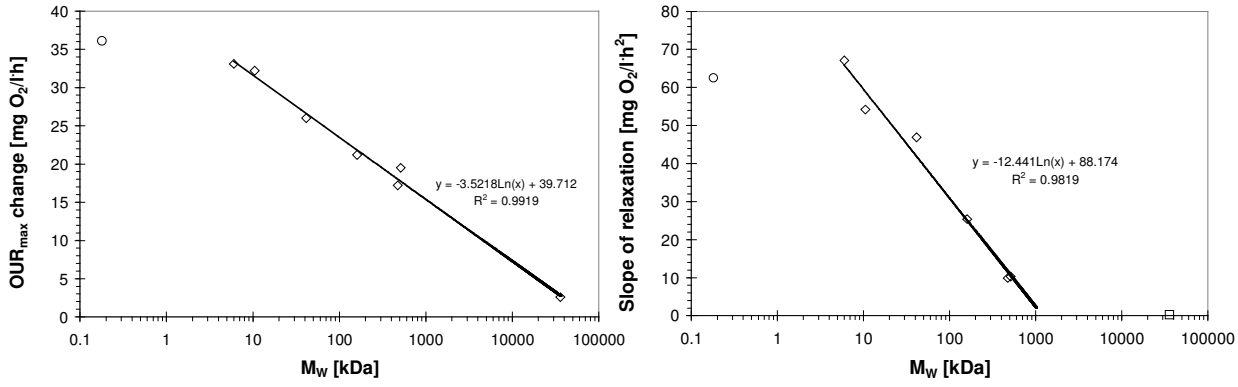


Figure 5-12. OUR change (left) and slope of relaxation plotted against initial molecular weight. The change of OUR was determined by subtracting the peak OUR value from the estimated endogenous respiration, while the slope of relaxation was determined by fitting a linear curve to the relaxation slope of the OUR curve. Correlation estimation relates to dissolved polymers (left) without the colloid particle (35 MDa) for the slope estimation (€, right). Circles represent Glucose.

parameter can be found as seen in the other plots. It may be interpreted as the first order degradation correlation, which is intrinsic in the model used here (Rittmann and McCarty, 2002). The OUR curves (Figure 5-11) also show OUR estimates based on the estimated areal degradation rates (5-2), and adjusted by the theoretical calculated stoichiometry between oxygen and Dextran/Glucose of 0.78 g $O_2$/g TOC. As the model applied does not take diffusive time nor biological time lags into account, OUR is overestimated during the initial phases of each batch. The relaxation back to background respiration levels is, however, relatively well described by the simple direct growth model applied, as the time scale is longer. As for the higher molecular weight standards of experiment 7, the model seems to be more accurate for them, indicating that the lower size standards are transport limited, while the higher are limited by the depolymerisation rate. Figure 5-11 also shows that the estimated OUR curves suggest higher total oxygen consumption than the measured. The stoichiometric coefficient used here is based on theoretical deduction as suggested by Heijnen (1999) by estimation, using thermodynamically based arguments, of the maximum theoretical heterotrophic yield on Glucose. Underlying this approach is the assumptions that maintenance requirements are negligible during growth, and that all assimilated substrate (carbon) is used for energy generation (catabolism) and cell growth (internal anabolism). This yield estimation does not take into account synthesis of EPS or other exogenous microbial products, and it represents the maximum yield. Thus, overestimation of OUR could easily be a result of too high $O_2$ to TOC yield factor. Using a standard trapezoidal integration rule (Kreyszig, 1988), an integration software was designed and programmed in LabView (6.0i), and each OUR diagram from the injected Dextran standards were integrated. Observed yield coefficients were found as the ratio between the sample standard initial TOC and the integrated OUR curve. The result of this estimation will be presented later. Replacing the calculated theoretical yield by the estimated, recalculation of the estimated OUR curve from the bulk phase TOC kinetics resulted in the OUR estimations shown in Figure 5-11, as thin lines. Naturally, these OUR estimations show better fit than the theoretical estimates, and illustrate that using true stoichiometric coefficients enable fairly good estimations of measured OUR based on the degradation kinetics estimated on TOC data.

Before turning to intermediate dynamics, a short evaluation of the assumptions made as part of the modelled data interpretation needs comments. The first assumption made was that the rate of hydrolysis is slower than the rate of mineralisation. This assumption was picked up above, and by comparing hydrolysis product OUR to Dextran OUR it is clear that this

assumption is valid as the OUR on glucose was faster and stronger (peak height) than subsequent Dextran polymers. The other major assumption is that the biofilm is partly penetrated by the sample standards. Harremoës and Henze (2002) suggested using the inverse Thiele modulus, $\Phi$, that represent the governing parameter for diffusional limited reactions in biomass gradients, to calculate the substrate penetration depth as:

$$L_P = \frac{L}{\Phi} = \beta \cdot L = \sqrt{\frac{2 \cdot D_{Xs} \cdot S}{k_{0f}}} \qquad (5\text{-}8)$$

where: $L_P$ is the penetration depth [m], $L$ is the real biofilm thickness [m], $S$ is the bulk phase limiting substrate concentration [g/m$^3$] and $\Phi$ is the Thiele modulus [1]. Assuming substrates are not restricted by the biofilm matrix (a conservative assumption which will overestimate the penetration depth, $D_{Xs} > D_{Xs,film}$), and using the maximum bulk phase concentrations occurring during experiments (i.e. 100 and 200 mg/l for exp. 10 and 7, respectively), estimated diffusion coefficients and zero order intrinsic reaction rates presented in Table 5-1 and Table 5-2 provides maximum penetration depths presented in Figure 5-13. Biofilm thickness was determined throughout experiment 5, and at the beginning of experiment 7 by microscopic determination (Bakke and Olsson, 1986) of removable coupons from the rotor surface. Comparison between biomass areal density on slides and the outer wall (the static cylinder) at the end of experiment 11 indicated, however, that the biofilm on the slides were thinner and more heterogeneous than the biofilms on the other surfaces inside the Rototorque. The optical thickness was found to be about 200 µm at the start of experiment 7. Effective biofilm thickness, as defined by Harremoës and Henze (2002) was determined by adding 100 mg/l Glucose (initial reactor concentration) to both reactors prior to experiment 7, and measuring OUR and bulk $O_2$ as the reactor turned anaerobic. The effective biofilm thickness is given as:

$$L_E = \frac{2 \cdot D_{O_2} \cdot S_{O_2}}{OUR_{A,max}} \qquad (5\text{-}9)$$

where: $S_{O2}$ is the limiting bulk phase $O_2$ concentration, $OUR_{A,max}$ is the maximum (zero order) OUR [mg $O_2$/m$^{2\cdot}$h]. The right panel of Figure 5-13 shows the transition from zero to half order kinetics defining the bulk phase $O_2$ concentration used for determination of the effective biofilm thickness. The areal removal rate may be found by dividing the $OUR_{max}$ by the

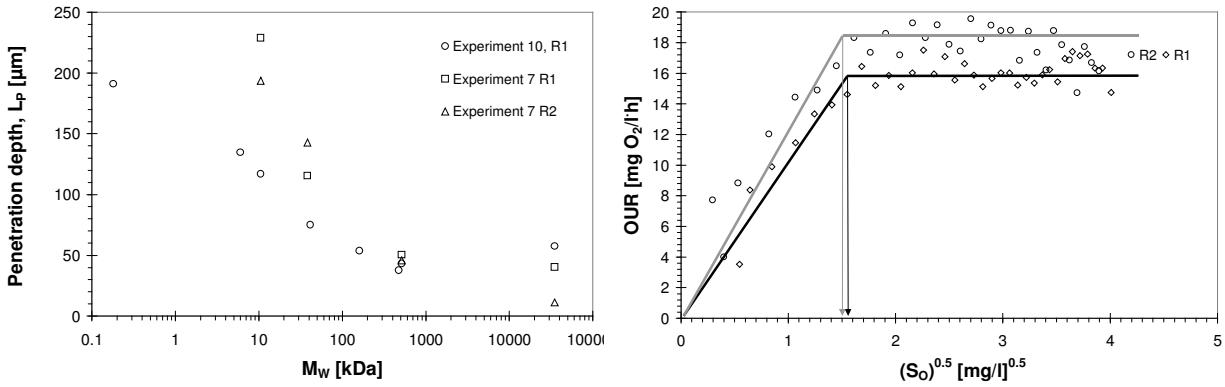


Figure 5-13. Estimated maximum penetration depths for $R_1$ and $R_2$ in experiment 7, and for $R_1$ in experiment 10 (left). Right panel show the determination of the effective thickness defined as the biofilm thickness estimated at the transition from 0. to ½ order kinetics.

specific area, *a*, and the tabulated diffusion coefficients in water ($2.1 \cdot 10^{-4}$ $m^2$/d, Cussler, 1984) compensated for biofilm diffusion resistance, ($0.58 \cdot D_{liq}$, Stewart, 2003a). The effective biofilm thickness was found to be 378 and 310 µm for $R_1$ and $R_2$, respectively, indicating that the optical density on coupons underestimated the biofilm thickness with as much as 89 %, most likely due to hydrodynamic shear force differences at the coupon surface, caused by small edges immediately upstream the coupon slide. It is therefore likely that the partly penetration assumption holds for all polymer standards, but that the Glucose sample standard could be close to fully penetrated in some parts of the biofilm, at least during the initial stages of the Glucose batch. However, as most of the rate estimation was conducted during lower batch concentrations (see Figure 5-9), the possible effect on the estimated kinetics is negligible. The third assumption of the batch experiments, that the biofilm was fully oxygen penetrated, was evaluated by assessing the Thiele modulus ratio of oxygen and substrate (Harremoës and Henze, 2002). The limiting oxygen concentration (bulk phase oxygen concentration where oxygen becomes limiting) may be determined by:

$$S_{O_2,lim} = \frac{D_S \cdot S}{D_{O_2} \cdot Y_{S/O_2}} \qquad (5\text{-}10)$$

where: $Y_{S/O2}$ is the Glucose to oxygen stoichiometric coefficient and *S* is the bulk substrate concentration [g/$m^3$]. For experiment 7 the limiting oxygen concentration during maximum bulk phase substrate concentration was 2.3 mg/l (for 10 kDa) or 21 mg/l for the monomer

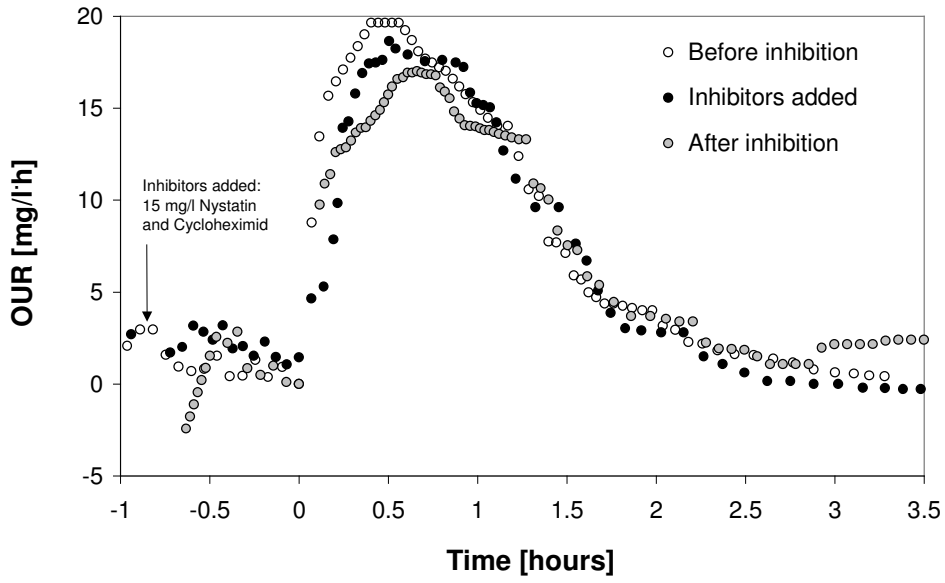


Figure 5-14. Eukaryotic inhibition experiment following the last batch injection of experiment 10 to $R_1$. Estimated OUR's are zeroed (by subtracting the lowest OUR before injection) for comparison.

(Glucose), whereas the limiting oxygen concentration for experiment 10 was 10.5 mg/l (based on initial Glucose concentration). As the oxygen minimum set point during these experiments was set at 22 mg/l, oxygen was never limiting the degradation of carbon sources during any of the batch experiments performed.

Figure 5-14 shows the result of adding eukaryotic inhibitors (Nystatin and Cycloheximid, Lee and Welander, 1994) to $R_1$ following experiment 10 batches. Inhibitors were added about 45 min before injection of 100 mg/l Dextran 160 kDa, and the batch were left for 19 hours. Injection of the same Dextran standard before (4 hours) and after (19 hours) did not significantly reduce OUR, indicating dominant bacterial respiration.

## 5.3 Intermediate formation and transport

Intermediate dynamics were studied in experiment 7 and 10. In addition, separate batch studies using pure enzymes and biofilm coupon samples were conducted. The main hypothesis to be evaluated is accumulation of intermediates in the bulk phase, and characterisation of size distribution during degradation. Due to the uncertainty and difficulties with slope calibration (see appendix 9.3), all results in this section is reported as refractive index output signal [mV] or units [nRIU].

### 5.3.1 Pure enzymes studies

Three purified enzymes with cited activity against Dextran were evaluated for degradation intermediate dynamics. Several sample standards were incubated in Pyrex vials with variable Dextranase (3.2.1.11), Oligo-1,6 Glucosidase (3.2.1.10, Isomaltase) and α-Glucosidase (3.2.1.20) activity. All activities are reported as enzyme activity units, U; for Dextranase: 1 mmole Isomaltose/min (substrate: 500 kDa Dextran, Fluka 31392 at pH 5.5 and T = 50°C), and for α-Glucosidase and Oligo-1,6 Glucosidase: activity as 2 µmole D-Glucose/min from Isomaltose and Maltose at pH 6.0 and 6.8, respectively (T=25°C).

No activity against Dextran was observed for Isomaltase. Figure 5-15 shows Dextranase depolymerisation of 250 mg/l initial concentration of 160m kDa Dextran at various initial Dextranase activity. Upper left panel show the result of 0.03 mU, right panel 3 mU, and lower panels the action of 0.8 and 0.6 mU (left, right). The first batch (0.03 mU) suggests

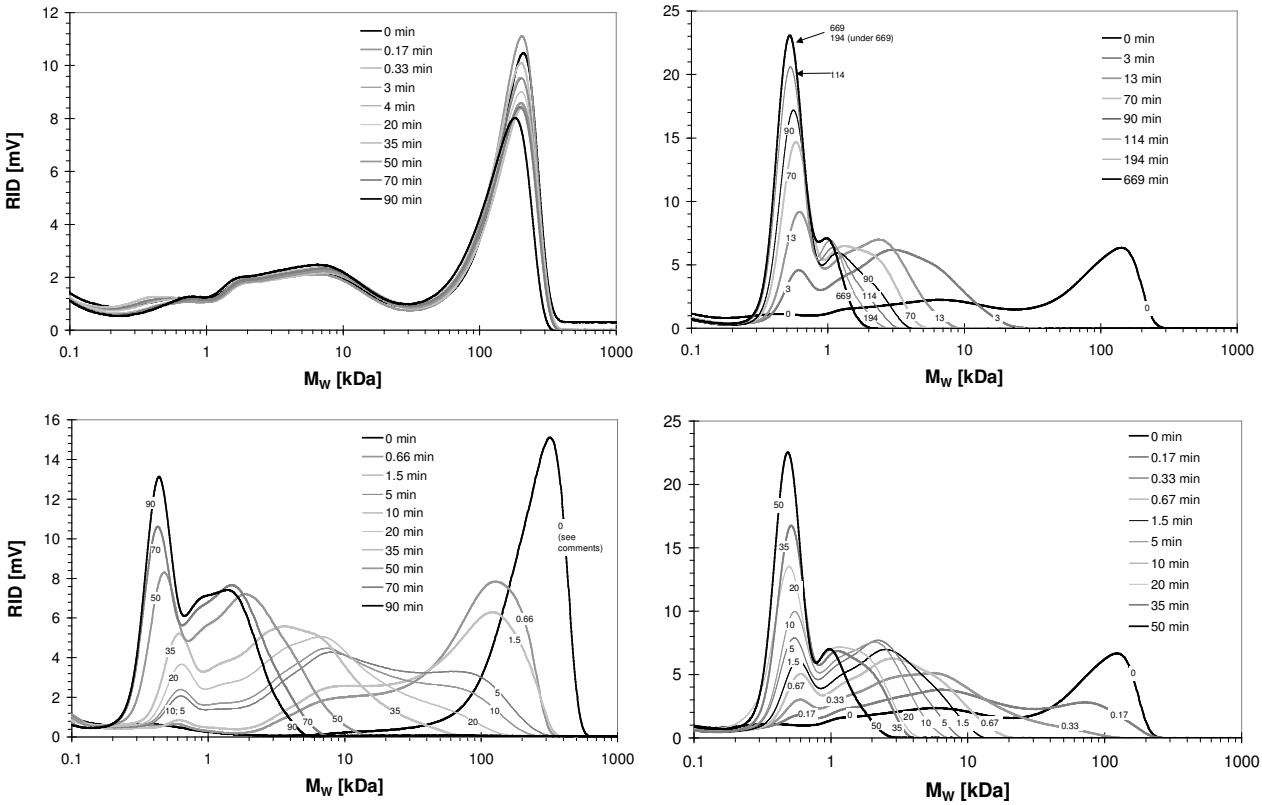


Figure 5-15. Intermediate dynamics during Dextranase depolymerisation of 160 kDa 250 mg/l initial concentration. Upper left panel show degradation by 0.03 mU Dextranase, while the upper right show the same by 3 mU enzyme. Lower panels show the action by 0.8 (left) and 0.6 mU and intermediate dynamics at high rate sampling.

Dextranase shortage, as only about 25% of the original 160 kDa peak is depolymerised within 1.5 hours. Increasing the initial enzyme concentration by 100 resulted in total depolymerisation of the initial peak within 3 minutes (Figure 5-15, upper right panel). No intermediates in the 10-100 kDa range appeared to occur, but peaks around 1 kDa accumulated in most samples. The final product accumulated at 0.514 kDa, very close to Isomaltotriose (0.504 kDa). In order to evaluate depolymerisation intermediates in the 10-100 kDa range, additional experiments were conducted at higher sampling frequencies. Lower panels (Figure 5-15) show that intermediates in all size classes were produced before being further depolymerised into lower fragments, again accumulating around 1 kDa. Most of this intermediate range dynamics was over within the first 10 -20 min. Pressure fluctuations during analysis of the 0.8 mU batch samples caused the initial peak to be skewed towards the higher $M_W$ range. This did not affect the other peaks. From the data in Figure 5-15 it is hard to conclude how the effect of initial Dextranase changed the kinetics. Comparing the to panels to the right (3 and 0.6 mU) there seems to be no major kinetic effect of lowering the enzyme

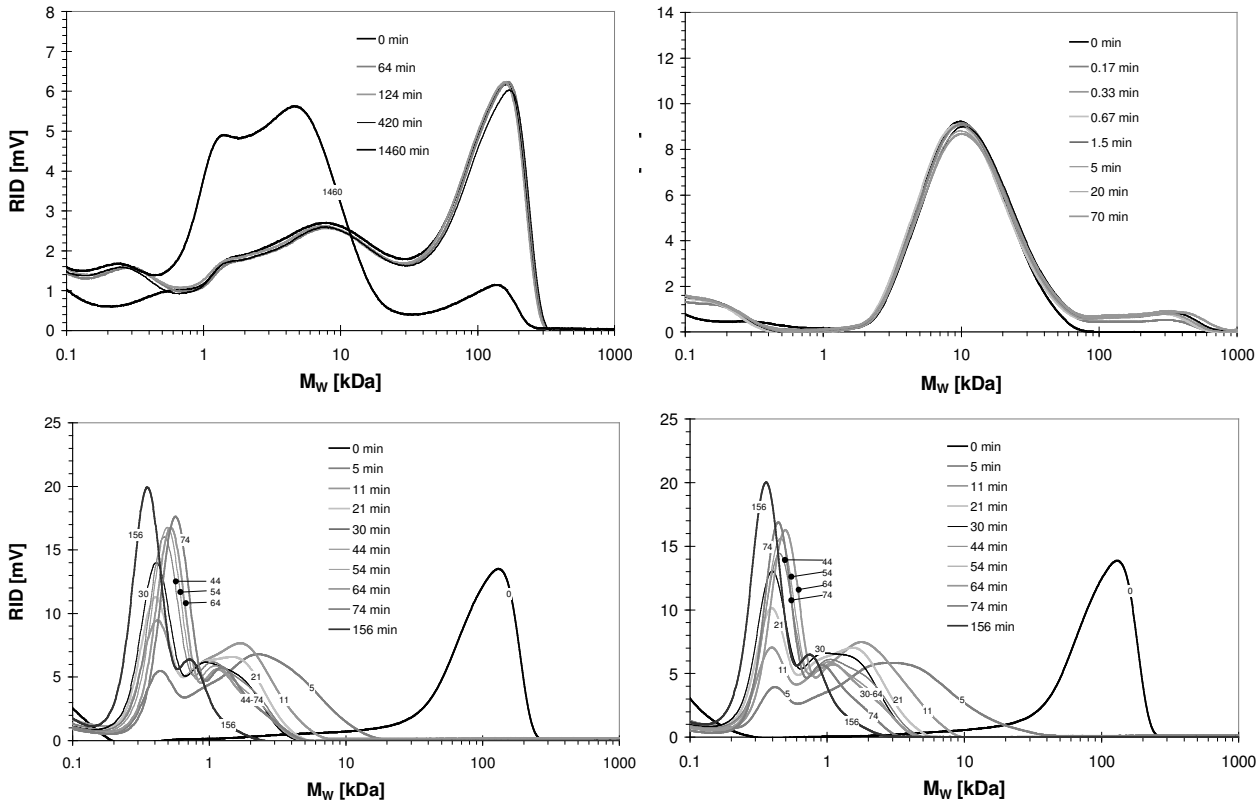


Figure 5-16. α-Glucosidase activity (3.7mU) against 160 kDa Dextran at 250 mg/l initial concentration (upper left), and Oligo-1,6-Glucosidase (3.75 mU) against 250 mg/l initial 12 kDa Dextran. Lower left panel show depolymerisation by 3.6 mU Dextranase and lower right the combined action of 3.6 mU Dextranase and 3.75 mU α-Glucosidase.

concentration by a factor of 5, an unexpected result it is hard to explain. Also, the slightly higher Dextranase concentration of the 0.8 mU batch (lower left) did not seem to cause the depolymerisation of the initial peak, nor intermediates, to occur faster. On the contrary, the intermediate peaks seem to show up later than the 0.6 mU (lower right). This can only be explained by pipetting errors and analytical variabilities. Interpretation of Figure 5-15 should therefore only be limited to the relative distributions of intermediates during depolymerisation of the model system, Dextranase and 160 kDa Dextran.

Figure 5-16 show α-Glucosidase activity against 160 kDa Dextran, and Oligo-1,6-Glucosidase incubated with 12 kDa. No α-Glucosidase activity can be detected the first hours, however, depolymerisation occurred after 24 hours. Depolymerisation was very similar for both 0.6 and 3.75 mU of enzyme (0.6 mU not shown), indicating that the depolymerisation detected is probably not caused by the α-Glucosidase, but could possibly be related to contamination. This enzyme is exo-acting and it is therefore suspicious that only medium range intermediates occurred, and no mono- or oligomeric products were detected. The intermediate range signal detected in all initial pure enzyme batches (Figure 5-15 and Figure 5-16) could result from limited contamination of the sample standard, however, it did not interfere with the high enzyme activity batches as the initial enzyme activity was comparably high. Oligo-1,6-Glucosidase activity was also very low. The low increase at around 0.1-0.2 kDa during the initial minute of the experiment is probably due to analytical variations as no decrease in the 12 kDa peak is found, and peak increase stop after 10 seconds.

Figure 5-16 also show results from a pure Dextranase and a combined Dextranase-α-Glucosidase batch (lower panels). No effect of additional α-Glucosidase activity could be detected, thus, depolymerisation could only be attributed to Dextranase. The end products of these batches were dominated by a 0.348 peak (Isomaltose at 342) and Isomaltotriose at 0.504 kDa, with preceding temporal accumulation between 1 and 2 kDa. One would expect exo-activity to bring the low $M_W$ product peak towards Glucose (0.18 kDa), but that did not occur, suggesting low α-Glucosidase activity also against Isomaltoses.

### 5.3.2 Coupon experiments (Exp. 6)

Batch tests in 60 ml Pyrex culture tubes were used to evaluate depolymerisation and mineralisation of products using biofilm samples from $R_1$ during the regrowth period between experiment 5 and 7. Experiment 6 involved evaluating three distinct biofilms (thin, medium

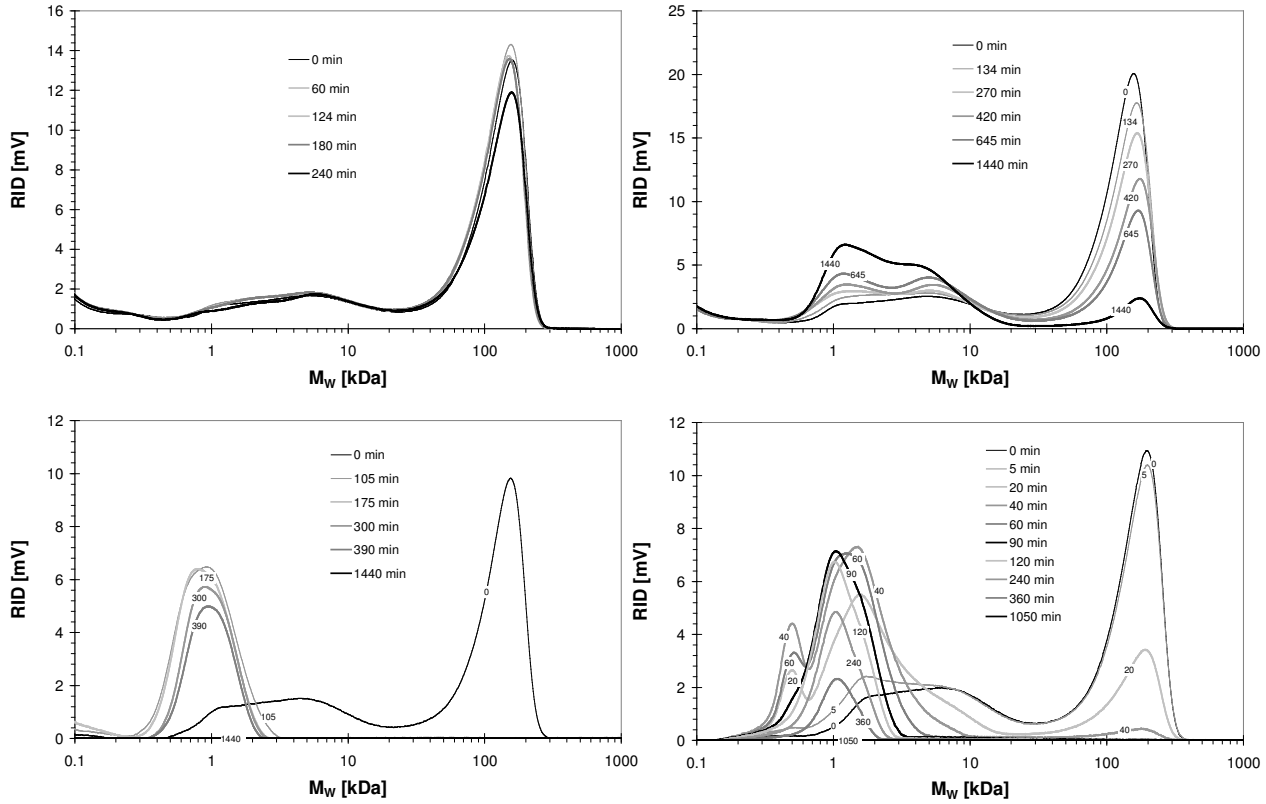


Figure 5-17. Pyrex batch tests using biofilm slides from $R_1$ dropped into 250 mg/l 160 kDa Dextran. Upper left is thin biofilm (0.7 g/m$^2$), upper right medium biofilm (3.7 g/m$^2$), lower plates show thick biofilms (5.2 g/m$^2$), one with high sampling rate (right) indicating details of intermediate formation. The high initial concentration in the medium biofilm batch is probably due to pipetting error. Termination sample was used for background correction for the thick biofilm tests.

and thick) and their effect on depolymerisation dynamics. $R_1$ had been operated on 20 mg/l inlet 160 kDa continuous operation for 15 hours, after thickness estimation using strong yeast extract and Glucose (500 mg/l, initial). Detachment/washout events were conducted daily. Figure 5-17 show the results of Pyrex batch experiments of thin (0.7 g/m$^2$, 0-10 µm), medium thick (3.7 g/m$^2$, ~ 60 µm) and thick biofilms (5.7 g/m$^2$, 150 µm) after slides were dropped into predefined media containing 250 mg/l Dextran 160 kDa. Biomass density seems to have a great effect upon depolymerisation of the initial polymer as hardly any reduction can be seen after 4 hours of the thin biofilm, and only modest amount being converted in the medium sized; complete conversion can be seen for the thick biofilm within 1 - 1.5 hours. Complete degradation was only observed for the thick biofilms, however, that is most likely due to the duration of the observations, rather than incomplete conversion. All samples (apart from the thin biofilm) showed bulk phase accumulation of intermediates in the lower $M_W$ range (below 10 kDa), and some interesting dynamics was observed for the thick biofilm shown in the right

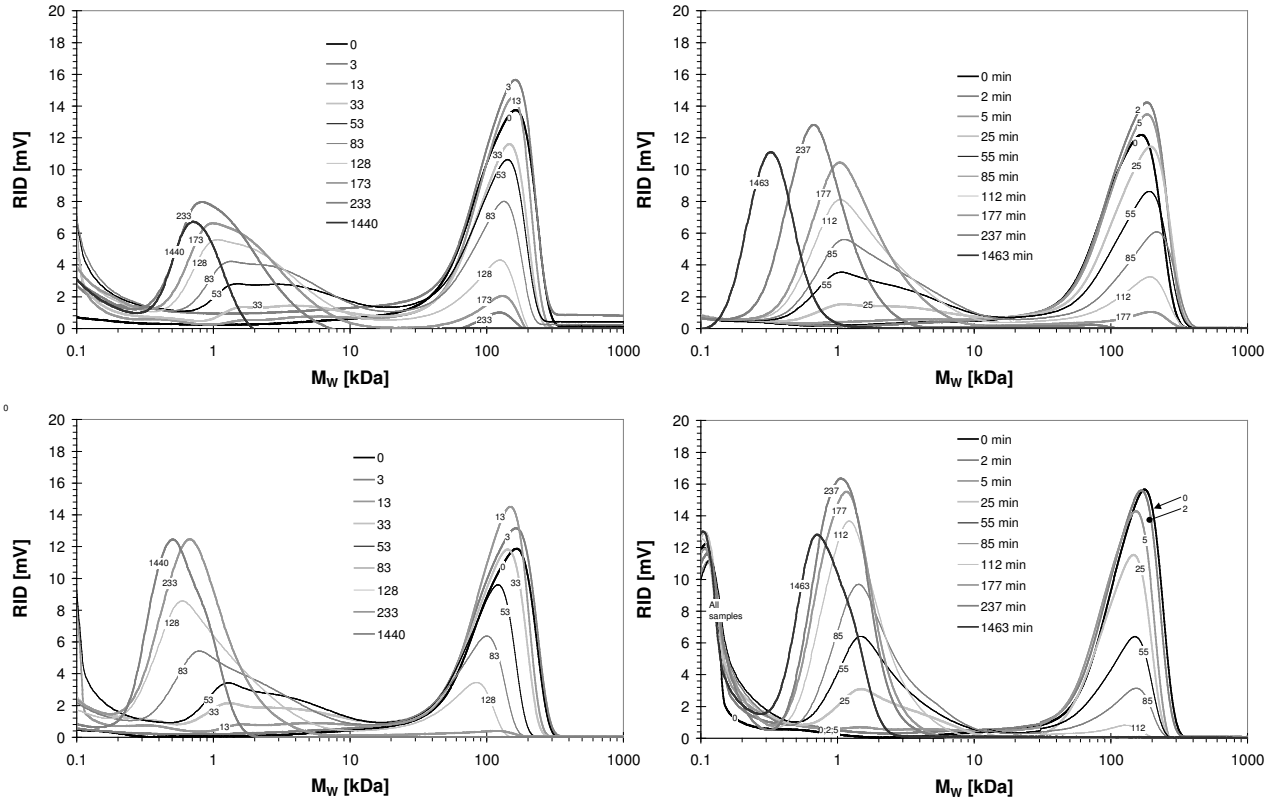


Figure 5-18. Results from Azide inactivation experiments showing Pyrex batch tests of 160 kDa Dextran 250 mg/l initial concentration of active growing biofilm (upper left), active but starved (upper right), inactivated growing (lower left) and inactivated starved biofilm (lower right). Azide eluted around 0.1 kDa and may be seen as a peak in the lower left panel.

lower panel of Figure 5-17. Following incubation, short chain polymers starts to accumulate immediately. No intermediates in the 10-100 kDa range seem to occur at significant levels. After about 20 minutes, a peak can be seen at 0.5 kDa, however, it disappears after 90 minutes appearing to go through a dynamic peak formation around 40 minutes. This peak suggests temporal accumulation of assimilable Isomaltose to Isomaltotetraose, and could indicate rapid surface depolymerisation combined with a lag-phase growth response and/or back diffusion to the bulk. The fact that no low $M_W$ intermediates appear during the rest of that batch indicates direct mineralisation or exo-oligo - Glucosidase activity. All samples also show consistent accumulation of intermediates in the lower kDa range (0.5 - 2 kDa). Another interesting detail is the disappearance of all intermediates above 2-3 kDa in the initial and 5 min sample shown in the lower right panel of Figure 5-17. Temporary accumulation below, and disappearance above this limit seems to indicate a shift in dynamics in this rather short range. The reason for that is not clear. Apart from the obvious mineralisation, the main difference between these experiments and the Dextranase experiments is that intermediate range (3-100 kDa) intermediates did not appear in any of the Pyrex batches. Isomaltotriose, the main product of

the pure enzyme studies, did occur as a temporal intermediate, but disappeared after about 60 min. This point towards dominating Dextranase activity, and that potential oligo-Glucosidase degradation occurred after induction, or not at all. Pyrex glass experiments were also carried out by comparing growing (active), starved and $NaN_3$ inactivated biofilms. The objective for these experiments was to see if inactivation by Azide would result in bulk phase accumulation of the assimilated depolymerisation product. By comparing active and inactivated samples this should appear in the bulk. Also, growth phase effects were evaluated by comparing kinetics and intermediate dynamics of biofilms in the exponential and endogenous growth phase (growing and starved biofilms). Results of inactivation experiments are presented in Figure 5-18. Due to pressure variations during analysis, resulting chromatograms were not aligned (using the buffer signal as internal standard reference), and had to be manually aligned by moving each sample peak according to the buffer elution peak. This caused some of the early peaks to appear slightly off the initial peak, and may have led to some dislocation of the accumulating peaks around 1 kDa. Still, as for the other Pyrex batches, accumulation of intermediates occurred around 1 kDa, and inactivation seemed to enhance this for both the active and starved biofilm. The starved biofilm showed the same depolymerisation rate as the active, but consumption of products was slower, and low $M_W$ intermediates accumulated more. Similar trend could be observed for the Azide treated biofilms. Comparing the growing biofilm batches, inactivation seemed to cause accumulation of oligo Dextrans, especially the low $M_W$'s at 0.5-1 kDa. This again coincides with the Isomaltotriose to Isomaltopentaose oligomers and could indicate that active biofilms assimilate these Dextranase products, or that growth linked induction of oligo-Glucosidase activity cease during inactivation.

### 5.3.3 Rototorque OUR experiments

Intermediate dynamics were followed during the OUR experiments reported in section 5.2.2 and 5.2.3 (Experiment 7 an 10). Figure 5-19 show intermediate dynamics in $R_1$ during the OUR experiment reported in section 5.2.2. Intermediates over the entire range appeared in the bulk phase for the low $M_W$ standards, while these did not occur for the 160 and 513 kDa. The lack of 10 - 100 kDa intermediates for the high $M_W$ batches is probably not due to inappropriate sampling frequency, as intermediate simultaneously occur at low $M_w$ and under the original peak. For all standards, oligomers accumulation to significant concentrations was

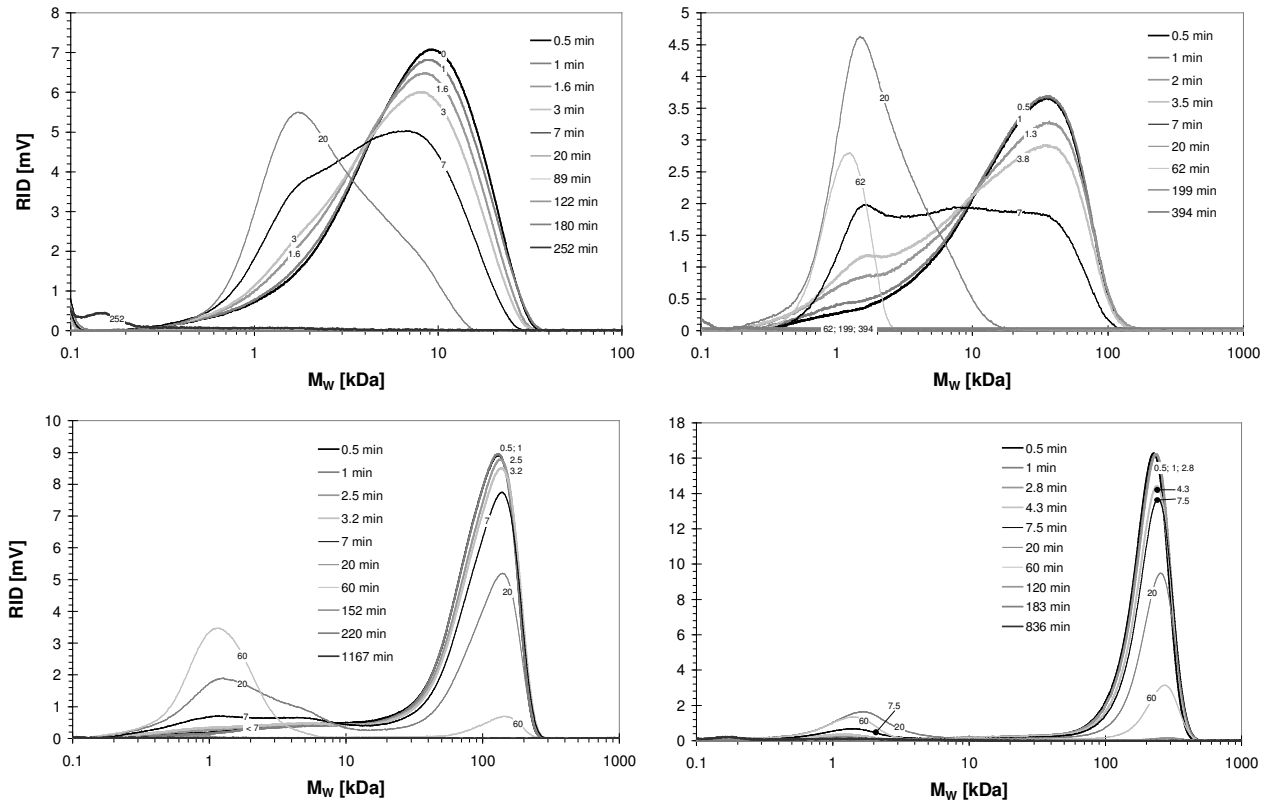


Figure 5-19. Intermediate dynamics in $R_1$ during OUR batch experiments as part of experiment 7 (section 5.2.2). Upper left to lower right show 10.5, 38.1, 160 and 513 kDa Dextran, initial concentration was 200 mg/l.

observed, very similar to the Pyrex batch coupon and pure enzymes results. By observing iso-time lines, a certain impression of the rate of polymer change can be seen. This is consistent with the observed OUR and TOC time series reported above, and support the kinetic implications inferred from Figure 5-7 and Figure 5-12. The 38.1 kDa injection deviates, however, to some extent as the 7 minute isotime line is skewed more too the lower $M_W$ intermediates as for the 10.5 kDa standard. That might be due to the fact that the 38.1 kDa standard was the last injection made during this campaign, and that growth may have enhanced the rate of the intermediate dynamics by higher biomass. Generally, the higher the molecular weight of the initial standard, the lower accumulation of bulk phase intermediates. That might be due to sampling intensity, but could also indicate rate dependant back diffusion or adsorption (i.e. the rate of low $M_W$ production is high enough to cause local intermediate accumulation that also increase back diffusion and limit adsorption). Figure 5-20 presents the same data for $R_2$, showing the same pattern and behaviour as observed in $R_1$. Here the kinetic behaviour is more consistent with the rate inferences made in section 3.3, and also consistent with the TOC and OUR observations (see Table 5-1, Table 5-2 and Figure 5-7). $R_2$ showed higher depolymerisation and mineralisation kinetics, probably due to biomass differences

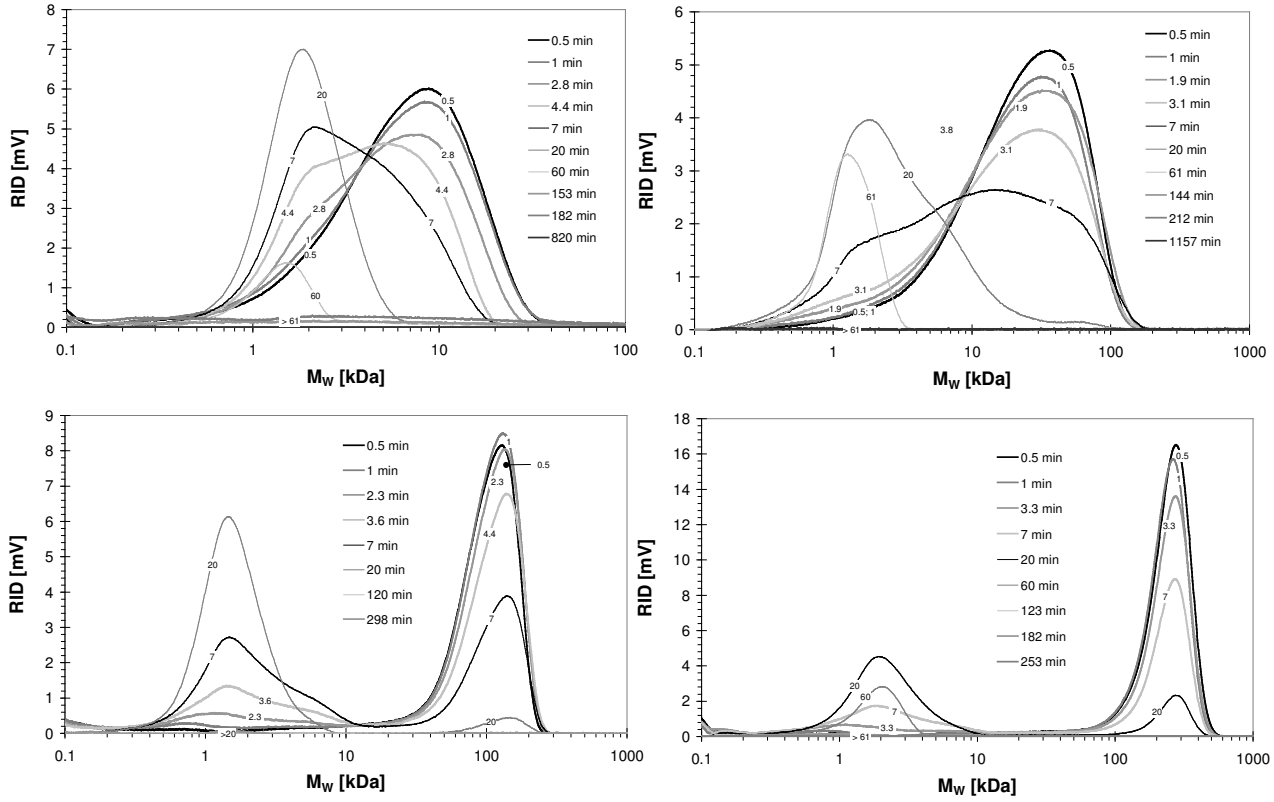


Figure 5-20. Intermediate dynamics in $R_2$ during OUR batch experiments as part of experiment 7 (section 5.2.2). Upper left to lower right show 10.5, 38.1, 160 and 513 kDa Dextran, initial concentration was 200 mg/l.

(with reference to the observed strong implications of biomass reported in section 5.3.2). In fact, comparison of estimated $k_{0f}$ coefficients (Table 5-1), reveals that $R_2$ was faster than $R_1$ for all standards except the unexpected rapid depolymerisation of 38.1 kDa in $R_1$. That also suggest that 38.1 kDa in $R_1$ should be considered as an outlayer during comparison of intermediate dynamics results and kinetic interpretation. Intermediate formation results from experiment 10 are presented in Figure 5-21. Lack of time resolution is due to less frequent sampling, as intermediate formation was not the main objective of this experiment. Low levels of intermediates appeared, but that could be the result of too low initial sampling rate, or could be attributed to the reduced initial concentration, as compared to experiment 7 results. Some accumulation was, however, detected, this time around 0.5 kDa (Isomaltotriose), similar to the pure enzyme accumulation observed in section 5.3.1. Comparison of the 35-60 min distribution curves indicates the same kinetic effect on depolymerisation of the initial peak as observed in experiment 7. The higher the initial $M_W$ standard is, the lower the initial peak reduction rate appears. This demonstrates consistency towards the TOC and OUR curves in section 5.2.3., and the kinetic relation presented in Figure 5-10.

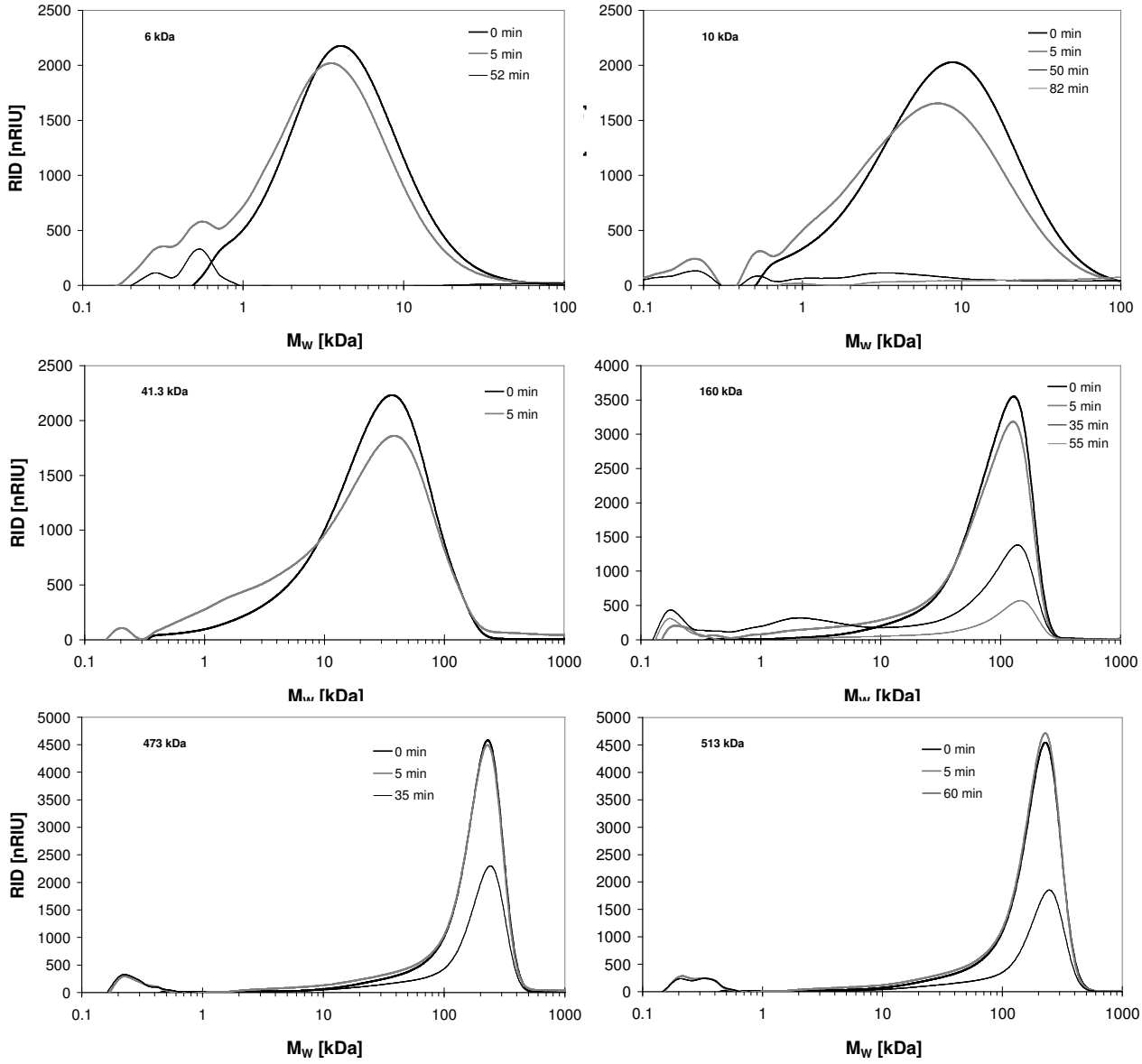


Figure 5-21. Intermediate formation in $R_1$ during OUR experiments of the Rototorque depolymerisation studies reported in section 5.2.3. Initial concentration was 100 mg/l, and initial Dextran standards are indicated. Signals have been background corrected by Blank injection.

## 5.4 Location of depolymerisation

Dextranase and α-Glucosidase assays were used to directly assess location of active enzymes in the biofilm reactor systems during experiment 8 (washout experiment). The results of Dextranase (endo-activity) assay of samples taken directly from the biofilm reactor bulk, void phase samples prepared by washing biofilm coupons with buffer, native biofilm samples and fractionated biofilm samples into loosely matrix bound and matrix bound (cell attached), is

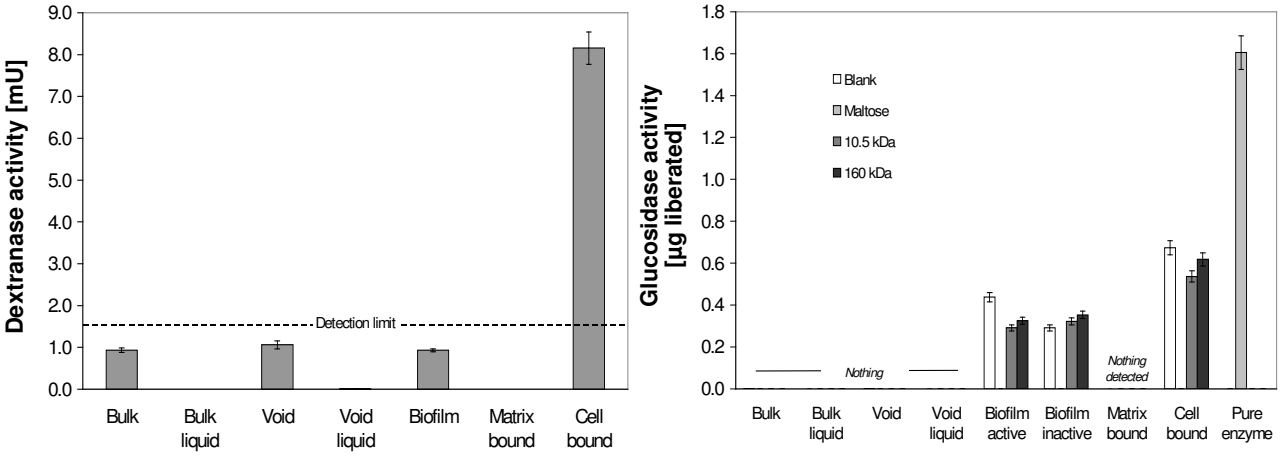


Figure 5-22. Dextranase (left) and α-Glucosidase activity (right) found in sub-compartments of the biofilm on coupons sampled from the Rototorque during experiment 8.

shown in Figure 5-22. Significant (i.e. over the detection limit) Dextranase activity was only found in the pellet after centrifugation of re-suspended biofilm sub-samples from the biofilm coupons. This indicates dominated cell bound dextranase activity (endo-depolymerisation). Surprisingly, the active un-fractionated biofilm sample did not show Dextranase activity similar to the pellet extract. That is probably due to less biomass on the slide used for this particular assay, and up-concentration during centrifugation. α-Glucosidase was detected in the cell containing biofilm fractions, the intact biofilm and the cellular extract. However, addition of Dextran did not increase the rate of Glucose formation, but actually decreased it. This result is probably due to residual glycosides in the freshly sampled biofilm. Reduction upon Dextran addition could indicate non-productive binding between α- Glucosidase and the Dextran substrate. Inactivation by Azide did not seem to affect the Glucose liberation rate. Pure α-Glucosidase was run in parallel as a method check, and it only showed significant activity against Maltose indicating that α-Glucosidase was active during testing. This strongly suggests that α-Glucosidase do not act upon α-1,6 bonds of terminal glucosidic linkages of Dextran, supporting the pure enzyme intermediate results in section 5.3.1 (Figure 5-16). Database information of this enzyme indicates activity against Dextran (as α-Glucosidase are known to depolymerise Starch and Oligo-Dextrans)[11], however, no direct evidence of activity on larger Dextrans is reported.

[11] A range of references is given in BRENDA (http://www.brenda.uni-koeln.de) under the 3.2.1.20 entry.

## 5.5 Degradation rate of wastewater particles

The sequencing batch operation of the tubular reactor system meant that a slightly different approach for data interpretation had to be used. Reactor concentration of extracted wastewater particles, $X_S$, was estimated by subtracting the amount TOC lost during each bulk phase refreshment, and the amount respired estimated from the OUR. The equation used for reactor $X_S$ estimation was:

$$X_S(t_n) = X_S(t_{n-1}) - \frac{\Delta O_2(t_n)}{Y_{O_2/X_S}} - X_{S_{out}}(t_n) \quad (5\text{-}11)$$

where: $X_S$ is the reactor concentration at $t_n$ and $t_{n-1}$, $\Delta O_2$ is the oxygen consumption at $t_n$, $Y_{O2/Xs}$ is the stoichiometric consumption of $O_2$ per TOC consumed and $X_{S,out}$ is the TOC in the drained bulk at time $t_n$. The oxygen consumption was calculated by trapezoidal integration of the OUR curve (Kreysig, 1990), as:

$$\Delta O_2(t_n) = \frac{OUR(t_n) + OUR(t_{n-1})}{2} \cdot (t_n - t_{n-1}) \quad (5\text{-}12)$$

The mass balance for the areal removal rate of particulate wastewater is given by:

$$V \cdot \frac{dX_s}{dt} = -r_A \cdot A_f \quad (5\text{-}13)$$

Under the assumption that depolymerisation is the rate limiting process during degradation, we may infer that the areal removal rate of depolymerisation products is first order in substrate, and may be treated as constant (pseudo steady state approximation):

$$V \frac{dS}{dt} = -k_{1,A} \cdot S \cdot A + r_A \cdot A \approx 0 \quad (5\text{-}14)$$

Bulk phase oxygen utilisation rate, as measured, may then be represented by:

$$OUR = -\frac{dO_2}{dt} = k_{1,A} \cdot S \cdot Y_{O_2/X_S} \cdot \frac{A}{V} + OUR_{end} \quad (5\text{-}15)$$

which, by insertion of (5-13) gives the areal depolymerisation rate as:

$$r_A = \frac{OUR - OUR_{end}}{Y_{O_2/X_S} \cdot a} \qquad (5\text{-}16)$$

where: $a$ is the area to surface ratio (A/V) [1/m] and $Y_{O2/Xs}$ is the stoichiometric oxygen consumption per mass unit POM consumed [g $O_2$/g $X_S$]. The stoichiometric coefficient may be determined from typical wastewater substrate stoichiometries. Assuming the substrate yield to be 0.5 g wastewater substrate ($C_{18}H_{19}O_9N$) (Henze, 2002), the oxygen consumption per wastewater substrate (POM) consumed is 1.49 g $O_2$/g POM, or 3.05 g $O_2$/g $TOC_{POM}$. By plotting $r_A$ against the estimated bulk phase POM data, kinetics and kinetic parameters may be determined. Figure 5-23 shows the time course of the preparative stages and the depolymerisation experiment on extracted wastewater particles from Knardalstrand WWTP, Porsgrunn, Norway, and the depolymerisation rate (here denoted as hydrolysis rate, $r_{h,A}$) plotted against the estimated total reactor (bulk and adsorbed) POM concentration. Assuming variable half order kinetics as used in section 5.2.2, equation (5-4), the half order variable depolymerisation/degradation rate coefficient may be determined. From Figure 5-23 (right) best fit by least squares approximation for the half order model adopts first order properties as the $K_S$ coefficient becomes very high (for the fit shown $K_S$ was limited

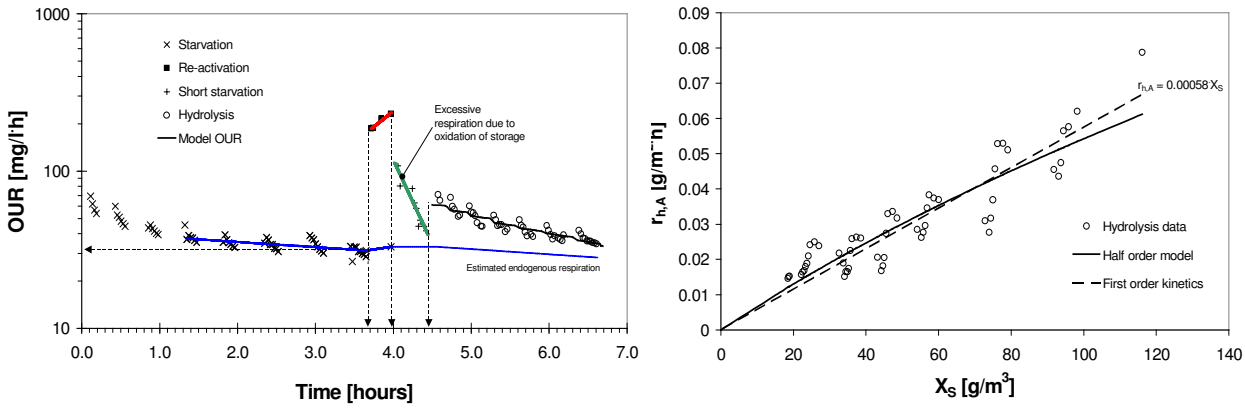


Figure 5-23. OUR during wastewater depolymerisation experiment (left) and determined relation between reactor POM (as TOC) and estimated (based on measured OUR) depolymerisation (here: hydrolysis) rate. Model estimation using the half order model described in section 5.2.2, and simple first order kinetics are shown. Lines in OUR diagram represent estimated endogenous-, reactivation and short starvation respiration, and respiration curve during POM depolymerisation and mineralisation.

to 100 mg TOC/l). The half order rate coefficient for this approximation is 0.01 $(g/m)^{1/2}/d$ which is half of the estimated 35 MDa Dextran degradation coefficient found in experiment 10 (see Figure 5-10 and Table 5-2). Anticipating fist order kinetics gives an areal first order removal rate coefficient, $k_{1,A}$ of 0.58 mm/h, or 0.014 m/d. By multiplying this with the area to surface ratio (a), one may obtain a rough estimate for the volumetric first order removal rate coefficient that may be compared to activated sludge literature values. A ratio of 333 $m^2/m^3$ gives a first order volumetric removal coefficient of 4.6 1/d, which is intermediate of literature values for hydrolytic first order coefficients for dissolved solids (i.e. particle diameters < 0.45 µm) of 3-20 1/d, and suspended solids of 0.6-1.4 1/d (Henze, 2002). The relative distributions of POM before and after the accumulation/adsorption phase of the experiment were determined by Laser diffraction analysis, and results are presented in Figure 5-24. Adsorption of primarily lower range POM seems to be the predominant mechanism as the curve moves towards the higher size fractions with a slightly tighter distribution. Interestingly, low µm POM seems to accumulate during the adsorption, indicating fragmentation or even microbial depolymerisation/degradation, or detached biomass during the anaerobic 30 minutes of adsorption.

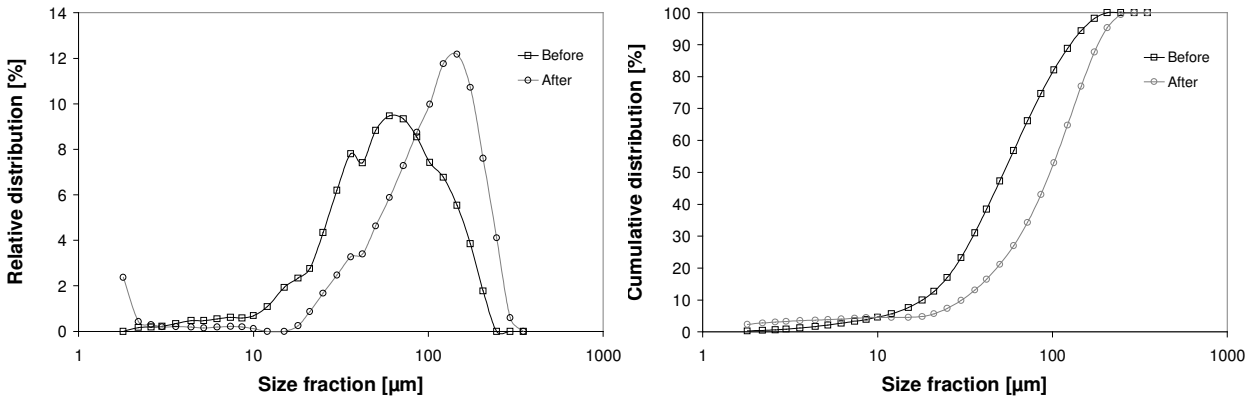


Figure 5-24. Relative and cumulative distribution of POM, before and after the adsorption phase. The difference between the curves represents the adsorbed POM onto the biofilm surface/matrix.

## 5.6 Depolymerisation modelling results

This section reports on modelling results obtained from simulations of the batch degradation process of experiment 7 and 10. The objective is to complement the analytical modelling results obtained in section 3.3, for comparison and further evaluation of kinetics and model identification. Three modelling strategies were tested: One step hydrolysis in a biofilm compartment, full range polymer dynamics by suspended Dextranase and full range polymer dynamics in a biofilm compartment. All models were implemented in Aquasim (Reichert, 1994; Reichert, 1998), and selected parameters were estimated by secant parameter estimation integrated by a fifth order Runge-Kutta algorithm (Reichert, 1998). Before reporting on depolymerisation dynamics, a short description of kinetic and stoichiometric biofilm characterisation is provided.

### 5.6.1 Biofilm characterisation

This section reports on data interpretation and estimations conducted to establish basal growth and stoichiometric parameters used for modelling Monod limited growth and simple endogenous respiration and maintenance substrate utilisation as described by Beeftink et al. (1991).

Theoretical maximum growth yield on easily biodegradable substrate was estimated using the method suggested by Heijnen (1999), compensated for the fact that Isomaltose, Isomaltotriose, Isomaltotetraose and Isomaltopentaose ($M_W$ 0.342-0.666 kDa) may be assimilated directly. This value was evaluated against estimated respirometric coefficients found by dividing the integrated OUR curve by the initial carbon (Glucose or Dextran) concentrations. Several parameters were estimated by splitting data sets into suitable ranges for the particular parameter in question (Dochain et al., 1995; Keesman et al., 1997; Weijers and Vanrolleghem, 1997). In this section, a simple ASM1 derived model as, suggested by Kommedal et al. (2002) without EPS synthesis and degradation, is applied.

Respirometric coefficients, defined as mass oxygen consumed per mass substrate converted, were determined using the integration routine as described in section 3.3, and results are presented in Figure 5-25. As noted above, oxygen to Glucose consumption was lower than the theoretical estimate, while the stoichiometric coefficients were higher for the medium sized fractions (10-500 kDa) and lower for 6 and 473 kDa (note that these size classes were

| Process | State Variables $S$ | $S_O$ | $X_S$ | $X_H$ | $X_I$ | Rate |
|---|---|---|---|---|---|---|
| Growth | $-1$ | $-\nu^{\mu}_{O_2/S}$ | | $Y_{X/S}$ | | $\mu_{max}\frac{S}{K_S+S}\cdot X_H$ |
| Maintenance consumption | $-1$ | $-\nu^{m}_{O_2/S}$ | | | | $k_m\frac{S}{K_S+S}\cdot X_H$ |
| Endogenous respiration | | $-\nu^{endo}_{O_2/X}$ | | $-1$ | $f_{X_I}$ | $k_d\frac{K_S}{K_S+S}\cdot X_H$ |
| Oxygenation | | 1 | | | | $K_L a\cdot\left(S_{O,sat}-S_O\right)$ |
| Detachment (surface→bulk) | | | | $-1,1$ | | $k_{det}\cdot X_{H,f}\cdot L_f^2$ |

Table 5-3. Process matrix for the model used for estimating endogenous and growth process parameters.

estimated from single data only). No systematic correlation was found between the initial concentrations of Dextran and the respirometric coefficient, $\nu_{O2/Dex}$.

Endogenous respiration data obtained from several long running time batches were used for estimation of the endogenous respiration coefficient, $k_d$, and initial biomass estimation as described by Ekama et al. (1986) and Keesman et al. (1998). Assuming no external substrate (neither slowly nor readily biodegradable) is present, and full oxygen penetration of the biofilm, the system may be represented by suspended mass balances as no substrate gradients are limiting:

$$\frac{dX}{dt} = -k_d \cdot X \qquad (5\text{-}17)$$

where $k_d$ is the endogenous respiration coefficient [1/h]. The oxygen mass balance is given by:

$$OUR(t) = -\frac{dO_2}{dt} = \frac{k_d}{Y_{X/O_2}} \cdot X \qquad (5\text{-}18)$$

Differentiating (5-18), inserting (5-17) into the differential and re-integrating, gives the following biomass independent equation for the endogenous respiration coefficient:

$$\frac{OUR(t)}{OUR(t_0)} = e^{-k_d \cdot t} \qquad (5\text{-}19)$$

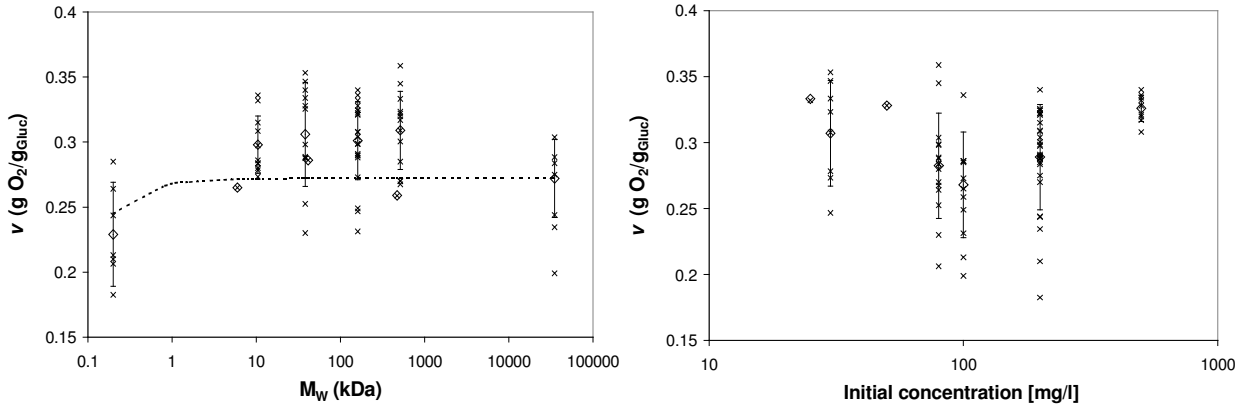


Figure 5-25. Estimated oxygen to substrate stoichiometric coefficients for all batch experiments conducted. Left panel show relation to initial molecular weight of the substrate, while right panel show the dependency to initial concentration. Dashed line indicates the theoretical stoichiometry between $O_2$ and Dextran as described by Heijnen (1999).

Figure 5-26 shows endogenous respirations for selected long runtime batches during the entire experimental campaign. Endogenous respiration coefficients, estimated by exponential fitting to each batch, are weight averaged based on the non-linear standard error estimate, and found to be 0.020 ± 0.005 1/h (n = 6) for $R_1$, and 0.017 ± 0.006 1/h (n = 8) for $R_2$. These values are about twice the lysis rate reported by Henze et al. (2000), and slightly higher than the theoretical estimate (0.012 1/h) found by using the approach suggested by Heijnen (1999). That could indicate remaining biodegradable material during the initial parts of the estimations, or storage effects not detected in the respirograms (Gujer et al., 2000). Endogenous respiration is further applied for the estimation of active heterotrophic biomass by inserting estimated $k_d$ values into (5-18), and estimating $X_{ini}$ at stable background respiration levels before each sample standard injection. The endogenous stoichiometric oxygen demand is estimated by thermodynamic balancing (Heijnen, 1999), and found to be

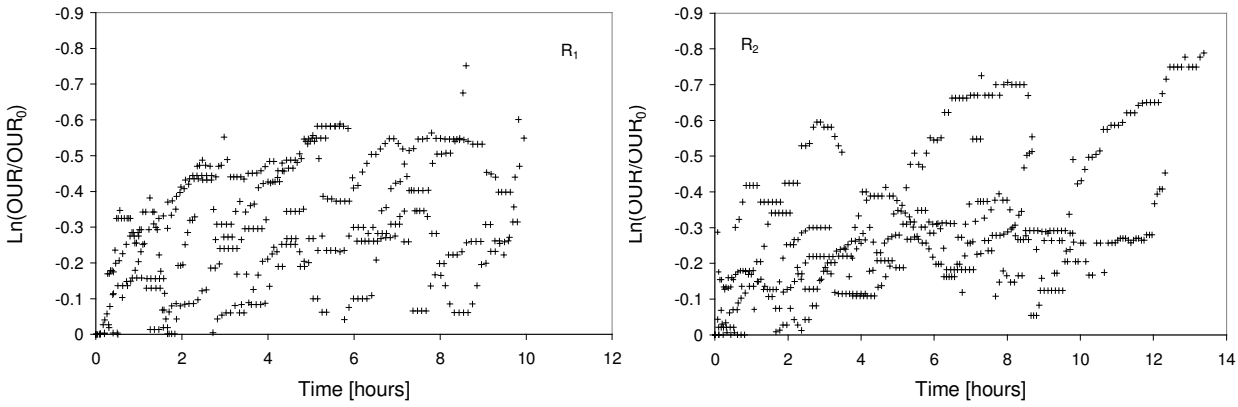


Figure 5-26. Endogenous respiration estimations used for estimation of $k_d$ ($R_1$ and $R_2$).

1.36 g $O_2$/g X. As described by Insel et al. (2002), respirograms may be separated into specific parameter sensitive ranges for optimum (reduction of estimation error) sensitivity. For biofilm systems, further complexity results from diffusional transport phenomena. Further investigation of the kinetic model (Table 5-3) therefore involved parameter estimation in Aquasim (Reichert, 1994), using defined substrate batch samples (i.e. blanks as diluted PBS) and Glucose standards. In order to reflect the plug-flow nature of the sampling point (top of the bubble column, see Figure 4-1), the plug flows of tubing and possible adsorption phenomena, a rather complicated model was designed and evaluated (Figure 5-27). However, model complexity resulted in very long simulation times, and led to program failure during parameter estimation. Therefore, model simplification by implementation of the oxygenation process in the CSTR-Bulk phase and removing plug flow sub-compartments was performed. Figure 5-28 show the results of sensitivity and error propagation analysis of both models on the 100 mg/l Glucose batch in experiment 10. Model complexity reduction does not reduce sensitivity for the parameters of interest for estimation, indeed the sensitivity of the simple model increase, reducing the estimated error propagating from the uncertainty of the parameters. The simple model is therefore the preferred, both for simulation simplicity and estimation accuracy. Figure 5-28 also shows that the model is sensitive and restricted to $k_d$ and $X_{ini}$ estimation before injection, and when the model relaxes back to background

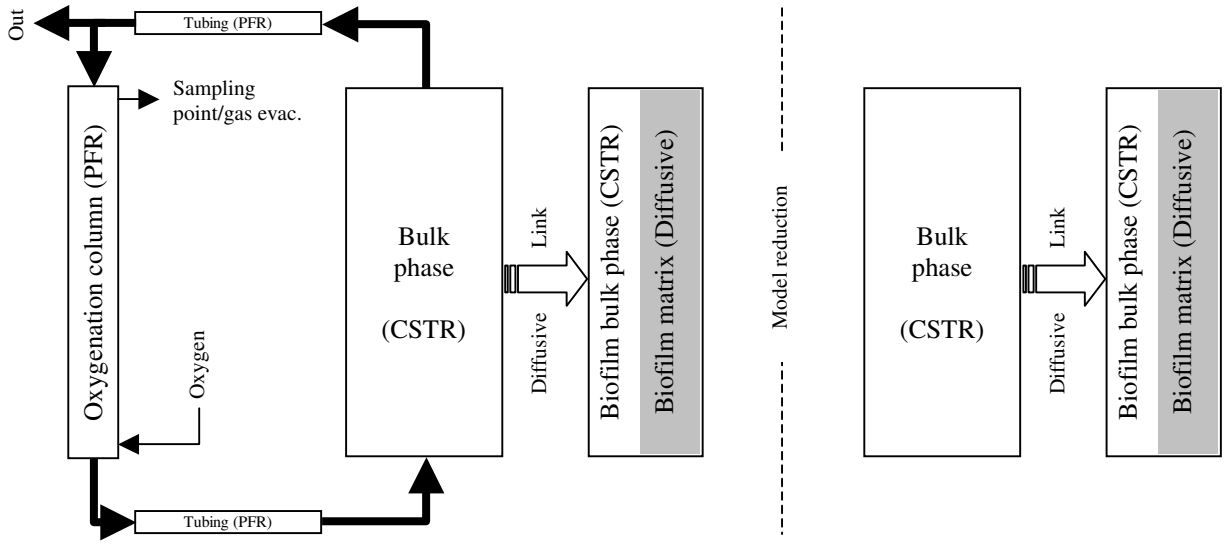


Figure 5-27. Block compartment description of realistic model (left) and model compartment structure of the simplified model. Dark arrows indicate advective flow links, while the broad represents the diffusive link across the biofilm boundary layer. The biofilm bulk phase is kept very small (at approx. 130 µm total thickness) and the major part of the bulk phase is represented by the CSTR Bulk phase compartment.

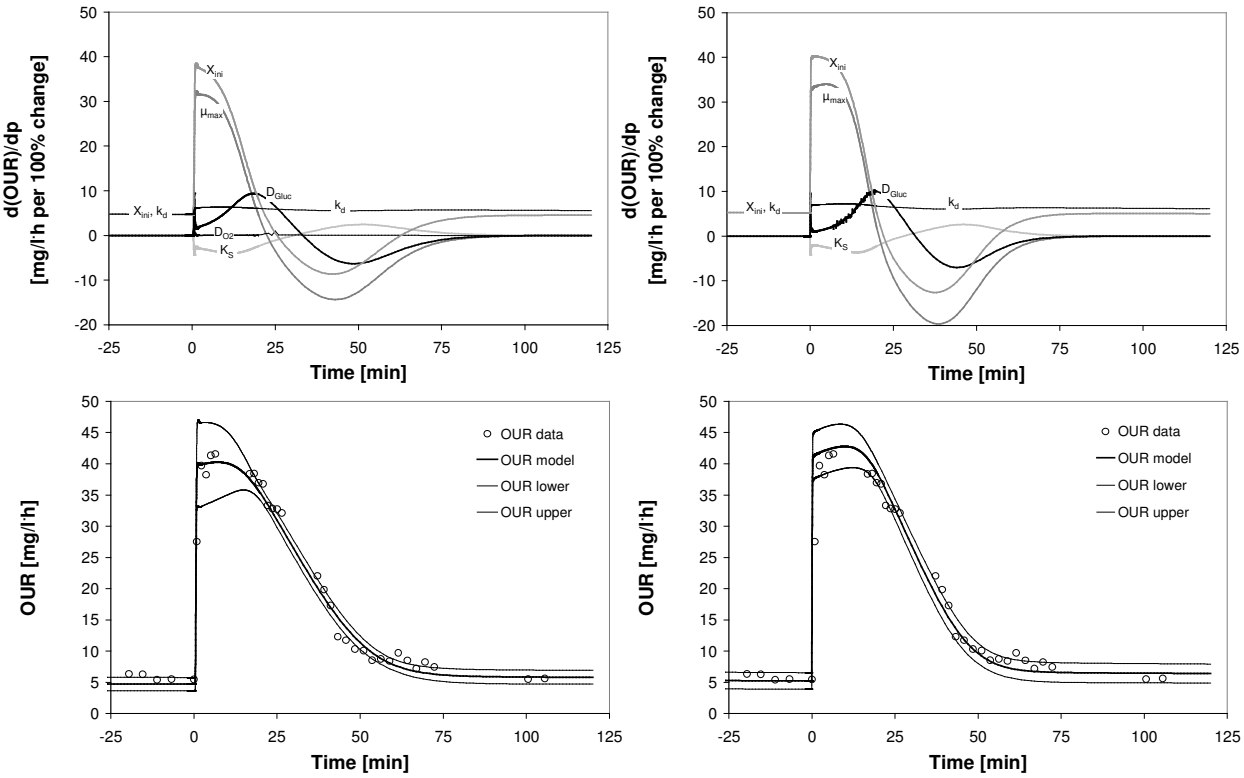


Figure 5-28. Model complexity evaluation by comparing sensitivity analysis on both models (complex to the left), and error contribution by selected parameters ($\mu_{max}$, $K_S$, $D_{Gluc}$, $k_d$, $X_{ini}$) to the simulated OUR response on initial 100 mg/l Glucose.

respiration (as assumed during analytical estimation above). Further, knowing $X_{ini}$ at $t_0$ enable estimation of $\mu_{max}$ during the peak phase, while $K_S$ may be estimated by the relaxation slope of the OUR response curve (as suggested by Insel et al., 2002), and from the bulk phase TOC concentrations (data not shown). Diffusion coefficients are not estimated here, both due to limited sensitivity and lack of measurements, and that literature values exist for liquid and biofilm applications (Stewart, 2003; Cussler, 1984). Table 5-4 presents estimated growth and substrate transport parameters adopted in the basal biofilm growth-maintenance-endogenous respiration model. Parameters ($u_{max}$ and $K_S$) are estimated from the 100 mg/l Glucose injection of experiment 10 (9. September), and validated against the 80 and 200 mg/l injections after experiment 6 (27 June) and experiment 7 (29 July). Biofilm detachment is modeled by the generic expression suggested by Wanner and Gujer (1986), and evaluated by Stewart (1993) and Kommedal et al. (2000). Biofilm intrinsic parameters (diffusion resistance factors, $\eta$, the biofilm surface detachment coefficient, $k_{det}$, biofilm density, $\rho_{Xf}$) are selected from relevant literature (Stewart, 2003; Kommedal et al., 2000; Kommedal and Bakke, 2003) adapted to biofilm areal density observations (6-10 g VSS/m$^2$).

| Parameter | Value | Unit | Reference |
|---|---|---|---|
| $\mu_{max}$ | 0.51 ±0.02 | 1/h | Estimated here |
| $K_S$ | 4.01 ± 0.09 | mg/l | Estimated here |
| $D_{O2}$ | $7.62 \cdot 10^{-6}$ | $m^2/h$ | Cussler, 1984 |
| $\eta_{O2,film}$ | 0.58 | 1 | Stewart, 2003 |
| $D_{Gluc}$ | $2.28 \cdot 10^{-6}$ | $m^2/h$ | Cussler, 1984 |
| $\eta_{Gluc,film}$ | 0.3 | 1 | Stewart, 2002 |
| $k_d$ | $R_1$: 0.017 ± 0.006<br>$R_2$: 0.020 ± 0.005 | 1/h | Estimated here |
| $Y_{X/S}$ | Glucose: 0.55<br>Dextran: 0.58 | g S/g X | Estimated here (Heijnen, 1999) |
| $\nu_{O/S}$ | Figure 5-25 | g $O_2$/g S | Estimated here |
| $\nu_{O2/S,maint}$ | 1.07 | g $O_2$/ g S | Estimated here (Heijnen, 1999) |
| $\nu_{O/X,end}$ | 1.36 | g $O_2$/g X | Estimated here (Heijnen, 1999) |
| $f_{Xi}$ | 0.1 | 1 | Henze et al (2000) |
| $k_{det}$ | 0.5 | $m^2/mg \cdot h$ | Kommedal et al. (2000) |
| $\rho_{Xf}$ | 105000 | $g/m^3$ | Estimated here |
| $L_b$ | 50 | µm | LaMotta (1976), Trulear and Characklis (1982) |

Table 5-4. Growth and substrate transport parameters estimated or adopted from literature for use in the growth-maintenance-endogenous decay basal biofilm model. Errors represent standard errors estimated by Aquasim ($\mu_{max}$ and $K_S$) and by non-linear regression analysis ($k_d$).

Initial biomass density, $X_{ini,f}$, is determined for each batch based on endogenous respiration, while initial biofilm thickness is estimated by parameter estimation of the OUR peak shape. While OUR peak height is determined by $X_{ini}$ and $\mu_{max}$, the peak width is determined by the initial active biofilm thickness. The biomass density inside the active layer is determined from endogenous respiration levels (i.e. that part of the OUR curve that is not experiencing mass transfer limitations). OUR and TOC degradation was found to be insensitive to the modeled diffusive boundary layer thickness in the biofilm reactor (data not shown in Figure 5-28). The small response detected was in addition correlated to the diffusion coefficients. This is consistent with LaMotta (1976) who found no effect of Rototorque rotational speed on Glucose removal rates above 1.5 1/s (in this study, 2 1/s) on a thin biofilm (≈ 8 µm), and with Trulear and Characklis (1982) that found the same for a thicker biofilm (110 µm). Both studies concluded no effects of a boundary layer thickness of 40-60 µm (Lb/D = 1-2 d/m). In this study an effective layer thickness of 50 µm is used (i.e. bulk biofilm reactor thickness, plus estimated boundary layer thickness). The biomass density was chosen based on the following reasoning. Assuming spherical bacteria, the densest biofilm possible is π/6 volume fraction (vol. cells/vol. biofilm).

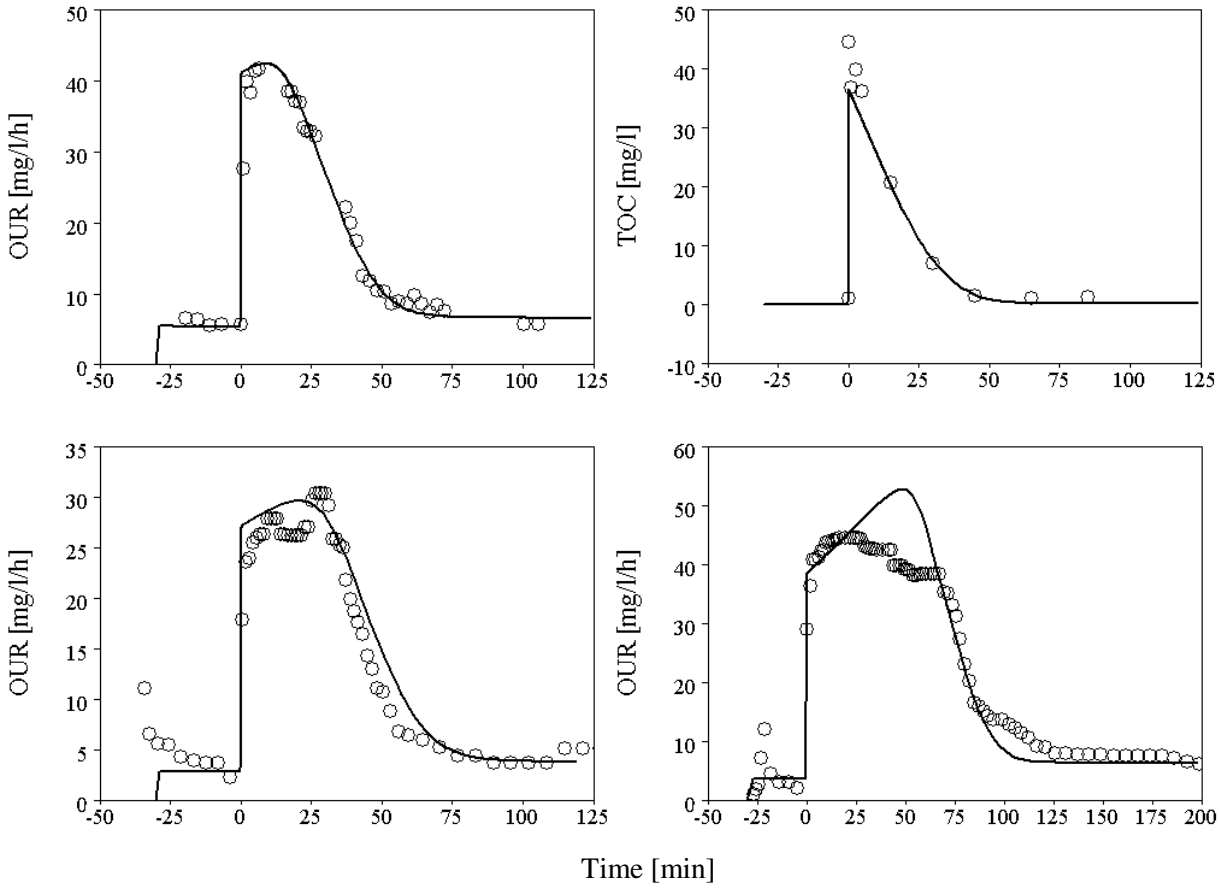


Figure 5-29. Calibration and validation of biofilm growth and endogenous process model. Upper panels show measured and simulated OUR (left) and bulk phase TOC (right) results from calibration of growth parameters ($\mu_{max}$ and $K_S$), and initial biomass $X_{ini}$ after injection of 100 mg/l Glucose. Lower panels show OUR validations of 80 (left) and 200 mg/l Glucose initial batch concentrations.

One cell consists of about 80 % water (Brock and Madigan, 1991) which gives a theoretically estimated maximum biofilm density of 105 kg/m$^3$.

Figure 5-29 presents the result of model calibration and validation described above. The model seems to reflect the main characteristics of the OUR curve even for batch experiments separated by more than 70 days. The ascending plateau of the peak OUR represents close to maximum growth, while the slope back to background respiration represents substrate limited growth. Deviations observed at the peak levels and transition between substrate limited and endogenous respiration may be attributed to storage phenomena (Insel et al., 2002; Gujer 2000). The inadequacy of precisely reflect the initial TOC dynamics is most likely due to the structural reduced model with no plug flow dynamics around the sampling point, and non-homogeneity during the initial stages of the batch operation. The estimated initial biomass densities are (initial concentrations in brackets) 13035 (100 mg/l), 6844 (80 mg/l) and 9027 (200 mg/l) g/m$^3$ and the initial biofilm thickness is 60 µm. These densities are about 1/10 of

the measured VS from coupon analysis (average June: 8 g/m$^2$), indicating that about 10% of the biomass (as VS) is actively respiring. Using the measured biofilm thickness (about 300 µm) this would indicate that the non-respiring fraction of the biofilm biomass (here lumped into the inert fraction parameter, $X_i$) is about 22000 g/m$^3$, and that the active biofilm layer is situated on top of a non-respiring layer of about 250 µm. For the remaining modeling, volumetric fractions are assumed to be constant (constant biomass densities), and differences in background respiration is attributed to variable thickness of the respiring layer. This strategy is based on the assumption that biofilm thickness is more dynamic than the biomass density of the biofilm matrix. Some reports indicate this to be the case (Bakke, 1986), and structurally it does not significantly change the modeling behavior. The main difference is that plateau shape will be more consistent and distinct.

### 5.6.2 One step depolymerisation model

Calibration of a one step hydrolysis model as suggested by the ASM group (Henze et al., 1987; Henze et al., 1995; Henze et al., 1999 and Gujer et al., 1999) and other workers (Orhon et al., 1999; Sollfrank et al., 1988; Spanjers and Vanrolleghem, 1995) was implemented using simple first order kinetics (references are listed in Table 2-3, model no. I). It can be easily shown that both the adsorption-hydrolysis model of Dold et al. (1980) adapted in the ASM1 and 2, and the equivalent adopted in ASM 3 (Gujer, 1999) will reduce to a simple first order depolymerisation expression in biofilms. The main reason for that is the high local biomass concentration in the biofilm matrix that makes the denominator of the switch function constant at most concentrations:

$$r_h = k_h^* \frac{X_S / X_h}{K_X + X_S / X_h} \cdot X_h \overset{X_h \gg X_S}{\Rightarrow} k_h^* \frac{X_S}{K_X} = k_h \cdot X_S \qquad (5\text{-}20)$$

The apparent biomass independence of this expression does not represent the observed biomass effects as found in the slide experiments and pure enzyme studies (section 5.3.1 and 5.3.2.). It is postulated here that the first order depolymerisation coefficient, $k_{1h}$, is biomass dependant, but with rather low short term sensitivity to the depolymerisation process during a single batch experiment. Thus, $k_{1h}$ is determined by the biomass at the beginning of each

| Process | State Variables | | | | | Rate |
|---|---|---|---|---|---|---|
| | $S$ | $S_O$ | $X_S$ | $X_H$ | $X_I$ | |
| Growth | $-1$ | $-\nu^{\mu}_{O_2/S}$ | | $Y_{X/S}$ | | $\mu_{max}\frac{S}{K_S+S}\cdot X_H$ |
| Maintenance consumption | $-1$ | $-\nu^{m}_{O_2/S}$ | | | | $k_m\frac{S}{K_S+S}\cdot X_H$ |
| Endogenous respiration | | $-\nu^{endo}_{O_2/X}$ | | $-1$ | $f_{X_I}$ | $k_d\frac{K_S}{K_S+S}\cdot X_H$ |
| Hydrolysis (depolymerisation) | 1 | | $-1$ | | | $k_h\cdot X_S$ |
| Oxygenation | | 1 | | | | $K_L a\cdot\left(S_{O,sat}-S_O\right)$ |
| Detachment (surface→bulk) | | | | $-1,1$ | | $k_{det}\cdot X_{H,f}\cdot L_f^2$ |

Table 5-5. Process matrix for the one step hydrolysis (depolymerisation) model.

batch, and the depolymerisation rate is modelled independent of biomass during batch execution. Hydrolysis of Dextran ($X_S$) to produce readily biodegradable substrate (Glucose), without any carbon loss (i.e. $Y_{Xs/S}$ = 1), were complimented by the basal growth and endogenous respiration model presented above. Table 5-5 shows the process matrix used for one step hydrolysis modelling. Figure 5-30 presents the results of the one step depolymerisation model applied on experiment 10 (section 5.2.3). The first order depolymerisation coefficient, $k_h$, was estimated by fitting to the observed OUR and bulk phase TOC concentrations. In addition, initial active biofilm thickness (layer of active biomass) was estimated by the initial respiration, keeping the biomass composition constant. Bulk phase TOC estimations show very good accordance with the measured values, while reasonable good fit is achieved for the OUR. Interestingly, the modelled bulk phase TOC indicate relatively high levels of Glucose (data not shown), peaking at 24 mg/l for the fastest degraded standard (6 kDa), decreasing to about 0.5 mg/l for the slowly standard (35 MDa). Initial OUR peaking and rapid bulk phase TOC reduction in the colloidal standard (35 MDa) required additional processes, here minimized by introducing two step hydrolysis (fast and slow) and large fraction Dextran adsorption. Simple linear mass transfer adsorption was implemented (Dold et al, 1980), and the fast fraction equaled the kinetics and diffusivities of the 160 kDa standard.

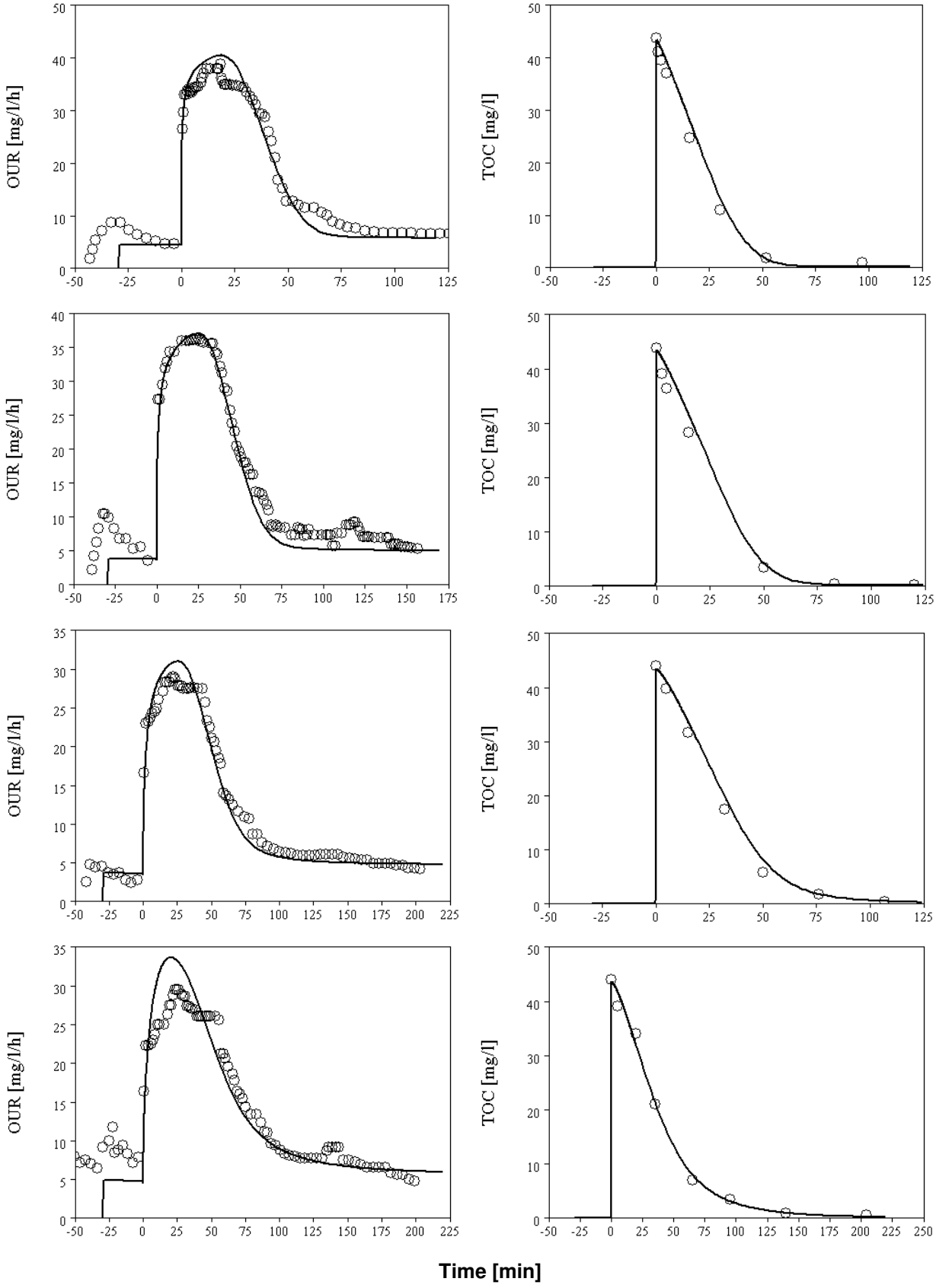


Figure 5-30. Estimated (circles) and modelled OUR and bulk phase TOC (solid lines) during experiment 10 batches. Panels show the results of injecting 100 mg/l Dextran of 6, 10.5, 41.3 and 160 kDa initial molecular weight (top to bottom).

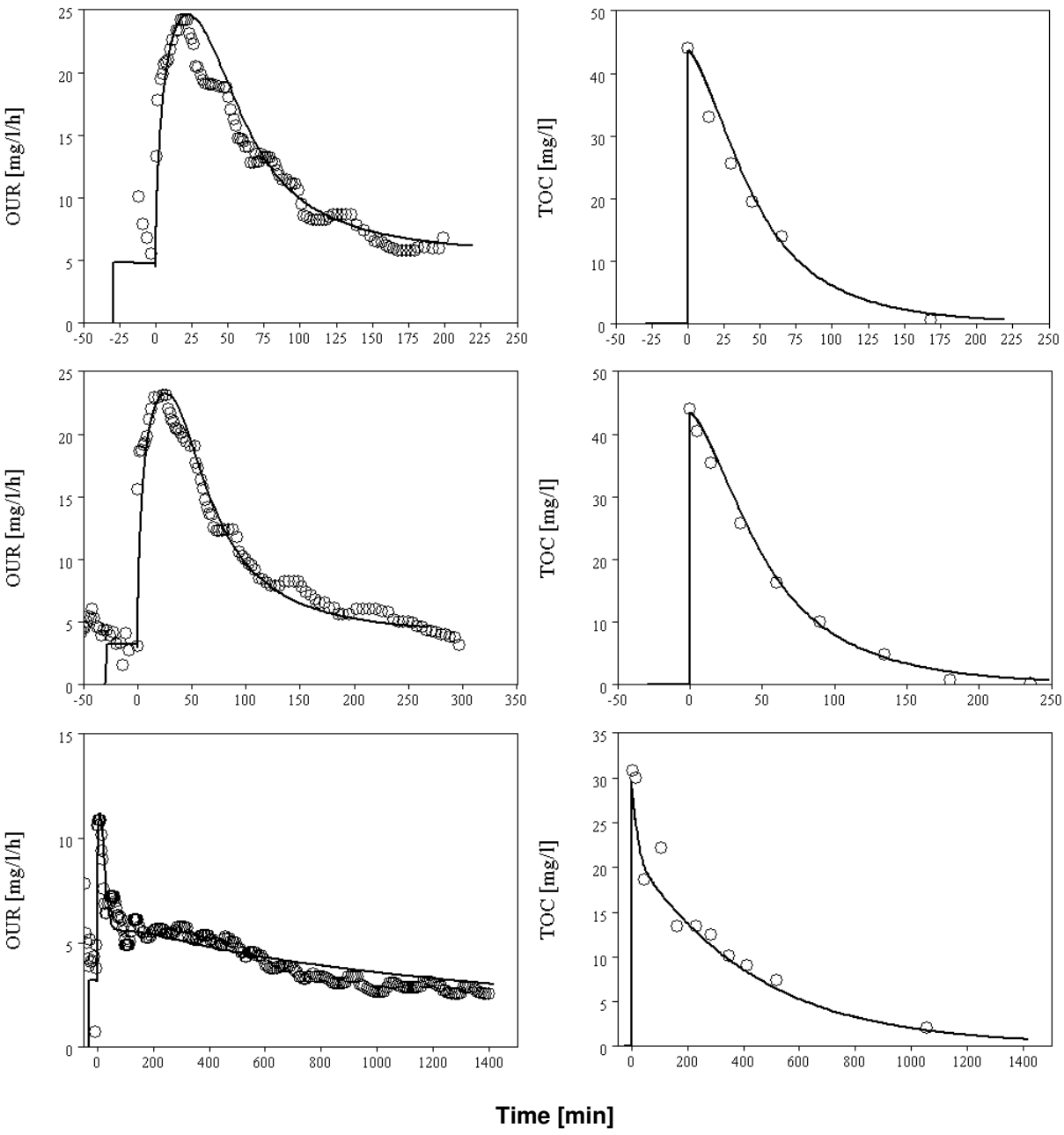


Figure 5-30 (cont). Estimated (circles) and modelled OUR and bulk phase TOC (solid lines) during experiment 10 batches. Panels show the results of injecting 100 mg/l Dextran of 473, 513, and 35000 kDa initial molecular weight (top to bottom). The 35 MDa standard was modelled using two step depolymerisation and adsorption (see text for details).

Structured biofilm modelling provides valuable information on biofilm development and substrate dynamics that are not accessible in the measured data. Biofilm thickness increased during the batch run by 10 µm, independent of the $M_W$ standard, and the relative volume fraction of active bacteria increased equally (inert particles were reduced), most at the surface (6%) and less at the active-inactive biofilm layer (0.6%). Bulk phase biomass increased (due

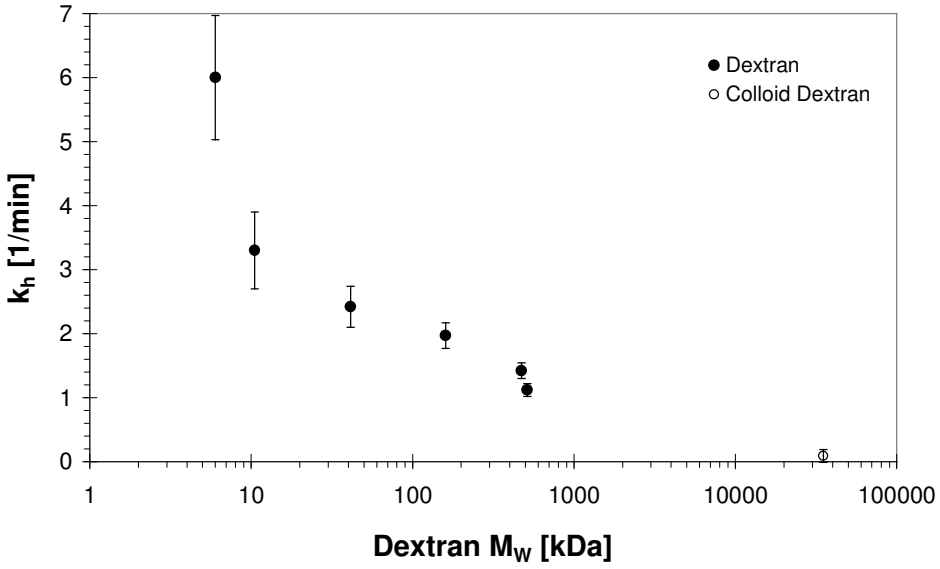


Figure 5-31. Estimated first order depolymerisation coefficient for the $M_W$ standards used in experiment 10, implemented in the one step depolymerisation model. Error bars represent estimated standard deviations during parameter estimation in Aquasim.

to growth and detachment) to about 1 g/m$^3$, or about 0.5 % of the active biomass in the reactor. These observations support the experimental assumption regarding negligible bulk phase contribution to the observed rates, and adjustments of the initial biofilm thickness according to the initial respirometric activity. Biofilm Glucose concentrations increased to high levels violating the assumption of constant and low Glucose levels assumed as part of the analytical variable half order approach presented in section 3.3. However, taking the modelling premise of an active layer on top of a thick inactive biomass layer as supported by the observed and estimated biofilm thickness, and the biomass measured on coupons, the structured model can still be regarded as non-penetrated, following variable zero to half order kinetics (high Glucose levels).

Figure 5-31 presents the estimated first order depolymerisation coefficients plotted against the initial molecular weight of the sample standards. This plot represents the same as Figure 5-7 and Figure 5-10, however, this time compensated for biofilm transport. The same logarithmic dependency is apparent for the intermediate size fractions (10-500 kDa), while the small standard (6 kDa) and the colloidal deviates as it did in the analytical analysis of section 3.3. The elevated kinetics of the small Dextran standard could be explained by the model structure allowing assimilation of monomer only (Glucose). Omitting intermediate dynamics would affect the Dextran of closest proximity to the assimilable fragments (Oligomers < 0.8-1 kDa) more than the higher $M_W$ standards.

The simple one step model clearly reflects some of the $M_W$ effects on depolymerisation kinetics as shown by the variable order model of Rittman and McCarty (1980; 2001), but still does not take intermediate dynamics into account, making evaluation of transport versus reaction limitation insufficient. Using the Thiele modulus (Levenspiel, 1972) as suggested by Harremoës and Henze (2002) the following conditions can be defined:

$$\text{reaction limited} \Leftarrow 1 > \Phi > 1 \Rightarrow \text{diffusion limited} \qquad (5\text{-}21)$$

where the Thiele Modulus for general kinetics is given as:

$$\Phi = \sqrt{\frac{(n+1)\cdot k_{n,f}\cdot L_f^2 \cdot S^{n-1}}{2\cdot D_{S,f}}} \qquad (5\text{-}22)$$

where: $n$ is the reaction order, $k_{n,f}$ is the n$^{th}$ reaction order coefficient, $L_f$ is the biofilm thickness, $S$ is the biofilm surface limiting substrate concentration and $Ds_f$ is the limiting substrate diffusion coefficient in the biofilm. Figure 5-32 shows bulk phase Glucose concentrations and estimated Thiele modulus concentration limits for reaction to diffusion limitations (below the dashed lines of left panel) given the active biofilm thickness. Interestingly, the biofilm system is reaction limited during the peak OURs for all standards

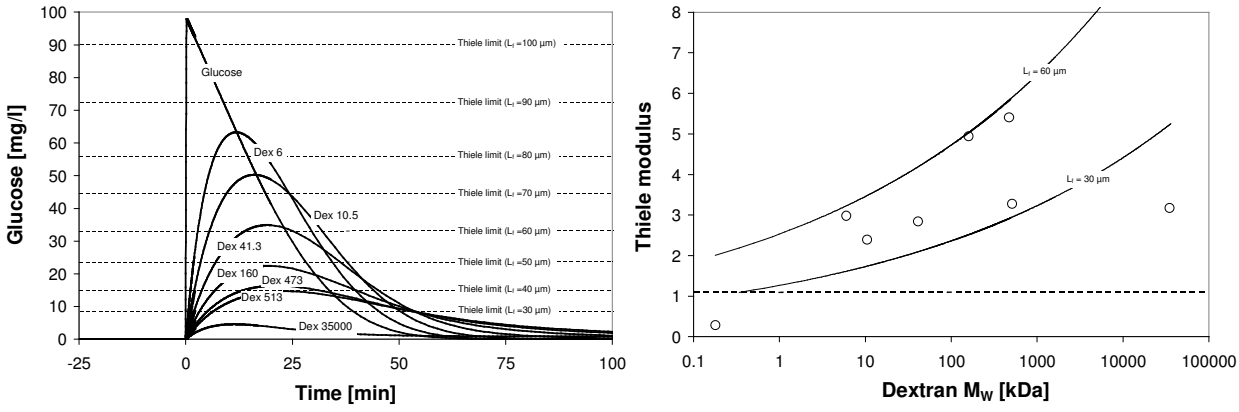


Figure 5-32. Simulated bulk Glucose concentrations during experiment 10 (left). Dashed lines represent Thiele modulus concentrations limits for the particular biofilm thickness where the system changes from being reaction to be diffusion limited (below lines). Right panel show the estimated Thiele modulus of the rate limiting first order depolymerisation process (values are based on the diffusion characteristics of the initial molecular standard). Solid lines represent estimated Thiele modulus based on $k_h$ estimates from Figure 5-31 and $D_{Xf}$ from Figure 5-6.

below 41.3-100 kDa. Figure 5-32 also show the estimated Thiele modulus of each batch injection during experiment 10, using the estimated first order depolymerisation coefficients and the estimated biofilm diffusion coefficients of the initial polymer standard (Figure 5-6). Also included is the Thiele modulus of the zero order ($\mu \approx \mu_{max}$) Glucose conversion rate, and a theoretical estimate using correlations of $k_h$ in Figure 5-31 and diffusion coefficients from Figure 5-6. As can be seen, depolymerisation is diffusion limited for all polymer standards, and the theoretical estimate indicate that it will be for all Dextrans above 0.35 kDa for biofilms thicker than 30 µm (solid lines). Variability within the 30 - 60 µm theoretical range is due to variable initial biofilm thicknesses during the simulations ($k_h$ estimations), and the error introduced by disregarding intermediate dynamics.

### 5.6.3 Full intermediate model; pure enzymes

Practical limitation regarding the number of active state variables restricts full intermediate modelling to the low size fractions. The full intermediate model is presented in the process matrix of . Due to the model size limitations, the maximum number of intermediates is set to 123 (i.e. 20 kDa). Initial concentrations are taken from the certified standard distribution provided by the producer (see Figure 4-3). Lack of pure enzyme depolymerisation data from ~ 10 kDa initial Dextran standards, limits this modelling section to simulations for qualitative comparison to the measured intermediate time series presented in section 5.3.1.

Figure 5-33 presents simulation results of endo-depolymerisation of the 12 kDa certified calibration standard. The maximum activity ($e_0 \cdot k_0 = V_{max}$) and Michaelis coefficient ($K_M$) are selected arbitrarily as no comparison with data or literature values are available. Comparison of different $K_M$ values showed that the same dynamics could be simulated by simultaneously adjusting the $V_{max}$ value (data not shown). In order to compare simulated intermediates and SEC-HPLC results, the simulated intermediates need to be superimposed the same way as the polymer intermediates were during SEC (ref. discussion in section 5.3). By grouping the simulated intermediates into elution intervals of 0.25 min it was possible to present simulation results for comparison with the RID signals from the SEC-HPLC. Figure 5-33 left panel show endo-activity end products (Isomaltose and Isomaltotriose) and intermediate (P4 to P120) time series, while the right panel presents intermediate dynamics after grouping plotted against molecular weight. This plot may be compared to the pure enzyme dynamic plots in

| Process | State Variables $S_1$ | $S_i$ | $S_{(j-1)}$ | $S_j$ | Rate |
|---|---|---|---|---|---|
| Endodepolymerisation | | $\frac{2i}{j^2-3j}$ | | $-1$ | $\sum_{j=i+2}^{m} \frac{k_0 \cdot e_0 \frac{P_j}{K_{M_j}}}{1+\sum_{l=4}^{m} \frac{P_l}{K_{M_l}}}$ |
| Exodepolymerisation | 1 | | 1 | $-1$ | $\sum_{j=2}^{m} \frac{k_0 \cdot e_0 \frac{P_j}{K_{M_j} \cdot (j-1)}}{1+\sum_{l=2}^{m} \frac{P_l}{K_{M_l} \cdot (l-1)}}$ |
| Comments: | | $i = 4,5,...m-4$ | | | |

Table 5-6. Process matrix for the pure enzymes simulation. *m* is all polymers susceptible for enzymatic activity, *j* is the actual polymer being depolymerised into intermediates *i* during endo-attack and into *j-1* and a monomer ($S_1$) during exo-activity.

section 5.3.1 (Figure 5-15), even though quantitative comparison is impossible (160 kDa data whereas simulations represents 12 kDa). Some quantitative evaluation can still be made though, by assuming the accumulating peak between 0.2 and 0.8 kDa of Figure 5-15 (right panels) to represent Dextranase end products (Isomaltose and Isomaltotriose) formation. By regarding the RID response to be fairly constant in the 0.1 to 3 kDa region (see Appendix 9.3 for validation), the peak values below 0.6 kDa may be regarded as the sum of the end products, while the 0.8-2 kDa represents residual fragments. Using the relative peak values,

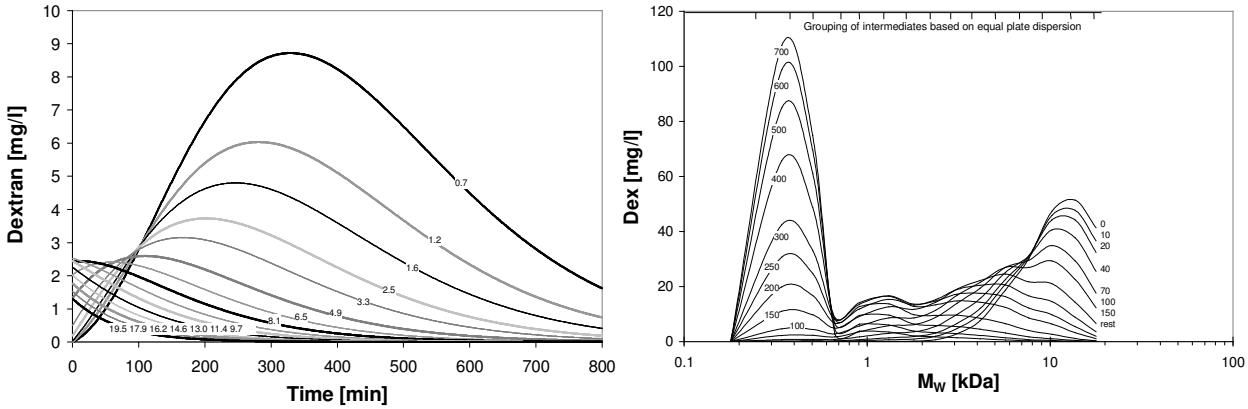


Figure 5-33. Simulation of intermediate dynamics using the pure Dextranase model with high $K_M$. Left panel show selected intermediates against time, while the right panel show intermediate concentrations at selected times as they would have appeared on the RID detector using 0.25 min grouping (peak overlapping; see text for details).

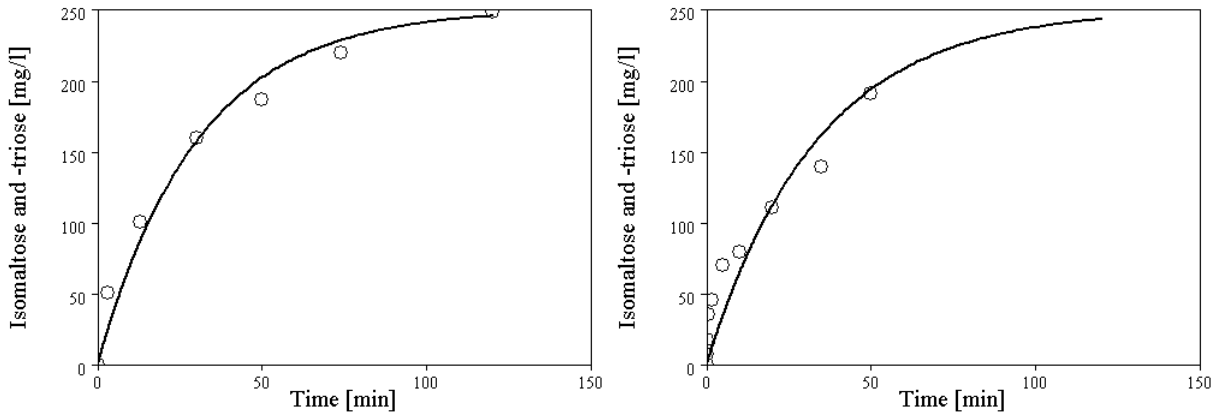


Figure 5-34. One step depolymerisation model (Michaelis Menten kinetics) calibrated on the pure Dextranase data of Figure 5-15 for 3 mU (left) and 0.6 mU Dextranase. Initial Dextran of 160 kDa and 250 mg/l.

these may be recalculated into concentrations by assuming the initial Dextran to be conserved. The inability of the Aquasim model to simulate larger than 20 kDa intermediates, also limits this simulation to one step analysis, Dextran → Isomaltose + Isomaltotriose. Figure 5-34 shows a calibrated one step model based on Michaelis-Menten kinetics applied on the data presented in Figure 5-15 for 0.6 and 3 mU. Michaelis-Menten parameters were estimated to 66 g/l for $K_M$, and 2.2 and 1.9 g Iso/l·min for $V_{max}$ for 3 and 0.6 mU, respectively. These coefficients effectively transform the Michaelis-Menten kinetics into first order kinetics with first order rate coefficients 0.037 and 0.029 g Iso/g Dex·min.

### 5.6.4 Full intermediate model; Biofilm application

The full intermediate model presented in  is combined with the basal growth and decay model (Table 5-3), using the calibrated growth and decay parameters in Table 5-4, and theoretically estimated diffusion coefficients presented in Figure 5-6. In response to the findings in section 5.4 on localisation of exogenous enzymes, only Dextranase (no exo-activity) is active as it is thought to dominate the overall depolymerisation. Growth and maintenance are incorporated for all Dextran oligomers below the uptake limit of 0.99 kDa (White, 2000). Kinetically, the substrates are subjected to competing substrate inhibition equivalent to the apparent substrate inhibition deduced for depolymerisation. Yield and respirometric coefficients are theoretically estimated by the method of Heijnen (1999). Table 5-7 presents the process matrix for the full intermediate biofilm model. An inactive fraction of 10 % (of dry mass) is introduced by endogenous decay (cell death). The biofilm has the same

| Process | State Variables | | | | | | | | | | | | Rate |
|---|---|---|---|---|---|---|---|---|---|---|---|---|---|
| | $S_1$ | $S_2$ | $S_3$ | $S_4$ | $S_5$ | $S_6$ | $S_O$ | $S_i$ | $S_{(j-1)}$ | $S_j$ | $X_H$ | $X_I$ | |
| Growth on "C" | −1 | | | | | | $-\nu^{\mu}_{O_2/1}$ | | | | $Y_{X/1}$ | | $\mu_{max}\frac{S_1}{K_S+\sum_i^6 S_{iC}}\cdot X_H$ |
| Growth on "2C" | | −1 | | | | | $-\nu^{\mu}_{O_2/2}$ | | | | $Y_{X/2}$ | | $\mu_{max}\frac{S_2}{K_S+\sum_i^6 S_{iC}}\cdot X_H$ |
| Growth on "3C" | | | −1 | | | | $-\nu^{\mu}_{O_2/3}$ | | | | $Y_{X/3}$ | | $\mu_{max}\frac{S_3}{K_S+\sum_i^6 S_{iC}}\cdot X_H$ |
| Growth on "4C" | | | | −1 | | | $-\nu^{\mu}_{O_2/4}$ | | | | $Y_{X/4}$ | | $\mu_{max}\frac{S_4}{K_S+\sum_i^6 S_{iC}}\cdot X_H$ |
| Growth on "5C" | | | | | −1 | | $-\nu^{\mu}_{O_2/5}$ | | | | $Y_{X/5}$ | | $\mu_{max}\frac{S_5}{K_S+\sum_i^6 S_{iC}}\cdot X_H$ |
| Growth on "6C" | | | | | | −1 | $-\nu^{\mu}_{O_2/6}$ | | | | $Y_{X/6}$ | | $\mu_{max}\frac{S_6}{K_S+\sum_i^6 S_{iC}}\cdot X_H$ |
| Endo-depolymer. | | | | | | | | $\frac{2\cdot i}{j^2-3\cdot j}$ | | −1 | | | $\sum_{j=i+2}^{m}\frac{k_0\cdot e_0\cdot P_j}{K_{M_l}+\sum_{l=4}^{m}P_l}$ |
| Exo-depolymer. | 1 | | | | | | | | 1 | −1 | | | $\sum_{j=2}^{m}\frac{k_0\cdot e_0\frac{P_j}{K_{M_j}\cdot(j-1)}}{1+\sum_{l=2}^{m}\frac{P_l}{K_{M_l}\cdot(l-1)}}$ |
| Maintenance on "C" | −1 | | | | | | $-\nu^{m}_{O_2/1}$ | | | | | | $k_e\frac{S_1}{K_S+\sum_{i=1}^6 S_i}\cdot X_H$ |
| Maintenance on "2C" | | −1 | | | | | $-\nu^{m}_{O_2/2}$ | | | | | | $k_e\frac{S_2}{K_S+\sum_{i=1}^6 S_i}\cdot X_H$ |
| Maintenance on "3C" | | | −1 | | | | $-\nu^{m}_{O_2/3}$ | | | | | | $k_e\frac{S_3}{K_S+\sum_{i=1}^6 S_i}\cdot X_H$ |
| Maintenance on "4C" | | | | −1 | | | $-\nu^{m}_{O_2/4}$ | | | | | | $k_e\frac{S_4}{K_S+\sum_{i=1}^6 S_i}\cdot X_H$ |
| Maintenance on "5C" | | | | | −1 | | $-\nu^{m}_{O_2/5}$ | | | | | | $k_e\frac{S_5}{K_S+\sum_{i=1}^6 S_i}\cdot X_H$ |
| Maintenance on "6C" | | | | | | −1 | $-\nu^{m}_{O_2/6}$ | | | | | | $k_e\frac{S_6}{K_S+\sum_{i=1}^6 S_i}\cdot X_H$ |
| Endogenous | | | | | | | $-\nu^{endo}_{O_2/X}$ | | | | −1 | $f_{X_I}$ | $k_d\frac{K_S}{K_S+\sum_{i=1}^6 S_i}\cdot X_H$ |
| Oxygenation | | | | | | | 1 | | | | | | $K_La\cdot(S_{O,sat}-S_O)$ |
| Comments: | | | | | | | | *i = 4,5,…m-4* | | | | | |

Table 5-7. Process matrix for the full intermediate model.

initial properties as described in section 5.6.1, while the initial Dextran distribution is taken from the sample standard analysis presented in Figure 5-21 for 6 and 10.5 kDa. The simplified model (Figure 5-27) described in section 5.6.2 is embedded in Aquasim 2.1 using the biofilm compartment, and loading of the initial Dextran is implemented by a inlet advective pulse of $50 \cdot 10^{-6}$ $m^3$/min active over 0.2 min (V = 10 ml) of 11.5 g Dextran/l at time 0 min, to the bulk phase compartment.

Figure 5-35 shows simulated and measured OUR and bulk phase TOC during depolymerisation and mineralisation of 100 mg/l (initial) 6 and 10.5 kDa Dextran. The results are similar to the one step depolymerisation model estimated by the same data (Figure 5-30, first and second panels), even though slightly better fit for both OUR and TOC is observed (Terminal Chi-Square results from Aquasim parameter estimation decreased from 2730 and 3464, to 2666 and 2346, when applying the full intermediate model, for the 6 and 10 kDa

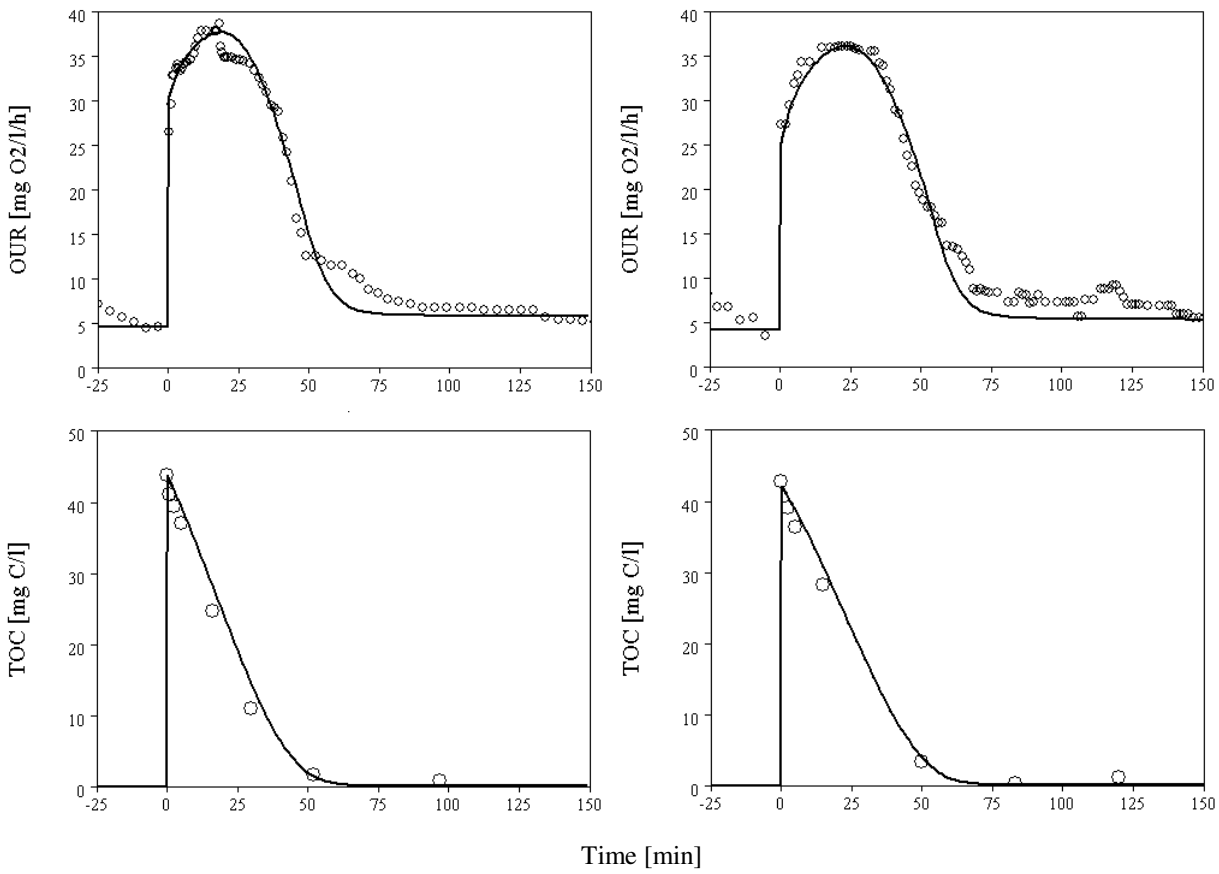


Figure 5-35. Modelled and measured OUR and bulk phase TOC during depolymerisation and mineralisation of initial $M_W$ of 6 (left panels) and 10.5 kDa Dextran (Experiment 10). Initial Dextran concentration was 100 mg/l.

standards, respectively). Thus, applying the complex model seems not to dramatically improve the overall observable performance. However, expanding the model from a one step process to a full intermediate depolymerisation model, without increasing the number of parameters by more than a single rate coefficient ($K_M$ of depolymerisation), clearly suggest model improvements in terms of generality and mechanistic reflection of the nature of Dextran depolymerisation. Parameter estimation of the two depolymerisation coefficients, $K_M$ and $V_{max}$, using the OUR and Bulk phase TOC data, gave half saturation concentrations of

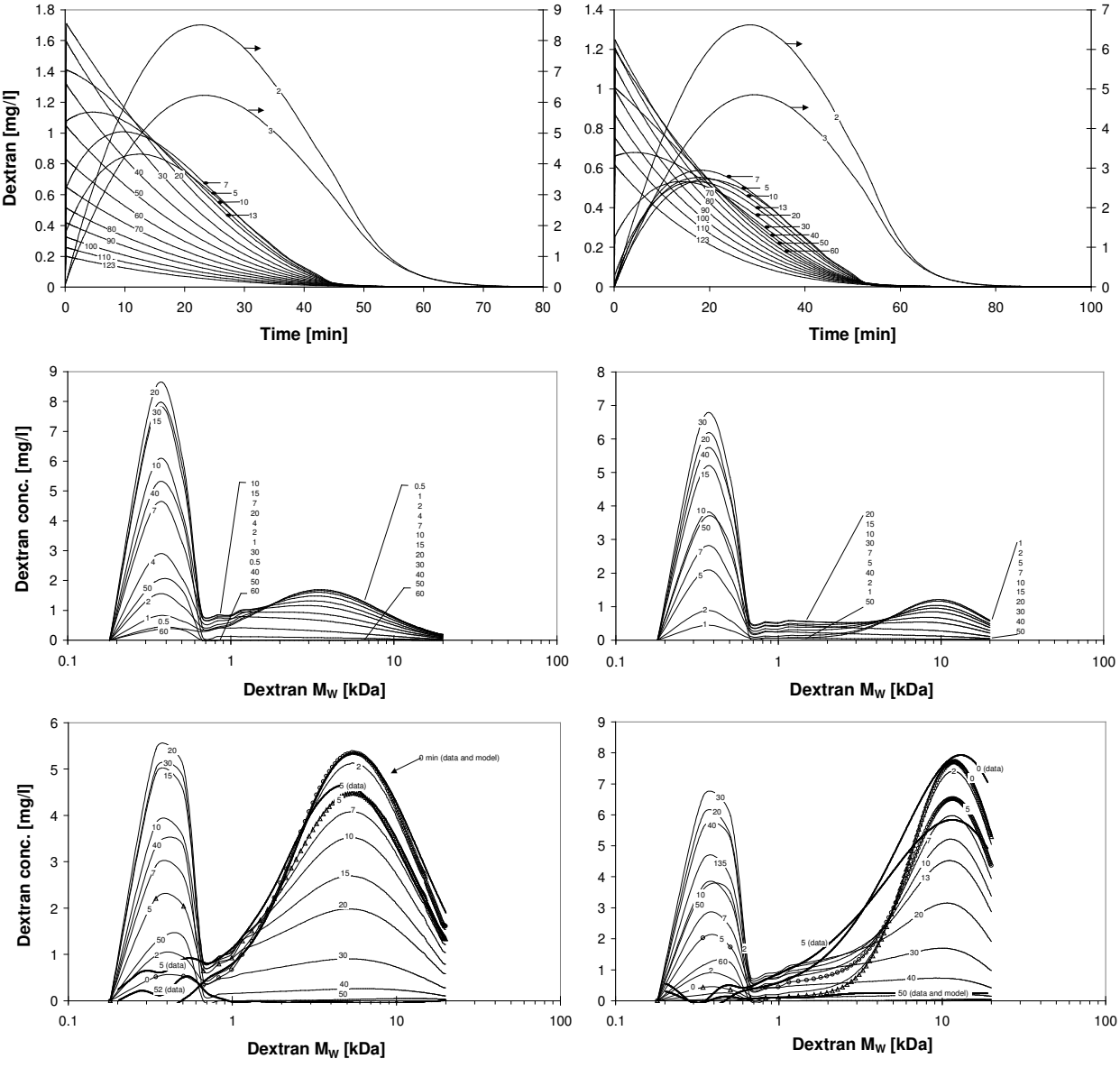


Figure 5-36. Simulated intermediate dynamics of 100 mg/l initial 6 (left panels), and 10.5 kDa Dextran sample standards. Upper row shows time series development of bulk phase intermediates. Middle plots presents simulated bulk phase $M_W$ distribution during degradation, while lower figures presents the same data compensated for superimposition and dispersion as they would appear from a calibrated RID signal (see text for details).

0.0254 and 0.0250 mg/l, and maximum Dextranase rates of 1554 and 1686 g/g·min, for 6 and 10 kDa, respectively. Even though the samples standards used for this estimation is close, and to a certain degree overlapping, the conformity of the estimated parameters, from two independent data sets of two separate state variables, support the model of size independent kinetic coefficients, with intrinsic $M_W$ effects as presented in Table 5-7 from the deduced expression in section 4.6. Figure 5-36 presents simulated intermediate dynamics during the depolymerisation of 6 and 10 kDa (initial concentration 100 mg/l), including the measured intermediates during experiment 10. Simulated intermediate data are compensated for peak overlapping and variable $M_W$ RID sensor response as discussed in section (5.1) and appendix 2, for qualitative comparison to the measured intermediate distributions. RID data are recalculated into Dextran concentrations using the slope/RID signal calibration presented in Appendix 2. Middle panels (Figure 5-36) show true simulated intermediate concentrations, while the lower panels indicate compensated distributions. Qualitatively, the simulated dynamics of the initial polymer peak resembles the measured distribution, however, simulations indicate accumulation of assimilable intermediates (especially P2 and P3) that are not seen in the data. Accumulation in the pre-assimilable range (1-5 kDa) does not occur during simulations.

This concludes the results section. Experimental data not reported here do not ad significant information to the results presented, or data are not interpretable using the methods applied. Raw data are available in Appendix 9.4 and 9.5.

# 6 Discussion

The main objectives of this study are evaluation of the effects of molecular weight on depolymerisation kinetics, the combined kinetic and transport effects of intermediate dynamics in diffusive gradient bio aggregates (here: biofilms) and location of depolymerisation in these systems.

## 6.1 Effect of molecular weight on depolymerisation kinetics

Degradation rate reductions due to increased substrate size, either as molecular weight or particle diameter, have to a certain degree been regarded *a priori* in the wastewater literature (Levine et al., 1991), and early studies on particle degradations confirmed that degradation rates of colloids are higher than degradation of supracolloidal particles (Balmat, 1957). The effect of molecular weight on polymer degradation in biofilm systems was investigated in this work by analysing bulk phase TOC (Figure 5-5 and Figure 5-9) and estimation of OUR (Figure 5-8 and Figure 5-11). While the OUR analysis provides qualitative evidence for the rate effects of $M_W$, analysis by the theory of Harremoës (1978) and Rittmann and McCarty (1980; 2001) of the bulk phase substrate concentration, enable quantitative evaluation. Figure 5-7 and Figure 5-10 show that degradation of polymers relates systematically to the molecular weight within the range above the membrane transport cut-off limit (or the direct assimilable range), and that above about 1-10 MDa the dependency change. The half order degradation coefficient decreased from about 1.5 to 0.057 $(g/m)^{1/2}/d$ when initial MW of the substrate was increased from 6 to 35000 kDa. This 26-fold decrease is similar to the size effects presented by Sollfrank and Gujer (1991) and Vollertsen and Hvitved-Jacobsen (1999) where 10-fold decrease in degradation of fast to slowly hydrolysable wastewater particles was found. The latter studies did not, however, separate the degradable fractions according to size, but by degradation. The biofilm removal rate of wastewater particles investigated here (section 5.5, Figure 5-23) correlated to first order kinetics in the range of values found in the literature. First order kinetics has been reported by many authors (see Table 2-3), and re-evaluation of the data of experiment 7 and 10 by first order kinetics showed that as the initial polymer become large, first order fitting becomes just as good as the variable order model by Rittmann and McCarty (1980; 2002).

The size effect on the observed removal rate may be due to reaction and/or transport limitations to the surface of, or into the biofilm matrix. From the mathematical definition of the areal removal coefficient, $k_{1/2,A}$ (5-3) , it is clear that both degradation rate effects and diffusion limitations are included in this parameter, by $k_{0,f}$ and $D_{Xs}$ respectively. Intrinsic reaction effects on the reaction coefficient may be due to the molar reduction of possible substrate molecules, combined with spatial limitations on the number of enzyme complexes per molecule. The initial concentration of Dextran in experiments 7 and 10 was kept constant at 100 and 200 mg/l, meaning that the initial number of available substrate molecules was inversely proportional to the molecular weight. As the substrate becomes smaller (number of polymer bonds per molecule decrease), the number of substrate molecules available for substrate-enzyme complex formation increase, yielding increased degradation rates.

An alternative explanation model for the observed size effect on the removal rate is the reduced substrate diffusion coefficient as the molecular size increase, described by the Stokes-Einstein equation (5-5). Figure 5-10 shows that $k_{1/2,A}$ relates to the molecular weight as ~ $M_W^{-0.19}$ while strictly mass transfer limitations should show a ~$M_W^{-0.5}$ relation (represented by the dotted line in Figure 5-10), not taking partitioning into account. Intermediate formation would reduce the average molecular weight during depolymerisation, and increase the effective diffusion coefficient. Therefore, the deviation between the observed reduction on $k_{1/2,A}$ and the theoretical estimate based on diffusion restrictions alone can be explained by intermediate formation effectively reducing the mean substrate molecular weight as the initial molecules are degraded. Bulk accumulation of small fragment intermediates has been observed in batch and continuous, suspended and biofilm cultures, and for pure and mixed populations (Haldane and Logan, 1994; Confer and Logan, 1998). These observations support the formation and accumulation of intermediates with increasing molecular mobility, resulting in increased penetration, degradation rates, and bulk phase accumulation. The shift from logarithmic reduction of $k_{1/2,A}$ as the initial molecular weight increase as depicted in Figure 5-10, to the less dependant removal rate of the high $M_W$ standards may be attributed to obstruction of the large molecules by the extracellular polymeric structure of the biofilm. Jimenez et al. (1988) found an upper biofilm diffusion limit of about 2 MDa, while Tanaka et al. (1984) indicated this limit to be lower (10-100 kDa) studying alginate gels resembling biofilm gel properties. More recently Stoodley et al. (1997) suggests the biofilm matrix to be microporous, with pore diameters between 50 - 200 Å, corresponding to spherical molecules of 20-200 kDa (see Figure 5-6). However, Bryers and Drummond (1998) points out that the biofilm matrix is heterogeneous in terms of porosity, and that macropores and channels are

common for heterogeneous biofilms, suggesting the matrix pore diameter to vary from micro- to macropores (0.2-10 MDa) within a considerable range of pore diameters. This is supported by Lawrence et al. (1994) who found spatial variability in the mobility of fluorescein labelled Dextrans of variable sizes in pure (*Pseudomonas fluorescens*) and mixed population biofilms using scanning confocal laser microscopy. Thus, the shift at 1-3 MDa observed in Figure 5-10 may very well be due to the inner filter effect of the biofilm matrix, indicating the limit of the effect of polymer/particle molecular weight on observed hydrolysis in biofilm systems. Above this limit the available area of the polymer/particle to biofilm surface area is more likely to be affecting the degradation rate indicated by the fat dotted line in Figure 5-10 as supported by other studies (Terashima and Lin, 2000).

By the analysis of the Thiele modulus (5-21) and (5-22) and the one step depolymerisation model (section 5.6.2) it is evident that the system was partly reaction limited by depolymerisation product utilisation during the peak OUR for Dextran below about 100 kDa. However, a similar analysis of the estimated first order depolymerisation rates and the Dextran diffusion coefficients shows that the depolymerisation process is at all times diffusion limited, even down to Isomaltose (0.342 kDa) for a biofilm as thin as 30 µm (Figure 5-32). This indicates that the overall removal rate of polymers is diffusion limited as long as depolymerisation is the rate limiting process. Accumulation of assimilable intermediates as shown in Figure 5-17 and partly in Figure 5-21, and from the full intermediate model (section 5.6.4) indicates, however, that depolymerisation is not rate limiting for degradation of low $M_W$ polymers, observations also supported by the Thiele modulus evaluation in Figure 5-32 (left). The logarithmic effect of $M_W$ on the overall degradation as presented in Figure 5-7 and Figure 5-10 can therefore be attributed to combined diffusion and reaction rate limitations, where reaction limitations are most likely to dominate for low $M_W$ intermediates and thin biofilms, and diffusion limitations gradually overtakes at higher $M_W$ (50 - 100 kDa).

## 6.2 Intermediate dynamics

Very limited information regarding intermediate formations and effects of such is found in the wastewater research and engineering literature. Investigations into the kinetics and stoichiometry of depolymerisation have been limited to one to three step processes of sequential degradation without measuring intermediate formation. Early studies by Banerji et al. (1968) showed that intermediate carbohydrates occurred in the liquid phase of activated

sludge systems degrading polysaccharides. Coulibaly et al. (2002) measured oligosaccharide accumulation during starch degradation in a model sewer bioreactor, and Larsen and Harremoës (1994) detected the same in a biofilm system. Haldane and Logan (1994) detected by ultrafiltration significant accumulation (14 and 54%) of intermediates in the size range below 1 and 10 kDa when studying 70 kDa Dextran degradation in batch and continuous monocultures. The same was observed by Confer and Logan (1997a; 1997b) when studying pure, limited mixed population and wastewater biofilm and suspended cultures degrading Bovine Albumin and Dextrans. In the latter study intermediates of 2-10 kDa accumulated during protein depolymerisation, while assimilable fractions (< 1 kDa) increased in the bulk phase of suspended pure and mixed biofilm and suspended cultures during Dextran and Dextrin (Starch hydrolysate) degradation. Depolymerisation fragments were released in a range of reactor and culture configurations, indicating that bulk phase accumulation of low $M_W$ intermediates is a general fundamental aspect of biological polymer degradation.

These findings are supported by the studies reported in this work. Using SEC-HPLC, intermediate dynamics could be presented as continuous distributions. The suspended pure enzyme studies reported in section 5.3.1 show that intermediates of all size fractions occur, and that low $M_W$ intermediates around the 1-5 kDa accumulate more than the intermediate fraction above 5 kDa, and that the formation of end products (di and trimers) are slightly delayed compared to the 1-5 kDa range. Similar delayed end product formation is also seen in the inactivated coupon experiments (Figure 5-18), but for these intact biofilm matrix studies no significant levels of larger intermediates (8-50 kDa) occurred. The absence of larger intermediates can be explained by the reduced diffusivity back to solution. A similar effect may account for the relative low removal effect on the initial polymers, as they will have to penetrate and not escape the biofilm matrix. Adsorption to biofilms is reported to correlate inversely to $M_W$ (Carlson and Silverstein, 1998), indicating marginal adsorption effects on the initial polymers. The colloidal standard may, however, be subjected to entrapment mechanisms to the surface, or inside the biofilm matrix (Drury et al., 1993), as the size of these particles is the order of biofilm cells (Stolzenbach, 1996). Rapid uptake, as seen in Figure 5-5 and Figure 5-9 (inserts), can only be explained by such mechanisms.

Accumulation of low $M_W$ intermediates was also observed by MacGregor et al. (1994). They suggested that multi-binding sites on the enzyme (α-Amylase) resulted in increased affinity for longer oligomers, $M_W$ > 1.5-1.7 kDa (DP>9-10), compared to the shorter intermediates. This resulted in intermittent accumulation of penta to octamers during degradation of amylose (0.8-1.3 kDa). No accumulation was observed for oligomers above this limit, and mono- di-

and trimers were only detected after the longer polymers were degraded. This dynamic pattern is very similar to the intermediate dynamics detected in this study, especially the pure enzyme experiment (section 5.3.1), experiment 7 and the coupon experiments (section 5.3.3 and 5.3.2). Naturally this is not reflected in the modelling results due to the assumption of equal enzyme affinity. This might indicate that Dextranase also posses a multi-binding sites active centre. It has been shown that the reaction mechanism of barley α-Amylase is similar to several bacterial α-Amylases (e.g. *Bacillus amyloliquefaciens*, Thoma, et al., 1971), so this model could also apply to other bacterial Glucanases. The combination of reduced reaction rates of the sub-DP10 oligomers combined with increased diffusivity by $M_W$ reduction may explain the observed dynamics.

Active biofilm coupon experiments show that assimilable fractions do accumulate intermittently similar to the observations by Haldane and Logan (1994) and Confer and Logan (1997b); however, accumulation of the low $M_W$ non-assimilable fractions (1-4 kDa) was more pronounced (Figure 5-17). Confer and Logan (1997a) observed this for protein degradation, but only to a limited extent during Dextran and Dextrin degradation. Assimilable fractions did not accumulate during the Rototorque degradation studies in experiment 7 (section 5.3.3), however, low $M_W$ non-assimilable intermediates accumulated similar to the coupon experiments (Figure 5-19 and Figure 5-20). Contrary to this, no intermediates accumulated at all in experiment 10 (Figure 5-21). The fundamental intermediate and assimilable fraction accumulation proposed by Confer and Logan (1997b; 1998) seems to be supported by these results. The model suggests that the production of low $M_W$ fractions proceed faster than assimilation and mineralisation by the culture responsible for the depolymerisation. However, they did not suggest mechanistic explanations to why this happens (though, necessity of reaching different enzymes are proposed), and from the data in this work there seems to be some circumstances where accumulation do not occur. In order to project fundamental systematic properties mechanistic understanding is necessary. Before entering that discussion, Figure 5-17 indicate that less accumulation is likely to occur during growth compared to starved biofilms. That indicates that accumulation is balanced by the uptake rate of depolymerisation products.

During sequential depolymerisation in a porous structure like biofilms, whereby a polymer is degraded into smaller fragments, the concentration of intermediates (and initial polymer) is very different from the equivalent distribution in the bulk. Intermediates formed in the biofilms are more likely to react further, than to diffuse back into the biofilm. As the products become smaller diffusivities within the biofilm increase, and the likelihood that products

diffuse back into the bulk solution increase. Depending on factors affecting the reaction kinetics and diffusion, such as the pore size and structure, temperature, enzyme activity, biofilm intrinsic advective transport, matrix surface charge, etc, intermediate concentrations in the bulk phase may occur. Varga and Malcata (1996) evaluated, by mathematical arguments, the behaviour of polymers diffusing into a structure holding immobilized enzymes. They evaluated the effect of the Thiele modulus (5-21) for saturated ($C_n >> K_M$) Michaelis Menten kinetics, defined as:

$$\Phi = \sqrt{\frac{L_f^2 \cdot k_{0,n} \cdot e_0}{C_n \cdot D_n}} \tag{6-1}$$

on the selectivity, $S_{i,i+1}$ (defined as the ratio of flux of $C_i$ to the flux of $C_{i+1}$ through the biofilm surface), of observable removal of polymer$_n$ ($C_n$) to polymer$_{n+1}$, following multisubstrate Michaelis-Menten kinetics (4-6):

$$S_{i,i+1} = \frac{D_i \cdot \left(\frac{dC_i}{dx}\right)_{x=L}}{D_{i+1} \cdot \left(\frac{dC_{i+1}}{dx}\right)_{x=L}} \quad for\ i = 2, 3, ..., n-2 \tag{6-2}$$

If the selectivity is positive and above 1, bulk phase intermediates will not form. In the selectivity range 0-1, substrate flux is higher than the product removal rate, indicating higher affinity for the substrate compared to the product (at equal diffusivities), or higher diffusivity of the products (at equal reaction rates) out of the biofilm (products are generated inside the matrix). Negative selectivity results when the intermediate formation is high enough to give net flux out of the biofilm surface. Depending on the bulk phase concentration of substrates and intermediates, intermediates may therefore form if the Thiele modulus of the intermediate is low and the bulk phase concentration is low. In this work reaction rate ($v_{max} = k_0 \cdot e_0$) is constant, while the diffusivity of the products always increased compared to the substrates. At higher $\Phi$ intermediates will not form due to diffusion limitations of products (intermediates) out of the biofilm slab. However, Thiele moduli will gradually decrease as the $M_W$ of the products decrease (diffusivity increase), and at some stage intermediates may occur (depending on the bulk phase concentration). This is in agreement with the theoretical investigation of Varga and Malcata (1996) who found that the selectivity of polymer removal gradually decreased first below 1, and then below 0 upon lowering the Thiele modulus of

depolymerisation reactions. In the range $\Phi \varepsilon$ [0.1,1] an abrupt shift occurred due to reversal of the intermediate concentration gradient in the matrix. Thus, in addition to the rate effects described by MacGregor et al. (1994), increased diffusivities due to reduced $M_W$ could also explain the accumulation of low $M_W$ intermediates. Combining these models do in fact explain accumulation of the non- assimilable as well as the delayed occurrence of the assimilable products in the pure enzyme and inactivated biofilm coupon experiment. For intermediates above the number of multicites of the endo-enzyme (10, MacGregor et al., 1994; 9-12 found by Thoma et al., 1971) the depolymerisation rate is constant. Reduced Thiele modulus by increased diffusivity, results in increased bulk phase intermediate formation. As the polymers are cleaved below the maximum active site number of the enzyme, the affinity is reduced leading to reduced conversion of the 4-9 DP fraction (0.67-1.5 kDa. This in turn increases the flux of these intermediates into the bulk, further enhancing the accumulation of these intermediates. As the depolymerisation of this fraction proceeds (at the reduced rate) the end products will finally dominate the bulk. During simultaneous assimilation of the assimilable fraction (0.18-0.9 kDa), the 1-2 kDa fraction will dominate in the bulk phase as observed for the active coupon experiments in section 5.3.2 (Figure 5-17), and the biofilm reactor experiment in section 5.3.3 (Figure 5-19 and Figure 5-20).

From the explanation model suggested above, the extent of intermediate release depends on the depolymerisation enzyme activity (amount and kinetics). Using the same enzyme as used in section 5.3.1 (Dextranase from *P. lilacinum* and Dextran from *L. mesenteroides* B 512), Mountzouris et al. (2002) also found Isomalto- and Isomaltotriose to be the major product (43 and 56 %, respectively). In addition, by HPLC-SEC they found intermediate accumulation in the 1-10 kDa region in a CSTR operated reactor when the enzyme activity was low combined with low residence time (60 min). As the enzyme activity (amount) and residence time increased, only di- to heptamers accumulated. Absence of intermediates due to high concentrations (activity) of depolymerising enzymes was also reported and discussed by Rollings et al. (1983). Their explanation suggests multi-binding of enzymes to single substrate polymers disabling release of the product sub/polymers until the polymers are small enough to be completely released by the enzymes. Whether high enzyme concentrations promote multi-bonding or limits the release and transport by the intermediates, both mechanisms suggest reductions in low $M_W$ intermediates due to elevated enzyme activity. Interestingly, limited substrate availability, as will be the case for degradation of non-hydrated dense colloids (like Starch granules), will significantly limit the amount of intermediate released to the bulk phase (Rollings and Thompson, 1984). Thus, high enzyme activities and low substrate availability

will limit accumulation of intermediates. This may explain the absence of significant amounts of intermediates during experiment 10 batches (Figure 5-21) compared to the ones in experiment 7. In experiment 10, half the initial Dextran concentration was added (100 as opposed to 200 mg/l), and the activity measured as OUR (reflecting synthesis of assimilable fractions) did not reduce by more than 16, 17 and 35 % for 10.5, 38.1/41.3 and 513 kDa, respectively (from Figure 5-8 and Figure 5-11). This suggests that the depolymerisation activity during experiment 10 was relatively higher than experiment 7. Reduced substrate availability and increased enzyme activity will both result in reduced accumulation of intermediates as seen in experiment 10 (Figure 5-21).

Another explanation to the accumulation in the 1-5 kDa range of pure enzyme studies is that Dextranase do not attack α1-2, α1-3 and α1-4 bonds of the branching points (Walker, 1978), nor adjacent α1-6 bonds (Walker and Pulkownik, 1974). Altered intermediate dynamics due to branching of Starch was reported by Sanroman et al. (1996). Branching also reduce depolymerisation of the polymer backbone by steric hindrances close to the branching positions. Open mixed cultures as applied in the coupon and biofilm reactor experiments probably house, or at least harbour the ability to synthesise, debranching enzymes. The observed accumulation of these fractions must in such circumstances be attributed to Thiele moduli effects as discussed above.

## 6.3 Enzyme location

Compared to the limited studies on intermediate dynamics during depolymerisation, identification and location mapping of extracellular enzymes are well studied for activated sludge and natural systems (see section 2.3 for references). For suspended cultures it seems evident that enzyme activity follows the cellular fraction (Banerji et al., 1967; Chóst 1991; Boczar et al., 1992; Frølund et al., 1995; Confer and Logan, 1997a; Confer and Logan; 1997b), even though reports of bulk phase dominated depolymerisation in pure cultures are available (Goel et al., 1997; Goel et al., 1998a; Goel et al., 1999), and several observations of secretion in natural habitats have been reported (see Wetzel, 1991, for a summary). Confer and Logan (1998a showed, by comparing suspended and biofilm cultures fed on polysaccharides (Dextran) and protein (Bovine Albumine), that hydrolytic activity was associated with the biofilm matrix, a minimum of five times higher than the biofilm filtrate. The results of this study support the proposed mechanism of Confer and Logan (1998b) of

depolymerisation activity in biofilms dominated by the biofilm matrix fraction, followed by possible back diffusion into the bulk phase by depolymerisation intermediate products. Further, it seems like the biofilm activity is compartmentalised with the cellular fraction of the biofilm, with no detectable activity in the filtered void water, EPS matrix or the bulk phase (Figure 5-22), and residual activity below the detection limit in the unfiltered non-cellular compartments. α-Glucosidase, associated with the cells of suspended and biofilm cultures by several workers (Confer and Logan (1998a; Goel et al., 1997; Goel et al., 1998a; Richards et al, 1984), detected through liberation of Glucose, was observed in the biofilm compartment. Addition of Dextran did not, however, increase the Glucose liberation rate, suggesting that the activity was not related to Dextran degradation. Inactivation by Azide did not alter this, indicating that the absence of Glucose was not related to rapid assimilation by the biofilm bacteria. Residual Glucose can be attributed to Glucose leakage from surplus intracellular Glucose during mineralisation of Dextranase products (Isomaltoses).

These data were obtained during continuous operation of the Rototorque reactors (experiment 8; see Table 4-1) at $\Theta_H$ of 75 min, and Dextran loading of 3.5 g/m$^2$·d. This is in the same range as full scale wastewater biofilters are operated (Tchobanoglous et al., 2003). Depolymerisation of polymers in biofilm systems are therefore not likely to be the result of bulk phase exogenous enzymes as suggested by Rohold and Harremoës (1993) and Larsen (1992), and conceptualised by the model suggested by Larsen and Harremoës (1994). The intermediate dynamics and enzyme locations observed in this work support the general model suggested by Confer and Logan (1998b) of cellular enzyme location and intermediate transport via the bulk (graphically presented in the conceptual model in Figure 3-2).

Releasing enzymes into the bulk phase has by several authors been viewed as energetically inefficient compared to cell-associated locations (Confer and Logan, 1998; Wentzel, 1991; Hoppe, 1983; Hollibaugh and Azam, 1983) due to increased susceptibility to degradation and chemical alteration, and the increased distance between the product releasing site and the enzyme producer. Wentzel (1991) argued, however, that releasing enzymes into solution still would benefit cells over distances as high as 500 µm. In biofilm systems, transport limitations will reduce the efficiency of polymer degradation, limitations that would be reduced if enzymes were released to the bulk, and more diffusible products return. However, bulk phase constituents are subjected to washout, and enzymes released to the bulk would very soon be transported out of energetically favourable zones (e.g. > 500 µm). As a community, though, coordinated release of enzymes could still be beneficial for harvesting limited diffusible substrates through collective harvesting, and mutualistic mechanisms have been proposed and

observed in these consortia (Costerton and Lewandowski, 1997; Watnick and Kolter, 2001; Stoodley et al., 2002). Location of exogenous enzymes may therefore be subjected to environmental regulation on gene and/or community level controlled by factors like residence time, growth rate, substrate availability/transport limitations, substrate properties, etc. The numerous observation of cell associated activity to the less frequent reports of extracellular may suggest that cell association is the most common location but certain conditions may induce release into the surrounding media. In biofilms, that would primarily imply release to the EPS matrix and void liquids, and subsequent release to the bulk. Thus, the model suggested by Larsen and Harremoës (1994) may be a contingency mechanism for polymer and particle degradation, while the standard scheme outlined by Confer and Logan (1998a; 1998b) prevail during "normal" conditions.

## 6.4 Modelling

Mathematical modelling is a very efficient way of organising and communicating quantitative concepts and hypothesis. In this work, three modelling exercises are used to 1) identify and calibrate growth and biofilm structure dynamics; 2) calibrate a one step depolymerisation model as suggested by the ASM group (see references in section 5.6.2) for evaluation of size effects on depolymerisation kinetics (as opposed to degradation kinetics by the approach suggested by Harremoës (1978) and Rittmann and McCarty (1980; 2002)); 3) further investigations into the cause of the observed size dependency; and 4) qualitative calibration of a full range intermediate model for simulation of intermediate dynamics, and qualitative comparison to observed intermediate distributions. Kinetics and stoichiometry for the applied models were based on first order kinetics in accordance with the ASM suggestions, adapted to biofilm conditions; and multi-substrate kinetics and stoichiometries developed from standard Michaelis-Menten expressions.

Calibration and validation of the biofilm characterisation model (Figure 5-25, Figure 5-26 and Figure 5-29) show acceptable fit to the measured bulk phase TOC and OUR data, and the growth and biofilm dynamics parameters estimated (Table 5-4) are within reported values for similar mixed culture biofilm systems (see references in section 5.6.1).

Using the calibrated growth model, one step depolymerisation was calibrated for all size classes investigated in experiment 10 (section 5.2.3), and results are presented in Figure 5-30. Compared to the modelling using the Rittmann and McCarty (1980; 2002) model, tight fitting

is achieved for both observed variables, OUR and bulk TOC. Estimated first order depolymerisation rate coefficients show similar logarithmic correlation to the substrate molecular weight as found by the analytical solution (Figure 5-7 and Figure 5-10), confirming the analytical direct degradation results, even though the three distinct regions identified on Figure 5-10 did not appear as clearly. By itself, this result indicates logarithmic reaction rate reduction by the substrate $M_W$. At the same time, transport limitations are evident from the evaluation of the Thiele moduli calculated using the depolymerisation coefficients estimated (Figure 5-32). As the Thiele moduli increase linear to the logarithm of the $M_W$ even though the linear reduction of $k_h$ to the logarithm of $M_W$ (Figure 5-31) is used for the Thiele moduli calculations, significant effects on the overall removal rate must in addition be attributed to transport limitations, especially for the larger polymers. Interestingly, the colloidal size standard show reduced Thiele modulus compared to the dissolved polymers, which means that for this fraction transport limitations are not as strong, but that reaction rate reduction becomes more significant. This may indicate that the colloid is not diffusing into the matrix (transport independent from size) but is depolymerised at the biofilm surface, and the reduction in overall removal rate is dominated by reaction rate reductions. Combining these

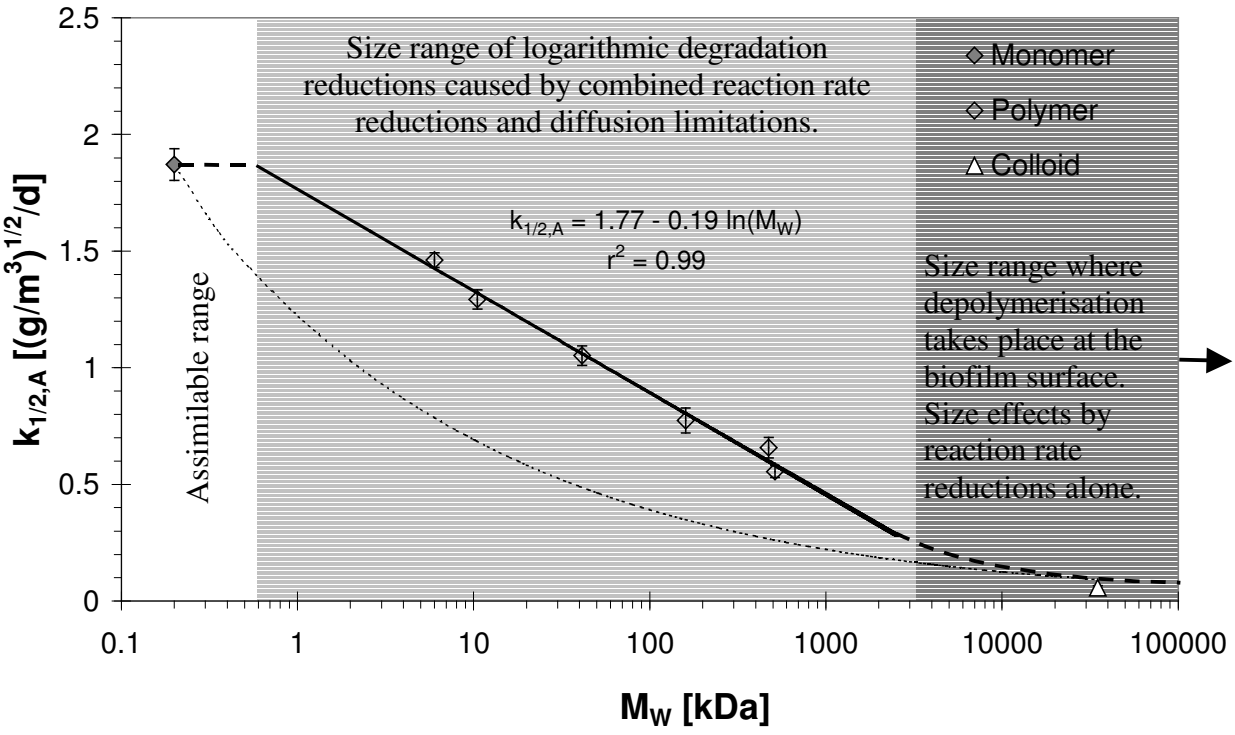


Figure 6-1. Conceptual model for the combined effect of transport and reaction rate on observed removal rate by substrate molecular size.

two observations, a unified degradation model for polymer and particle degradation in biofilms may be suggested. Dissolved polymers able to penetrate the biofilm matrix are subjected to logarithmic reduction of observed removal rate due to reaction rate and transport limitations. Non-diffusible polymers, colloids and particles are subjected to reaction rate reductions only, and show less dependency towards substrate molecular weight. The unified degradation model concept is presented in Figure 6-1.

Kinetic expressions presented in section 4.6 were developed by assuming: single active site - single substrate bond enzyme-substrate complex formation, equal complex formation probability (constant $K_M$) and no $M_W$ effects on the product rate formation ($k_0$). These are standard assumptions underlying the gross of continuous multi-substrate Michaelis-Menten kinetics (Suga et al., 1974; Costa and Malcata, 1994; Silva and Malcata, 1994; Varga and Malcata, 1996; Sehanputri and Hill Jr., 2000). Kinetic expressions and stoichiometry developed for endo activity (4-2 and 4-3) and exo depolymerisation (4-6, 4-7 and 4-8) are equivalent to the molar expressions by Suga et al. (1974).

Inability to extract single polymer intermediates from the HPLC-SEC data made quantitative calibration and validation of the full intermediate model impossible. However, by grouping simulated intermediates by a constant time factor, column dispersion and intrinsic calibration uncertainty could be mimicked for qualitative comparison to real data. This introduced artefacts, especially pronounced in the low $M_W$ region, and care should be exercised during interpretation.

Suspended pure enzyme simulation results (Figure 5-33) indicate formation of all possible intermediates similar to the observations in section 5.3.1, and resemble the simulated distribution dynamics reported in the early works of Montroll and Simha (1940). For the biofilm plots (Figure 5-36), assimilable (0.18-0.9 kDa) product formation dominates bulk phase accumulation (especially the Dextranase end products), while non-assimilable low $M_W$ accumulation is not significant. Comparing the grouped simulation results to the observed distributions in experiment 10 (Figure 5-36, low panels) it is clear that the calibrated model overestimates assimilable substrate accumulation, while the higher $M_W$ intermediates show better fit.

The full intermediate biofilm model was calibrated against measured OUR and bulk TOC by tuning the endo- activity maximum, $v_{max}$, (as Dextranase was the only depolymerising enzyme detected) and the Michaelis coefficient, while exo-activity was set to zero. Figure 5-35 show the result of the calibration. The estimated $K_M$ values are remarkably close, and similar to literature reports on *Penicillium lilacinum* Dextranase (Das and Dutta, 1996). As literature

values are hard to implement in a structured multisubstrate model (most of the literature values are estimated using one step Michaelis-Menten models), further interpretation cannot be done. This is seen by the fact that most reported affinities are very low[12], indicating competitive substrate inhibition rather than true low affinities (ref. equation 4-2). However, it is interesting that the estimated parameters are pair wise close (both $K_M$ and $v_{max}$), and that the overall model performance is close to the observed OUR and TOC.

By leaving out the exo-glucanase activity, reported synergistic effects found for celluloses (Okazaki and Moo-Young, 1978; Fujii) and Starch degradation (Fujii and Kawamura, 1985) is not included. Dean III and Rollings (1992) showed that synergism becomes significant for homogenous endo, and to *endo* + *exo* activity ratios in the range 0.3 - 0.7, using a model very similar to the one proposed here. As the measured ratio is very close to unity, synergism may not have been a major mechanism during the experiment herein. Moreover, the same authors also found that log $(K_M/S_0)_{\text{endo}}$ values above zero exhibited most synergism, values that are very far from the ones obtained in this study (here about -3.5).

Multi-substrate modelling as suggested here exhibits the drawback of complexity on parameter estimation and model identification. Even though the full intermediate model does not contain many parameters, inability to identify intermediates and enzyme concentrations precisely, makes estimation of kinetic parameters very uncertain, if not impossible. Applications should therefore be restricted to qualitative evaluations. Lumped substrate modelling, like the ones reported in section 5.6.2 or generic limited number intermediate models, should be used for macro scale evaluations. Nevertheless, the model framework is *a priori* and from observations more consistent with the micro scale dynamics of the process. Further investigations into the process should therefore be based on the full intermediate mechanistic model, in order to develop a sound basis for data interpretation. That would require development or adaptations of refined analytical methodologies for enzyme and intermediate quantification, and implementation of the mathematical model in powerful numerical software. From detailed knowledge of the fundamentals, lumped models may be used for applied reactor modelling, restricted by necessary assumptions evaluated against the detailed model. It is better to do qualified simplifications on the known, than guessing the unknown.

[12] BRENDA (http://www.brenda.uni-koeln.de/php/result_flat.php3?ecno=3.2.1.11)

## 6.5 Implication for wastewater treatment systems

This section presents a short attempt to project the results and discussion on polymer and colloid degradation to wastewater engineering applications. Some ideas on how intermediate dynamics may be used for the development of novel designs are suggested.

Renewed interest for the application of biofilm reactors for treating municipal and industrial wastewater has been catalysed by the development of quantitative mechanistic models for biofilm dynamics the past 25 years. Removal of dissolved and colloidal organics following primary treatment, nitrification and denitrification using packed and suspended biofilters, are now standard wastewater engineering applications. Adsorption of smaller fragments, mainly dissolved polymers (Carlson and Silverstain, 1998), and physical retention (entrapment) by the heterogeneous biofilm structure (Bouwer, 1987), removes polymer and particulate organic matter to the bio aggregate (also valid for suspended biofilms: activated sludge flocs). Retention close to the active biomass enhance degradation by depolymerisation and mineralisation, and by sludge return (activated sludge) and substratum growth (biofilms), particles are given sufficient retention time for complete depolymerisation. As suggested in the present study, depolymerisation by exogenous enzymes in the biofilm matrix cause readily biodegradable substrates to diffuse back into bulk solution, whereby these are subjected to advective transport further into the biofilter (packed bed). Thus, hydraulic retention time significantly determines the COD dynamics in biofilters, and successful design for COD removal must take the size effects and dynamics of particulate/polymeric organic matter into account.

Biofilters have also been used successfully to oxidise ammonium, and for nitrogen removal (Harremoës and Henze, 2002). Use of treatment plant internal carbon sources for post-denitrification is interesting in order to minimize sludge production, and reduce operation costs (Janning, 1998). Particles extracted after pre-treatment are bypassed the secondary BOD removal and nitrification process, and fed denitrifying biofilters (la Cour Jansen et al., 2002). Entrapment and adsorption of SBOD will, by depolymerisation, provide carbon source for the biofilm downstream. Again, design and operation of such filters must take size effects on depolymerisation and transport dynamics into account. Bulk phase intermediate formation will, by the plug flow advection, distribute RBCOD deeper into the filter with consequences for the location of denitrification.

Biofilters may be designed for one stage nitrogen removal in post aerobic RBCOD removal systems, by bypassing SBCOD from primary treatment to combined nitrification-denitrification filters. Particles and colloids entering the filter will adsorb to surface biofilm in the inlet region, and release intermediates to the advective bulk for transport deeper into the filter. Aerobic ammonium rich inlet water with limited RBCOD may select for nitrifying cultures below the limited heterotrophic surface layer, loaded with particulate and colloidal SBCOD. As the RBCOD is relatively low, nitrifiers are able to compete with the heterotrophs for oxygen, maintaining viable autotrophic cultures in the deeper part of the biofilm in the inlet stages of the filter. Autotrophic growth may even cause extended surface detachment of adsorbed SBCOD and heterotrophs, carrying them deeper into the filter. Depending on organic loading and hydraulic retention time, a pseudo steady state could be achieved where nitrifiers dominate the first stage of the filter, consuming oxygen and releasing nitrate, followed by anoxic sections deeper in the filter receiving electron donor from the depolymerisation of SBCOD in the upstream aerobic and anoxic sections. Combined nitrification- denitrification could also be achieved in a suspended biofilm reactor low in bulk phase RBCOD, but with high SBCOD and ammonium. Under such conditions, fast growing autotrophs may be able to compete with the heterotrophs in the upper layers, resulting in sharp oxygen gradients (due to the high OUR of nitrifiers) and formation of anoxic layers in the deeper biofilm sections. In such a regime, particles retained on the surface and/or transported into the upper regions of a biofilm, will be depolymerised into diffusive intermediates and products that may enter deeper into the biofilm, where anoxic respiring heterotrophs create a sink for depolymerisation products and nitrate. Limited depolymerisation rate could enable steady state conditions of autotrophic surface layers growing on top heterotrophs growing at limited rate under anoxic conditions. The key factor for this condition is the concentration of bulk phase RBCOD and oxygen.

Intermediate dynamics will also have an effect on mathematical modelling of wastewater systems. In the ASM group (Henze et al., 2000), depolymerisation, or hydrolysis, is treated as a one step model not taking the size of substrates into account. In gradient systems, biofilms and activated sludge flocs, sequential depolymerisation into more and more diffusive intermediates will affect the observed removal rates, causing overestimation of kinetic parameters, or SBCOD fraction. By the same reasons, generalisation of parameters is also difficult, something that might be the reason for the relatively large range of hydrolysis parameters reported, and the emphasis by the ASM group on hydrolysis parameters as a major source of uncertainty of the ASM models (Henze et al. 2000).

# 7 Conclusion

Depolymerisation in biofilms was investigated for the purpose of obtaining general knowledge on degradation of dissolved polymers and colloidals using the polysaccharide Dextran as model substrate. Oxygen utilisation rates and bulk phase TOC measurements during batch operation of a rototorque biofilm reactor were used to investigate the effect of initial molecular weight on the observed removal rates. Bulk phase size distribution of depolymerisation intermediates was measured by HPLC-SEC using pure enzymes and biofilms, and specific enzyme assays were used for identifying the location of depolymerisation. Calibration of a mixed population biofilm model was used to compare simulated substrate dynamics with mineralisation rate (OUR), and bulk phase substrate dynamics. By theoretical analysis of the estimated depolymerisation rates and literature data on polymer diffusivity in biofilms, a conceptual model for the combined effect of polymer and particle size on depolymerisation and transport in biofilms is suggested.

The main conclusions are:

1. Dextran removal rate decrease with increasing Dextran molecular weight. The observed areal half order removal rate coefficient, $k_{1/2,A}$, show negative logarithmic correlation to the initial $M_W$ of Dextran in the 1-500 kDa range.

2. Depolymerisation intermediates accumulated in the bulk phase over the entire Dextran size range during pure Dexranase (3.2.1.11) studies. Final products were oligoisomaltoses (DP 2-6). Dextran was not depolymerised by α-Glucosidase (3.2.1.20) nor Oligo-α-1,6 Glucosidase.

3. Removal of Dextran is biomass dependent in what appears to be a non-linear dependency on biofilm thickness, expressed as biomass areal density ($g/m^2$), with no depolymerisation observed for thin biofilms (0.7 $g/m^2$), slow for medium (3.7 $g/m^2$) and high for thicker biofilms (5.2 $g/m^2$).

4. Low $M_W$ Dextran intermediates (1-10 kDa) accumulated in the bulk during depolymerisation of 160 kDa Dextran at 250 and 200 mg/l initial concentrations, but were not detected during experiments with 100 mg/l initial concentrations. Intermediate range Dextran (10-100 kDa) did not accumulate in either case. At the

same conditions, some assimilable range Dextran (0.2-0.9 kDa) accumulated during initial 250 and 200 mg/l batches, but was not detected during 100 mg/l initial concentrations. The extent of bulk phase accumulation seems to depend on the biofilm growth rate, where more bulk phase accumulation is observed during experiments with starved compared to more actively growing biofilms. More intermediates accumulate during low $M_W$ initial standards, compared to higher. These observations indicate that the extent of bulk phase intermediate accumulation is balanced by the rate of depolymerisation, and the substrate uptake rate (growth). Accumulation in biofilm systems is therefore depending on the SBCOD loading rate.

5. Dextranase was detected in the cellular fraction of the biofilms. Dextranase activity was not detected in any other biofilm sub compartments.

6. The observed bulk phase intermediate accumulation and enzymatic activity in the cellular fraction, support the conceptual model of Confer and Logan (1998), implying that bulk phase intermediate accumulation observed in this study and by others, is not a result of enzymatic activity in the bulk phase, but transport of intermediates from the biofilm matrix.

7. Evaluation of Thiele moduli from one step depolymerisation modelling suggests that the logarithmic reduction in observed removal rate is caused by combined reaction rate and transport limitations. Transport limitations dominates as the polymeric substrate size increase and inhibit biofilm matrix diffusion, and the removal rate becomes a surface limited reaction

.

# 8 References


Amon, R.M.W. and Benner, R. (1994) Rapid cycling of high molecular weight dissolved organic matter in the ocean, Nature, **369**, pp. 549-552

Andrews, G.F. and Tien, C. (1977) New approach to bacterial kinetics in wastewater, *J. Env. Eng. Div. ASCE*, **103**(6), pp. 1057-1074

Argaman, Y. (1995) A steady state model for the single sludge activated sludge system - I. Model description, *Wat. Res.*, **29**(1), pp. 137-145

Arnosti, C. (1995) Measurement of depth- and site-related differences in polysaccharide hydrolysis rates in marine sediments, *Geochim. Cosmochim Acta*, **59**(29), pp. 4247-4257

Arnosti, C. and Repta, D.J. (1994) Extracellular enzyme activity in anaerobic bacterial cultures: Evidence of Pullulanase activity among mesophilic marine bacteria, *Appl. Environ. Microbiol*., **60**(3), pp. 840-846

Ashwell, G. (1957) Colorimetric analysis of sugars, *Meth. Enzymol*. **3**, pp. 73-105

Atlas,R.M. and Bartha, R. *Microbial Ecology: Fundamentals and Applications*, 4th ed., Benjamin/Cummings Publishing Company Inc., Manlo Park (CA), 1998

Bailey, J.E. and Ollis, D.F *Biochemical engineering fundamentals*, 2nd. ed., McGraw-Hill, Singapore, 1986

Bakke R., Trulear, M.G, Robinson , J.A, and Characklis, W.G. (1984) Activity of *Pseudomonas aeruginosa* in biofilms: steady state. *Biotechnol. Bioeng* **26**(12), pp.1418-1424.

Bakke, R. *Biofilm detachment*, Ph.D. thesis, Montana State University, MT, 1986

Bakke, R. and Olsson, P.Q. (1986) Biofilm thickness measurements by light microscopy, *J. Microbiol. Meth.*, **5**, pp. 93-98

Balmat, J.L. (1957) Biochemical oxidation of various particulate fractions of sewage, *Sewage & Industrial Wastes*, **29**(7), pp. 757-761

Banjeri, S.K., Ewing, B.B., Engelbrecht, R.S. and Speece, R.E: (1968a) Mechanism of starch removal in the activated sludge process, *J. Wat. Poll. Contr. Fed.* **40**(1), pp.16-29

Banjeri, S.K., Ewing, B.B., Engelbrecht, R.S. and Speece, R.E: (1968b) Kinetics of removal of starch in activated sludge systems, *J. Wat. Poll. Contr. Fed.* **40**(2), pp.161-173

Baty III, A.M., Diwu, Z., Dunham, G., Eastburn, C.C., Geesey, G.G., Goodman, A.E., Suci, P.A. and Techkarnjanaruk, S. (2001) Characterization of extracellular chitinolytic activities in biofilms, in *Methods in Enzymology Part A*, **336**, *Microbial growth in biofilms*, Doyle R.J. (ed.), Academic Press, San Diego 2001

Bayer, E.A., Shimon, L.J.W., Shoham, Y. and Lamed, R. (1998) Cellulosomes - Structure and ultra structure, *J. Struct. Biol*., **124**(2-3), pp. 221-234

Beeftink, H.H., van der Heijden, R.T.J.M. and Heijnen, J.J. (1990) Maintenance requirements: energy supply from simultaneous endogenous respiration and substrate consumption, *FEMS Microbiol Ecol*, **73**, pp. 203-210

Beguin, P. and Aubert, J.P. (1994) The biological degradation of cellulose, *FEMS Microbiol. Rev*., **13**, pp. 25-58

Benner, R., Pakulski, J.D., McCarthy, M., Hedges, J.I. and Hatcher, P.G. (1992) Bulk chemical characteristics of dissolved organic matter in the ocean, *Science*, **255**, pp. 1561-1564

Bjerre,H.L. (1996) *Transformation of wastewater in an open sewer: The Emscher River, Germany*, Ph.D. thesis, Aalborg University, Aalborg, Denmark

Boczar, B.A., Begley, W.M. and Larson, R.J. (1992) Characterization of enzyme activity in activated sludge using rapid analysis for specific hydrolases, *Wat. Env. Res.*, **64**, pp. 792-797

Boetius, A and Lochte, K. (1994) Regulation of marine enzymatic degradation of organic matter in deep sea sediments, *Mar. Ecol. Prog. Ser.*, **104**, pp. 299-307

Boetius, A and Lochte, K. (1996) Effect of organic enrichment on hydrolytic potentials and growth of bacteria in deep sea sediments, *Mar. Ecol. Prog. Ser.*, **140**, pp.239-250

Boos, W. and Shuman, H. (1998) Maltose/Maltodextrin system of *Escherichia coli*: Transport, metabolism and regulation, *Microbiol. Mol. Biol. Rev*., **62**(1), pp. 204-229

Boyd, A., and Chakrabarty, A.M. (1994) Role of alginate lyase in cell detachment of *Pseudomonas aeruginosa*, *Appl. Env. Microbiol.,* **60**(7), pp. 2355-2359

Boyd, A., and Chakrabarty, A.M. (1995) *Pseudomonas aeruginosa* biofilms - Role of the alginate exopolysaccharide, *J. Ind. Microbiol.,* **15**(3), pp. 162-168

Bryers, J.D. and Mason, C.A. (1987) Biopolymer particulate turnover in biological waste treatment, *Bioproc. Eng.*, **2**, pp. 95-109

Bryers, J.D. *Biofilms* II, *process analysis and applications*, Bryers, J.D. (ed.), Wiley series in ecological and applied microbiology, New York, 2000

Carbonell, J.V., Izquierdo, L., Sendra, J.M. and Manzannares, P. (1998) A Monte Carlo simulation of the depolymerisation of linear homopolymers by endo-enzymes exhibiting random attack probability and single attack mechanism: Application to the (1→3), (1→4)- β-D-Glucan/endo-(1→3),(1→4)-β-D-Glucanase system, *Biotechnol. Bioeng*., **60**(1), pp. 105-113

Carlson, G. and Silverstein, J. (1998) Effect of molecular size and charge on biofilm sorption of organic matter, *Wat.Res.*, **32**(5), pp. 1580-1592

Cembella, A.D., Antia, N.J. and Harrison, P.J. (1984) The utilisation of inorganic and organic phosphorous compounds as nutrients by eukaryotic micro algae: A multidisciplinary perspective. Part 1, *CRC Crit. Rev. Microbiol*., **10**, pp. 317-391

Cheryan, M. *Ultrafiltration and Microfiltration Handbook*, Technomic Publishing, Lancaster Pennsylvania, 1998

Characklis, W.G. (1990a) Biofilms: A basis for an interdisciplinary approach, in *Biofilms*, Characklis, W.G. and Marshall, K.C. (ed.), pp. 195-231, John Wiley and Sons Inc., New York, 1990

Characklis, W.G. (1990b) Laboratory biofilm reactors, in *Biofilms*, Characklis, W.G. and Marshall, K.C. (ed.), pp. 55-89, John Wiley and Sons Inc., New York, 1990

Characklis, W.G. and Marshall, K.C. (1990) Biofilms: A basis for an interdisciplinary approach, in *Biofilms*, Characklis, W.G. and Marshall, K.C. (ed.), pp. 3-16, John Wiley and Sons Inc., New York, 1990

Characklis, W.G., Turakhia, M.H. and Zelver, N. (1990) Transport and interfacial transfer phenomena, in *Biofilms*, Characklis, W.G. and Marshall, K.C. (ed.), pp. 265-340, John Wiley and Sons Inc., New York, 1990

Christensen, B.E. and Characklis, W.G. (1990) Physical and chemical properties of biofilm systems, in *Biofilms*, Characklis, W.G. and Marshall, K.C. (ed.), pp. 93-130 John Wiley and Sons Inc., New York, 1990

Chróst, R.J. (1991) Environmental control of the synthesis and activity of aquatic microbial ectoenzymes, in *Microbial Enzymes in Aquatic Environments*, Chróst, R.J. (ed)., Brock/Springer Series in Contemporary Bioscience, Springer Verlag, New York, 1991

Chróst, R.J. (1990) Microbial ectoenzymes in aquatic environments, in *Aquatic Microbial Ecology: Biochemical and Molecular Approaches,* Overbeck, J. and Chróst, R.J. (ed.), Springer Verlag, New York, 1990

Clesceri, L.S., Greenberg, A.E. and Eaton *Standard Methods for the examination of water and wastewater*, American Public Health Association/American Water Works Association/Water Environment Federation, Washington, 1998

Cliff, R.C. (1980) *A dynamic model for predicting oxygen utilization in activated sludge processes,* Ph.D. thesis, University of Huston, TX

Confer, D.R. and Logan, B.E. (1991) Increased bacterial uptake of macromolecular substrates with fluid shear, *Appl. Env. Microb.*, **57**(11), pp. 3093-3100

Confer, D.R. and Logan, B.E. (1997a) Molecular weight distribution of hydrolysis products during biodegradation of model macromolecules in suspended and biofilm cultures .1. Bovine serum albumin, *Wat. Res.*, **31**(9), pp. 2127-2136

Confer, D.R. and Logan, B.E. (1997b) Molecular weight distribution of hydrolysis products during the biodegradation of model macromolecules in suspended and biofilm cultures. 2. Dextran and dextrin. *Wat. Res.*, **31**, (9), 2137-2145

Confer, D.R. and Logan, B.E. (1998a) Location of protein and polysaccharide hydrolytic activity in suspended and biofilm wastewater cultures, *Wat. Res.*, **32**(1), pp. 31-38.

Confer, D.R. and Logan, B.E. (1998b) A conceptual model describing macromolecule degradation by suspended cultures and biofilms, *Wat. Sci. Tech.*, **37**(4-5), pp. 231-234

Cornish-Bowden, A. *Fundamentals of enzyme kinetics*, Rev. edition, Portland Press, London 1995

Costa, R.M. and Malcata, F.X. (1994) Multisubstrate Michaelis-Menten kinetics: Explicit dependence of substrate concentration on the time for batch reactors, *Bioproc. Eng.*, **10**(4), pp. 155-159

Costerton, J.W., Lewandowski, Z., Caldwell, D.E., Korber, D.R. and Lappin-Schott, H.M. (1995) Microbial biofilms, *Ann. Rev. Microbiol.*, **49**, pp. 711-745

Costerton, J.W. and Lewandowski, Z. (1997) The Biofilm Lifestyle, *Advances in Dental Research*, **11**(1), pp. 192-195

Costerton, J.W., Cook, G. and Lamont, R. (1999) The Community Architecture of Biofilms: Dynamic Structures and Mechanisms, in *Proc. Dental Plaque Revisted*: *Oral Biofilms in Health and Disease*, Newman, H.N. and Wilson, M. (ed), BioLine, pp 5-14

Cotner, J.B. and Wentzel, R.G. (1991) Bacterial phosphatase from different habitats in a small hard water lake, in *Microbial Enzymes in Aquatic Environments*, Chróst, R.J. (ed)., Brock/Springer Series in Contemporary Bioscience, Springer Verlag, New York, 1991

Coughlan, M.P. (1985) The properties of fungal and bacterial cellulases with comment on their production and application, *Biotechnol. Genetic Eng. Rev*., **3**, pp. 39-109

Coughlan, M.P. (1992) Enzymatic hydrolysis of cellulose: An overview, *Bioresource Technol*., **39**(2), pp. 107-115

Coulibaly, L., Naveau, H. and Agathos, S.N. (2002) A tank-in-series bioreactor to simulate macromolecule laden wastewater pre-treatment under sewer conditions by *Aspergillus niger*, *Wat. Res.*, **36**(16), pp. 3941-3948

Das, D.K. and Dutta, S.K. (1996) Purification, biochemical characterization and mode of action an extracellular endo-dextranase from the culture filtrate of *Penicillium lilacinum*, Int. *J. Biochem. Cell Biol.*, **28**(1), pp. 107-113

Davies, D.G., Parsek, M.R., Pearson, J.P., Iglewski, B.H., Costerton, J.W. and Greenberg, E.P. (1998) The involvement of cell-to-cell signals in the development of a bacterial biofilm, *Science*, **280**(5361), pp. 295-298

Dean III, S.W. and Rollings, J.E. (1992) Analysis and quantification of a mixed exo-acting and endo-acting polysaccharide depolymerisation system, *Biotechnol. Bioeng.*, **39**(9), pp. 968-976

de Beer, D., Stoodley, P. and Lewandowski, Z. (1994a) Liquid flow in heterogeneous biofilms, *Biotechnol. Bioeng*. **44**(6), pp. 636-641.

de Beer, D., Stoodley, P., Roe, F. and Lewandowski, Z. (1994b) Effects of biofilm structures on oxygen distribution and mass transport. *Biotechnol. Bioeng*. **43** pp. 1131-1138

de Beer, D., Stoodley, P. (1997) Relation between the structure of an anaerobic biofilm and transport phenomena, *Wat. Sci Tech*., **32**(8), pp. 11-18

de Beer, D., Stoodley, P. and Lewandowski, Z. (1997) Measurement of local diffusion coefficients in biofilms by micro-injection and confocal microscopy. *Biotechnol. Bioeng.* **53**, pp. 151-158.

de la Sota, A., Larrea, L., Novak, L., Grau, P. and Henze, M. (1994) Performance and model calibration of R-D-N- process in pilot plant, *Wat. Sci Tech.*, **30**(6), pp. 355-364

Dennis, R.W. and Irvine, R.L. (1981) A stoichiometric model of bacterial growth, *Wat.Res.*, **15**(12), pp. 1363-1373

Dochain, D, Vanrolleghem, P.A. and Van Daele, M. (1995) Structural identifiability of biokinetic models of activated sludge respiration, *Wat. Res.*, **29**(11), pp. 2571-2579

Dold, P.L., Ekama, G.A. and Marais, G.v.R. (1980) A general model for the activated sludge process, *Prog. Wat. Technol*, **12**, pp. 47-77

Dold, P.L., Fleit, E., Han, J. and Copp, J.B. (1995) Assay for determination of α-Amylase activity in activated sludge mixed bacterial communities, *Environ. Technol*., **16**, pp. 181-188

Drury, W.J., Stewart, P.S. and Characklis, W.G. (1993) Transport of 1-μm latex-particles in *Pseudomonas aeruginosa* biofilms, *Biotechnol. Bioeng.*, **42**(1), pp. 111-117.

Eastman J.A. and Ferguson, J.F. (1981) Solubilisation of particulate organic carbon during acid phase of anaerobic digestion, *J. Wat. Pollut. Control Fed.*, **53**, pp. 352-366

Ekama, G.A. and Marais, G.v.R. (1977) The activated sludge process part II: Dynamic behaviour, W*ater SA.*, **3**(1), pp. 17

Ekama, G.A. and Marais, G.v.R. (1978) Adsorption in the activated sludge process, W*ater SA.*, **4**(1), pp. 39-48

Ekama, G.A. and Marais, G.v.R. (1979) Dynamic behaviour of the activated sludge process, *J Water Pollut. Control Fed.*, **51**, pp. 534

Ekama, G. A., Dold, P.L. and Marais, G.v.R. (1986) Procedures for determining einfluent COD fractions and the maximum specific growth rate of heterotrophs in activated sludge systems, *Wat.Sci.Tech.*, **18**(6), pp.91-114

Eliosov, B. and Argaman, Y. (1995) Hydrolysis of particulate organics in activated sludge systems, *Wat. Res.*, **29**(1), pp. 155-163

Elster, H.J. and Einsele, W. (1937) Beiträge zur hydrographie des Bodensees (Obersee), *Internationale Revue der Hydrobiologie*, **35**, pp. 522-585

Escher, A. and Characklis, W.G. (1990) Modeling the initial events in biofilm accumulation, in *Biofilms*, Characklis, W.G. and Marshall, K.C. (ed.), pp. 445-486, John Wiley and Sons Inc., New York, 1990

Fermi, C. (1906) The presence of enzymes in soil, water and dust, *Zentralblatt für Bakteriologie und Parasitenkunde*, **26**, pp.330-334

Flemming, H-C. (1995) Sorption sites in biofilms, *Wat. Sci. Tech.,* **32**(8), pp. 27-33

Flemming H-C. and Wingender, J. (2001) Relevance of microbial extracellular polymeric substances (EPSs) - Part I: Structural and ecological aspects, *Wat Sci. Tech*., **43**(6), pp. 1-8

Frigon, D., Oerther, D.B., Morgenroth, E. and Raskin, L. (2001) Oligonucleotide probe hybridization and modeling results suggest that populations consuming readily biodegradable substrate have high cellular RNA levels, *Proceedings of the Fifth Kollekolle Seminar on Activated Sludge Modelling*, IWA, pp. 147-158

Frølund,B., Griebe,T. and Nielsen,P.H. (1995) Enzymatic-activity in the activated-sludge floc matrix, *Appl Microbiol Biotechnol.nol*, **43**(4), pp. 755-761.

Fujii, M. and Kawamura, Y. (1985) Synergistic action of α-Amylase and Glucoamylase on hydrolysis of starch, *Biotechnol. Bioeng*., **27**(3), pp. 260-265

Geesey, G.G. (1982) Microbial exopolymers: Ecological and economic considerations, *ASM News*, **48**, pp. 9-14

Gilbert, H.J. and Hazlewood, G.P. (1993) Bacterial cellulases and xylanases, J. Gen. Microbiol., **139**(part II), pp. 187-194

Goldberg, R.N. and Tewari, Y.B. (1994) Thermodynamics of enzyme-catalyzed reactions: Part 3. Hydrolases, *J. Phys. Chem. Ref. Data*, **23**, pp. 1035

Goldberg, R.N. and Tewari, Y.B. (1995) Thermodynamics of enzyme-catalyzed reactions: Part 4. Lyases, *J. Phys. Chem. Ref. Data*, **24**, pp. 1669

Goel, R., Mino, T., Satoh, H. and Matsuo, T. (1997) Effect of electron acceptor conditions on hydrolytic enzyme synthesis in bacterial cultures, *Wat.Res.*, **31**(10), pp. 2597-2603

Goel, R., Mino, T., Satoh, H. and Matsuo, T. (1998a) Comparison of hydrolytic enzyme systems in pure culture and activated sludge under different electron acceptor conditions, *Wat.Sci.Tech.*, **37**(4-5), pp. 335-343

Goel, R., Mino, T., Satoh, H. and Matsuo, T. (1998b) Enzyme activities under anaerobic and aerobic conditions inactivated sludge sequencing batch reactor, *Wat.Res.*, **32**(7), pp. 2081-2088

Goel, R., Mino, T., Satoh, H. and Matsuo, T. (1998c) Intracellular storage compounds, oxygen uptake rates and biomass yield with readily and slowly degradable substrates, *Wat.Sci.Tech.*, **38**(8-9), pp. 85-93

Goel, R., Mino, T., Satoh, H. and Matsuo, T. (1999) Modeling hydrolysis processes considering intracellular storage, *Wat.Sci.Tech.*, **39**(1), pp. 97-105

Goronszy, M.C. and Eckenfelder, W.W. (1991) The role of the degradation of primary solids in activated sludge plants, in: *64th annual conference WPCF*, Toronto, Oct. 1991.

Grau, P., Sutton, P.M., Henze, M., Elmaleh, S., Grady, C.P.L.Jr., Gujer, W. and Koller, J. (1982) Recommended notation for use in the description of biological wastewater treatment processes, *Wat. Res.*, **16**(11), pp. 1501-1505

Gujer, W. (1980) The effect of particulate organic material on activated sludge yield and oxygen requirement, *Prog. Wat. Technol*, **6**, pp. 79-95

Gujer, W. and Wanner, O. (1990) Modelling mixed population biofilms, , in *Biofilms*, Characklis, W.G. and Marshall, K.C. (ed.), pp. 397-443, John Wiley and Sons Inc., New York, 1990

Gujer, W., Henze, M., Mino, T. and van Loosdrecht, M.C.M. (1999) Activated sludge model no. 3, *Wat. Sci. Tech.*, **39**(1), pp. 183-193

Haldane,G. and Logan,B.E. (1994) Molecular size distribution of a macromolecular polysaccharide (Dextran) during its biodegradation in batch and continuous cultures, *Wat. Res.*, **28**(9), pp. 1873-1878

Hamilton, M.A., Johnson, K.R., Camper, A.K., Stoodley, P., Harkin, G.J., Gillis, R.J., and Shope, P.A. (1994) Analysis of bacterial spatial patterns at the initial stage of biofilm formation, *Biometrical Journal*, **37**, pp. 393-408.

Harremoës, P. (1978) Biofilm kinetics, in *Water Pollution Microbiology* Mitchell, R. (ed.), **2**, pp. 71-109, John Wiley & Sons, New York , 1978

Harremoës, P. and Henze, M. (2002) Biofilters, in: *Wastewater Treatment: Biological and Chemical Processes*, 3rd ed., Henze, M., Harremoës, P., la Cour Jansen, J. and Arvin, E., Springer Verlag, pp. 157-203, Berlin, 2002

Hartenstein, R. (1982) Soil macroinvertebrates, aldehyde oxidase, catalase, cellulase and peroxidase, *Soil. Biol. Biochem.* **14**(4), pp. 387-391

Harth, G., and Horwitz, M.A. (1999) Export of recombinant Mycobacterium tuberculosis superoxide dismutase is dependent upon both information in the protein and mycobacterial export machinery - A model for studying export of leaderless proteins by pathogenic mycobacteria, *J. Biol. Chem.*, **274**(7), pp. 4281-4292

Harvey, H.W. (1925) Oxidation in sea water, *Journal of Marine Biology Association UK*, **13**, pp. 953-969

Hashimoto,W., Momma,K., Miki,H., Mishima,Y., Kobayashi,E., Miyake,O., Kawai,S., Nankai,H., Mikami,B. and Murata,K. (1999) Enzymatic and genetic bases on assimilation, depolymerization, and transport of heteropolysaccharides in bacteria. *Journal of Bioscience and Bioengineering*, **87**(2), pp. 123-136.

Heijnen, J.J. (1999) A thermodynamically based description of chemotrophic microbial growth stoichiometry and kinetics, in *Encyclopedia of Bioprocess Technology: Fermentation, Biocatalysis and Biodeparation*, Flickinger, M.C. and Drew, S.W. (ed.), John Wiley & Sons, New York, 1999

Henze, M. (1979) Sewage treatment by activated sludge - A model with emphasis on oxygen consumption and sludge composition, *Progr. Wat. Tech*., Supplement 1, pp. 41-60

Henze, M., Grady, C.P.L. Jr., Gujer, W., Marais, G.v.R. and Matsuo, T. *Activated sludge model No. 1*, IAWPRC Scientific and Technical Report no. 3, London 1987

Henze, M. and Mladenovski, C. (1991) Hydrolysis of particulate substrate by activated-sludge under aerobic, anoxic and anaerobic conditions, *Wat. Res.*, **25**(1), pp. 61-64

Henze, M. (1992) Characterisation of wastewater for modelling of activated sludge process, *Wat. Sci. Tech*., **25**(6), pp. 1-15

Henze, M., Gujer, W., Mino, T., Matsuo, T., Wentzel, M.C. and Marais, G.v.R *Activated Sludge Model No. 2,* Scientific and Technical Reports, No.3, IAWQ Publishing. London, 1995

Henze, M., Gujer, W., Mino, T., Matsuo, T., Wentzel, M.C., Marais, G.v.R. and van Loosdrecht, M.C.M. (1999) Activated sludge model No.2d, ASM 2d, *Wat. Sci. Tech.*, **39**(1), pp. 165-182

Henze, M., Gujer, W., Mino, T. and van Loosdrecht, M.C.M. *Activated sludge models ASM 1, ASM 2, ASM 2D and ASM 3*, Scientific and Technical Report no.9, IWA Publishing, London, 2000

Henze, M., Harremoës, P., la Cour Jansen, J. and Arvin E. *Wastewater Treatment, Biological and Chemical Processes*, 3$^{d}$ ed., Springer Verlag, Berlin, 2002

Hermanowicz, S.W. (1998) A model for two dimensional biofilm morphology, *Wat. Sci. Tech.,* **37**(4-5), pp. 219-222

Heukelekian, H. and Balmat, J.L. (1959) Chemical composition of the particulate fractions of domestic sewage, *Sewage & Industrial Wastes*, **31**(4), pp. 413-423

Hollibaugh, J.T. and Azam, F. (1983) Microbial degradation of dissolved proteins in seawater, *Limnol. Oceanogr*., **28**(6), pp. 1104-1116

Hoppe, H.G. (1983) Significance of exoenzymatic activities in the ecology of brackish water-measurements by means of Methylumbelliferryl-substrates, *Mar. Ecol. Prog. Ser.*, **11**(3), pp. 299-308

Horan, N.J. and Eccles, C.R. (1986) Purification and characterisation of extracellular polysaccharide from activated sludge, *Wat. Res*., **20**(11), pp. 1427-1432

Horn, H., Neu, T.R. and Wulkow, M. (2001) Modelling the structure and function of extracellular polymeric substances in biofilms with new numerical techniques, *Wat. Sci. Tech*., **43**(6), pp. 121–127

Hsieh, K.M., Murgel, G.A., Lion, L.W. and Schuler, M.L. (1994) Interactions of microbial biofilms with toxic trace metals: 1. Observation and modeling of cellular growth, attachment and production of extracellular polymer, *Biotechnol. Bioeng.*, **44**(2), pp. 219-231

Hulett, F.M. (1986) The secreted alkaline phosphatase of *Bacillus licheniformis* MC14: Identification of a possible precursor, in *Cacillus molecular genetics and Biotechnol.nology applications*, Ganesan A.T. and Hoch, J.A. (ed.), Academic Press Inc., New York 1986

Janning,K.F. (1998) *Hydrolysis and oxidation of particulate organic matter in biofilters* Ph.D. thesis, Technical University of Denmark, Lyngby

Jimenez, B., Noyola, A., Capdeville, B., Roustan, M. and Faup, G. (1988) Dextran blue colorant as a reliable tracer in submerged filters, *Wat. Res.*, **22**(10), pp. 1253-1257

Jones, J.G. (1979) Microbial activity in lake sediments with particular reference to electrode potential gradients, *J. Gen. Microbiol*., **54**(4), pp. 784-790

Jones, S.E. and Lock, M.A. (1991) Peptidase activity in river biofilms by product analysis, in *Microbial Enzymes in Aquatic Environments*, Chróst, R.J. (ed)., Brock/Springer Series in Contemporary Bioscience, Springer Verlag, New York, 1991

Jones, S., Yu, B., Bainton, N.J., Birdsall, M., Bycroft, B.W., Chhabra, S.R., Cox, A.J.R., Golby, P., Reeves, P.J., Stephens, S., Winson, M.K., Salmond, G.P.C., Stewart,G.S.A.B. and

Kappeler, J. and Gujer, W. (1992) Estimation of kinetic parameters of heterotrophic biomass under aerobic conditions and characterisation of wastewater for activated sludge modelling, *Wat. Res. Tech.,* **25**(6), pp.125-140

Keesman, K.J., Spanjers, H. and van Straten, G. (1998) Analysis of endogenous process behaviour in activated sludge, *Biotechnol. Bioeng.*, **57**(2), pp. 155-163

Keiding, K. and Nielsen, P.H. (1997) Desorption of organic macromolecules from activated sludghe flocs: effects of ionic composition, *Wat. Res.,* **31**(7), pp. 1665-1672

Keiding, K., Wybrandt, L. and Nielsen, P.H. (2001) Remember the water - a comment on EPS colligative properties, *Wat. Sci. Tech*., **43**(6), pp. 17–23

Kepkay, P.E. (1994) Particle aggregation and the biological reactivity of colloids. *Marine Ecology-Progress Series*, **109**(2-3), pp. 293-304

Kharazmi, A. (1991) Mechanisms involved in the evasion of the host defence by Pseudomonas aeruginosa, *Immunol. Lett*., **30**(2), pp. 293-304

Klapwijk, A., Drent, J. and Steenwvoorden, J.H.A.M. (1974) A modified procedure for the TTC-dehydrogenase test in activated sludge, *Wat.Res.*, **8**(2), pp. 121

Koch G., Kühl, M., Gujer, W. and Siegrist, H. (2000) Calibration and validation of activated sludge model no. 3 for Swiss municipal wastewater, *Wat. Res*., **34**(14), 3580-3590

Kommedal, R. and Bakke, R. (2000a) Modelling *Pseudomonas aeruginosa* EPS production, in *"Biofilms 2000", American Society for Microbiology conference proceedings*, July 16-20, 2000, Big Sky, MT, USA

Kommedal, R. and Bakke, R. (2000b) *Pseudomonas aeruginosa* biofilm detachment, in *"Biofilms 2000", American Society for Microbiology conference proceedings*, July 16-20, 2000, Big Sky, MT, USA

Kommedal, R. and Bakke, R. (2003) Modelling *Pseudomonas aeruginosa* biofilm detachment, HiT Working Papers no. 3/2003, ISSN: 1501-8520, 29 p.

Kommedal, R., Bakke R., Dockery, J. and Stoodley, P. (2001) Modelling production of extracellular polymeric substances in a pseudomonas aeruginosa chemostat culture, *Wat. Sci. Tech*., **43**(6), pp. 129-134

Köster, M., Jensen, P. and Meyer-Reil, L.A. (1991) Hydrolytic activities of organisms and biogenic structures in deep sea sediments, in *Microbial Enzymes in Aquatic Environments*, Chróst, R.J. (ed)., Brock/Sprinmger Series in Contemporary Bioscience, Springer Verlag, New York, 1991

Kreft, J.U. and Wimpenny, J.W. (2001) Effect of EPS on biofilm structure and function as revealed by an individual-based model of biofilm growth, *Wat. Sci. Tech*., **43**(6), pp. 135–135

Kreps, E. (1934)Organic catalysts or enzymes in sea water, in *James Johnstone memorial volume*, University of Liverpool Press, Liverpool 1934

Kreyszig, E. *Advanced engineering mathematics*, 6th ed., John Wiley & Sons, New York, 1988

Insel, G, Karahan Gül, Ö, Orhon, D., Vanrolleghem, P.A. and Henze, M. (2002) Important limitations in the modelling of activated sludge: biased calibration of the hydrolysis process, *Wat. Sci. Tech.*, **45**(12), pp. 23-36

la Cour Jansen, J., Harremoës, P and Henze, M. (2002) Treatment plants for denitrification, in *Wastewater Treatment: Biological and Chemical Processes*, 3rd ed., Henze, M., Harremoës, P., la Cour Jansen, J. and Arvin, E., Springer Verlag, pp. 239-284, Berlin, 2002

Ladd, J.N. (1972) Origin and range of enzymes in soil, in *Soil Enzymes*, Burns, R.G. (Ed.) Academic Press, London 1972

LaMotta, E.J. (1976) External mass transfer in a biological film reactor, *Biotechnol. Bioeng.*, **18**(10), pp. 1359-1370

Larsen, T.A. and Harremoës, P. (1994) Degradation mechanisms of colloidal organic matter in biofilm reactors. *Wat.Res.*, **28**(6), pp. 1443-1452

Larsen, T. A. *Degradation of colloidal organic matter in biofilm reactors,* Ph.D. thesis at Department of Environmental Science and Engineering, Technical University of Denmark, Lyngby, 1992

Lawrence, J.R., Wolfaardt, G.M. and Korber, D.R. (1994) Determination of diffusion coefficients in biofilms by confocal laser microscopy, *Appl. Env. Microbiol.*, **60**(4), pp. 1166-1173

Lee, J.M. and Fox, P.F. (1985) Purification and characterisation of *Paecilomyces lilacinus* dextranase, *Enzyme Micob. Tech.*, **7**(11), pp. 573-577

Lee, N.M. and Welander, T. (1994) Influence of predators on nitrification in aerobic biofilm processes, *Wat. Sci. Tech.,* **29**(7), pp. 355-363

Lehninger, A.L., Nelson, D.L. and Cox, M.M. *Principles of Biochemistry*, 3rd ed., Worth Publishers, New York 2000

Levine, A. D., Tchobanoglous, G. and Asano, T. (1991) Size distributions of particulate contaminants in wastewater and their impact on treatability, *Wat. Res.*, **25**(8), pp. 911-922

Levenspiel, O. *Chemical Reaction Engineering*, 2nd ed., John Wiley & Sons, New York, 1972

Lewandowski, Z., Stoodley, P. and Altobelli, S. (1995) Experimental and conceptual studies on mass transport in biofilms. *Water Sci. Tech.* **31**(1), pp. 153-162

Lochte, K., Boetius, A. and Petry, C. (2000) Microbial food webs under severe nutrient limitations: Life in the deap sea, in *Microbial Biosystems: New frontiers*, Bell, C.R., Brylinsky M and Johnson-Green, P. (ed.), Proc. 8th Int. Symp. Microb. Ecol., Atlantic Can. Soc. Microb. Ecol., Halifax, pp. 95-102

MacGregor, E.A., MacGregor, A.W., Macri, L.J. and Morgan, J.E. (1994) Models of the action of barley alfa-amylase isozymes on linear substrates, *Carb. Res.*, **257**(2), pp. 249-268

Mathews, C.K and van Holde, K.E. *Biochemistry*, Benjamin/Cummings Publishing Company Inc., Redwood City (CA), 1990

Mattiason, B. (1980) A simple method involving aqueous two phase separation systems for activity determination of enzymes hydrolysing macromolecular substrates, *Analytical Lett.,* **13**(B10), pp. 851-860

Maxham, V.J. and Majer, J.W. (1978) Bacterial growth on organic polymers, *Biotechnol. Bioeng.*, **20**, pp. 865-898

McDermott, J.B., Libanati, C. LaMarca, C. and Klein, M.T. (1990) Quantitative use of model compound information: Monte Carlo simulation of the reactions of complex macromolecules, *Ind. Eng. Chem. Res.*, **29**(1), pp. 22-29

McKinney, R.E. and Ooten, R.J. (1969) Concepts of complete mixing activated sludge, *Transcripts of the 19th Sanitation Engineering Conference*, University of Kansas, pp. 32-59

McLoughlin, A.J. and Cromie-Quilty, M.B. (1983) The kinetics of protein removal by activated sludge, *Wat. Res*., **17**(2), pp. 161-166

Meyer-Reil, L.A. (1991) Ecological aspects of enzymatic activity in marine sediments, in *Microbial Enzymes in Aquatic Environments*, Chróst, R.J. (ed)., Brock/Springer Series in Contemporary Bioscience, Springer Verlag, New York, 1991

Milferstedt, K. *Depolymerization enzyme activity and liberation of intermediates in biofilm systems*, M.Sc. thesis, Lehrstuhl für Hydrologie, University of Bayreuth, Germany, 2001

Mino, T., San Pedro, D.C. and Matsuo, T. (1995) Estimation of the rate of slowly biodegradable cod (SBCOD) hydrolysis under anaerobic, anoxic and aerobic conditions by experiments using starch as model substrate, *Wat. Sci. Tech.*, **31**(2), pp. 95-103

Miranda, M., Murado, M.A., Sanroman, A. and Lema, J.M. (1991) Mass transfer control of enzymatic hydrolysis of polysaccharides by glucoamylase, *Enzyme. Microb. Technol.,* **13**(2), pp. 142-147

Montroll, E.W. and Simha, R. (1940) Theory of depolymerisation of long chain molecules, *J. Chem. Phys.*, **8**, pp. 721-727

Morgan, J.W., Forster, C.F. and Evison, L. (1990) A comparative study of the nature of biopolymers extracted from anaerobic and activated sludges, Wat. Res., **24**(6), pp. 743-750

Morgenroth, E., Kommedal, R. and Harremoës, P. (2001): Processes and modeling of hydrolysis of particulate organic matter in aerobic wastewater treatment - A review, *Wat. Sci. Tech.*, **45**(6), pp. 25-40

Mortimer, R.G. *Physical Chemistry*, 2nd ed., Academic Press, London, 2000

Mosquera-Corral, A., Montras, A., Heijnen, J.J. and van Loosdrecht, M.C.M. (2003) Degradation of polymers in a biofilm airlift suspension reactor, *Wat. Res.*, **37**(3), pp. 485-492

Nakatani, H. (1996) Monte Carlo simulation of multiple attack mechanism of α-Amylase, *Biopolymers*, **39**(5), pp. 665-669

Neu, T.R. and Lawrence, J.R. (1997) Development and structure of microbial biofilms in river water studied by confocal laser scanning microscopy, *FEMS Microbiol. Ecol.*, **24**, pp. 11-25

Nielsen, P.H., Jahn, A. and Palmgren, R. (1997) Conceptual model for production and composition of exopolymers in biofilms, *Wat. Sci. Tech.*, **36**(1), pp. 11-19

Novak, L., Larrea, L. and Wanner, J. (1995) Mathematical model for soluable carbonaceous substrate sorption, *Wat. Sci. Tech.,* **31**(2), pp. 67-77

Novitsky, J.A. (1986) Degradation of dead microbial biomass in a marine sediment, *Appl. Environ. Microbiol.*, **52**(3), pp. 504-509

Nybroe, O., Jorgensen, P.E. and Henze, M. (1992) Enzyme-activities in waste-water and activated-sludge, *Wat.Res.*, **26**(5), pp. 579-584

Ohnishi, Y., Kubo, S., Ono, Y., Nozaki, M., Gonda, Y., Okano, H., Matsuya, T., Matsushiro, A. and Morita, T. (1995) Cloning and sequensing of the gene coding for Dextranase from *Streptococcus salivarius*, *Gene*, **156**, pp. 93-96

O'Melia, C.R. (1987) Particle-particle interactions, in *Aquatic Surface Chemistry*, Stumm (ed.), Wiley, New York 1987

Ohron, D. and Çokgör, E.U. (1997) COD fractionation in wastewater characterisation - The state of the art, J. *Chem. Tech. Biotechnol.*, **68**, pp. 283-293

Okazaki, M. and Moo-Young, M. (1978) Kinetics of enzymatic hydrolysis of cellulose: Analytical description of a mechanistic model, *Biotechnol. Bioeng.*, **20**(5), pp. 637-663

Picioreanu, C., van Loosdrecht, M.C.M. and Heijnen, J.J. (1998) Mathematical modeling of biofilm structure with a hybrid differential-discrete cellular automaton approach, *Biotechnol. Bioeng.*, **58**(1), pp. 101-116

Priest, F.G. (1992) Synthesis and secretion of extracellular enzymes in bacteria, in Microbial degradation of natural products, Winkelmann (ed.),

Priest, F.G. *Extracellular Enzyme*, Aspects of Microbiology 9, van Nostrand Reihold Co.Ltd., Wokingham. Berkshire (UK), 1984

Reichert, P. (1994) AQUASIM - a tool for simulation and data analysis of aquatic systems, Wat. Sci. TEch., **29**(2), pp. 21-30

Reichert, P. and Wanner, O. (1997) Movement of solids in biofilms: Significance of liquid phase transport, *Wat. Sci. Tech.*, **36**(1), pp. 321-328

Reichert, P. *AQUASIM: Computer program for the identification and simulation of aquatic systems*, User Manual, version 2.0, EAWAG, Dubendorf 1998

Revsbech, N.P. and Jørgensen, B.B. (1986) Microelectrodes: Their use in microbial ecology, *Adv. Micr. Ecol.*, **9**, pp. 293-352

Richards, S.R., Hastwell, C. and Davies, M. (1984) Comparative examination of 14 activated sludge plants using enzymatic techniques, *Wat. Pollut. Control*, **83**(3), pp. 301-313

Rittmann, B.E. and McCarty, P.L. (1980) Model of steady state biofilm kinetics, *Biotechnol. Bioeng.,* **22**(11), pp. 2343-2357

Rittmann, B.E. and McCarty, P.L., *Environmental Biotechnology: Principals and Applications*, McGraw-Hill, New York, 2001

Roger, P., Mattisson, C., Axelsson, A. and Zacchi, G. (2000) Use of holographic laser interferometry to study the diffusion of polymers in gels, *Biotechnol. Bioeng*., **69**(6), pp. 654-663

Rohold, L. and Harremoës, P. (1993) Degradation of non-diffusible organic matter in biofilm reactors, *Wat.Res.*, **27**(11), pp. 1689-1691

Rollings, J.E., Okos, M.R. and Tsao, G.T. (1983) Molecular size distributions of Starch during enzymatic hydrolysis, in: *Foundations of Biochemical Engineering: Kinetics and Thermodynamics in Biological systems* (ed. Blanck, H.W., Papoutsakis, E.T. and Stephanopolous, G.), American Chemical Society, Washington, 1983

Rollings, J.E. and Thompson, R.W. (1984) Kinetics of enzymatic Starch liquefication: Simulation of the high molecular weight product distribution, *Biotechnol. Bioeng.*, **26**(12), pp. 1475/1484

Rydman, P.S. and Bamford, D.H. (2002) Phage enzymes digest peptidoglycan tp deliver DNA, *ASM News*, **68**(7), pp. 330-335

San Pedro,D.C., Mino,T. and Matsuo,T. (1994) Evaluation of the rate of hydrolysis of slowly biodegradable COD (SBCOD) using starch as substrate under anaerobic, anoxic and aerobic conditions, *Wat.Sci.Tech.*, **30**(11), pp. 191-199

Sanders, W.T.M., Zeeman, G. and Lettinga, G. (2002) Hydrolysis kinetics of dissolved polymer substrates, *Wat. Sci. Tech*, **45**(10), pp. 99-104

Sanroman, A., Murado, M.A. and Lema, J.M. (1996) The influence of substrate structure on the kinetics of the hydrolysis of Starch by Glucoamylase, *Appl. Biochem. Biotechnol.*, **59**(3), pp. 329-336

Sauer, K. and Camper, A.K. (2001) Characterization of phenotypic changes in *Pseudomonas putida* in response to surface-associated growth, *J. Bacteriol*., **183**(22), pp. 6579-6589

Sauer, K., Camper, A.K., Ehrlich, G.D., Costerton, J.W. and Davies, D.G. (2002) *Pseudomonas aeruginosa* displays multiple phenotypes during development as a biofilm, *J. Bacteriol*., **184**(2), pp. 1140-1154

Schellhorn, H.E. and Forsberg, C.W. (1984) Multiplicity of extracellular β-(1-4)-endoglucanase of Bacteroides succinogenes, *Biochim. Biophys. Acta*, **523**, pp. 930-937

Schomburg, D., Schomburg, I *Handbook of enzymes*, 2nd edition, Springer Verlag, Berlin, 2002

Schramm, A., Hauer Larsen, L., Revsbeck, N.P., Ramsing, N.B., Amann, R. and Schleifer, K.H. (1997) Structure and function of a nitrifying biofilm as determined by in situ hybridisation and the use of microelectrodes, *Appl. Env. Microbiol.*, **62**(12), pp. 4641-4647

Sehanputri, P.S. and Hill Jr., C.G. (2000) Biotechnology for the production of nutraceuticals enriched in conjugated Linoleic acid: II. Multiresponse kinetics of the hydrolysis of corn oil by a *Pseudomonas sp.* Lipase immobilized in a hollow fiber reactor, *Biotechnol. Bioeng.*, **69**(4), pp. 450-4456

Silva, T.R. and Malcata, F.X. (1994) On the appropriateness of use of a continuous formulation fo the modelling of discrete multireactant systems following Michaelis-Menten kinetics, *Bioproc. Eng.*, **10**(5-6), pp. 235-240

Smidsrød, O. and Moe, S.T. *Biopolymer chemistry* (Biopolymerkjemi), Tapir Forlag, Trondheim, 1995

Smucker, R.A. and Kim, C.K. (1991) Chitinase activity in estuarine waters, in *Microbial Enzymes in Aquatic Environments*, Chróst, R.J. (ed)., Brock/Springer Series in Contemporary Bioscience, Springer Verlag, New York, 1991

Sollfrank U. and Gujer, W. (1991) Characterisation of domestic wastewater for mathematical modelling of the activated sludge process, *Wat. Sci. Tech*., **23**(Kyoto), pp. 1057-1066

Spanjers, H. and Vanrolleghem, P.A. (1995) Respirometry as a tool for rapid characterization of wastewater and activated sludge, *Wat. Sci. Tech.*, **31**(2), pp. 105-114

Spérandio, M. and Paul, E. (2000) Estimation of wastewater biodegradable COD fractions by combining respirometric experiments in various So/Xo ratios, *Wat. Res.*, **34**(4), pp. 1233-1246

Sprouse, G. and Rittmann, B.E. (1990) Colloid removal in fluidised bed biofilm reactor*, J. Environ. Eng.*, ASCE, **116**(2), pp. 314-329

Sridhar,M.K.C. and Pallai,C. (1973): Protease activity in sewage, sludge and effluents, *Wat.Waste Treat.*, **16**(8), pp.35

Stolzenbach, K. (1996) Particle transport and attachment, in *Structure and function of biofilms*, Characklis, W.G. and Wilderer, P.A. (ed.), Wiley and Sons Inc., New York, 1996

Stenstrøm, M.K. *A dynamic model and computer compatible control strategies for wastewater treatment plants*, Ph.D. thesis, Clemson University, Clemson, SC, 1975

Stewart, P. (2003a) Diffusion in biofilms, *J. Bacteriol.*, **185**(5), pp. 1485-1491

Stewart P. (2003b) A review of experimental measurements of effective diffusive permeabilities and effective diffusion coefficients in biofilms, *Biotechnol. Bioeng.*, **59**(3), pp. 261-272

Stewart, P.S. (1993) A model of Biofilm Detachment, *Biotechnol. Bioeng*., **41**(1), pp. 111-117

Stoodley, P., Yang, S., Lappin-Scott, H. and Lewandowski, Z. (1997) Relationship between mass transfer coefficient and liquid flow velocity in heterogeneous biofilms using microelectrodes and confocal microscopy, *Biotehnol.. Bioeng.*, **56**(), pp. 681-688

Stoodley, P., Sauer, K., Davies, D.G. and Costerton, J.W. (2002) Biofilms as Complex Differentiated Communities, *Annu. Rev. Microbiol.*, **56**, pp. 187-209

Suga, K., van Dedem, G and Moo-Young, M. (1975) Degradation of polysaccharides by endo and exo enzymes: A theoretical analysis, *Biotechnol. Bioeng.* **17**(3), pp. 433-439

Tamburini, C., Garcin, J., Ragot, M. and Bianchi, A. (2002) Biopolymer hydrolysis and bacterial production under ambient hydrostatic pressure through a 2000 m water column in the NW Mediterranean, *Deep Sea Res. II*, **49**, pp. 2109-2123

Tanaka, H., Matsumura, M. and Veliky, I.A. (1984) Diffusion characteristics in Ca-alginate beads, *Biotechnol. Bioeng.*, **26**(1), pp. 53-58

Tanyolac, A. and Beyenal, H. (1997) Prediction of average biofilm density and performance of a spherical bioparticle under substrate inhibition, *Biotechnol. Bioeng*., **56**(3), pp. 319-329

Tauber,H. *The chemistry and technology of enzymes*, Wiley and Sons, New York, 1948

Taylor, J.R. *An introduction to error analysis*, University Science Books, Mill Valley, CA, 1982

Tchobanoglous, G., Burton, F.L. and Stensel, H.D. *Wastewater Engineering: Treatment, and Reuse*, 4rd ed., Metcalfe & Eddy Inc., McGraw-Hill Inc. New York, 2003

Terashima, Y. and Lin, S. (2000) On the modelling of microbiological hydrolysis of organic solids, *Wat. Sci. Tech.*, **42**(12), pp. 11-19

Teuber,M. and Brodisch,K.E.U. (1976) Enzymatic activities of activated sludge as potential measures of active biomass, *Proc. Soc. Gen. Microbiol*, **3**, pp. 119

Thiel,P.G. and Hattingh,W.H.J. (1967) Determination of hydrolytic enzyme activities in anaerobic digesting sludge, *Wat.Res.*, **1**(3), pp. 191

Tholosan, O., Lamy, F., Garcin, J. Polychronaki, T. and Bianchi, A. (1999) Biphasic extracellular proteolytic enzyme activity in the benthic water and sediment in the northwestern Mediterranean Sea, *Appl.Environ. Microbiol.*, **65**(4), pp. 1619-1626

Thoma, J.A., Rao, G.V.K., Brothers, C., Spradlin, J. and Li, L.H. (1971) Substrate mapping of enzymes correlation of product patterns with Michaelis parameters and substrate induced strain, *J. Biol. Chem*., **246**(18), pp. 5621-5635

Trulear, M.G. and Characklis, W.G. (1982) Dynamics of biofilm processes, *J. Wat. Poll.Contr. Fed.*, **54**(9), pp. 1288-1301

Trulear, M.G. *Cellular reproduction and extracellular polymer formation in the development of biofilms*, Ph.D. thesis, Montana State University, Bozeman MT, 1983

Tsuno, H. (1978) Kinetic model of activated sludge metabolism and its application to the response of qualitative shock loads, *Wat.Res.*, **12**(8), pp. 513-522

Turakhia, M.H. *The influence of calcium on biofilm processes*, Ph.D. thesis, Montana State University, Bozeman MT, 1986

Ubukata, Y. (1992) Kinetics of polymeric substrate removal by activated sludge: Hydrolysis of polymers is the rate limiting step, *Wat. Sci. Tech.*, **26**(9-11), pp. 2457-2460

Ubakata, Y. (1997) Kinetics of polymeric substrate (Dextrin or Peptone) removal by activated sludge: Hydrolysis of polymers to monomers is the rate limiting step, *Wat. Sci. Tech*. **26**(12), pp. 159-167

Ubukata, Y. (1999) Kinetics and fundamental mechanisms of Starch removal by activated sludge: Hydrolysis of starch to Maltose and Maltotriose is the rate determining step, *Wat. Sci. Tech.*, **40**(1), pp. 61-68

Vaicum,L., Gruia,E. and Godeanu,S. (1965) The determination of some enzymatic activities as a research method in activated sludge, *Rev. Roum. Biochim.*, **2**(1), pp. 87

van Loosdrecht, M.C.M., Eikelboom, E., Gjaltema, A., Mulder, A., Tijhuis, L. and Heijnen, J.J. (1995) Biofilm structures, *Wat. Sci. Tech.*, **32**(8). pp. 35-44

van Loosdrecht, M.C.M., Heijnen, J.J., Eberl, H., Kreft, J. and Picioreanu, C. (2002) Mathematical modelling of biofilm structures, *Antonie van Leeuwenhoek*, **81**(1-4), pp. 245-256

Varga, S. and Malcata, F.X. (1996) Enhancement of product selectivity via enzyme immobilisation in sequential degradation reactions of polymeric substrates, *Bioproc. Eng.*, **15**, pp. 189-194

Vetter, Y.A., Deming, P.A., Jumars, P.A. and Krieger-Brockett, B.B. (1998) A predictive model of bacterial foraging by means of freely released extracellular enzymes, *Microbial Ecology*, **36**, pp. 75-92

Vollertsen, J. and Hvitved-Jacobsen, T. (1999) Stoichiometric and kinetic model parameters for microbial transformations of suspended solids in combined sewer systems, *Wat.Res.*, **33**(14), pp. 3127-3141.

Walker, G.J. (1978) Dextrans, in *International Review of Biochemistry: Biochemistry of Charbohydrates* II, Manners, D.J (ed.), **16**, pp. 75-126, University Park Press, Baltimore, 1978

Walker G.J. and Pulkownik, A. (1974) Action of α-1,6-glucan glucohydrolase on oligosaccharide derived from dextran, *Carbohydr. Res.*, **36**(1), pp. 53-66

Wanner, O. and Gujer, W. (1986) A multi species biofilm model, *Biotechnol. Bioeng.*, **28**(3), pp. 314-328

Wanner, O., and Reichert, P. (1996) Mathematical modelling of mixed-culture biofilms, *Biotechnol. Bioeng*., **49**(2), pp. 172-184

Watnick, P. and Kolter, P. (2001) Biofilm, city of microbes, *J. Bacteriol*., **182**(10), pp. 2675-2679

Webb, E.C. *Enzyme nomenclature: Recommendations of the Nomenclature Committee of the International Union of Biochemistry and Molecular Biology on the nomenclature and classification of enzymes*, Academic Press, San Diego, 1992

Weijers, S.R. and Vanrolleghem, P.A. (1997) A procedure for selecting the most important parameters in calibrating the activated sludge model no. 1 with full scale plant data, *Wat. Sci. Tech.*, **36**(5), pp. 69-79

Weiss, M.S., Abele, U., Weckesser, J., Welte, W., Schiltz, E. and Schulz, G.E. (1991) Molecular architecture and electrostatic properties of a bacterial porin, *Science*, **254**(5038), pp. 1627-1630

White, D., *The Physiology and Biochemistry of Prokaryotes*, 2nd ed., Oxford University Press Inc., Oxford, 2000

Wicker-Böckelmann, U., Wingender, J. and Winkler, U. (1987) Alginate Lyase release cell bound Lipase from mucoid strains of *Pseudomonas aeruginosa*, *Zentralblatt für bakteriologie mikrobiologie und hygiene series A*, **266**(3-4), pp. 379-389

Williams, P. (1993) The *lux* autoinducer regulates the production of exoenzyme virulence determinants in *Erwinia cartotovora* and *Pseudomonas aeruginosa*, EMBO Journal, **12**(6), pp. 2477-2482

Wojciechowski, P.M., Koziol, A. and Noworyta, A. (2001) Iteration model of starch hydrolysis by amylolytic enzymes, *Biotechnol. Bioeng.*, **75**(5), pp. 530-539

Wu, C. (1993) Laser Light Scattering Characterization of the molecular weight distribution of Dextran, *Macromolecules*, **26**, pp. 3821-3825

Wuertz, S., Bishop, P.L. and Wilderer, P. *Biofilms in wastewater treatment: An interdisciplinary approach*, IWA Publishing, London 2003

Ziff, R.M. and McGrady, E.D. (1986) Kinetics of polymer degradation, *Macromolecules*, **19**, pp. 2513-2519

Zita, H. and Hermansson, M. (1994) Effects of ionic strength on bacterial adhesion and stability of activated flocs in wastewater activated sludge systems, *Appl. Environ. Micobiol.*, **60**(9), pp. 3041-3048

Zita A, Hermansson M. (1997) Effects of bacterial cell surface structures and hydrophobicity on attachment to activated sludge flocs, *Appl. Environ. Micobiol.*, **63**(3), pp. 1168-1170

Zobell, C.E. and Allen, E.C. (1935) The significance of marine bacteria in the fouling of submerged surfaces, *J. Bacteriol.*, **29**(3), pp. 230-251

Zobell, C.E. and Anderson, D.Q. (1937) Observations on the multiplication of bacteria in different volumes of stored sea water and the influence of oxygen tension and solid surfaces, *Biological Bulletin*, **71**, pp. 324-342

Zobell, C.E: and Rittenburg, S.C. (1937) The occurrence and characteristics of chitinoclastic bacteria in the sea, *J. Bacteriol.*, **35**(3), pp. 275-287

# 9 Appendix

## 9.1 EC Group 3 Hydrolases

**EC 3.1 Acting on Ester Bonds**

**EC 3.1.1 Carboxylic Ester Hydrolases**

EC 3.1.1.1 carboxylesterase
EC 3.1.1.2 arylesterase
EC 3.1.1.3 triacylglycerol lipase
EC 3.1.1.4 phospholipase $A_2$
EC 3.1.1.5 lysophospholipase
EC 3.1.1.6 acetylesterase
EC 3.1.1.7 acetylcholinesterase
EC 3.1.1.8 cholinesterase
EC 3.1.1.10 tropinesterase
EC 3.1.1.11 pectinesterase
EC 3.1.1.13 sterol esterase
EC 3.1.1.14 chlorophyllase
EC 3.1.1.15 L-arabinonolactonase
EC 3.1.1.17 gluconolactonase
EC 3.1.1.19 uronolactonase
EC 3.1.1.20 tannase
EC 3.1.1.21 retinyl-palmitate esterase
EC 3.1.1.22 hydroxybutyrate-dimer hydrolase
EC 3.1.1.23 acylglycerol lipase
EC 3.1.1.24 3-oxoadipate *enol*-lactonase
EC 3.1.1.25 1,4-lactonase
EC 3.1.1.26 galactolipase
EC 3.1.1.27 4-pyridoxolactonase
EC 3.1.1.28 acylcarnitine hydrolase
EC 3.1.1.29 aminoacyl-tRNA hydrolase
EC 3.1.1.30 D-arabinonolactonase
EC 3.1.1.31 6-phosphogluconolactonase
EC 3.1.1.32 phospholipase $A_1$
EC 3.1.1.33 6-acetylglucose deacetylase
EC 3.1.1.34 lipoprotein lipase
EC 3.1.1.35 dihydrocoumarin hydrolase
EC 3.1.1.36 limonin-D-ring-lactonase
EC 3.1.1.37 steroid-lactonase
EC 3.1.1.38 triacetate-lactonase
EC 3.1.1.39 actinomycin lactonase
EC 3.1.1.40 orsellinate-depside hydrolase
EC 3.1.1.41 cephalosporin-C deacetylase
EC 3.1.1.42 chlorogenate hydrolase
EC 3.1.1.43 a-amino-acid esterase
EC 3.1.1.44 4-methyloxaloacetate esterase
EC 3.1.1.45 carboxymethylenebutenolidase
EC 3.1.1.46 deoxylimonate A-ring-lactonase
EC 3.1.1.47 1-alkyl-2-acetylglycerophosphocholine esterase
EC 3.1.1.48 fusarinine-C ornithinesterase
EC 3.1.1.49 sinapine esterase
EC 3.1.1.50 wax-ester hydrolase
EC 3.1.1.51 phorbol-diester hydrolase
EC 3.1.1.52 phosphatidylinositol deacylase
EC 3.1.1.53 sialate *O*-acetylesterase
EC 3.1.1.54 acetoxybutynylbithiophene deacetylase
EC 3.1.1.55 acetylsalicylate deacetylase
EC 3.1.1.56 methylumbelliferyl-acetate deacetylase
EC 3.1.1.57 2-pyrone-4,6-dicarboxylate lactonase
EC 3.1.1.58 *N*-acetylgalactosaminoglycan deacetylase
EC 3.1.1.59 juvenile-hormone esterase
EC 3.1.1.60 bis(2-ethylhexyl)phthalate esterase
EC 3.1.1.61 protein-glutamate methylesterase
EC 3.1.1.63 11-*cis*-retinyl-palmitate hydrolase
EC 3.1.1.64 *all-trans*-retinyl-palmitate hydrolase
EC 3.1.1.65 L-rhamnono-1,4-lactonase
EC 3.1.1.66 5-(3,4-diacetoxybut-1-ynyl)-2,2'-bithiophene deacetylase
EC 3.1.1.67 fatty-acyl-ethyl-ester synthase
EC 3.1.1.68 xylono-1,4-lactonase
EC 3.1.1.70 cetraxate benzylesterase
EC 3.1.1.71 acetylalkylglycerol acetylhydrolase
EC 3.1.1.72 acetylxylan esterase
EC 3.1.1.73 feruloyl esterase
EC 3.1.1.74 cutinase
EC 3.1.1.75 poly(3-hydroxybutyrate) depolymerase
EC 3.1.1.76 poly(3-hydroxyoctanoate) depolymerase
acyloxyacyl hydrolase
EC 3.1.1.77 acyloxyacyl hydrolase
EC 3.1.1.78 polyneuridine-aldehyde esterase

**EC 3.1.2 Thiolester Hydrolases**

EC 3.1.2.1 acetyl-CoA hydrolase
EC 3.1.2.2 palmitoyl-CoA hydrolase
EC 3.1.2.3 succinyl-CoA hydrolase
EC 3.1.2.4 3-hydroxyisobutyryl-CoA hydrolase
EC 3.1.2.5 hydroxymethylglutaryl-CoA hydrolase
EC 3.1.2.6 hydroxyacylglutathione hydrolase
EC 3.1.2.7 glutathione thiolesterase
EC 3.1.2.10 formyl-CoA hydrolase
EC 3.1.2.11 acetoacetyl-CoA hydrolase
EC 3.1.2.12 *S*-formylglutathione hydrolase
EC 3.1.2.13 *S*-succinylglutathione hydrolase
EC 3.1.2.14 oleoyl-[acyl-carrier-protein] hydrolase
EC 3.1.2.15 ubiquitin thiolesterase
EC 3.1.2.16 [citrate-(*pro*-3*S*)-lyase] thiolesterase
EC 3.1.2.17 (*S*)-methylmalonyl-CoA hydrolase
EC 3.1.2.18 ADP-dependent short-chain-acyl-CoA hydrolase
EC 3.1.2.19 ADP-dependent medium-chain-acyl-CoA hydrolase
EC 3.1.2.20 acyl-CoA hydrolase
EC 3.1.2.21 dodecanoyl-[acyl-carrier protein] hydrolase
EC 3.1.2.22 palmitoyl-(protein) hydrolase
EC 3.1.2.23 4-hydroxybenzoyl-CoA thioesterase
EC 3.1.2.24 2-(2-hydroxyphenyl)benzenesulfinate hydrolase

**EC 3.1.3 Phosphoric Monoester Hydrolases**

EC 3.1.3.1 alkaline phosphatase
EC 3.1.3.2 acid phosphatase
EC 3.1.3.3 phosphoserine phosphatase
EC 3.1.3.4 phosphatidate phosphatase
EC 3.1.3.5 5'-nucleotidase
EC 3.1.3.6 3'-nucleotidase
EC 3.1.3.7 3'(2'),5'-bisphosphate nucleotidase
EC 3.1.3.8 3-phytase
EC 3.1.3.9 glucose-6-phosphatase
EC 3.1.3.10 glucose-1-phosphatase
EC 3.1.3.11 fructose-bisphosphatase
EC 3.1.3.12 trehalose-phosphatase
EC 3.1.3.13 bisphosphoglycerate phosphatase
EC 3.1.3.14 methylphosphothioglycerate phosphatase
EC 3.1.3.15 histidinol-phosphatase
EC 3.1.3.16 phosphoprotein phosphatase
EC 3.1.3.17 [phosphorylase] phosphatase
EC 3.1.3.18 phosphoglycolate phosphatase
EC 3.1.3.19 glycerol-2-phosphatase
EC 3.1.3.20 phosphoglycerate phosphatase
EC 3.1.3.21 glycerol-1-phosphatase
EC 3.1.3.22 mannitol-1-phosphatase
EC 3.1.3.23 sugar-phosphatase
EC 3.1.3.24 sucrose-phosphatase
EC 3.1.3.25 inositol-1(or 4)-monophosphatase
EC 3.1.3.26 4-phytase
EC 3.1.3.27 phosphatidylglycerophosphatase
EC 3.1.3.28 ADPphosphoglycerate phosphatase
EC 3.1.3.29 *N*-acylneuraminate-9-phosphatase
EC 3.1.3.31 nucleotidase
EC 3.1.3.32 polynucleotide 3'-phosphatase
EC 3.1.3.33 polynucleotide 5'-phosphatase
EC 3.1.3.34 deoxynucleotide 3'-phosphatase
EC 3.1.3.35 thymidylate 5'-phosphatase
EC 3.1.3.36 phosphoinositide 5-phosphatase
EC 3.1.3.37 sedoheptulose-bisphosphatase
EC 3.1.3.38 3-phosphoglycerate phosphatase
EC 3.1.3.39 streptomycin-6-phosphatase
EC 3.1.3.40 guanidinodeoxy-*scyllo*-inositol-4-phosphatase
EC 3.1.3.41 4-nitrophenylphosphatase
EC 3.1.3.42 [glycogen-synthase-D] phosphatase
EC 3.1.3.43 [pyruvate dehydrogenase (lipoamide)]-phosphatase
EC 3.1.3.44 [acetyl-CoA carboxylase]-phosphatase
EC 3.1.3.45 3-deoxy-*manno*-octulosonate-8-phosphatase
EC 3.1.3.46 fructose-2,6-bisphosphate 2-phosphatase
EC 3.1.3.47 [hydroxymethylglutaryl-CoA reductase (NADPH)]-phosphatase
EC 3.1.3.48 protein-tyrosine-phosphatase
EC 3.1.3.49 [pyruvate kinase]-phosphatase
EC 3.1.3.50 sorbitol-6-phosphatase
EC 3.1.3.51 dolichyl-phosphatase
EC 3.1.3.52 [3-methyl-2-oxobutanoate dehydrogenase (lipoamide)]-phosphatase
EC 3.1.3.53 myosin-light-chain-phosphatase
EC 3.1.3.54 fructose-2,6-bisphosphate 6-phosphatase
EC 3.1.3.55 caldesmon-phosphatase
EC 3.1.3.56 inositol-polyphosphate 5-phosphatase
EC 3.1.3.57 inositol-1,4-bisphosphate 1-phosphatase
EC 3.1.3.58 sugar-terminal-phosphatase
EC 3.1.3.59 alkylacetylglycerophosphatase
EC 3.1.3.60 phospho*enol*pyruvate phosphatase
EC 3.1.3.62 multiple inositol-polyphosphate phosphatase
EC 3.1.3.63 2-carboxy-D-arabinitol-1-phosphatase
EC 3.1.3.64 phosphatidylinositol-3-phosphatase
EC 3.1.3.66 phosphatidylinositol-3,4-bisphosphate 4-phosphatase
EC 3.1.3.67 phosphatidylinositol-3,4,5-trisphosphate 3-phosphatase
EC 3.1.3.68 2-deoxyglucose-6-phosphatase
EC 3.1.3.69 glucosylglycerol 3-phosphatase
EC 3.1.3.70 mannosyl-3-phosphoglycerate phosphatase
EC 3.1.3.71 2-phosphosulfolactate phosphatase
EC 3.1.3.72 5-phytase

**EC 3.1.4 Phosphoric Diester Hydrolases**

EC 3.1.4.1 phosphodiesterase I
EC 3.1.4.2 glycerophosphocholine phosphodiesterase
EC 3.1.4.3 phospholipase C
EC 3.1.4.4 phospholipase D
EC 3.1.4.11 phosphoinositide phospholipase C
EC 3.1.4.12 sphingomyelin phosphodiesterase
EC 3.1.4.13 serine-ethanolaminephosphate phosphodiesterase
EC 3.1.4.14 [acyl-carrier-protein] phosphodiesterase
EC 3.1.4.15 adenylyl-[glutamate—ammonia ligase] hydrolase
EC 3.1.4.16 2',3'-cyclic-nucleotide 2'-phosphodiesterase
EC 3.1.4.17 3',5'-cyclic-nucleotide phosphodiesterase
EC 3.1.4.35 3',5'-cyclic-GMP phosphodiesterase
EC 3.1.4.37 2',3'-cyclic-nucleotide 3'-phosphodiesterase
EC 3.1.4.38 glycerophosphocholine cholinephosphodiesterase
EC 3.1.4.39 alkylglycerophosphoethanolamine phosphodiesterase
EC 3.1.4.40 CMP-*N*-acylneuraminate phosphodiesterase
EC 3.1.4.41 sphingomyelin phosphodiesterase D
EC 3.1.4.42 glycerol-1,2-cyclic-phosphate 2-phosphodiesterase
EC 3.1.4.43 glycerophosphoinositol inositolphosphodiesterase
EC 3.1.4.44 glycerophosphoinositol glycerophosphodiesterase
EC 3.1.4.45 *N*-acetylglucosamine-1-phosphodiester a-*N*-acetylglucosaminidase
EC 3.1.4.46 glycerophosphodiester phosphodiesterase
EC 3.1.4.48 dolichylphosphate-glucose phosphodiesterase
EC 3.1.4.49 dolichylphosphate-mannose phosphodiesterase
EC 3.1.4.50 glycosylphosphatidylinositol phospholipase D
EC 3.1.4.51 glucose-1-phospho-D-mannosylglycoprotein phosphodiesterase

**EC 3.1.5 Triphosphoric Monoester Hydrolases**

EC 3.1.5.1 dGTPase

**EC 3.1.6 Sulfuric Ester Hydrolases**

EC 3.1.6.1 arylsulfatase
EC 3.1.6.2 steryl-sulfatase
EC 3.1.6.3 glycosulfatase
EC 3.1.6.4 *N*-acetylgalactosamine-6-sulfatase
EC 3.1.6.6 choline-sulfatase
EC 3.1.6.7 cellulose-polysulfatase
EC 3.1.6.8 cerebroside-sulfatase
EC 3.1.6.9 chondro-4-sulfatase
EC 3.1.6.10 chondro-6-sulfatase
EC 3.1.6.11 disulfoglucosamine-6-sulfatase
EC 3.1.6.12 *N*-acetylgalactosamine-4-sulfatase
EC 3.1.6.13 iduronate-2-sulfatase
EC 3.1.6.14 *N*-acetylglucosamine-6-sulfatase
EC 3.1.6.15 *N*-sulfoglucosamine-3-sulfatase
EC 3.1.6.16 monomethyl-sulfatase
EC 3.1.6.17 D-lactate-2-sulfatase
EC 3.1.6.18 glucuronate-2-sulfatase

**EC 3.1.7 Diphosphoric Monoester Hydrolases**

EC 3.1.7.1 prenyl-diphosphatase
EC 3.1.7.2 guanosine-3',5'-bis(diphosphate) 3'-diphosphatase
EC 3.1.7.3 monoterpenyl-diphosphatase

**EC 3.1.8 Phosphoric Triester Hydrolases**

EC 3.1.8.1 aryldialkylphosphatase
EC 3.1.8.2 diisopropyl-fluorophosphatase

**EC 3.1.11 Exodeoxyribonucleases Producing 5'-Phosphomonoesters**

EC 3.1.11.1 exodeoxyribonuclease I
EC 3.1.11.2 exodeoxyribonuclease III
EC 3.1.11.3 exodeoxyribonuclease (lambda-induced)
EC 3.1.11.4 exodeoxyribonuclease (phage SP3-induced)
EC 3.1.11.5 exodeoxyribonuclease V
EC 3.1.11.6 exodeoxyribonuclease VII

**EC 3.1.13 Exoribonucleases Producing 5'-Phosphomonoesters**

EC 3.1.13.1 exoribonuclease II
EC 3.1.13.2 exoribonuclease H
EC 3.1.13.3 oligonucleotidase
EC 3.1.13.4 poly(A)-specific ribonuclease

**EC 3.1.14 Exoribonucleases Producing 3'-Phosphomonoesters**

EC 3.1.14.1 yeast ribonuclease

**EC 3.1.15 Exonucleases Active with either Ribo- or Deoxyribonucleic Acids and Producing 5'-Phosphomonoesters**

EC 3.1.15.1 venom exonuclease

**EC 3.1.16 Exonucleases Active with either Ribo- or Deoxyribonucleic Acids and Producing 3'-Phosphomonoesters**

EC 3.1.16.1 spleen exonuclease

**EC 3.1.21 Endodeoxyribonucleases Producing 5'-Phosphomonoesters**

EC 3.1.21.1 deoxyribonuclease I
EC 3.1.21.2 deoxyribonuclease IV (phage-$T_4$-induced)
EC 3.1.21.3 type 1 site-specific deoxyribonuclease
EC 3.1.21.4 type II site-specific deoxyribonuclease
EC 3.1.21.5 type III site-specific deoxyribonuclease

EC 3.1.21.6 CC-preferring endodeoxyribonuclease
EC 3.1.21.7 deoxyribonuclease V

**EC 3.1.22 Endodeoxyribonucleases Producing 3'-Phosphomonoesters**

EC 3.1.22.1 deoxyribonuclease II
EC 3.1.22.2 *Aspergillus* deoxyribonuclease $K_1$
EC 3.1.22.4 crossover junction endoribonuclease
EC 3.1.22.5 deoxyribonuclease X

**EC 3.1.25 Site-Specific Endodeoxyribonucleases Specific for Altered Bases**

EC 3.1.25.1 deoxyribonuclease (pyrimidine dimer)
**EC 3.1.26 Endoribonucleases Producing 5'-Phosphomonoesters**

EC 3.1.26.1 *Physarum polycephalum* ribonuclease
EC 3.1.26.2 ribonuclease alpha
EC 3.1.26.3 ribonuclease III
EC 3.1.26.4 calf thymus ribonuclease H
EC 3.1.26.5 ribonuclease P
EC 3.1.26.6 ribonuclease IV
EC 3.1.26.7 ribonuclease P4
EC 3.1.26.8 ribonuclease M5
EC 3.1.26.9 ribonuclease [poly-(U)-specific]
EC 3.1.26.10 ribonuclease IX
EC 3.1.26.11 RNase Z

**EC 3.1.27 Endoribonucleases Producing 3'-Phosphomonoesters**

EC 3.1.27.1 ribonuclease $T_2$
EC 3.1.27.2 *Bacillus subtilis* ribonuclease
EC 3.1.27.3 ribonuclease $T_1$
EC 3.1.27.4 riblonuclease $U_2$
EC 3.1.27.5 pancreatic ribonuclease
EC 3.1.27.6 *Enterobacter* ribonuclease
EC 3.1.27.7 ribonuclease F
EC 3.1.27.8 ribonuclease V
EC 3.1.27.9 tRNA-intron endonuclease
EC 3.1.27.10 rRNA endonuclease

**EC 3.1.30 Endoribonucleases Active with either Ribo- or Deoxyribonucleic Acids and Producing 5'-Phosphomonoesters**

EC 3.1.30.1 *Aspergillus* nuclease $S_1$
EC 3.1.30.2 *Serratia marcescens* nuclease

**EC 3.1.31 Endoribonucleases Active with either Ribo- or Deoxyribonucleic Acids and Producing 3'-Phosphomonoesters**

EC 3.1.31.1 micrococcal nuclease

**EC 3.2 Glycosylases**

**EC 3.2.1 Glycosidases, i.e. enzymes hydrolysing *O*- and *S*-glycosyl compounds**

EC 3.2.1.1 a-amylase
EC 3.2.1.2 b-amylase
EC 3.2.1.3 glucan 1,4-a-glucosidase
EC 3.2.1.4 cellulase
EC 3.2.1.6 endo-1,3(4)-b-glucanase
EC 3.2.1.7 inulinase
EC 3.2.1.8 endo-1,4-b-xylanase
EC 3.2.1.10 oligo-1,6-glucosidase
EC 3.2.1.11 dextranase
EC 3.2.1.14 chitinase
EC 3.2.1.15 polygalacturonase
EC 3.2.1.17 lysozyme
EC 3.2.1.18 exo-a-sialidase
EC 3.2.1.20 a-glucosidase
EC 3.2.1.21 b-glucosidase
EC 3.2.1.22 a-galactosidase
EC 3.2.1.23 b-galactosidase
EC 3.2.1.24 a-mannosidase
EC 3.2.1.25 b-mannosidase
EC 3.2.1.26 b-fructofuranosidase
EC 3.2.1.28 a,a-trehalase
EC 3.2.1.31 b-glucuronidase
EC 3.2.1.32 xylan endo-1,3-b-xylosidase
EC 3.2.1.33 amylo-1,6-glucosidase
EC 3.2.1.35 hyalurononglucosaminidase
EC 3.2.1.36 hyaluronoglucuronidase
EC 3.2.1.37 xylan 1,4-b-xylosidase
EC 3.2.1.38 b-D-fucosidase
EC 3.2.1.39 glucan endo-1,3-b-D-glucosidase
EC 3.2.1.40 a-L-rhamnosidase
EC 3.2.1.41 pullulanase
EC 3.2.1.42 GDP-glucosidase
EC 3.2.1.43 b-L-rhamnosidase
EC 3.2.1.44 fucoidanase
EC 3.2.1.45 glucosylceramidase
EC 3.2.1.46 galactosylceramidase
EC 3.2.1.47 galactosylgalactosylglucosylceramidase
EC 3.2.1.48 sucrose a-glucosidase
EC 3.2.1.49 a-*N*-acetylgalactosaminidase
EC 3.2.1.50 a-*N*-acetylglucosaminidase
EC 3.2.1.51 a-L-fucosidase
EC 3.2.1.52 b-L-*N*-acetylhexosaminidase
EC 3.2.1.53 b-*N*-acetylgalactosaminidase
EC 3.2.1.54 cyclomaltodextrinase
EC 3.2.1.55 a-*N*-arabinofuranosidase
EC 3.2.1.56 glucuronosyl-disulfoglucosamine glucuronidase
EC 3.2.1.57 isopullulanase
EC 3.2.1.58 glucan 1,3-b-glucosidase
EC 3.2.1.59 glucan endo-1,3-a-glucosidase
EC 3.2.1.60 glucan 1,4-a-maltotetraohydrolase
EC 3.2.1.61 mycodextranase
EC 3.2.1.62 glycosylceramidase
EC 3.2.1.63 1,2-a-L-fucosidase
EC 3.2.1.64 2,6-b-fructan 6-levanbiohydrolase
EC 3.2.1.65 levanase
EC 3.2.1.66 quercitrinase
EC 3.2.1.67 galacturan 1,4-a-galacturonidase
EC 3.2.1.68 isoamylase
EC 3.2.1.70 glucan 1,6-a-glucosidase
EC 3.2.1.71 glucan endo-1,2-b-glucosidase
EC 3.2.1.72 xylan 1,3-b-xylosidase
EC 3.2.1.73 licheninase
EC 3.2.1.74 glucan 1,4-b-glucosidase
EC 3.2.1.75 glucan endo-1,6-b-glucosidase
EC 3.2.1.76 L-iduronidase
EC 3.2.1.77 mannan 1,2-(1,3)-a-mannosidase
EC 3.2.1.78 mannan endo-1,4-b-mannosidase
EC 3.2.1.80 fructan b-fructosidase
EC 3.2.1.81 agarase
EC 3.2.1.82 exo-poly-a-galacturonosidase
EC 3.2.1.83 k-carrageenase
EC 3.2.1.84 glucan 1,3-a-glucosidase
EC 3.2.1.85 6-phospho-b-galactosidase
EC 3.2.1.86 6-phospho-b-glucosidase
EC 3.2.1.87 capsular-polysaccharide endo-1,3-a-galactosidase
EC 3.2.1.88 b-L-arabinosidase
EC 3.2.1.89 arabinogalactan endo-1,4-b-galactosidase
EC 3.2.1.91 cellulose 1,4-b-cellobiosidase
EC 3.2.1.92 peptidoglycan b-*N*-acetylmuramidase
EC 3.2.1.93 a,a-phosphotrehalase
EC 3.2.1.94 glucan 1,6-a-isomaltosidase
EC 3.2.1.95 dextran 1,6-a-isomaltotriosidase
EC 3.2.1.96 mannosyl-glycoprotein endo-b-*N*-acetylglucosaminidase
EC 3.2.1.97 glycopeptide a-*N*-acetylgalactosaminidase
EC 3.2.1.98 glucan 1,4-a-maltohexaosidase
EC 3.2.1.99 arabinan endo-1,5-a-L-arabinosidase
EC 3.2.1.100 mannan 1,4-mannobiosidase
EC 3.2.1.101 mannan endo-1,6-b-mannosidase
EC 3.2.1.102 blood-group-substance endo-1,4-b-galactosidase
EC 3.2.1.103 keratan-sulfate endo-1,4-b-galactosidase
EC 3.2.1.104 steryl-b-glucosidase
EC 3.2.1.105 strictosidine b-glucosidase
EC 3.2.1.106 mannosyl-oligosaccharide glucosidase
EC 3.2.1.107 protein-glucosylgalactosylhydroxylysine glucosidase
EC 3.2.1.108 lactase
EC 3.2.1.109 endogalactosaminidase
EC 3.2.1.110 mucinaminylserine mucinaminidase
EC 3.2.1.111 1,3-a-L-fucosidase
EC 3.2.1.112 2-deoxyglucosidase
EC 3.2.1.113 mannosyl-oligosaccharide 1,2-a-mannosidase
EC 3.2.1.114 mannosyl-oligosaccharide 1,3-1,6-a-mannosidase
EC 3.2.1.115 branched-dextran exo-1,2-a-glucosidase
EC 3.2.1.116 glucan 1,4-a-maltotriohydrolase
EC 3.2.1.117 amygdalin b-glucosidase
EC 3.2.1.118 prunasin b-glucosidase
EC 3.2.1.119 vicianin b-glucosidase
EC 3.2.1.120 oligoxyloglucan b-glycosidase
EC 3.2.1.121 polymannuronate hydrolase
EC 3.2.1.122 maltose-6'-phosphate glucosidase
EC 3.2.1.123 endoglycosylceramidase
EC 3.2.1.124 3-deoxy-2-octulosonidase
EC 3.2.1.125 raucaffricine b-glucosidase
EC 3.2.1.126 coniferin b-glucosidase
EC 3.2.1.127 1,6-a-L-fucosidase
EC 3.2.1.128 glycyrrhizinate b-glucuronidase
EC 3.2.1.129 endo-a-sialidase
EC 3.2.1.130 glycoprotein endo-a-1,2-mannosidase
EC 3.2.1.131 xylan a-1,2-glucuronosidase
EC 3.2.1.132 chitosanase
EC 3.2.1.133 glucan 1,4-a-maltohydrolase
EC 3.2.1.134 difructose-anhydride synthase
EC 3.2.1.135 neopullulanase
EC 3.2.1.136 glucuronoarabinoxylan endo-1,4-b-xylanase
EC 3.2.1.137 mannan exo-1,2-1,6-a-mannosidase
EC 3.2.1.138 anhydrosialidase
EC 3.2.1.139 a-glucuronidase
EC 3.2.1.140 lacto-*N*-biosidase
EC 3.2.1.141 4-a-D-{(1-4)-a-D-glucano}trehaose trehalohydrolase
EC 3.2.1.142 limit dextrinase
EC 3.2.1.143 poly(ADP-ribose) glycohydrolase
EC 3.2.1.144 3-deoxyoctulosonase
EC 3.2.1.145 galactan 1,3-b-galactosidase
EC 3.2.1.146 b-galactofuranosidase
EC 3.2.1.147 thioglucosidase
EC 3.2.1.148 ribosylhomocysteinase
EC 3.2.1.149 b-primeverosidase

**EC 3.2.2 Hydrolysing *N*-Glycosyl Compounds**

EC 3.2.2.1 purine nucleosidase
EC 3.2.2.2 inosine nucleosidase
EC 3.2.2.3 uridine nucleosidase
EC 3.2.2.4 AMP nucleosidase
EC 3.2.2.5 NAD nucleosidase
EC 3.2.2.6 NAD(P) nucleosidase
EC 3.2.2.7 adenosine nucleosidase
EC 3.2.2.8 ribosylpyrimidine nucleosidase
EC 3.2.2.9 adenosylhomocysteine nucleosidase
EC 3.2.2.10 pyrimidine-5'-nucleotide nucleosidase
EC 3.2.2.11 b-aspartyl-*N*-acetylglucosaminidase
EC 3.2.2.12 inosinate nucleosidase
EC 3.2.2.13 1-methyladenosine nucleosidase
EC 3.2.2.14 NMN nucleosidase
EC 3.2.2.15 DNA-deoxyinosine glycosylase
EC 3.2.2.16 methylthioadenosine nucleosidase
EC 3.2.2.17 deoxyribodipyrimidine endonucleosidase
EC 3.2.2.19 ADPribosylarginine hydrolase
EC 3.2.2.20 DNA-3-methyladenine glycosylase I
EC 3.2.2.21 DNA-3-methyladenine glycosylase II
EC 3.2.2.22 rRNA *N*-glycosylase
EC 3.2.2.23 DNA-formamidopyrimidine glycosylase
EC 3.2.2.24 ADP-ribosyl-[dinitrogen reductase] hydrolase

**EC 3.2.3 Hydrolysing *S*-Glycosyl Compounds**

**EC 3.3 Acting on Ether Bonds**

**EC 3.3.1 Trialkylsulfonium hydrolases**

EC 3.3.1.1 adenosylhomocysteinase
EC 3.3.1.2 adenosylmethionine hydrolase
**EC 3.3.2 Ether Hydrolases**

EC 3.3.2.1 isochorismatase
EC 3.3.2.2 alkenylglycerophosphocholine hydrolase
EC 3.3.2.3 epoxide hydrolase
EC 3.3.2.4 *trans*-epoxysuccinate hydrolase
EC 3.3.2.5 alkenylglycerophosphoethanolamine hydrolase
EC 3.3.2.6 leukotriene-$A_4$ hydrolase
EC 3.3.2.7 hepoxilin-epoxide hydrolase
EC 3.3.2.8 limonene-1,2-epoxide hydrolase

**EC 3.4 Acting on peptide bonds (Peptidases)**

**EC 3.4.11 Aminopeptidases**

EC 3.4.11.1 leucyl aminopeptidase
EC 3.4.11.2 membrane alanyl aminopeptidase
EC 3.4.11.3 cystinyl aminopeptidase
EC 3.4.11.4 tripeptide aminopeptidase
EC 3.4.11.5 prolyl aminopeptidase
EC 3.4.11.6 arginyl aminopeptidase
EC 3.4.11.7 glutamyl aminopeptidase
EC 3.4.11.9 X-Pro aminopeptidase
EC 3.4.11.10 bacterial leucyl aminopeptidase
EC 3.4.11.13 clostridial aminopeptidase
EC 3.4.11.14 cytosol alanyl aminopeptidase
EC 3.4.11.15 lysyl aminopeptidase
EC 3.4.11.16 X-Trp aminopeptidase
EC 3.4.11.17 tryptophanyl aminopeptidase
EC 3.4.11.18 methionyl aminopeptidase
EC 3.4.11.19 D-stereospecific aminopeptidase
EC 3.4.11.20 aminopeptidase Ey
EC 3.4.11.21 aspartyl aminopeptidase
EC 3.4.11.22 aminopeptidase I

**EC 3.4.12 Peptidylamino-Acid Hydrolases or Acylamino-Acid Hydrolases**

**EC 3.4.13 Dipeptidases**

EC 3.4.13.3 X-His dipeptidase
EC 3.4.13.4 X-Arg dipeptidase
EC 3.4.13.5 X-methyl-His dipeptidase
EC 3.4.13.7 Glu-Glu dipeptidase
EC 3.4.13.9 X-Pro dipeptidase
EC 3.4.13.12 Met-X dipeptidase
EC 3.4.13.17 non-stereospecific dipeptidase
EC 3.4.13.18 cytosol nonspecific dipeptidase
EC 3.4.13.19 membrane dipeptidase
EC 3.4.13.20 b-Ala-His dipeptidase
EC 3.4.13.21 dipeptidase E

**EC 3.4.14 Dipeptidyl-peptidases and tripeptidyl-peptidases**

EC 3.4.14.1 dipeptidyl-peptidase I
EC 3.4.14.2 dipeptidyl-peptidase II
EC 3.4.14.4 dipeptidyl-peptidase III
EC 3.4.14.5 dipeptidyl-peptidase IV
EC 3.4.14.6 dipeptidyl-dipeptidase
EC 3.4.14.9 tripeptidyl-peptidase I
EC 3.4.14.10 tripeptidyl-peptidase II
EC 3.4.14.11 X-Pro dipeptidyl-peptidase

**EC 3.4.15 Peptidyl-dipeptidases**

EC 3.4.15.1 peptidyl-dipeptidase A
EC 3.4.15.4 peptidyl-dipeptidase B
EC 3.4.15.5 peptidyl-dipeptidase Dcp

**EC 3.4.16 Serine-type carboxypeptidases**

EC 3.4.16.2 lysosomal Pro-X carboxypeptidase
EC 3.4.16.4 serine-type D-Ala-D-Ala carboxypeptidase
EC 3.4.16.5 carboxypeptidase C
EC 3.4.16.6 carboxypeptidase D

**EC 3.4.17 Metallocarboxypeptidases**

EC 3.4.17.1 carboxypeptidase A
EC 3.4.17.2 carboxypeptidase B
EC 3.4.17.3 lysine carboxypeptidase
EC 3.4.17.4 Gly-X carboxypeptidase
EC 3.4.17.6 alanine carboxypeptidase
EC 3.4.17.8 muramoylpentapeptide carboxypeptidase
EC 3.4.17.10 carboxypeptidase E
EC 3.4.17.11 glutamate carboxypeptidase
EC 3.4.17.12 carboxypeptidase M
EC 3.4.17.13 muramoyltetrapeptide carboxypeptidase
EC 3.4.17.14 zinc D-Ala-D-Ala carboxypeptidase
EC 3.4.17.15 carboxypeptidase A2
EC 3.4.17.16 membrane Pro-X carboxypeptidase
EC 3.4.17.17 tubulinyl-Tyr carboxypeptidase
EC 3.4.17.18 carboxypeptidase T
EC 3.4.17.19 carboxypeptidase Taq
EC 3.4.17.20 carboxypeptidase U
EC 3.4.17.21 glutamate carboxypeptidase II
EC 3.4.17.22 metallocarboxypeptidase D

**EC 3.4.18 Cysteine-type carboxypeptidases**

EC 3.4.18.1 cathepsin X

**EC 3.4.19 Omega peptidases**

EC 3.4.19.1 acylaminoacyl-peptidase
EC 3.4.19.2 peptidyl-glycinamidase
EC 3.4.19.3 pyroglutamyl-peptidase I
EC 3.4.19.5 b-aspartyl-peptidase
EC 3.4.19.6 pyroglutamyl-peptidase II
EC 3.4.19.7 *N*-formylmethionyl-peptidase
EC 3.4.19.9 g-glutamyl hydrolase
EC 3.4.19.11 g-D-glutamyl-*meso*-diaminopimelate peptidase I
EC 3.4.19.12 ubiquitinyl hydrolase 1

**EC 3.4.21 Serine endopeptidases**

EC 3.4.21.1 chymotrypsin
EC 3.4.21.2 chymotrypsin C
EC 3.4.21.3 metridin
EC 3.4.21.4 trypsin
EC 3.4.21.5 thrombin
EC 3.4.21.6 coagulation factor Xa
EC 3.4.21.7 plasmin
EC 3.4.21.9 enteropeptidase
EC 3.4.21.10 acrosin
EC 3.4.21.12 a-Lytic endopeptidase
EC 3.4.21.19 glutamyl endopeptidase
EC 3.4.21.20 cathepsin G
EC 3.4.21.21 coagulation factor VIIa
EC 3.4.21.22 coagulation factor IXa
EC 3.4.21.25 cucumisin
EC 3.4.21.26 prolyl oligopeptidase
EC 3.4.21.27 coagulation factor XIa
EC 3.4.21.32 brachyurin
EC 3.4.21.34 plasma kallikrein
EC 3.4.21.35 tissue kallikrein
EC 3.4.21.36 pancreatic elastase
EC 3.4.21.37 leukocyte elastase
EC 3.4.21.38 coagulation factor XIIa
EC 3.4.21.39 chymase

EC 3.4.21.41 complement subcomponent C

EC 3.4.21.42 complement subcomponent C
EC 3.4.21.43 classical-complement-pathway C3/C5 convertase
EC 3.4.21.45 complement factor I
EC 3.4.21.46 complement factor D
EC 3.4.21.47 alternative-complement-pathway C3/C5 convertase
EC 3.4.21.48 cerevisin
EC 3.4.21.49 hypodermin C
EC 3.4.21.50 lysyl endopeptidase
EC 3.4.21.53 endopeptidase La
EC 3.4.21.54 g-renin
EC 3.4.21.55 venombin AB
EC 3.4.21.57 leucyl endopeptidase
EC 3.4.21.59 tryptase
EC 3.4.21.60 scutelarin
EC 3.4.21.61 kexin
EC 3.4.21.62 subtilisin
EC 3.4.21.63 oryzin
EC 3.4.21.64 endopeptidase K
EC 3.4.21.65 thermomycolin
EC 3.4.21.66 thermitase
EC 3.4.21.67 endopeptidase So
EC 3.4.21.68 t-plasminogen activator
EC 3.4.21.69 protein C (activated)
EC 3.4.21.70 pancreatic endopeptidase E
EC 3.4.21.71 pancreatic elastase II
EC 3.4.21.72 IgA-specific serine endopeptidase
EC 3.4.21.73 u-plasminogen activator
EC 3.4.21.74 venombin A
EC 3.4.21.75 furin
EC 3.4.21.76 myeloblastin
EC 3.4.21.77 semenogelase
EC 3.4.21.78 granzyme A
EC 3.4.21.79 granzyme B
EC 3.4.21.80 streptogrisin A
EC 3.4.21.81 streptogrisin B
EC 3.4.21.82 glutamyl endopeptidase II
EC 3.4.21.83 oligopeptidase B
EC 3.4.21.84 limulus clotting factor
EC 3.4.21.85 limulus clotting factor
EC 3.4.21.86 limulus clotting enzyme
EC 3.4.21.87 omptin
EC 3.4.21.88 repressor LexA
EC 3.4.21.89 signal peptidase I
EC 3.4.21.90 togavirin
EC 3.4.21.91 flavivirin
EC 3.4.21.92 endopeptidase Clp
EC 3.4.21.93 proprotein convertase 1
EC 3.4.21.94 proprotein convertase 2
EC 3.4.21.95 snake venom factor V activator
EC 3.4.21.96 lactocepin
EC 3.4.21.97 assemblin
EC 3.4.21.98 hepacivirin
EC 3.4.21.99 spermosin
EC 3.4.21.100 pseudomonapepsin
EC 3.4.21.101 xanthomonapepsin
EC 3.4.21.102 C-terminal processing peptidase

**EC 3.4.22 Cysteine endopeptidases**

EC 3.4.22.1 cathepsin B
EC 3.4.22.2 papain
EC 3.4.22.3 ficain
EC 3.4.22.6 chymopapain
EC 3.4.22.7 asclepain
EC 3.4.22.8 clostripain
EC 3.4.22.10 streptopain
EC 3.4.22.14 actinidain
EC 3.4.22.15 cathepsin L
EC 3.4.22.16 cathepsin H
EC 3.4.22.17 calpain
EC 3.4.22.24 cathepsin T
EC 3.4.22.25 glycyl endopeptidase
EC 3.4.22.26 cancer procoagulant
EC 3.4.22.27 cathepsin S
EC 3.4.22.28 picornain 3C
EC 3.4.22.29 picornain 2A
EC 3.4.22.30 caricain
EC 3.4.22.31 ananain
EC 3.4.22.32 stem bromelain
EC 3.4.22.33 fruit bromelain
EC 3.4.22.34 legumain
EC 3.4.22.35 histolysain
EC 3.4.22.36 caspase-1
EC 3.4.22.37 gingipain R
EC 3.4.22.38 cathepsin K
EC 3.4.22.39 adenain
EC 3.4.22.40 bleomycin hydrolase
EC 3.4.22.41 cathepsin F
EC 3.4.22.42 cathepsin O
EC 3.4.22.43 cathepsin V
EC 3.4.22.44 nuclear-inclusion-a endopeptidase
EC 3.4.22.45 helper-component proteinase
EC 3.4.22.46 L-peptidase

**EC 3.4.23 Aspartic endopeptidases**

EC 3.4.23.1 pepsin A
EC 3.4.23.2 pepsin B
EC 3.4.23.3 gastricsin
EC 3.4.23.4 chymosin
EC 3.4.23.5 cathepsin D
EC 3.4.23.12 nepenthesin
EC 3.4.23.15 renin
EC 3.4.23.16 HIV-1 retropepsin
EC 3.4.23.17 Pro-opiomelanocortin converting enzyme
EC 3.4.23.18 aspergillopepsin I
EC 3.4.23.19 aspergillopepsin II
EC 3.4.23.20 penicillopepsin
EC 3.4.23.21 rhizopuspepsin
EC 3.4.23.22 endothiapepsin
EC 3.4.23.23 mucorpepsin
EC 3.4.23.24 candidapepsin
EC 3.4.23.25 saccharopepsin
EC 3.4.23.26 rhodotorulapepsin
EC 3.4.23.27 physaropepsin
EC 3.4.23.28 acrocylindropepsin
EC 3.4.23.29 polyporopepsin
EC 3.4.23.30 pycnoporopepsin
EC 3.4.23.31 scytalidopepsin A
EC 3.4.23.32 scytalidopepsin B
EC 3.4.23.34 cathepsin E
EC 3.4.23.35 barrierpepsin
EC 3.4.23.36 signal peptidase II
EC 3.4.23.38 plasmepsin I
EC 3.4.23.39 plasmepsin II
EC 3.4.23.40 phytepsin
EC 3.4.23.41 yapsin 1
EC 3.4.23.42 thermopsin
EC 3.4.23.43 prepilin peptidase
EC 3.4.23.44 nodavirus endopeptidase

**EC 3.4.24 Metalloendopeptidases**

EC 3.4.24.1 atrolysin A
EC 3.4.24.3 microbial collagenase
EC 3.4.24.6 leucolysin
EC 3.4.24.7 interstitial collagenase
EC 3.4.24.11 neprilysin
EC 3.4.24.12 envelysin
EC 3.4.24.13 IgA-specific metalloendopeptidase
EC 3.4.24.14 procollagen N-endopeptidase
EC 3.4.24.15 thimet oligopeptidase
EC 3.4.24.16 neurolysin
EC 3.4.24.17 stromelysin 1
EC 3.4.24.18 meprin A
EC 3.4.24.19 procollagen C-endopeptidase
EC 3.4.24.20 peptidyl-Lys metalloendopeptidase
EC 3.4.24.21 astacin
EC 3.4.24.22 stromelysin 2
EC 3.4.24.23 matrilysin
EC 3.4.24.24 gelatinase A
EC 3.4.24.25 vibriolysin
EC 3.4.24.26 pseudolysin
EC 3.4.24.27 thermolysin
EC 3.4.24.28 bacillolysin
EC 3.4.24.29 aureolysin
EC 3.4.24.30 coccolysin
EC 3.4.24.31 mycolysin
EC 3.4.24.32 b-lytic metalloendopeptidase
EC 3.4.24.33 peptidyl-Asp metalloendopeptidase
EC 3.4.24.34 neutrophil collagenase
EC 3.4.24.35 gelatinase B
EC 3.4.24.36 leishmanolysin
EC 3.4.24.37 saccharolysin
EC 3.4.24.38 gametolysin
EC 3.4.24.39 deuterolysin
EC 3.4.24.40 serralysin
EC 3.4.24.41 atrolysin B
EC 3.4.24.42 atrolysin C
EC 3.4.24.43 atroxase
EC 3.4.24.44 atrolysin E
EC 3.4.24.45 atrolysin F
EC 3.4.24.46 adamalysin
EC 3.4.24.47 horrilysin
EC 3.4.24.48 ruberlysin
EC 3.4.24.49 bothropasin
EC 3.4.24.50 bothrolysin
EC 3.4.24.51 ophiolysin
EC 3.4.24.52 trimerelysin I
EC 3.4.24.53 trimerelysin II
EC 3.4.24.54 mucrolysin
EC 3.4.24.55 pitrilysin
EC 3.4.24.56 insulysin
EC 3.4.24.57 *O*-sialoglycoprotein endopeptidase
EC 3.4.24.58 russellysin
EC 3.4.24.59 mitochondrial intermediate peptidase
EC 3.4.24.60 dactylysin
EC 3.4.24.61 nardilysin
EC 3.4.24.62 magnolysin
EC 3.4.24.63 meprin B
EC 3.4.24.64 mitochondrial processing peptidase
EC 3.4.24.65 macrophage elastase
EC 3.4.24.66 choriolysin L
EC 3.4.24.67 choriolysin H
EC 3.4.24.68 tentoxilysin
EC 3.4.24.69 bontoxilysin
EC 3.4.24.70 oligopeptidase A
EC 3.4.24.71 endothelin-converting enzyme
EC 3.4.24.72 fibrolase
EC 3.4.24.73 jararhagin
EC 3.4.24.74 fragilysin
EC 3.4.24.75 lysostaphin
EC 3.4.24.76 flavastacin
EC 3.4.24.77 snapalysin

**EC 3.4.25 Threonine endopeptidases**

EC 3.4.25.1 proteasome endopeptidase complex

**EC 3.4.99 Endopeptidases of unknown catalytic mechanism**

**EC 3.5.1 In Linear Amides**

EC 3.5.1.1 asparaginase
EC 3.5.1.2 glutaminase
EC 3.5.1.3 w-amidase
EC 3.5.1.4 amidase
EC 3.5.1.5 urease
EC 3.5.1.6 b-ureidopropionase
EC 3.5.1.7 ureidosuccinase
EC 3.5.1.8 formylaspartate deformylase
EC 3.5.1.9 arylformamidase
EC 3.5.1.10 formyltetrahydrofolate deformylase
EC 3.5.1.11 penicillin amidase
EC 3.5.1.12 biotinidase
EC 3.5.1.13 aryl-acylamidase
EC 3.5.1.14 aminoacylase
EC 3.5.1.15 aspartoacylase
EC 3.5.1.16 acetylornithine deacetylase
EC 3.5.1.17 acyl-lysine deacylase
EC 3.5.1.18 succinyl-diaminopimelate desuccinylase
EC 3.5.1.19 nicotinamidase
EC 3.5.1.20 citrullinase
EC 3.5.1.21 *N*-acetyl-b-alanine deacetylase
EC 3.5.1.22 pantothenase
EC 3.5.1.23 ceramidase
EC 3.5.1.24 choloylglycine hydrolase
EC 3.5.1.25 *N*-acetylglucosamine-6-phosphate deacetylase
EC 3.5.1.26 $N^4$-(b-*N*-acetylglucosaminyl)-L-asparaginase
EC 3.5.1.27 *N*-formylmethionylaminoacyl-tRNA deformylase
EC 3.5.1.28 *N*-acetylmuramoyl-L-alanine amidase
EC 3.5.1.29 2-(acetamidomethylene)succinate hydrolase
EC 3.5.1.30 5-aminopentanamidase
EC 3.5.1.31 formylmethionine deformylase
EC 3.5.1.32 hippurate hydrolase
EC 3.5.1.33 *N*-acetylglucosamine deacetylase
EC 3.5.1.35 D-glutaminase
EC 3.5.1.36 *N*-methyl-2-oxoglutaramate hydrolase
EC 3.5.1.38 glutamin-(asparagin-)ase
EC 3.5.1.39 alkylamidase
EC 3.5.1.40 acylagmatine amidase
EC 3.5.1.41 chitin deacetylase
EC 3.5.1.42 nicotinamide-nucleotide amidase
EC 3.5.1.43 peptidyl-glutaminase
EC 3.5.1.44 protein-glutamine glutaminase
EC 3.5.1.46 6-aminohexanoate-dimer hydrolase
EC 3.5.1.47 *N*-acetyldiaminopimelate deacetylase
EC 3.5.1.48 acetylspermidine deacetylase
EC 3.5.1.49 formamidase
EC 3.5.1.50 pentanamidase
EC 3.5.1.51 4-acetamidobutyryl-CoA deacetylase
EC 3.5.1.52 peptide-$N^4$-(*N*-acetyl-b-glucosaminyl)asparagine amidase
EC 3.5.1.53 *N*-carbamoylputrescine amidase
EC 3.5.1.54 allophanate hydrolase
EC 3.5.1.55 long-chain-fatty-acyl-glutamate deacylase
EC 3.5.1.56 *N,N*-dimethylformamidase

EC 3.5.1.57 tryptophanamidase
EC 3.5.1.58 *N*-benzyloxycarbonylglycine hydrolase
EC 3.5.1.59 *N*-carbamoylsarcosine amidase
EC 3.5.1.60 *N*-(long-chain-acyl)ethanolamine deacylase
EC 3.5.1.61 mimosinase
EC 3.5.1.62 acetylputrescine deacetylase
EC 3.5.1.63 4-acetamidobutyrate deacetylase
EC 3.5.1.64 $N^6$-benzyloxycarbonylleucine hydrolase
EC 3.5.1.65 theanine hydrolase
EC 3.5.1.66 2-(hydroxymethyl)-3-(acetamidomethylene)succinate hydrolase
EC 3.5.1.67 4-methyleneglutaminase
EC 3.5.1.68 *N*-formylglutamate deformylase
EC 3.5.1.69 glycosphingolipid deacylase
EC 3.5.1.70 aculeacin-A deacylase
EC 3.5.1.71 *N*-feruloylglycine deacylase
EC 3.5.1.72 D-benzoylarginine-4-nitroanilide amidase
EC 3.5.1.73 carnitinamidase
EC 3.5.1.74 chenodeoxycholoyltaurine hydrolase
EC 3.5.1.75 urethanase
EC 3.5.1.76 arylalkyl acylamidase
EC 3.5.1.77 *N*-carbamoyl-D-amino acid hydrolase
EC 3.5.1.78 glutathionylspermidine amidase
EC 3.5.1.79 phthalyl amidase
EC 3.5.1.81 *N*-acyl-D-amino-acid deacylase
EC 3.5.1.82 *N*-acyl-D-glutamate deacylase
EC 3.5.1.83 *N*-acyl-D-aspartate deacylase
EC 3.5.1.84 biuret amidohydrolase
EC 3.5.1.85 (*S*)-*N*-acetyl-1-phenylethylamine hydrolase
EC 3.5.1.86 mandelamide amidase
EC 3.5.1.87 *N*-carbamoyl-L-amino-acid hydrolase
EC 3.5.1.88 peptide deformylase
EC 3.5.1.89 *N*-acetylglucosaminylphosphatidylinositol deacetylase

**EC 3.5.2 In Cyclic Amides**

EC 3.5.2.1 barbiturase
EC 3.5.2.2 dihydropyrimidinase
EC 3.5.2.3 dihydroorotase
EC 3.5.2.4 carboxymethylhydantoinase
EC 3.5.2.5 allantoinase
EC 3.5.2.6 b-lactamase
EC 3.5.2.7 imidazolonepropionase
EC 3.5.2.9 5-oxoprolinase (ATP-hydrolysing)
EC 3.5.2.10 creatininase
EC 3.5.2.11 L-lysine-lactamase
EC 3.5.2.12 6-aminohexanoate-cyclic-dimer hydrolase
EC 3.5.2.13 2,5-dioxopiperazine hydrolase
EC 3.5.2.14 *N*-methylhydantoinase (ATP-hydrolysing)
EC 3.5.2.15 cyanuric acid amidohydrolase
EC 3.5.2.16 maleimide hydrolase

**EC 3.5.3 In Linear Amidines**

EC 3.5.3.1 arginase
EC 3.5.3.2 guanidinoacetase
EC 3.5.3.3 creatinase
EC 3.5.3.4 allantoicase
EC 3.5.3.5 formiminoaspartate deiminase
EC 3.5.3.6 arginine deiminase
EC 3.5.3.7 guanidinobutyrase
EC 3.5.3.8 formimidoylglutamase
EC 3.5.3.9 allantoate deiminase
EC 3.5.3.10 D-arginase
EC 3.5.3.11 agmatinase
EC 3.5.3.12 agmatine deiminase
EC 3.5.3.13 formiminoglutamate deiminase
EC 3.5.3.14 amidinoaspartase
EC 3.5.3.15 protein-arginine deiminase
EC 3.5.3.16 methylguanidinase
EC 3.5.3.17 guanidinopropionase
EC 3.5.3.18 dimethylargininase
EC 3.5.3.19 ureidoglycolate hydrolase
EC 3.5.3.20 diguanidinobutanase
EC 3.5.3.21 methylenediurea deaminase

**EC 3.5.4 In Cyclic Amidines**

EC 3.5.4.1 cytosine deaminase
EC 3.5.4.2 adenine deaminase
EC 3.5.4.3 guanine deaminase
EC 3.5.4.4 adenosine deaminase
EC 3.5.4.5 cytidine deaminase
EC 3.5.4.6 AMP deaminase
EC 3.5.4.7 ADP deaminase
EC 3.5.4.8 aminoimidazolase
EC 3.5.4.9 methenyltetrahydrofolate cyclohydrolase
EC 3.5.4.10 IMP cyclohydrolase
EC 3.5.4.11 pterin deaminase
EC 3.5.4.12 dCMP deaminase
EC 3.5.4.13 dCTP deaminase
EC 3.5.4.14 deoxycytidine deaminase
EC 3.5.4.15 guanosine deaminase
EC 3.5.4.16 GTP cyclohydrolase I
EC 3.5.4.17 adenosine-phosphate deaminase
EC 3.5.4.18 ATP deaminase
EC 3.5.4.19 phosphoribosyl-AMP cyclohydrolase
EC 3.5.4.20 pyrithiamine deaminase
EC 3.5.4.21 creatinine deaminase
EC 3.5.4.22 1-pyrroline-4-hydroxy-2-carboxylate deaminase
EC 3.5.4.23 blasticidin-S deaminase
EC 3.5.4.24 sepiapterin deaminase
EC 3.5.4.25 GTP cyclohydrolase II
EC 3.5.4.26 diaminohydroxyphosphoribosylaminopyrimidine deaminase
EC 3.5.4.27 methenyltetrahydromethanopterin cyclohydrolase
EC 3.5.4.28 *S*-adenosylhomocysteine deaminase

**EC 3.5.5 In Nitriles**

EC 3.13.1.1 UDPsulfoquinovose synthase
EC 3.5.5.1 nitrilase
EC 3.5.5.2 ricinine nitrilase
EC 3.5.5.4 cyanoalanine nitrilase
EC 3.5.5.5 arylacetonitrilase
EC 3.5.5.6 bromoxynil nitrilase
EC 3.5.5.7 aliphatic nitrilase
EC 3.5.5.8 thiocyanate hydrolase

**EC 3.5.99 In Other Compounds**

EC 3.5.99.1 riboflavinase
EC 3.5.99.2 thiaminase

EC 3.5.99.3 hydroxydechloroatrazine ethylaminohydrolase
EC 3.5.99.4 *N*-isopropylammelide isopropylaminohydrolase
EC 3.5.99.5 2-aminomuconate deaminase
EC 3.5.99.6 glucosamine-6-phosphate deaminase
EC 3.5.99.7 1-aminocyclopropane-1-carboxylate deaminase

**EC 3.6 Acting on Acid Anhydrides**

**EC 3.6.1 In Phosphorus-Containing Anhydrides**

EC 3.6.1.1 inorganic diphosphatase
EC 3.6.1.2 trimetaphosphatase
EC 3.6.1.3 adenosinetriphosphatase
EC 3.6.1.5 apyrase
EC 3.6.1.6 nucleoside-diphosphatase
EC 3.6.1.7 acylphosphatase
EC 3.6.1.8 ATP diphosphatase
EC 3.6.1.9 nucleotide diphosphatase
EC 3.6.1.10 endopolyphosphatase
EC 3.6.1.11 exopolyphosphatase
EC 3.6.1.12 dCTP diphosphatase
EC 3.6.1.13 ADP-ribose diphosphatase
EC 3.6.1.14 adenosine-tetraphosphatase
EC 3.6.1.15 nucleoside-triphosphatase
EC 3.6.1.16 CDP-glycerol diphosphatase
EC 3.6.1.17 bis(5'-nucleosyl)-tetraphosphatase (asymmetrical)
EC 3.6.1.18 FAD diphosphatase
EC 3.6.1.19 nucleoside-triphosphate diphosphatase
EC 3.6.1.20 5'-acylphosphoadenosine hydrolase
EC 3.6.1.21 ADP-sugar diphosphatase
EC 3.6.1.22 NAD diphosphatase
EC 3.6.1.23 dUTP diphosphatase
EC 3.6.1.24 nucleoside phosphoacylhydrolase
EC 3.6.1.25 triphosphatase
EC 3.6.1.26 CDP-diacylglycerol diphosphatase
EC 3.6.1.27 undecaprenyl-diphosphatase
EC 3.6.1.28 thiamine-triphosphatase
EC 3.6.1.29 bis(5'-adenosyl)-triphosphatase
EC 3.6.1.30 $m^7$G(5')pppN diphosphatase
EC 3.6.1.31 phosphoribosyl-ATP diphosphatase
EC 3.6.1.39 thymidine-triphosphatase
EC 3.6.1.40 guanosine-5'-triphosphate,3'-diphosphate diphosphatase
EC 3.6.1.41 bis(5'-nucleosyl)-tetraphosphatase (symmetrical)
EC 3.6.1.42 guanosine-diphosphatase
EC 3.6.1.43 dolichyldiphosphatase
EC 3.6.1.44 oligosaccharide-diphosphodolichol diphosphatase
EC 3.6.1.45 UDP-sugar diphosphatase
EC 3.6.1.46 heterotrimeric G-protein GTPase
EC 3.6.1.47 small monomeric GTPase
EC 3.6.1.48 protein-synthesizing GTPase
EC 3.6.1.49 signal-recognition-particle GTPase
EC 3.6.1.50 dynamin GTPase
EC 3.6.1.51 tubulin GTPase
EC 3.6.1.52 diphosphoinositol-polyphosphate diphosphatase

**EC 3.6.2 In Sulfonyl-Containing Anhydrides**

EC 3.6.2.1 adenylylsulfatase
EC 3.6.2.2 phosphoadenylylsulfatase

**EC 3.6.3 Acting on acid anhydrides; catalysing transmembrane movement of substances**

EC 3.6.3.1 $Mg^{2+}$-ATPase
EC 3.6.3.2 $Mg^{2+}$-importing ATPase
EC 3.6.3.3 $Cd^{2+}$-exporting ATPase
EC 3.6.3.4 $Cu^{2+}$-exporting ATPase
EC 3.6.3.5 $Zn^{2+}$-exporting ATPase
EC 3.6.3.6 $H^+$-exporting ATPase
EC 3.6.3.7 $Na^+$-exporting ATPase
EC 3.6.3.8 $Ca^{2+}$-transporting ATPase
EC 3.6.3.9 $Na^+/K^+$-exchanging ATPase
EC 3.6.3.10 $H^+/K^+$-exchanging ATPase
EC 3.6.3.11 $Cl^-$-transporting ATPase
EC 3.6.3.12 $K^+$-transporting ATPase
EC 3.6.3.14 $H^+$-transporting two-sector ATPase
EC 3.6.3.15 $Na^+$-transporting two-sector ATPase
EC 3.6.3.16 arsenite-transporting ATPase
EC 3.6.3.17 monosaccharide-transporting ATPase
EC 3.6.3.18 oligosaccharide-transporting ATPase
EC 3.6.3.19 maltose-transporting ATPase
EC 3.6.3.20 glycerol-3-phosphate-transporting ATPase
EC 3.6.3.21 polar-amino-acid-transporting ATPase
EC 3.6.3.22 nonpolar-amino-acid-transporting ATPase
EC 3.6.3.23 oligopeptide-transporting ATPase
EC 3.6.3.24 nickel-transporting ATPase
EC 3.6.3.25 sulfate-transporting ATPase
EC 3.6.3.26 nitrate-transporting ATPase
EC 3.6.3.27 phosphate-transporting ATPase
EC 3.6.3.28 phosphonate-transporting ATPase
EC 3.6.3.29 molybdate-transporting ATPase
EC 3.6.3.30 $Fe^{3+}$-transporting ATPase
EC 3.6.3.31 polyamine-transporting ATPase
EC 3.6.3.32 quaternary-amine-transporting ATPase
EC 3.6.3.33 vitamin $B_{12}$-transporting ATPase
EC 3.6.3.34 iron-chelate-transporting ATPase
EC 3.6.3.35 manganese-transporting ATPase
EC 3.6.3.36 taurine-transporting ATPase
EC 3.6.3.37 guanine-transporting ATPase
EC 3.6.3.38 capsular-polysaccharide-transporting ATPase
EC 3.6.3.39 lipopolysaccharide-transporting ATPase
EC 3.6.3.40 teichoic-acid-transporting ATPase
EC 3.6.3.41 heme-transporting ATPase
EC 3.6.3.42 b-glucan-transporting ATPase
EC 3.6.3.43 peptide-transporting ATPase
EC 3.6.3.44 xenobiotic-transporting ATPase
EC 3.6.3.45 steroid-transporting ATPase
EC 3.6.3.46 cadmium-transporting ATPase
EC 3.6.3.47 fatty-acyl-CoA-transporting ATPase
EC 3.6.3.48 a-factor-transporting ATPase
EC 3.6.3.49 channel-conductance-controlling ATPase
EC 3.6.3.50 protein-secreting ATPase
EC 3.6.3.51 mitochondrial protein-transporting ATPase
EC 3.6.3.52 chloroplast protein-transporting ATPase
EC 3.6.3.53 $Ag^+$-exporting ATPase

**EC 3.6.4 Acting on acid anhydrides; involved in cellular and subcellular movement**

EC 3.6.4.1 myosin ATPase
EC 3.6.4.2 dynein ATPase
EC 3.6.4.3 microtubule-severing ATPase
EC 3.6.4.4 plus-end-directed kinesin ATPase
EC 3.6.4.5 minus-end-directed kinesin ATPase
EC 3.6.4.6 vesicle-fusing ATPase
EC 3.6.4.7 peroxisome-assembly ATPase
EC 3.6.4.8 proteasome ATPase
EC 3.6.4.9 chaperonin ATPase
EC 3.6.4.10 non-chaperonin molecular chaperone ATPase
EC 3.6.4.11 nucleoplasmin ATPase

**EC 3.7 Acting on Carbon-Carbon Bonds**

**EC 3.7.1 In Ketonic Substances**

EC 3.7.1.1 oxaloacetase
EC 3.7.1.2 fumarylacetoacetase
EC 3.7.1.3 kynureninase
EC 3.7.1.4 phloretin hydrolase
EC 3.7.1.5 acylpyruvate hydrolase
EC 3.7.1.6 acetylpyruvate hydrolase
EC 3.7.1.7 b-diketone hydrolase
EC 3.7.1.8 2,6-dioxo-6-phenylhexa-3-enoate hydrolase
EC 3.7.1.9 2-hydroxymuconate-semialdehyde hydrolase
EC 3.7.1.10 cyclohexane-1,3-dione hydrolase

**EC 3.8 Acting on Halide Bonds**

**EC 3.8.1 In C-Halide Compounds**

EC 3.8.1.1 alkylhalidase
EC 3.8.1.2 2-haloacid dehalogenase
EC 3.8.1.3 haloacetate dehalogenase
EC 3.8.1.4 thyroxine deiodinase
EC 3.8.1.5 haloalkane dehalogenase
EC 3.8.1.6 4-chlorobenzoate dehalogenase
EC 3.8.1.7 4-chlorobenzoyl-CoA dehalogenase
EC 3.8.1.8 atrazine chlorohydrolase

**EC 3.8.2 In P-Halide Compounds**

**EC 3.9 Acting on Phosphorus-Nitrogen Bonds**

EC 3.9.1.1 phosphoamidase

**EC 3.10 Acting on Sulfur-Nitrogen Bonds**

EC 3.10.1.1 *N*-sulfoglucosamine sulfohydrolase
EC 3.10.1.2 cyclamate sulfohydrolase

**EC 3.11 Acting on Carbon-Phosphorus Bonds**

EC 3.11.1.1 phosphonoacetaldehyde hydrolase
EC 3.11.1.2 phosphonoacetate hydrolase

**EC 3.12 Acting on Sulfur-Sulfur Bonds**

EC 3.12.1.1 trithionate hydrolase

**EC 3.13 Acting on Carbon-Sulfur Bonds**

# 9.2 EC Group 4 Lyases

EC 4.1 Carbon-Carbon Lyases

**EC 4.1.1 Carboxy-Lyases**

EC 4.1.1.1 pyruvate decarboxylase
EC 4.1.1.2 oxalate decarboxylase
EC 4.1.1.3 oxaloacetate decarboxylase
EC 4.1.1.4 acetoacetate decarboxylase
EC 4.1.1.5 acetolactate decarboxylase
EC 4.1.1.6 aconitate decarboxylase
EC 4.1.1.7 benzoylformate decarboxylase
EC 4.1.1.8 oxalyl-CoA decarboxylase
EC 4.1.1.9 malonyl-CoA decarboxylase
EC 4.1.1.10 deleted, included in EC 4.1.1.12
EC 4.1.1.11 aspartate 1-decarboxylase
EC 4.1.1.12 aspartate 4-decarboxylase
EC 4.1.1.13 deleted
EC 4.1.1.14 valine decarboxylase
EC 4.1.1.15 glutamate decarboxylase
EC 4.1.1.16 hydroxyglutamate decarboxylase
EC 4.1.1.17 ornithine decarboxylase
EC 4.1.1.18 lysine decarboxylase
EC 4.1.1.19 arginine decarboxylase
EC 4.1.1.20 diaminopimelate decarboxylase
EC 4.1.1.21 phosphoribosylaminoimidazole carboxylase
EC 4.1.1.21 phosphoribosylaminoimidazole carboxylase
EC 4.1.1.22 histidine decarboxylase
EC 4.1.1.23 orotidine-5'-phosphate decarboxylase
EC 4.1.1.24 aminobenzoate decarboxylase
EC 4.1.1.25 tyrosine decarboxylase
EC 4.1.1.26 deleted, included in EC 4.1.1.28
EC 4.1.1.27 deleted, included in EC 4.1.1.28
EC 4.1.1.28 aromatic-L-amino-acid decarboxylase
EC 4.1.1.29 sulfoalanine decarboxylase
EC 4.1.1.30 pantothenoylcysteine decarboxylase
EC 4.1.1.31 phospho*enol*pyruvate carboxylase
EC 4.1.1.32 phospho*enol*pyruvate carboxykinase (GTP)
EC 4.1.1.33 diphosphomevalonate decarboxylase
EC 4.1.1.34 dehydro-L-gulonate decarboxylase
EC 4.1.1.35 UDP-glucuronate decarboxylase
EC 4.1.1.36 phosphopantothenoylcysteine decarboxylase
EC 4.1.1.37 uroporphyrinogen decarboxylase
EC 4.1.1.38 phospho*enol*pyruvate carboxykinase (diphosphate)
EC 4.1.1.39 ribulose-bisphosphate carboxylase
EC 4.1.1.40 hydroxypyruvate decarboxylase
EC 4.1.1.41 methylmalonyl-CoA decarboxylase
EC 4.1.1.42 carnitine decarboxylase
EC 4.1.1.43 phenylpyruvate decarboxylase
EC 4.1.1.44 4-carboxymuconolactone decarboxylase
EC 4.1.1.45 aminocarboxymuconate-semialdehyde decarboxylase
EC 4.1.1.46 *o*-pyrocatechuate decarboxylase
EC 4.1.1.47 tartronate-semialdehyde synthase
EC 4.1.1.48 indole-3-glycerol-phosphate synthase
EC 4.1.1.49 phospho*enol*pyruvate carboxykinase (ATP)
EC 4.1.1.50 adenosylmethionine decarboxylase
EC 4.1.1.51 3-hydroxy-2-methylpyridine-4,5-dicarboxylate 4-decarboxylase
EC 4.1.1.52 6-methylsalicylate decarboxylase
EC 4.1.1.53 phenylalanine decarboxylase
EC 4.1.1.54 dihydroxyfumarate decarboxylase
EC 4.1.1.55 4,5-dihydroxyphthalate decarboxylase
EC 4.1.1.56 3-oxolaurate decarboxylase
EC 4.1.1.57 methionine decarboxylase
EC 4.1.1.58 orsellinate decarboxylase
EC 4.1.1.59 gallate decarboxylase
EC 4.1.1.60 stipitatonate decarboxylase
EC 4.1.1.61 4-hydroxybenzoate decarboxylase
EC 4.1.1.62 gentisate decarboxylase
EC 4.1.1.63 protocatechuate decarboxylase
EC 4.1.1.64 2,2-dialkylglycine decarboxylase (pyruvate)
EC 4.1.1.65 phosphatidylserine decarboxylase
EC 4.1.1.66 uracil-5-carboxylate decarboxylase
EC 4.1.1.67 UDP-galacturonate decarboxylase
EC 4.1.1.68 5-oxopent-3-ene-1,2,5-tricarboxylate decarboxylase
EC 4.1.1.69 3,4-dihydroxyphthalate decarboxylase
EC 4.1.1.70 glutaconyl-CoA decarboxylase
EC 4.1.1.71 2-oxoglutarate decarboxylase
EC 4.1.1.72 branched-chain-2-oxoacid decarboxylase
EC 4.1.1.73 tartrate decarboxylase
EC 4.1.1.74 indolepyruvate decarboxylase
EC 4.1.1.75 5-guanidino-2-oxopentanoate decarboxylase
EC 4.1.1.76 arylmalonate decarboxylase
EC 4.1.1.77 4-oxalocrotonate decarboxylase
EC 4.1.1.78 acetylenedicarboxylate decarboxylase
EC 4.1.1.79 sulfopyruvate decarboxylase
EC 4.1.1.80 4-hydroxyphenylpyruvate decarboxylase

**EC 4.1.2 Aldehyde-Lyases**

EC 4.1.2.1 deleted, included in EC 4.1.3.16
EC 4.1.2.2 ketotetrose-phosphate aldolase
EC 4.1.2.3 deleted
EC 4.1.2.4 deoxyribose-phosphate aldolase
EC 4.1.2.5 threonine aldolase
EC 4.1.2.6 deleted
EC 4.1.2.7 deleted, included in EC 4.1.2.13
EC 4.1.2.8 deleted
EC 4.1.2.9 phosphoketolase
EC 4.1.2.10 mandelonitrile lyase
EC 4.1.2.11 hydroxymandelonitrile lyase
EC 4.1.2.12 ketopantoaldolase
EC 4.1.2.13 fructose-bisphosphate aldolase
EC 4.1.2.14 2-dehydro-3-deoxy-phosphogluconate aldolase
EC 4.1.2.15 now EC 2.5.1.54
EC 4.1.2.16 now EC 2.5.1.55
EC 4.1.2.17 L-fuculose-phosphate aldolase
EC 4.1.2.18 2-dehydro-3-deoxy-L-pentonate aldolase
EC 4.1.2.19 rhamnulose-1-phosphate aldolase
EC 4.1.2.20 2-dehydro-3-deoxyglucarate aldolase
EC 4.1.2.21 2-dehydro-3-deoxy-6-phosphogalactonate aldolase
EC 4.1.2.22 fructose-6-phosphate phosphoketolase
EC 4.1.2.23 3-deoxy-D-*manno*-octulosonate aldolase
EC 4.1.2.24 dimethylaniline-*N*-oxide aldolase
EC 4.1.2.25 dihydroneopterin aldolase
EC 4.1.2.26 phenylserine aldolase
EC 4.1.2.27 sphinganine-1-phosphate aldolase
EC 4.1.2.28 2-dehydro-3-deoxy-D-pentonate aldolase
EC 4.1.2.29 5-dehydro-2-deoxyphosphogluconate aldolase
EC 4.1.2.30 17a-hydroxyprogesterone aldolase
EC 4.1.2.31 deleted, included in EC 4.1.3.16
EC 4.1.2.32 trimethylamine-oxide aldolase
EC 4.1.2.33 fucosterol-epoxide lyase
EC 4.1.2.34 4-(2-carboxyphenyl)-2-oxobut-3-enoate aldolase
EC 4.1.2.35 propioin synthase
EC 4.1.2.36 lactate aldolase
EC 4.1.2.37 acetone-cyanhydrin lyase
EC 4.1.2.38 benzoin aldolase
EC 4.1.2.39 hydroxynitrilase
EC 4.1.2.40 tagatose-bisphosphate aldolase
EC 4.1.2.41 vanillin synthase

**EC 4.1.3 Oxo-Acid-Lyases**

EC 4.1.3.1 isocitrate lyase
EC 4.1.3.2 now EC 2.3.3.9
EC 4.1.3.3 *N*-acetylneuraminate lyase
EC 4.1.3.4 hydroxymethylglutaryl-CoA lyase
EC 4.1.3.5 now EC 2.3.3.10
EC 4.1.3.6 citrate (*pro-3S*)-lyase
EC 4.1.3.7 now EC 2.3.3.1
EC 4.1.3.8 now EC 2.3.3.8
EC 4.1.3.9 now EC 2.3.3.11
EC 4.1.3.10 now EC 2.3.3.7
EC 4.1.3.11 now EC 2.3.3.12
EC 4.1.3.12 now EC 2.3.3.13
EC 4.1.3.13 oxalomalate lyase
EC 4.1.3.14 3-hydroxyaspartate aldolase
EC 4.1.3.15 now EC 2.2.1.5
EC 4.1.3.16 4-hydroxy-2-oxoglutarate aldolase
EC 4.1.3.17 4-hydroxy-4-methyl-2-oxoglutarate aldolase
EC 4.1.3.18 now EC 2.2.1.6
EC 4.1.3.19 now EC 2.5.1.56
EC 4.1.3.20 now EC 2.5.1.57
EC 4.1.3.21 now EC 2.3.3.14
EC 4.1.3.22 citramalate lyase
EC 4.1.3.23 now EC 2.3.3.2
EC 4.1.3.24 malyl-CoA lyase
EC 4.1.3.25 citramalyl-CoA lyase
EC 4.1.3.26 3-hydroxy-3-isohexenylglutaryl-CoA lyase
EC 4.1.3.27 anthranilate synthase
EC 4.1.3.28 now EC 2.3.3.3
EC 4.1.3.29 now EC 2.3.3.4
EC 4.1.3.30 methylisocitrate lyase
EC 4.1.3.31 now EC 2.3.3.5
EC 4.1.3.32 2,3-dimethylmalate lyase
EC 4.1.3.33 now EC 2.3.3.6
EC 4.1.3.34 citryl-CoA lyase
EC 4.1.3.35 (1-hydroxycyclohexan-1-yl)acetyl-CoA lyase
EC 4.1.3.36 naphthoate synthase
EC 4.1.3.37 now EC 2.2.1.7

**EC 4.1.99 Other Carbon-Carbon Lyases**

EC 4.1.99.1 tryptophanase
EC 4.1.99.2 tyrosine phenol-lyase
EC 4.1.99.3 deoxyribodipyrimidine photo-lyase
EC 4.1.99.4 now EC 3.5.99.7
EC 4.1.99.5 octadecanal decarbonylase
EC 4.1.99.6 now EC 4.2.3.6
EC 4.1.99.7 now EC 4.2.3.9
EC 4.1.99.8 now EC 4.2.3.14
EC 4.1.99.9 now EC 4.2.3.15
EC 4.1.99.10 now EC 4.2.3.16
EC 4.1.99.11 benzylsuccinate synthase

**EC 4.2 Carbon-Oxygen Lyases**

**EC 4.2.1 Hydro-Lyases**

EC 4.2.1.1 carbonate dehydratase
EC 4.2.1.2 fumarate hydratase
EC 4.2.1.3 aconitate hydratase
EC 4.2.1.4 citrate dehydratase
EC 4.2.1.5 arabinonate dehydratase
EC 4.2.1.6 galactonate dehydratase
EC 4.2.1.7 altronate dehydratase
EC 4.2.1.8 mannonate dehydratase
EC 4.2.1.9 dihydroxy-acid dehydratase
EC 4.2.1.10 3-dehydroquinate dehydratase
EC 4.2.1.11 phosphopyruvate hydratase
EC 4.2.1.12 phosphogluconate dehydratase
EC 4.2.1.13 now EC 4.3.1.17
EC 4.2.1.14 now EC 4.3.1.18
EC 4.2.1.15 now EC 4.4.1.1
EC 4.2.1.16 now EC 4.3.1.19
EC 4.2.1.17 enoyl-CoA hydratase
EC 4.2.1.18 methylglutaconyl-CoA hydratase
EC 4.2.1.19 imidazoleglycerol-phosphate dehydratase
EC 4.2.1.20 tryptophan synthase
EC 4.2.1.21 now EC 4.2.1.22
EC 4.2.1.22 cystathionine b-synthase
EC 4.2.1.23 deleted
EC 4.2.1.24 porphobilinogen synthase
EC 4.2.1.25 L-arabinonate dehydratase
EC 4.2.1.26 now EC 4.3.1.21
EC 4.2.1.27 malonate-semialdehyde dehydratase
EC 4.2.1.28 propanediol dehydratase
EC 4.2.1.29 indoleacetaldoxime dehydratase
EC 4.2.1.30 glycerol dehydratase
EC 4.2.1.31 maleate hydratase
EC 4.2.1.32 L(+)-tartrate dehydratase
EC 4.2.1.33 3-isopropylmalate dehydratase
EC 4.2.1.34 (*S*)-2-methylmalate dehydratase
EC 4.2.1.35 (*R*)-2-methylmalate dehydratase
EC 4.2.1.36 homoaconitate hydratase
EC 4.2.1.37 now EC 3.3.2.4
EC 4.2.1.38 now EC 4.3.1.20
EC 4.2.1.39 gluconate dehydratase
EC 4.2.1.40 glucarate dehydratase
EC 4.2.1.41 5-dehydro-4-deoxyglucarate dehydratase
EC 4.2.1.42 galactarate dehydratase
EC 4.2.1.43 2-dehydro-3-deoxy-L-arabinonate dehydratase
EC 4.2.1.44 *myo*-inosose-2 dehydratase
EC 4.2.1.45 CDP-glucose 4,6-dehydratase
EC 4.2.1.46 dTDP-glucose 4,6-dehydratase
EC 4.2.1.47 GDP-mannose 4,6-dehydratase
EC 4.2.1.48 D-glutamate cyclase
EC 4.2.1.49 urocanate hydratase
EC 4.2.1.50 pyrazolylalanine synthase
EC 4.2.1.51 prephenate dehydratase
EC 4.2.1.52 dihydrodipicolinate synthase
EC 4.2.1.53 oleate hydratase
EC 4.2.1.54 lactoyl-CoA dehydratase
EC 4.2.1.55 3-hydroxybutyryl-CoA dehydratase
EC 4.2.1.56 itaconyl-CoA hydratase
EC 4.2.1.57 isohexenylglutaconyl-CoA hydratase
EC 4.2.1.58 crotonoyl-[acyl-carrier-protein] hydratase
EC 4.2.1.59 3-hydroxyoctanoyl-[acyl-carrier-protein] dehydratase
EC 4.2.1.60 3-hydroxydecanoyl-[acyl-carrier-protein] dehydratase
EC 4.2.1.61 3-hydroxypalmitoyl-[acyl-carrier-protein] dehydratase
EC 4.2.1.62 5a-hydroxysteroid dehydratase
EC 4.2.1.63 now EC 3.3.2.3
EC 4.2.1.64 now EC 3.3.2.3
EC 4.2.1.65 3-cyanoalanine hydratase
EC 4.2.1.66 cyanide hydratase
EC 4.2.1.67 D-fuconate dehydratase
EC 4.2.1.68 L-fuconate dehydratase
EC 4.2.1.69 cyanamide hydratase
EC 4.2.1.70 pseudouridylate synthase
EC 4.2.1.71 acetylenecarboxylate hydratase
EC 4.2.1.72 now EC 4.1.1.78
EC 4.2.1.73 protoaphin-aglucone dehydratase (cyclizing)
EC 4.2.1.74 long-chain-enoyl-CoA hydratase
EC 4.2.1.75 uroporphyrinogen-III synthase
EC 4.2.1.76 UDP-glucose 4,6-dehydratase
EC 4.2.1.77 *trans*-L-3-hydroxyproline dehydratase
EC 4.2.1.78 (*S*)-norcoclaurine synthase
EC 4.2.1.79 2-methylcitrate dehydratase
EC 4.2.1.80 2-oxopent-4-enoate hydratase
EC 4.2.1.81 D(-)-tartrate dehydratase
EC 4.2.1.82 xylonate dehydratase
EC 4.2.1.83 4-oxalmesaconate hydratase
EC 4.2.1.84 nitrile hydratase
EC 4.2.1.85 dimethylmaleate hydratase
EC 4.2.1.86 16-dehydroprogesterone hydratase
EC 4.2.1.87 octopamine dehydratase
EC 4.2.1.88 synephrine dehydratase
EC 4.2.1.89 carnitine dehydratase
EC 4.2.1.90 L-rhamnonate dehydratase
EC 4.2.1.91 carboxycyclohexadienyl dehydratase
EC 4.2.1.92 hydroperoxide dehydratase
EC 4.2.1.93 ATP-dependent $H_2$NAD(P)OH dehydratase
EC 4.2.1.94 scytalone dehydratase
EC 4.2.1.95 kievitone hydratase
EC 4.2.1.96 4a-hydroxytetrahydrobiopterin dehydratase
EC 4.2.1.97 phaseollidin hydratase
EC 4.2.1.98 16a-hydroxyprogesterone dehydratase
EC 4.2.1.99 2-methylisocitrate dehydratase
EC 4.2.1.100 cyclohexa-1,5-dienecarbonyl-CoA hydratase
EC 4.2.1.101 *trans*-feruloyl-CoA hydratase
EC 4.2.1.102 now EC 4.2.1.100
EC 4.2.1.103 cyclohexyl-isocyanide hydratase
EC 4.2.1.104 cyanate hydratase

**EC 4.2.2 Acting on Polysaccharides**

EC 4.2.2.1 hyaluronate lyase
EC 4.2.2.2 pectate lyase
EC 4.2.2.3 poly(b-D-mannuronate) lyase
EC 4.2.2.4 chondroitin ABC lyase
EC 4.2.2.5 chondroitin AC lyase
EC 4.2.2.6 oligogalacturonide lyase
EC 4.2.2.7 heparin lyase
EC 4.2.2.8 heparin-sulfate lyase
EC 4.2.2.9 pectate disaccharide-lyase
EC 4.2.2.10 pectin lyase
EC 4.2.2.11 poly(a-L-guluronate) lyase
EC 4.2.2.12 xanthan lyase
EC 4.2.2.13 exo-(1-4)-a-D-glucan lyase
EC 4.2.2.14 glucuronan lyase

**EC 4.2.3 Acting on phosphates**

EC 4.2.3.1 threonine synthase
EC 4.2.3.2 ethanolamine-phosphate phospho-lyase
EC 4.2.3.3 methylglyoxal synthase
EC 4.2.3.4 3-dehydroquinate synthase
EC 4.2.3.5 chorismate synthase
EC 4.2.3.6 trichodiene synthase
EC 4.2.3.7 pentalenene synthase
EC 4.2.3.8 casbene synthase
EC 4.2.3.9 aristolochene synthase
EC 4.2.3.10 (-)-*endo*-fenchol synthase
EC 4.2.3.11 sabinene-hydrate synthase
EC 4.2.3.12 6-pyruvoyltetrahydropterin synthase
EC 4.2.3.13 (+)-d-cadinene synthase
EC 4.2.3.14 pinene synthase
EC 4.2.3.15 myrcene synthase
EC 4.2.3.16 (-)-(4*S*)-limonene synthase
EC 4.2.3.17 taxadiene synthase
EC 4.2.3.18 abietadiene synthase
EC 4.2.3.19 *ent*-kaurene synthase

**EC 4.2.99 Other Carbon-Oxygen Lyases**

EC 4.2.99.1 now EC 4.2.2.2
EC 4.2.99.2 now EC 4.2.3.1
EC 4.2.99.3 now EC 4.2.2.2
EC 4.2.99.4 now EC 4.2.2.3
EC 4.2.99.5 deleted
EC 4.2.99.6 deleted, included in EC 4.2.2.4 and EC 4.2.2.5
EC 4.2.99.7 now EC 4.2.3.2
EC 4.2.99.8 now EC 2.5.1.47
EC 4.2.99.9 now EC 2.5.1.48
EC 4.2.99.10 now EC 2.5.1.49
EC 4.2.99.11 now EC 4.2.3.3
EC 4.2.99.12 carboxymethyloxysuccinate lyase
EC 4.2.99.13 now EC 2.5.1.50
EC 4.2.99.14 now EC 2.5.1.51
EC 4.2.99.15 now EC 2.5.1.52
EC 4.2.99.16 now EC 2.5.1.53
EC 4.2.99.17 now EC 4.2.99.14
EC 4.2.99.18 DNA-(apurinic or apyrimidinic site) lyase
EC 4.2.99.19 2-hydroxypropyl-CoM lyase

**EC 4.3 Carbon-Nitrogen Lyases**

**EC 4.3.1 Ammonia-Lyases**

EC 4.3.1.1 aspartate ammonia-lyase
EC 4.3.1.2 methylaspartate ammonia-lyase
EC 4.3.1.3 histidine ammonia-lyase
EC 4.3.1.4 formiminotetrahydrofolate cyclodeaminase
EC 4.3.1.5 phenylalanine ammonia-lyase
EC 4.3.1.6 b-alanyl-CoA ammonia-lyase
EC 4.3.1.7 ethanolamine ammonia-lyase
EC 4.3.1.8 hydroxymethylbilane synthase
EC 4.3.1.9 glucosaminate ammonia-lyase
EC 4.3.1.10 serine-sulfate ammonia-lyase
EC 4.3.1.11 dihydroxyphenylalanine ammonia-lyase
EC 4.3.1.12 ornithine cyclodeaminase
EC 4.3.1.13 carbamoyl-serine ammonia-lyase
EC 4.3.1.14 3-aminobutyryl-CoA ammonia-lyase
EC 4.3.1.15 diaminopropionate ammonia-lyase
EC 4.3.1.16 *threo*-3-hydroxyaspartate ammonia-lyase
EC 4.3.1.17 L-serine ammonia-lyase
EC 4.3.1.18 D-serine ammonia-lyase
EC 4.3.1.19 threonine ammonia-lyase
EC 4.3.1.20 *erythro*-3-hydroxyaspartate ammonia-lyase

**EC 4.3.2 Amidine-Lyases**

EC 4.3.2.1 argininosuccinate lyase
EC 4.3.2.2 adenylosuccinate lyase
EC 4.3.2.3 ureidoglycolate lyase
EC 4.3.2.4 purine imidazole-ring cyclase
EC 4.3.2.5 peptidylamidoglycolate lyase

**EC 4.3.3 Amine-Lyases**

EC 4.3.3.1 3-ketovalidoxylamine C-N-lyase
EC 4.3.3.2 strictosidine synthase
EC 4.3.3.3 deacetylisoipecoside synthase
EC 4.3.3.4 deacetylipecoside synthase

**EC 4.3.99 Other Carbon-Nitrogen Lyases**

EC 4.3.99.1 now EC 4.2.1.104

**EC 4.4 Carbon-Sulfur Lyases**

EC 4.4.1.1 cystathionine g-lyase
EC 4.4.1.2 homocysteine desulfhydrase
EC 4.4.1.3 dimethylpropiothetin dethiomethylase
EC 4.4.1.4 alliin lyase
EC 4.4.1.5 lactoylglutathione lyase
EC 4.4.1.6 *S*-alkylcysteine lyase
EC 4.4.1.7 deleted, included in EC 2.5.1.18
EC 4.4.1.8 cystathionine b-lyase
EC 4.4.1.9 L-3-cyanoalanine synthase
EC 4.4.1.10 cysteine lyase
EC 4.4.1.11 methionine g-lyase
EC 4.4.1.12 sulfoacetaldehyde lyase
EC 4.4.1.13 cysteine-*S*-conjugate b-lyase
EC 4.4.1.14 1-aminocyclopropane-1-carboxylate synthase
EC 4.4.1.15 D-cysteine desulfhydrase
EC 4.4.1.16 selenocysteine lyase
EC 4.4.1.17 holocytochrome-*c* synthase
EC 4.4.1.18 now EC 1.8.3.5

**EC 4.5 Carbon-Halide Lyases**

EC 4.5.1.1 DDT-dehydrochlorinase
EC 4.5.1.2 3-chloro-D-alanine dehydrochlorinase
EC 4.5.1.3 dichloromethane dehalogenase
EC 4.5.1.4 L-2-amino-4-chloropent-4-enoate dehydrochlorinase
EC 4.5.1.5 *S*-carboxymethylcysteine synthase

**EC 4.6 Phosphorus-Oxygen Lyases**

EC 4.6.1.1 adenylate cyclase
EC 4.6.1.2 guanylate cyclase
EC 4.6.1.3 now EC 4.2.3.4
EC 4.6.1.4 now EC 4.2.3.5
EC 4.6.1.5 now EC 4.2.3.7
EC 4.6.1.6 cytidylate cyclase
EC 4.6.1.7 now EC 4.2.3.8
EC 4.6.1.8 now EC 4.2.3.10
EC 4.6.1.9 now EC 4.2.3.11
EC 4.6.1.10 now EC 4.2.3.12
EC 4.6.1.11 now EC 4.2.3.13
EC 4.6.1.12 2-*C*-methyl-D-erythritol 2,4-cyclodiphosphate synthase
EC 4.6.1.13 phosphatidylinositol diacylglycerol-lyase
EC 4.6.1.14 glycosylphosphatidylinositol diacylglycerol-lyase
EC 4.6.1.15 FAD-AMP lyase (cyclizing)

**EC 4.99 Other Lyases**

EC 4.99.1.1 ferrochelatase
EC 4.99.1.2 alkylmercury lyase

## 9.3 Calibration of SEC-HPLC system

Calibration of SEC-HPLC system involved calibration of peak elution times versus known molecular weight standards (column calibration), and calibration of the refractive index detectors (RID) response to concentration standards (sensor calibration). As two slightly different systems were used for the analysis of experiment 7 and 10 (see Table 4-5), two calibration results are shown here.

Column calibration was performed according to the method described in materials and methods. The size standards used are listed in table xx. Peak elution times were determined as the mean of all standards injected (variable concentrations, see below). By plotting mean elution times versus certified molecular weight means (weight means), the ideal elution curve was constructed. The slight deviations from the expected logarithmic curve are most pronounced towards the ends of the calibration range (column set) of 0.2 - 250 kDa (even though the Zorbax column may be pushed towards 400 kDa using non-linear calibration). Omitting these data would bring the calibration curve close to the ideal correlation. However, these data points are very important for interpretation of the degradation data, and could not be left out. The deviation from the ideal will result in a slight over estimation of low molecular weight molecules (about 0.1 to 0.2 kDa) up to about 1 kDa, while an underestimation of the high molecular weight fragments over 200 kDa of 50 -100 kDa is expected. The concentration of each eluted polymer was found by calibrating the peak response using the certified calibration standards. As the concentration response of the detector proved to be

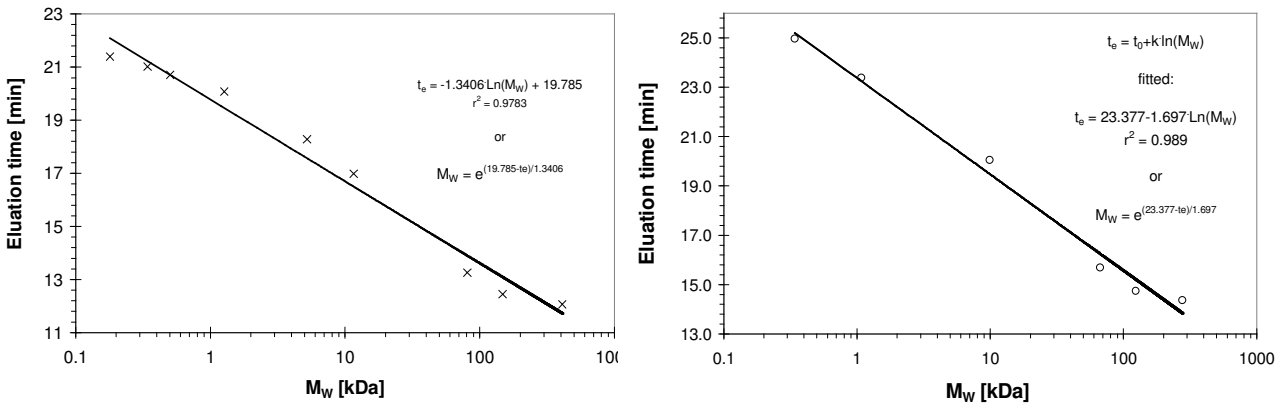


Figure 9-1. Elution curves of the Dextran calibration procedure. Indicated are calibrated $M_W$ transformation functions used for the rest of the HPLC-SEC analysis of experiment 10 (left) and 7 (right).

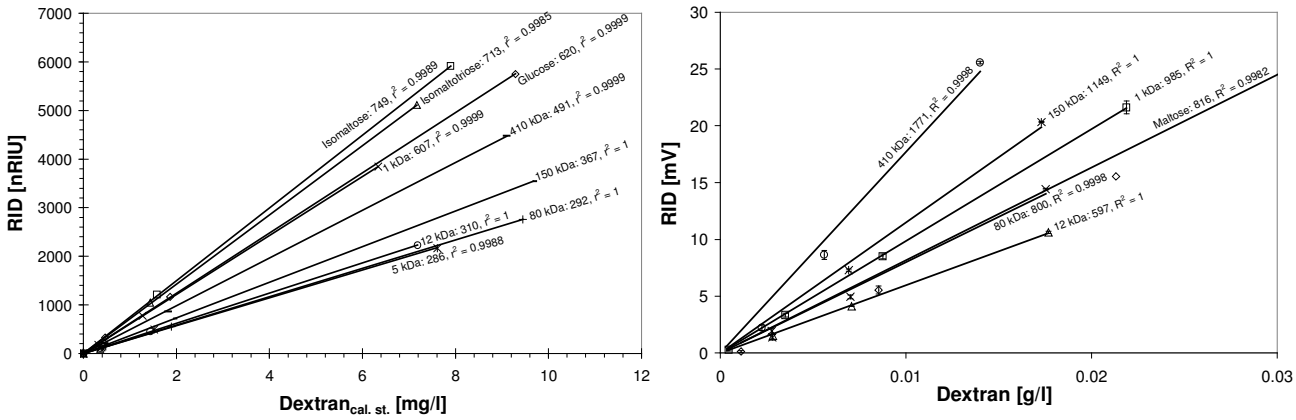


Figure 9-2. Sensor calibration for experiment 10 (right) and 6 (left) using certified (DIN) Dextran standards and >99% pure glucose, Isomaltose (Maltose) and Isomaltotriose as calibration standards. Legend show MW standard, slope of the "forced through zero" linear fitting curves and the linear correlation coefficient for 4 concentrations.

varying according to the molecular weight of the standards, sensor calibration had to be performed for each molecular weight standard (Figure 9-2). Calibration standards were distributed over a considerable range of polymer molecular weights (section 4.1.2). That implicated that the actual concentration at the peak was considerably lower than the total concentration of the standard. In order to calibrate the sensor response to the instantaneous molecular weight (given by the elution curve, Figure 9-1) passing through the sensor, the actual calibration standard peak concentrations would have to be determined. By the HPLC system used here, that is not possible since a high degree of overlapping was intrinsic of the molecular weight standards, and the high injection volume imposed a rather high degree of systematic superimposition that could not be resolved by traditional HPLC manipulations (mobile phase focusing, gradient elution, etc.). Peak concentration (i.e. the concentration of polymers integrated around the peak) of experiment 6 was therefore chosen to be the ± 5 % ($M_W$) range around each peak. A Gaussian curve (to the log $M_w$) was fitted to the DIN certified distribution following each standard. The ± 5 % area was determined by integrating the fitted Gauss curve, and defining the peak concentration as the ratio between the peak area and the total integrated area multiplied by the sample standard concentration (total concentration of the calibration standard).

Figure 9-3 show the slope to the elution time plot, indicating the relation between the slope of the calibration curve and the molecular weight (or elution time) of he standards. The fitted slope to elution time curves are "best fit" polynomials that were chosen solely on the degree

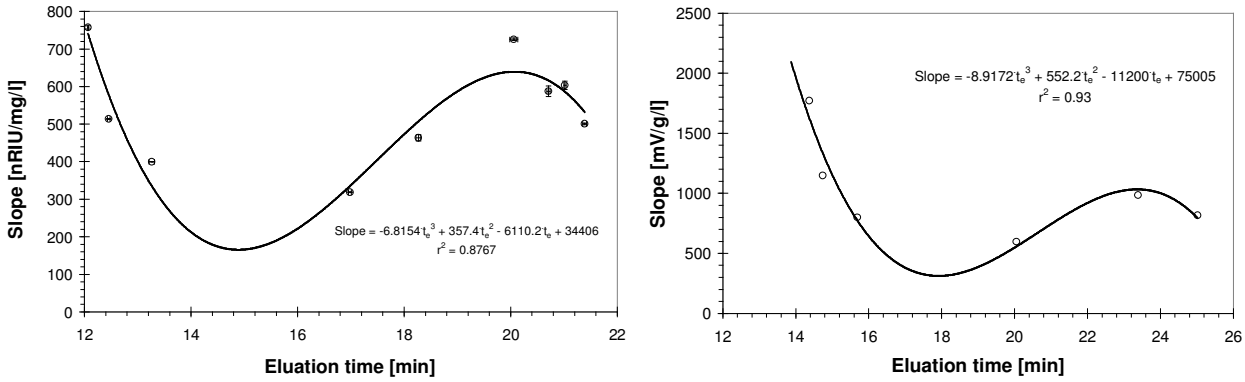


Figure 9-3. Calibration slope to elution time data for experiment 10 (left) and 6 and 7 (right). Models fitted are "best fitted" calibration curves (polynomial fitting). Error bars represent estimated slope and elution time standard deviations of the calibration standards (four concentrations).

of fitting, without any expected/presumed relation between the two. The lack of mechanistic relation weakens the method, but it should be remembered that the calibration does not represent a "true" single polymer to sensor response calibration, but rather a qualitative indication between the relative concentrations between size classes in a sample. By applying the integration method described above on one single polymer range (i.e. integrating over a single molecular weight polymer range of 0.162 kDa), a theoretical correlation between the slope value and the molecular weight could be constructed.

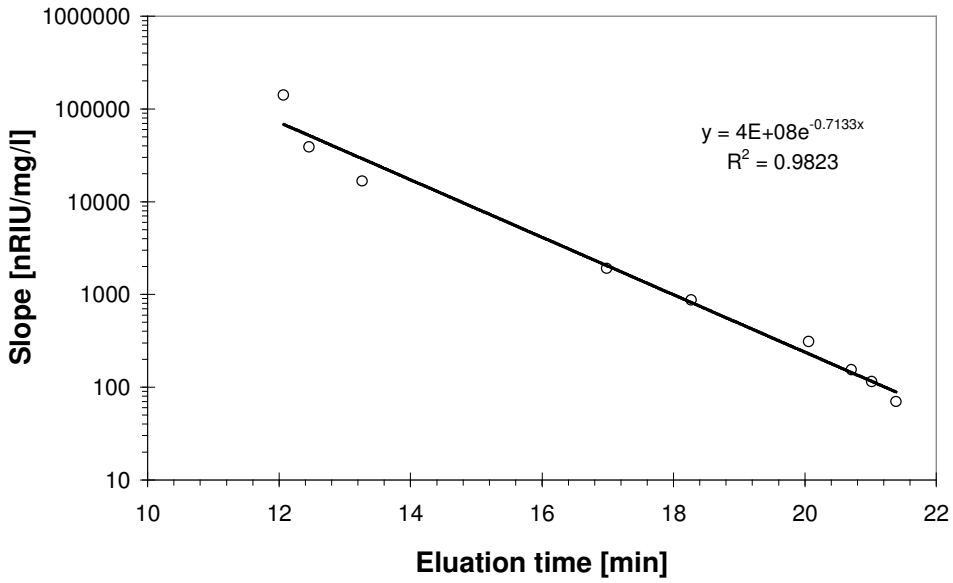


Figure 9-4. Theoretical Slope - Elution time plot based on single polymer peak integration range. Data from the experiment 10 calibration.

Figure 9-4 show the result of single peak slope to elution time calibration. The observed exponential relation is dominated by the exponential relation between the molecular weight separation and the elution time. The lower the molecular weight, the better separation (an intrinsic property of the SEC-HPLC technique).

## 9.4 Pilot testing results, Experiment 5.

Figure 9-5 and Figure 9-6 show the resulting OUR responses after Dextran sample standard injections during experiment 5. Legends provide information on batch date, initial $M_W$ standard and initial concentrations.

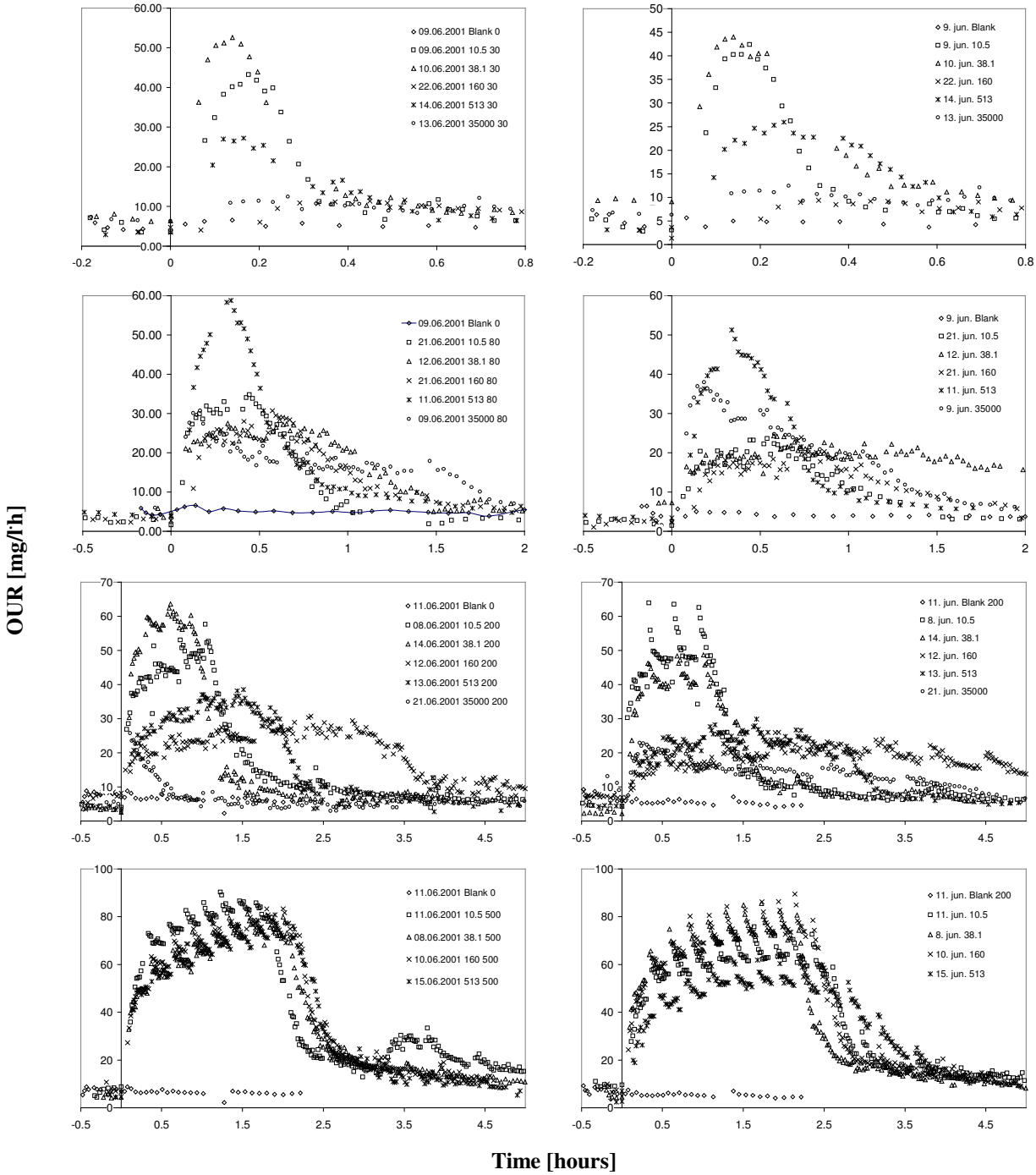


Figure 9-5. Respirograms of experiment 5 batches of 30 (top row), 80, 200 and 500 mg/l (bottom row) initial concentrations of indicated Dextran standards. The right column shows reactor 1 data, while column 2 contains the equivalent respirograms of reactor 2.

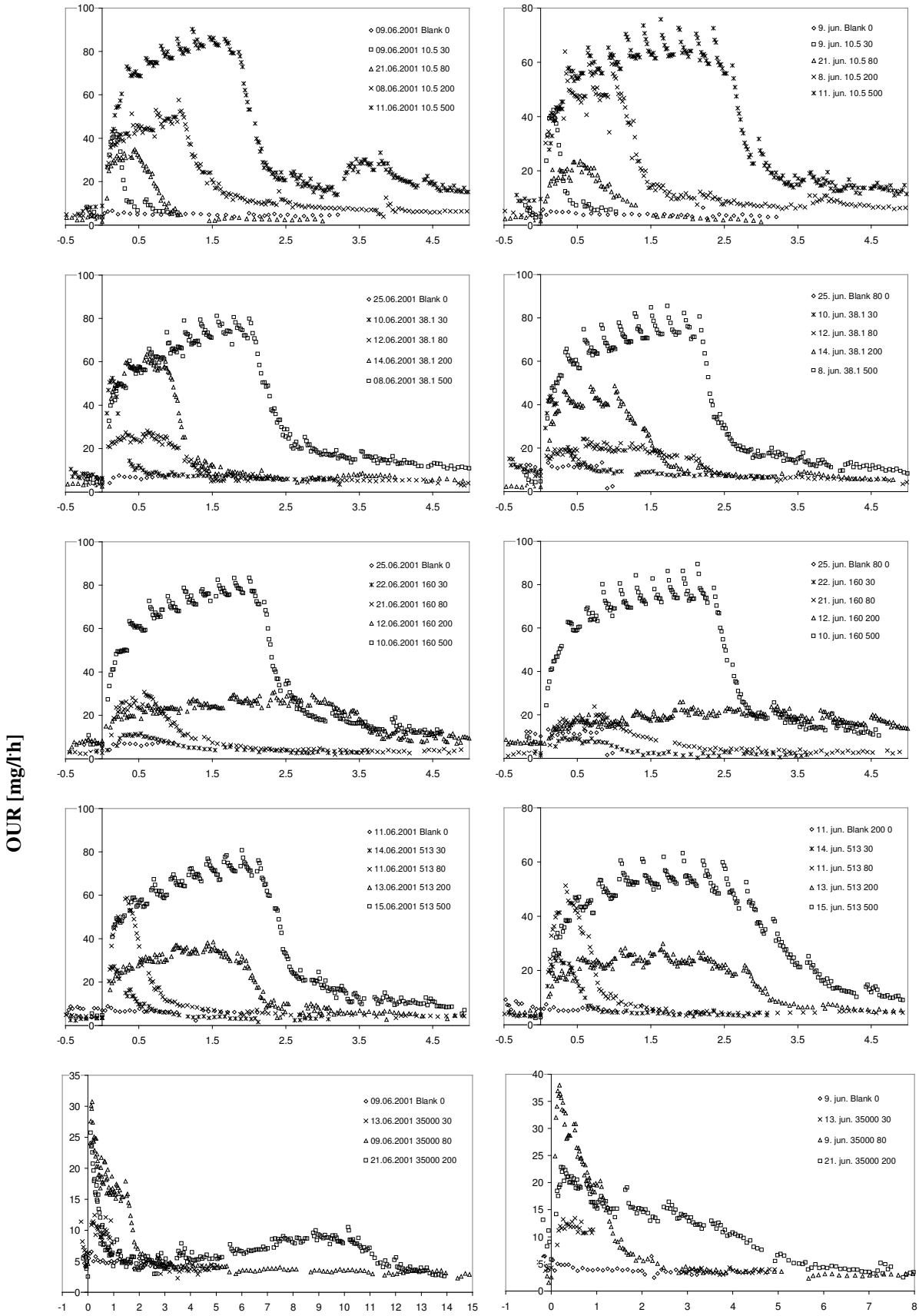


Figure 9-6. Respirograms from experiment 5 grouped as constant $M_W$ standards (rows) for R1 and $R_2$ (right).

Figure 9-5 show the OUR curves of the same initial standard concentration and variable initial $M_W$ (for $R_1$ and $R_2$, same samples applied at the same time). Dates of injection are indicated, and should be compared to the date of system failure (June 12, see Results section 5.2.1). Figure 9-6 show the same data grouped by plotting the same initial molecular weight sample standard, at variable initial batch concentrations.

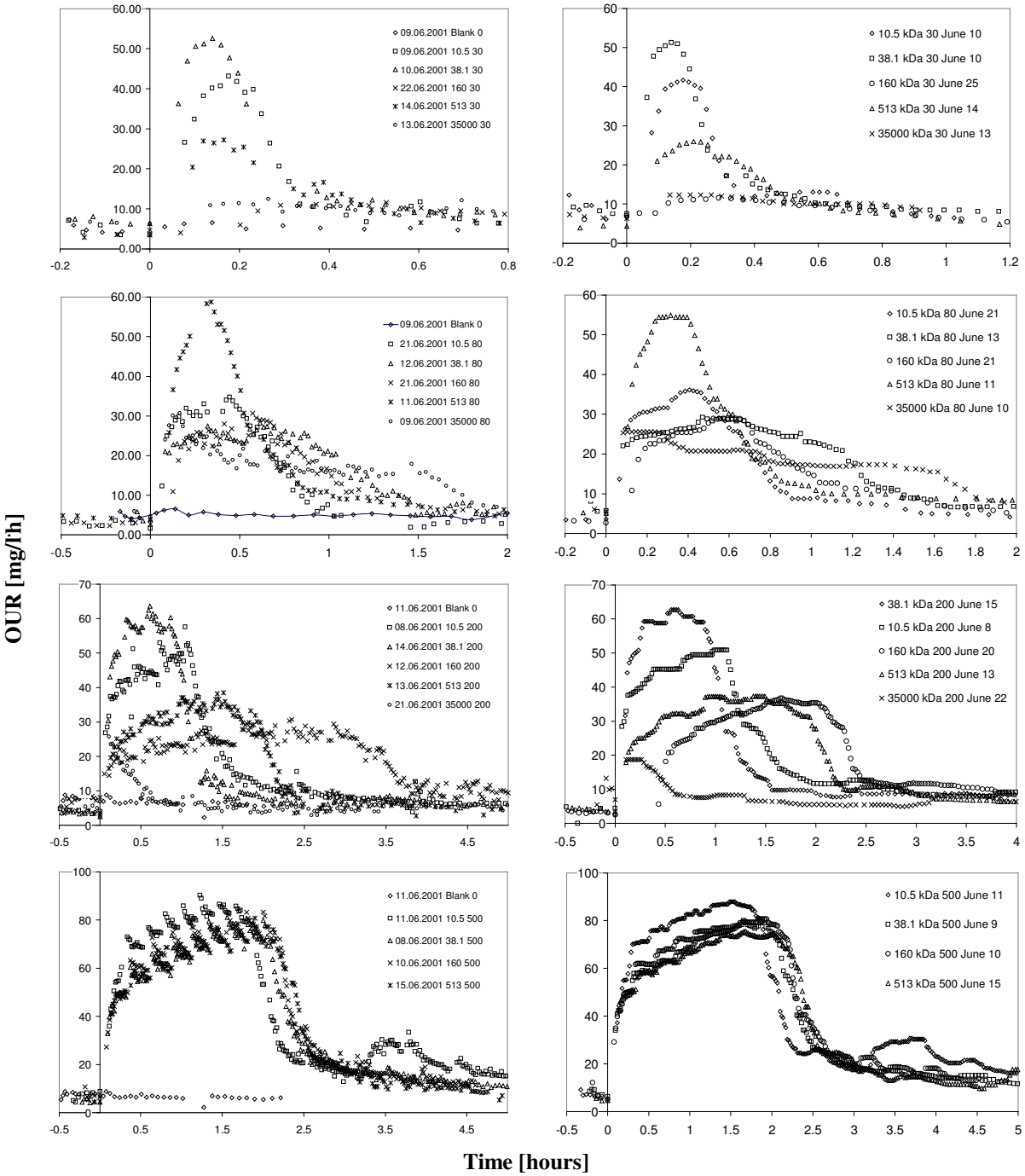


Figure 9-7. Example of data reprocessing (right column) conducted on the $R_1$ equal initial concentration raw data in order to compensate for data spreading and re-oxygenation effects.

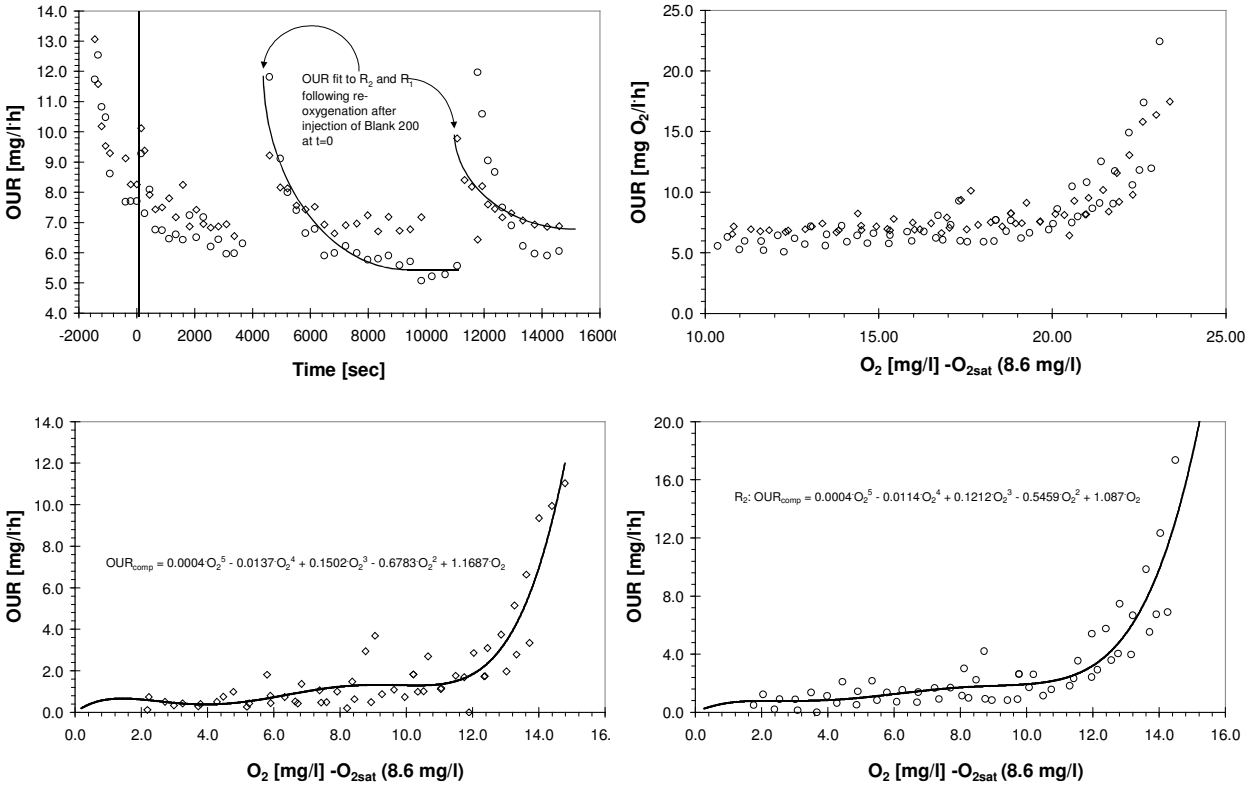


Figure 9-8. Observation that led to (upper plates) and compensation curve fitted for both reactors when analysing injection of a Blank sample.

In order to compensate for abnormally high OUR estimation just after a re-oxygenation cycle, the data were subtracted the blank re-oxygenation behaviour and smoothened using a Median filter in the data acquisition software (filter used was the "median.vi" of LabView, National Instruments, using variable data grouping). Figure 9-7 show the equal initial concentration of variable initial molecular weight batches smoothened by the Median filter, and compensated for high initial OUR rates following re-oxygenation. This processing reduced the fuzzy plots, but did not change the main features of the batches. Compensation for abnormal high OUR was apparent from the respirograms above (Figure 9-5 and Figure 9-6) by the systematic deviation from the OUR curves following oxygenation. This effect can easily be seen from the Blank injection shown in Figure 9-8 were the OUR curves of both reactors are plotted after injection of saline at $t_0$. By plotting OUR of endogenous respiring batches against the bulk phase $O_2$ concentration, a non-linear curve was fitted (Figure 9-8, lower plates) and implemented in the OUR data acquisition software for compensation of this unknown effect. Figure 9-9 show the result on the Blank (June 11) injection, and the effect on the 38.1 and 513 kDa samples on both reactors. Outlayers introduced after oxygenation is compensated

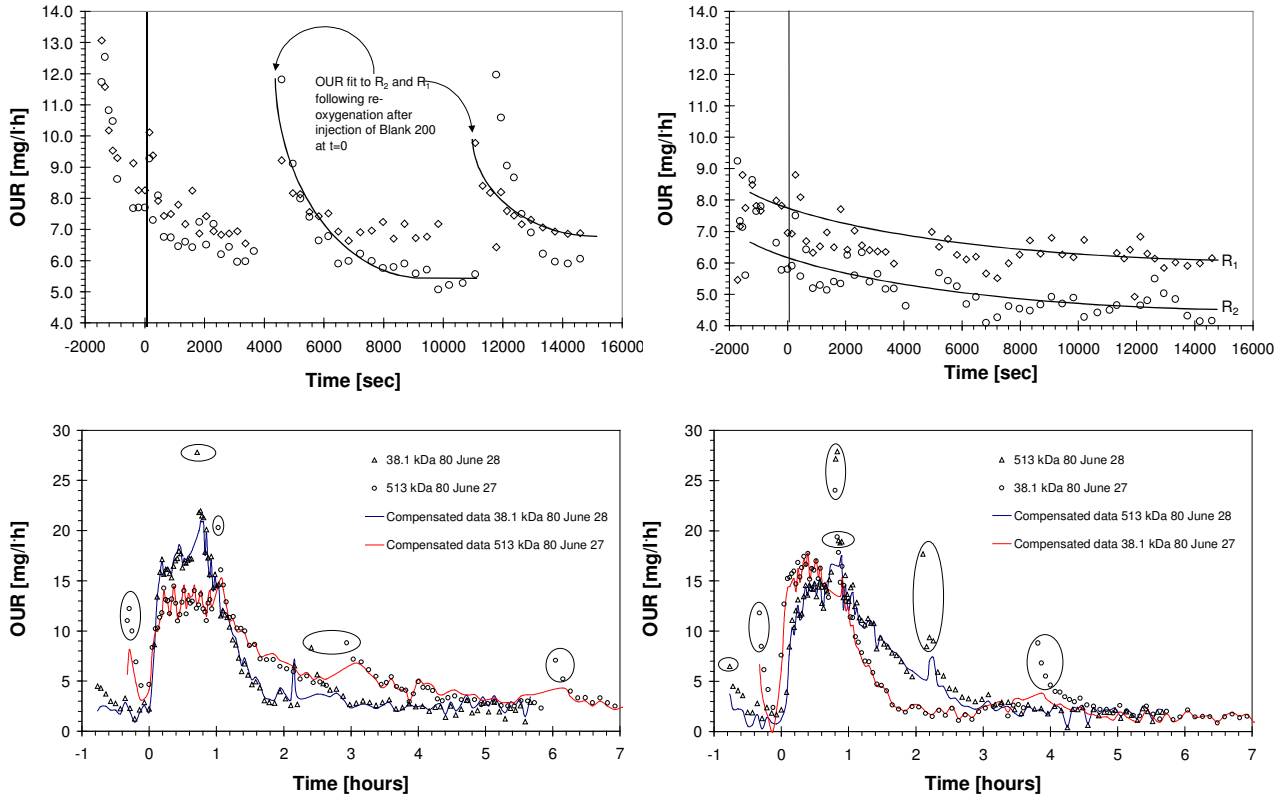


Figure 9-9. Upper plates illustrate compensation applied on the Blank injection (June 11; uncompensated left), and the comparisons between compensated and uncompensated batches of June 27 injections (513 vs 38.1 kDa) of $R_1$ (left) and $R_2$ (lower plates). Circled areas indicate data outlayers introduced after oxygenation and compensated for by the compensation equations of Figure 9-8.

for by the compensation equations presented in Figure 9-8 as can be seen from the difference between the lines (compensated data) and the raw data points.

Compensation and Median filter smoothening were only applied to the experiment 5 data as increased $O_2$ range level, system set up modifications (higher diffuser levels) and strict gas evacuation of the reactors before each experiment (accumulation of gas was checked before each sample injection) reduced the post-oxygenation artificial high OUR to expected (coherent) levels.

## 9.5 Effect of initial Dextran 160 kDa concentrations, experiment 9.

Evaluation of the initial concentration of Dextran was subject of experiment 9. Dextran 160 kDa of 25, 50, 100, 200 and 500 mg/l initial concentrations were injected to $R_1$, and depolymerisation rates were evaluated using observed mineralisation rates, and bulk phase TOC. The order of injection was 50, 100, 25, 500 and 200 mg/l.

Figure 9-10 show bulk phase OUR and TOC during degradation of the standards. The peak OUR, as mentioned in section 5.2.3, follow systematically the initial concentration, while the slope OUR (section 5.2.3) do not behave the same way. It seems like the high concentration standard proceed slower than the intermediate ones, something that may indicate overall substrate inhibiting mechanisms. Indeed, such mechanisms have been observed at high substrate concentrations (Miranda et al. 1991), and the TOC plot (Figure 9-10, right) indicates the same. First order degradation rate fittings indicate the substrate inhibitory effect (simplification of the half order kinetics applied in section 5.2), however, implementing a substrate inhibition model, as proposed by Bailey and Ollis (1986), in the one step depolymerisation model (section 5.6.2), did not reflect the OUR nor the TOC data (results not shown). As discussed in section 7, the high bulk phase TOC levels during the high initial batches could be due to extensive intermediate back diffusion to the bulk. This may offer an explanation to the observed inhibitory behaviour, however, that must be evaluated by bulk phase analysis and simulations.

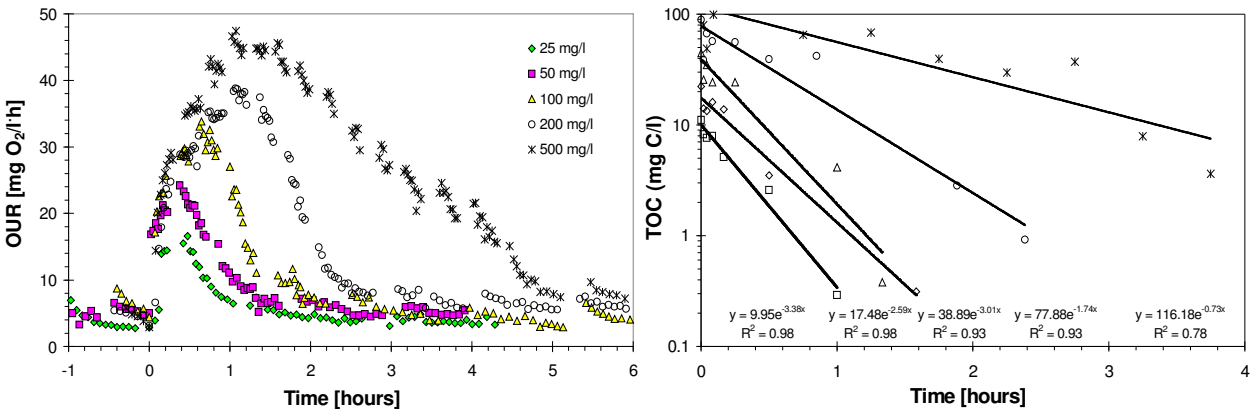


Figure 9-10. Oxygen utilisation rates (left) and bulk phase TOC during degradation of 160 kDa Dextran in $R_1$.